University of Massachusetts Medical School

eScholarship@UMMS

GSBS Dissertations and Theses   Graduate School of Biomedical Sciences

2012-03-28

A New Murine Model For Enterohemorrhagic Escherichia coli Infection Reveals That Actin Pedestal Formation Facilitates Mucosal Colonization and Lethal Disease: A Dissertation

Emily M. Mallick
University of Massachusetts Medical School

Let us know how access to this document benefits you.

Follow this and additional works at: https://escholarship.umassmed.edu/gsbs_diss

Part of the Amino Acids, Peptides, and Proteins Commons, Animal Experimentation and Research Commons, Bacteria Commons, Bacterial Infections and Mycoses Commons, Biological Factors Commons, Enzymes and Coenzymes Commons, Female Urogenital Diseases and Pregnancy Complications Commons, Hemic and Lymphatic Diseases Commons, Immunology and Infectious Disease Commons, and the Male Urogenital Diseases Commons

A NEW MURINE MODEL FOR ENTEROHEMORRHAGIC *ESCHERICHIA*

COLI INFECTION REVEALS THAT ACTIN PEDESTAL FORMATION

FACILITATES MUCOSAL COLONIZATION AND LETHAL DISEASE

A Dissertation Presented

By

EMILY M. MALLICK

Submitted to the Faculty of the University of Massachusetts Graduate School of

Biomedical Sciences, Worcester in partial fulfillment of the requirements for the degree

of

DOCTOR OF PHILOSOPHY

MARCH 28, 2012

MICROBIOLOGY AND PHYSIOLOGICAL SYSTEMS

A NEW MURINE MODEL FOR ENTEROHEMORRHAGIC *ESCHERICHIA COLI*
INFECTION REVEALS THAT ACTIN PEDESTAL FORMATION FACILITATES
MUCOSAL COLONIZATION AND LETHAL DISEASE

A Dissertation Presented By
EMILY M. MALLICK

The signatures of the Dissertation Defense Committee signifies completion and approval
as to style and content of Dissertation

_____

John M. Leong M.D., Ph.D., Thesis Advisor

_____

Victor Boyartchuk Ph.D., Member of Committee

_____

Jon Goguen Ph.D., Member of Committee

_____

Beth McCormick Ph.D., Member of Committee

_____

Chris Sassetti Ph.D., Member of Committee

_____

Cheleste Thorpe M.D., Member of Committee

The signature of the Chair of the Committee signifies that the written dissertation meets
the requirements of the Dissertation Committee

_____

Brian Akerley Ph.D., Chair of Committee

The signature of the Dean of the Graduate School of Biomedical Sciences signifies that
the student has met all graduation requirements of the school.

_____

Anthony Carruthers Ph.D.,
Dean of the Graduate School of Biomedical Sciences

Microbiology and Physiological Systems

March 28, 2012

ACKNOWLEDGEMENTS

I would like to thank all the people who have helped, encouraged, and inspired me throughout my graduate career and Ph.D. studies.

I especially thank my mentor, Dr. John Leong for his guidance, encouragement, understanding, and continuous support. He has taught me so much about thinking critically about my results and exploring many avenues of experimentation, while giving me the freedom to always reach my own conclusions and take my project in the direction of my choice. I am always thankful for his generosity, patience, feedback, and advice. I have become a much better presenter and writer because of him. Lastly, I am thankful for the fact that John always pushes me toward thinking on my own and has groomed me into a very independent, young scientist.

I thank my thesis committee Dr. Brian Akerley, Dr. Beth McCormick, Dr. Victor Boyartchuk, Dr. Jon Goguen, and Dr. Chris Sassetti for advice, support, and suggestions. I thank Dr. Cheleste Thorpe for agreeing to participate as my outside examiner and for finding time to take part in my defense.

I owe special thanks to Dr. Brian Akerley for letting me finish up my Ph.D. work in his lab. I also thank Dr. Jeff Gawronski and Dr. Sandy Wong for their company, advice, and help during my stay in the Akerley lab.

I thank my collaborators: Dr. David Schauer (MIT) who was an expert on *Citrobacter*, Dr. Megan McBee (MIT) who taught how to do *Citrobacter* mouse infections and was always available to answer questions related to the project, Dr. Steve Luperchio (MIT) for contributing data towards my first publication, Drs. Angela Melton-

I am grateful for all the members of the Leong Lab, both past and present that I have had the opportunity to work with and learn from: Dr. Brian Skehan for his mentorship when I first started in the lab, Doug Robbins, Dr. Rudra Bhowmick, Dr. Priya Kailasan Vanaja who I thank tremendously for always being willing and eager to edit my manuscripts, Dr. Mike Brady, Dr. Didier Vingadassalom for helping me throughout my graduate career and suggesting many useful experiments, Loranne Magoun, Dr. Nang Maung, Dr. Vivian Benoit, Cindy Lai, Dr. Yi-Pin Lin for all his humor, Dr. Qiang Chen, and Dr. Sowmya Balasubramanian.

I would like to thank my friends who were always there for moral support and made graduate school fun.

I would like to especially thank my family: mom, Edie Mallick, dad, Michael Mallick, and brother, Andrew Mallick. Without their support and generosity, I would not have been able to complete my graduate work.

Finally, I am incredibly grateful for my wonderful and supportive boyfriend, Chris, for his endless encouragement, patience, and support throughout my graduate career.

ABSTRACT

Enterohemorrhagic *Escherichia coli* (EHEC) colonizes the intestine and produces the

phage-encoded Shiga toxin (Stx) which is absorbed systemically and can lead to

hemolytic uremic syndrome (HUS) characterized by hemolytic anemia,

thrombocytopenia, and renal failure. EHEC, and two related pathogens,

Enteropathogenic *E. coli* (EPEC), and the murine pathogen, *Citrobacter rodentium*, are

attaching and effacing (AE) pathogens that intimately adhere to enterocytes and form

actin "pedestals" beneath bound bacteria. The actin pedestal, because it is a unique

characteristic of AE pathogens, has been the subject of intense study for over 20 years.

Investigations into the mechanism of pedestal formation have revealed that to generate

AE lesions, EHEC injects the type III effector, Tir, into mammalian cells, which

functions as a receptor for the bacterial adhesin intimin. Tir-intimin binding then triggers

a signaling cascade leading to pedestal formation. In spite of these mechanistic insights,

the role of intimin and pedestal formation in EHEC disease remains unclear, in part

because of the paucity of murine models for EHEC infection. We found that the

pathogenic significance of EHEC Stx, Tir, and intimin, as well as the actin assembly

triggered by the interaction of the latter two factors, could be productively assessed

during murine infection by recombinant *C. rodentium* expressing EHEC virulence

factors. Here we show that EHEC intimin was able to promote colonization of *C.

rodentium* in conventional mice. Additionally, previous *in vitro* data indicates that

intimin may have also function in a Tir-independent manner, and we revealed this

function using streptomycin pre-treated mice. Lastly, using a toxigenic *C. rodentium*

strain, we assessed the function of pedestal formation mediated by Tir-intimin interaction and found that Tir-mediated actin polymerization promoted mucosal colonization and a systemic Stx-mediated disease that shares several key features with human HUS.

TABLE OF CONTENTS

LIST OF TABLES

APPENDIX

LIST OF FIGURES

CHAPTER III: A NOVEL MURINE MODEL FOR SHIGA TOXIN-MEDIATED DISEASE BY ENTEROHEMORRHAGIC *ESCHERICHIA COLI*

APPENDIX

COPYRIGHT INFORMATION

Chapters in this thesis dissertation were taken from the following publications:

Chapter II: Mallick EM, Brady MJ, Luperchio SA, Vanguri VK, Magoun L, Liu H, Sheppard BJ, Mukherjee J, Donohue-Rolfe A, Tzipori S, Leong JM and Schauer DB (2012) Allele- and Tir-independent functions of intimin in diverse animal infection models. *Front. Microbio.* **3**:11. doi: 10.3389/fmicb.2012.00011.

LIST OF SYMBOLS, ABBREVIATIONS OR NOMENCLATURE

12-LOX	12-lipoxygenase
AE	Attaching and effacing
AJC	apical junction complex
Arp-2/3	actin related protein 2/3
Bfp	bundle-forming pilus
BUN	blood urea nitrogen
CFU	colony forming unit
CNS	central nervous system
EAEC	Enteroaggregative *Escherichia coli*
EHEC	Enterohemorrhagic *Escherichia coli*
EPEC	Enteropathogenic *Escherichia coli*
EAF	EPEC adherence factor
F-actin	Filamentous actin
FAS	Filamentous actin staining assay
Gb_3	globotriaosylceramide receptors
GBD	GTP-ase binding region
G-CSF	granulocyte colony stimulating factor
H&E	hematoxylin/eosin
HUS	Hemolytic uremic syndrome
IF	immunofluorescence
IF	intermediate filaments
iNWKO	conditional, intestinal N-WASP knockout mouse
IRSp53	Insulin receptor substrate p53
IRTKS	insulin receptor tyrosine kinase substrate
IV	intravenous
Kb	kilobase
KC	keratinocyte chemoattractant
LEE	Locus of Enterocyte Effacement
LMC	littermate controls
LPF	Long polar fimbriae
LPS	Lipopolysaccharide
MCP-1	monocyte chemoattractant protein
MEFs	Mouse embryonic fibroblasts
MIP-1β	macrophage inflammatory protein 1β
MOI	multiplicity of infection
MYD88	Myeloid differentiation primary response gene (88)
NPY	Asparagine-Proline-Tyrosine
N-WASP	neuronal Wiskott–Aldrich Syndrome protein
ORF	open reading frame
PAI	pathogenicity island
PAMPS	Pattern associated molecular patterns
PAS	Periodic acid-Schiff

PBS	phosphate buffered saline
RANTES	(aka CCL5) Regulated upon Activation, Normal T-cell Expressed, and Secreted
SH-2	Src homology domain 2
STEC	Shiga toxin producing *Escherichia coli*
Stx	Shiga toxin
T2SS	Type II secretion system
T3SS	Type III secretion system
TCA	trichloroacetic acid
TEM	Transmission electron microscopy
TER	Transepithelial resistance
Tir	Translocated intimin receptor
TNF-α	tumor necrosis factor α
TVSS	Type V secretion system
UMMS	University of Massachusetts Medical School
VCA	veroprolin homology, central hydrophobic, and acidic regions

CHAPTER I.

INTRODUCTION

I. Overview of attaching and effacing pathogens

Enterohemorrhagic *Escherichia coli* (EHEC)

EHEC belongs to the group of pathogenic *Escherichia coli* and is a member of the larger group of Shiga-toxin (Stx) producing *E. coli* (STEC). STEC strains produce Stx and may or may not contain the Locus of Enterocyte Effacement (LEE), which will be explained in detail below. EHEC was initially described in the early 1980's and the first infection in the United States was reported in 1983 (Riley et al., 1983). Today, EHEC remains a frequent cause of food-related outbreaks of diarrhea nationwide as well as in Europe and Japan (reviewed in (Kaper et al., 2004)). Cattle and other ruminants are important reservoirs of EHEC carriage (Borczyk et al., 1987; Caprioli et al., 2005a), and human infection usually occurs from the ingestion of contaminated food such as beef, produce, and dairy products, or through direct contact with infected animals (Cody et al., 1999; Crump et al., 2002). Serious outbreaks resulting in life-threatening hemolytic uremic syndrome (HUS) in the United States and worldwide are commonly due to serotype O157:H7 (Croxen and Finlay, 2010; Gansheroff and O'Brien, 2000; Kaper et al., 2004). In fact, it has been estimated by the Centers for Disease Control and Prevention (CDC) and others that EHEC O157:H7 causes more than 73,000 cases of illness, 2,000 hospitalizations, and 50-60 deaths annually in the United States (Mead and Griffin, 1998). Several non-O157 serotypes such as O26, O103, O55, and O111 have also associated with human disease (Jenkins et al., 2003; Pearce et al., 2004), and these

serotypes have been suggested to account for up to 20-50 percent of all STEC infections (Johnson et al., 2006). However, the prevalence of human infection by non-O157 STEC is probably underestimated due to the fact that many laboratories do not screen for these strains. Importantly, the CDC estimates that approximately 265,000 STEC infections (including EHEC O157:H7 and other STEC serotypes) occur each year.

Upon infection, EHEC localizes to the large intestine, colonizing the intestinal mucosa. Most infections result in local disease with severe abdominal cramping, watery diarrhea, and/or hemorrhagic colitis (bloody diarrhea). These infections are typically self-resolving, yet approximately five-to-ten percent of infected individuals go on to develop HUS that may be accompanied by long-term sequelae (Chandler et al., 2002; Siegler, 2003). Interestingly, an ever higher incidence of HUS (16 percent) was reported during a particularly virulent outbreak of EHEC associated with spinach in the United States in 2006 (Kulasekara et al., 2009). HUS occurs more often in children than adults and is the leading cause of renal failure in children in United States, with a mortality rate of five percent (Gerber et al., 2002). The clinical symptoms of HUS include the triad of hemolytic anemia, thrombocytopenia (low platelet count), and renal failure (for review, see (Paton and Paton, 1998; Proulx et al., 2001; Ruggenenti et al., 2001)). In severe cases, HUS can result in central nervous system (CNS) impairment (Cimolai et al., 1992; Neild, 1994). Unfortunately, there is no specific treatment of HUS and current management of infections usually consists of supportive therapy (MacConnachie and Todd, 2004).

Enteropathogenic *E. coli* (EPEC) and *Citrobacter rodentium*

EHEC, along with two related pathogens, Enteropathogenic *E. coli* (EPEC), and *Citrobacter rodentium*, are referred to collectively as attaching and effacing (AE) pathogens. EPEC colonizes the small intestine and is a major etiological agent of infantile diarrhea in the developing world (Chen and Frankel, 2005; Spears et al., 2006). *C. rodentium* is murine pathogen that causes transmissible colonic hyperplasia characterized by colonic epithelial cell proliferation and high mortality in suckling mice (reviewed in (Borenshtein et al., 2008; Luperchio and Schauer, 2001; Mundy et al., 2005)). In addition, *C. rodentium* is the only AE pathogen that is capable of efficiently colonizing conventional mice and therefore, has been used extensively as a small animal model for EHEC and EPEC pathogenesis (Barthold et al., 1978; Borenshtein et al., 2008; Deng et al., 2003; Luperchio and Schauer, 2001; Mundy et al., 2005). All three pathogens induce striking, ultra-structural changes on intestinal epithelial cells known as AE lesions (for review see (Kaper et al., 2004) (**Figure 1**)).

Attaching and effacing lesions

Unique changes in the intestinal epithelium following *E. coli* infection were first observed in piglets by Staley and co-workers in 1969 (Staley et al., 1969). Several years later, Takeuchi and colleagues described similar lesions on the intestinal epithelium of rabbits infected with *E. coli* O15 (Takeuchi et al., 1978) and following this, Moon and co-workers named the lesions "attaching and effacing" (Moon et al., 1983). These
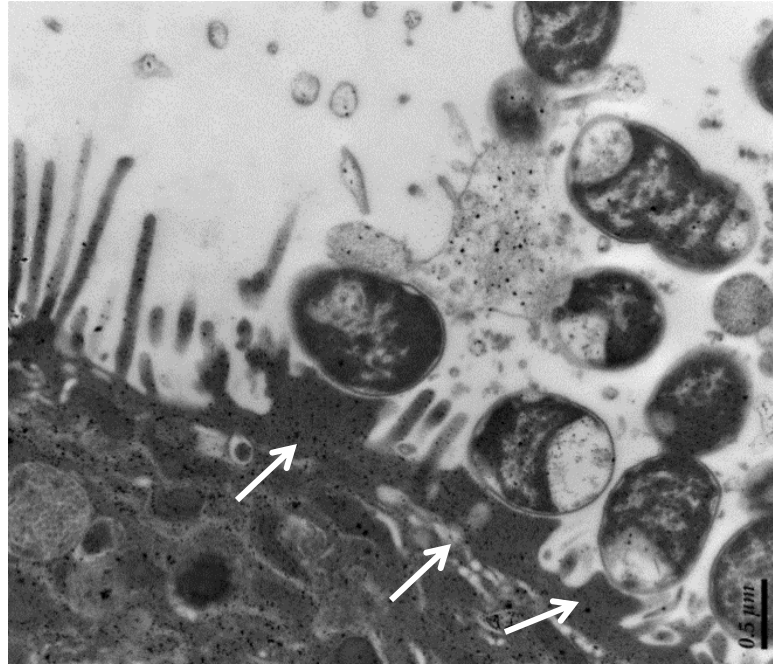
Figure 1. AE lesion formation by *C. rodentium*. An electron micrograph of the distal mouse colon upon infection by *C. rodentium* (λstx_{2dact}) revealing the presence of actin-rich pedestals (see white arrows). Magnification is at 20,500x and scale bar represents 0.5 μm.

remarkable lesions consist of intimate attachment of the bacteria to the host cells, localized effacement of brush-border microvilli, and the formation of highly organized filamentous (F-) actin pedestals beneath bound bacteria that lift bacteria above the plane of the host cell membrane (**Figure 1**). The detailed mechanisms of actin pedestal formation will be discussed below.

Effects of AE lesions on host cells

AE lesions and bacterial effector proteins (which will be described below; see **Table 1**) dramatically alter the function of intestinal cells, leading to the development of diarrhea. For instance, effacement of microvilli and formation of actin pedestals modifies the apical cytoskeletal domain of the intestinal enterocyte, which functions to maintain epithelial cell integrity and regulate fluid and solute exchange. Additionally, it has been predicted that microvillar effacement diminishes the absorptive capacity of the intestine. Furthermore, certain effector proteins secreted from the bacteria into the host cell disrupt tight junctions, which govern the paracellular movement of water and ions. Indeed, all three AE pathogens have been shown to diminish transepithelial electrical resistance (TEER) of polarized monolayers, an indication of tight junction disruption (Flynn and Buret, 2008; Hanajima-Ozawa et al., 2007; Ma et al., 2006). This has also been demonstrated *in vivo* (Canil et al., 1993; Dean and Kenny, 2004; Guttman et al., 2006a; Guttman et al., 2006b; Shifflett et al., 2005).

II. Host cell attachment by AE pathogens

Infection and passage through stomach

Once ingested, AE pathogens encounter a critical barrier to bacterial infection—the stomach, which has a pH as low as 1.5 – 2.5 (Gorden and Small, 1993). Therefore, an important property of AE pathogens is the ability to pass through this acidic environment and colonize the mammalian gastrointestinal tract to cause disease. The infectious dose of EHEC is extremely low (<100 organisms), which implies that it is able to pass through the stomach with high efficiency (Doyle and Pariza, 2001; Nataro and Kaper, 1998; Tilden et al., 1996; Yoon and Hovde, 2008). Indeed, EHEC and EPEC are extremely acid-resistant, similar to commensal *E. coli* (Lin et al., 1996), and adapt to acidic conditions by enabling acid resistance systems ((Richard and Foster, 2003), for review, see (Foster, 2004)). These acid resistance systems secrete protons from the bacteria, prevent extracellular protons from entering the bacterial cytoplasm, and induce changes in the membrane composition of the bacteria (Castanie-Cornet et al., 1999; Lin et al., 1995; Small et al., 1994). In addition to low pH, in order to cause infection, AE pathogens must also resist other harsh conditions including antimicrobial and digestive enzymes, peristalsis, cellular exfoliation, and innate immune responses (which will be discussed briefly in **Appendix B**).

Initial adhesins and non-intimate attachment

Upon transit through the stomach, AE pathogens must adhere to intestinal epithelial cells in order to effectively colonize the host and compete with normal microbiota. EHEC and *C. rodentium* establish infection on the luminal surface of the

large bowel, while EPEC colonizes the mucosal surface of the small intestine. Like many other pathogens, AE pathogens encode a multitude of surface factors which mediate the initial interaction with the host mucosa. Initial adhesins include: fimbriae (including pili and curli), outer-membrane proteins, surface proteins, effector proteins, and flagella (for review, see (Bardiau et al., 2010; Nougayrede et al., 2003; Torres et al., 2005)). For the purpose of this introduction, initial, non-intimate adhesins will be divided into two main groups: (1) fimbrial adhesins and (2) non-fimbrial adhesins.

Fimbrial adhesins

Fimbriae are filamentous structures that protrude from the bacterial surface and enable bacteria to adhere to host cells. Despite the assortment of EHEC genes putatively involved in fimbriae synthesis, as well as evidence suggesting some defined fimbriae promote colonization and disease (La Ragione et al., 2000; Lane and Mobley, 2007; Perna et al., 2001), the role these adhesins play in attachment has not been entirely clarified. One defined EHEC adhesin, however, long polar fimbriae (LPF) (Perna et al., 2001; Torres et al., 2002; Torres et al., 2004) was recently implicated in intestinal colonization of infant rabbits (Lloyd et al., 2012). Additionally, a Type IV pilus restricted to EHEC O157:H7, termed hemorrhagic coli pilus (HCP) (Xicohtencatl-Cortes et al., 2007), has been recognized in the serum of patients with HUS, but not healthy patients, suggesting that these pili are produced during infections *in vivo*. Moreover, infection of bovine gut explants with bacteria deficient in HCP production resulted in a significant reduction of bacterial adherence (Xicohtencatl-Cortes et al., 2007).

Like EHEC, EPEC and *Citrobacter* have putative and defined fimbriae and pili associated with colonization and virulence (Adams et al., 1997; Bieber et al., 1998; Fiederling et al., 1997; Giron et al., 1991; Mundy et al., 2003). *C. rodentium* has a type IV pilus termed colonization factor *Citrobacter* (CFC) that is required for intestinal colonization in mice (Mundy et al., 2003). EPEC is unique from EHEC and *C. rodentium* because it harbors the bundle-forming pilus (Bfp), a type IV pilus, expressed from 14 genes located on EPEC adherence factor (EAF) plasmid (Giron et al., 1993; Giron et al., 1991). While Bfp is important for localized adhesion and microcolony formation *in vitro* (Giron et al., 1993; Giron et al., 1991), its role *in vivo* is unclear (Hicks et al., 1998; Knutton et al., 1991). Nevertheless, a volunteer study demonstrated that Bfp plays an important role in human disease (Bieber et al., 1998) and humans develop Bfp-specific immune responses (Loureiro et al., 1998; Martinez et al., 1999).

Non-fimbrial adhesins

One non-fimbrial adhesin present in EHEC and EPEC is the outer-membrane protein, OmpA, which is important for binding to cells in culture (Torres and Kaper, 2003). This phenotype, however, has not been further investigated *in vivo*. Bacterial factors secreted from the type III secretion system (T3SS) of AE pathogens, most notably EspA, have also been suggested to be adhesins because they mediate the initial interaction between host cells and bacteria (Cleary et al., 2004; Daniell et al., 2001; Ebel et al., 1998; Knutton et al., 1998). In addition, there is evidence that proteins secreted independently of the T3SS play a role in adherence of AE pathogens to mammalian cells.

For example, EHEC harbors a type II secretion system (T2SS) and two secreted effectors, YodA and StcE, have been recognized to promote EHEC adherence *in vitro* as well as *in vivo* during colonization of infant rabbits (Grys et al., 2005; Ho et al., 2008). Finally, AE pathogens utilize flagella to adhere to host cells and data suggests that EPEC flagellar expression can be induced by eukaryotic factors secreted from host cells (Giron et al., 2002). Specifically, H7 of EHEC and H6 of EPEC have been hypothesized to adhere to mucus within the host intestinal tract and also bind host extracellular matrix proteins (Erdem et al., 2007).

Intimin-dependent adhesion

Despite the plethora of adhesins described above, the most thoroughly characterized adhesin absolutely required for attachment and intimate adherence of AE pathogens to epithelial cells, as well as for intestinal colonization and virulence (Donnenberg et al., 1993a; Donnenberg et al., 1993b; Marches et al., 2000; McKee et al., 1995; Schauer and Falkow, 1993b), is intimin (a ~94 kDa outer-membrane protein), encoded by the gene *eae.* The most distinguished function of intimin is to bind its own receptor, the translocated intimin receptor (Tir) (Hartland et al., 1999; Kenny et al., 1997). The interaction between Tir and intimin, referred to as intimate adherence, will be discussed below.

Biochemical and biophysical studies revealed that intimin can be divided into three domains: the flexible N-terminal region (including a periplasmic domain), a central membrane β-barrel, and a surface-exposed C-terminal domain (Ross and Miller, 2007; Yi

et al., 2010). This 280 amino acid C-terminal domain is considered the receptor binding

domain (Frankel et al., 1995) and because of allelic differences within this domain, at

least ten different intimin subtypes have been described (Adu-Bobie et al., 1998; Oswald

et al., 2000; Torres et al., 2005). EPEC, *C. rodentium*, and EHEC O157:H7 produce

intimin-α, intimin-β, and intimin-γ, respectively.

Allelic variation in intimin and tissue tropism and species host range

    Although EPEC and EHEC intimin have proven interchangeable for pedestal

formation on cultured cells, intimin exhibits considerable allelic variation in the C-

terminal domain responsible for adhesive activity (Frankel et al., 1994). Because of this

variation, intimin alleles from canonical EHEC, EPEC, and *C. rodentium* strains are

distinct and have been associated with differences in function, such as tissue tropism. For

example, infection of intestinal tissue *ex vivo* suggests that intimin of EHEC O157:H7

(intimin γ) promotes colonization of different epithelial types than intimin of canonical

EPEC (intimin α) or *C. rodentium* (intimin β) (Fitzhenry et al., 2002; Girard et al., 2005;

Mundy et al., 2007; Phillips and Frankel, 2000). In addition, whereas wild type EHEC

colonizes the large bowel of gnotobiotic piglets, an EHEC strain harboring a plasmid

expressing EPEC intimin acquired the additional ability to colonize the small intestine

(Tzipori et al., 1995). Allelic differences in intimin have also been shown to contribute to

species host range. For example, while *C. rodentium* expressing EPEC intimin is able to

efficiently colonize Swiss NIH and C3H/HeJ mice (Frankel et al., 1996b; Hartland et al.,

2000; Schauer and Falkow, 1993b), *C. rodentium* expressing a derivative of EPEC

intimin harboring the adhesive domain of EHEC intimin provided only poor colonization in these animals (Hartland et al., 2000; Mundy et al., 2007). **Chapter II** of this thesis will explore the allele-dependent and independent functions of intimin *in vitro* and in *vivo* and determine if these differences result in variation in tissue tropism and species host range.

Tir-independent functions of intimin

In addition to binding Tir, it has been suggested that intimin from both EPEC and EHEC can bind to uninfected, cultured epithelial cells (Frankel et al., 1994; Hartland et al., 1999; McKee and O'Brien, 1995). Additionally, it has been hypothesized that intimin possesses host receptor adhesive activities that also contribute to colonization and based on mutagenesis studies, the regions within intimin that mediate adherence to host cells are distinct from the Tir-binding region of intimin (Frankel et al., 1998). For example, the intimin-related *Yersinia pseudotuberculosis* invasin protein binds to β_1-chain integrins (Isberg et al., 1987), and EPEC intimin was shown to be capable of recognizing β_1-chain integrins, albeit with apparently much lower affinity (Frankel et al., 1996a). The eukaryotic protein nucleolin which is expressed on the surface of many cell types (Ginisty et al., 1999) and has also been implicated in serving as a receptor for some viruses (Callebaut et al., 1998; de Verdugo et al., 1995), is recognized by EHEC intimin (Sinclair and O'Brien, 2002) and localized beneath cell-associated EPEC during infection of cultured monolayers (Dean and Kenny, 2011). Finally, intimin, but not Tir contributes to the disruption of epithelial barrier function (Dean and Kenny, 2004), suggesting that

Tir-independent functions of intimin exist. **Chapter II** of this thesis will address the Tir-independent functions of intimin for the first time *in vivo* using a murine model.

Locus of enterocyte effacement and type III secretion

Generation of AE lesions depends on the ~35 kb, chromosomally-encoded pathogenicity island termed the Locus of Enterocyte Effacement (LEE), which is present in EHEC, EPEC, and *C. rodentium* (Barba et al., 2005; Deng et al., 2001; McDaniel et al., 1995; McDaniel and Kaper, 1997). (It should be noted that some STEC strains do not possess a LEE and have Stx as their main virulence factor, specifically STEC strains such as B2F1 and EC1720a that produce mucus-activatable toxin (Gobius et al., 2003; Ito et al., 1990; Melton-Celsa et al., 2002).) The LEE encodes the bacterial outer membrane adhesin intimin (described above) (Donnenberg and Kaper, 1991; Jerse, 1990), the T3SS machinery (Jarvis et al., 1995; Lee, 1997), and many effector proteins (see **Table 1**). The T3SS is a multiprotein basal export complex that including an ATPase, EscN, critical for the function of the apparatus, spans the inner and outer membranes of the bacterium (Daniell et al., 2001; Wilson et al., 2001). Distal to the basal body are components that form a filamentous appendage extending from the bacteria to the host cell (Knutton et al., 1998). Two translocators, EspB and EspD, that promote pore formation in mammalian membranes, are thought to be localized at the tip of this appendage, allowing the T3SS to act as a conduit through which effectors are delivered directly into the host cell cytoplasm (Ide et al., 2001; Ogino et al., 2006; Sekiya et al., 2001).

Tir and intimate attachment

Tir is an essential bacterial effector protein absolutely required for AE lesion formation and for colonization in many animal models (Deng et al., 2003; Marches et al., 2000; Ritchie et al., 2003). Upon injection into the host cell via the T3SS, Tir integrates into the host cell membrane in a hairpin loop conformation and serves as the receptor for the bacterial adhesin intimin, through its extracellular domain (Batchelor et al., 2000; Liu et al., 2002; Luo et al., 2000). Tir-intimin interaction induces Tir clustering (Touze et al., 2004) and permits the cytoplasmic N- and C-terminal domains of Tir to coordinate a downstream signaling cascade resulting in the formation of F-actin pedestals (Caron, et al., 2006; Hayward et al., 2006, Campellone et al., 2004). While the N-terminus of Tir has been shown to interact with actin-binding proteins such as α-actinin and cortactin (Cantarelli et al., 2002; Goosney et al., 2000; Mousnier et al., 2008), Tir mutants lacking the N-terminus are still able to generate actin pedestals, suggesting the key residues necessary for actin assembly reside in the C-terminus (Brady et al., 2007; Campellone et al., 2006; Campellone et al., 2004a). Although the requirement of Tir for colonization in animal models has been well established, the role of Tir-mediated actin assembly and pedestal formation in colonization and disease remains to be well characterized and will be discussed in **Chapters III and IV** of this thesis.

Additional effector proteins

Other effector proteins encoded on the LEE include the cytoskeletal modulating proteins EspF, Map, EspH, EspG, and EspK. EspF and Map disrupt epithelial barrier

function (Dean and Kenny, 2004; McNamara et al., 2001). EspH downregulates filopodium formation and promotes pedestal formation (Tu et al., 2003) and has been implicated in promoting colonization in animal models (Deng et al., 2004; Mundy et al., 2004; Ritchie and Waldor, 2005). EspG is responsible for destabilizing microtubule networks, triggering actin stress fiber assembly, and damaging the Golgi apparatus (Clements et al., 2011; Matsuzawa et al., 2004). Finally, EspK was reported to have no effect on actin nucleation in HeLa cells, but seems to promote persistence in an orally infected calf model (Vlisidou et al., 2006b). **Table 1** lists the common LEE and non-LEE encoded effector proteins and their functions in EHEC, EPEC, and *C. rodentium*. The *in vitro* and *in vivo* function of some of these cytoskeletal-modulating effectors in *C. rodentium* will be discussed in **Appendix A**.

Table 1. LEE-encoded and non-LEE encoded effector proteins.

Effector	Size or predicted molecular weight, location	Function or activity and associated AE pathogen	Reference(s)
Tir	56-68 kDa, LEE-encoded	bacterial receptor for intimin; required for AE lesion formation and for colonization and virulence in many animal infection models (EHEC, EPEC, Citro)	(Deng et al., 2003; Garmendia et al., 2005; Kenny et al., 1997; Marches et al., 2000; Ritchie et al., 2003)
EspF$_U$/ TccP	42.4 kDa, prophage encoded	required for AE lesion formation (EHEC); not typically present in EPEC or Citro	(Campellone et al., 2004b; Garmendia et al., 2004)
		no measurable effect on colonization of bovine intestine	(Vlisidou et al., 2006a)
		important for late stage colonization of rabbit intestine; may promote expansion beyond initial sites of infection in gnotobiotic piglets (EHEC)	(Ritchie et al., 2008)
		Can cooperate with *C. rodentium* Tir but addition of EspF$_U$ has no effect on colonization	(Girard et al., 2009a)
		binds to the autoinhibitory GBD in WASP proteins and displaces it from the VCA domain to activate N-WASP	(Cheng et al., 2008)
Map	~20-23 kDa, LEE-encoded	WxxxE family member; Targeted to and disrupts function of mitochondria (EPEC, EHEC); Disrupts tight junctions (EPEC); involved in intimin-dependent, Tir-independent barrier dysfunction (EPEC)	(Dean and Kenny, 2004; Kenny and Jepson, 2000)
		Functions as the active form of Cdc42; Promotes transient, Cdc42-dependent filopodia (EPEC)	(Alto et al., 2006; Kenny et al., 2002)
		Promotes colonization of small intestine of infant rabbits (EHEC)	(Ritchie and Waldor, 2005)
		Binds EBP50/NHERF1 which regulates ion channels in the intestine	(Simpson et al., 2006)
		Contributes to diarrhea and causes mitochondrial dysfunction and epithelial	(Ma et al., 2006; Simpson et al., 2006)

		barrier disruption *in vivo* (Citro)	
		C-terminal region of the protein is necessary for actin disruption and toxicity, but not for mitochondrial localization	(Rodriguez-Escudero et al., 2005)
		Not required for colonization but may confer competitive advantage in murine infection (Citro)	(Deng et al., 2004; Mundy et al., 2004);
EspH	21 kD, LEE-encoded	Diminishes filopodium formation and enhances pedestal formation (EHEC and EPEC); plays role in brush border remodeling and production of AE lesions	(Shaw et al., 2005a; Tu et al., 2003)
		Promotes colonization and diarrhea in infant rabbits (EHEC); not required for colonization or disease (Citro); Marginally promotes colonization in mice (Citro)	(Deng et al., 2004; Mundy et al., 2004; Ritchie and Waldor, 2005)
EspF	20-31, LEE-encoded	required for loss of TER, increased monolayer permeability; disrupts epithelial barrier function by altering distribution of occludin in tight junctions (EPEC)	(Guttman et al., 2006a; McNamara et al., 2001; Viswanathan et al., 2004a)
		induces apoptosis in HeLa cells (EPEC)	(Crane et al., 2001)
		Mild colonization defect early in infection (Citro); Appears to control inflammation in infant rabbit infection (EHEC); disrupts barrier function *in vivo* (EPEC)	(Deng et al., 2004; Mundy et al., 2004; Nagai et al., 2005; Ritchie and Waldor, 2005; Shifflett et al., 2005)
		required for inhibition of bacterial phagocytosis (EHEC, EPEC)	(Marches et al., 2008; Martinez-Argudo et al., 2007; Quitard et al., 2006)
		modulates architecture of the IF network within cells	(Viswanathan et al., 2004b)
		Binds sorting nexin 9 (EPEC)	(Marches et al., 2006)
EspG	44 kDa, LEE-encoded	destabilizes microtubule networks and triggers actin stress fiber assembly (EPEC)	(Matsuzawa et al., 2004)
		Possibly contributes to colonization and disease/colonic hyperplasia in mice (Citro)	(Hardwidge et al., 2005; Mundy et al., 2004)

		alters epithelial paracellular permeability (EPEC)	(Matsuzawa et al., 2005)
		promotes colonization in rabbit small intestine (EHEC)	(Ritchie and Waldor, 2005)
		Localizes to Golgi apparatus and disrupts Golgi function	(Clements et al., 2011)
EspG2	42 kDa, encoded on EspC PAI	interacts with tubulin and triggers the dissociation of microtubules beneath adherent bacteria	(Shaw et al., 2005b; Smollett et al., 2006)
		alters epithelial paracellular permeability (EPEC)	(Matsuzawa et al., 2005; Matsuzawa et al., 2004)
EspK	~47 kDa, non-LEE encoded; encoded on cryptic prophage CP-933N	inactivation of *espK* affected persistence of EHEC in intestines of orally inoculated calves; localizes to cytoplasm when expressed in COS-7 cells	(Vlisidou et al., 2006b)
EspI (NleA)	54 kDa, prophage-encoded	plays role in bacterial colonization and hyperplasia in mice (Citro)	(Mundy et al., 2004)
		targeted to Golgi apparatus	(Gruenheid et al., 2004)
EspZ (SepZ)	9.5 kDa, LEE-encoded	Contributes to protection against rapid cell death (EPEC); targeted to mitochondria	(Kanack et al., 2005; Shames et al., 2011; Shames et al., 2010)
		sepZ mutant has an intermediate colonization phenotype in some mouse strains (Citro)	(Deng et al., 2004)
EspM	~21 kDa, non-LEE encoded	Member of WxxxE family; modulates actin dynamics by activating RhoA signaling pathway	(Arbeloa et al., 2008)
		induces stress fibers	(Alto et al., 2006)
		More commonly found in EHEC and EPEC serotypes that are associated with severe disease	(Arbeloa et al., 2009)
		Inhibits pedestal formation (EHEC and	(Simovitch et al.,

		EPEC)	2010)
EspJ	25 kDa, prophage encoded	*C. rodentium*Δ*espJ* showed altered colonization and clearance dynamics in murine infection; EHEC *espJ* mutant has a clearance defect in infection of lambs late in infection; possible role in host survival and pathogen transmission (Citro (mice); EHEC (lambs))	(Dahan et al., 2005)
		responsible for trans-inhibition of macrophage opsonophagocytosis; impairs CR3-mediated uptake (EPEC, EHEC)	(Marches et al., 2008)
EspC	110 kDa, non-LEE encoded	secreted from cells by TVSS secretion; translocated into cells by T3SS (EPEC) causes cytotoxic effects including cytoskeletal damage	(Vidal and Navarro-Garcia, 2006, 2008)
NleH	33 kDa, non-LEE encoded	shares identity with the OspG effector in *Shigella* and YspK of *Y. entercolitica*; mutant has moderate defects in colonization of mice at early stages of infection (Citro)	(Garcia-Angulo et al., 2008; Hemrajani et al., 2008)
		Blocks apoptosis (EPEC)	(Hemrajani et al., 2010)
NleF	24 kDa, encoded on O island 71	localizes to host cytoplasm, important for bacterial colonization in mice (Citro) and gnotobiotic piglets (EHEC)	(Echtenkamp et al., 2008)
NleB	39 kDa, encoded on O-island 122/CP-933K	important for colonization and colonic hyperplasia of mice (Citro)	(Kelly et al., 2006)
NleC	40 kDa, encoded on prophage	Not required for AE lesion *in vitro* or for colonization of calves of lambs (EHEC)	(Marches et al., 2005)

	CP-933K		
NleD	28 kDa, encoded on prophage CP-933K	Not required for AE lesions *in vitro* and or for colonization in calves of lambs (EHEC)	(Marches et al., 2005)
		identified by signature-tagged mutagenesis screen as essential for full virulence in the gut by EHEC	(Dziva et al., 2004)
Cif	~32 kDa, encoded on lambdoid prophage	cycle inhibiting factor; not required for AE lesion formation; induces host cell cycle arrest and reorganization of actin cytoskeleton (EPEC, EHEC)	(Marches et al., 2005)
		required for inducible cytopathic effect, progressive recruitment of focal adhesion plaques, assembly of stress fibers, inhibition of cell cycle G2/M transition; leads to accumulation of inactive phosphorylated Cdk1	(Marches et al., 2003)
EspT	~22 kDa, non-LEE encoded	Member of WxxxE/SopE family of GEF's; activates RhoGTPases; induces formation of lamellipodia and membrane ruffles through activation of Rac-1 and Cdc42	(Bulgin et al., 2009)
		Has not been found in EHEC isolates; rarely found in EPEC and Citro	(Arbeloa et al., 2009)
		Triggers expression of immune mediators in an Erk/JNK and NF-Kb dependent manner	(Raymond et al., 2011)

Mechanisms of pedestal formation

Though EHEC, EPEC, and *C. rodentium* translocate highly related Tir molecules that are required for the formation of morphologically indistinguishable pedestals, the signaling pathway by which EHEC triggers F-actin assembly differs from that of EPEC and *C. rodentium* (Campellone, 2010; Caron et al., 2006; Hayward et al., 2006). In fact, even though the three AE pathogens have nearly identical LEEs and highly similar Tir proteins, EPEC Tir is not interchangeable with EHEC Tir (Kenny, 1999; Kenny, 2001) and EPEC Tir, but not EHEC Tir, can complement a *C. rodentium tir* mutant for pedestal formation *in vitro* or colonization *in vivo* (Deng et al., 2003). A key difference in the Tir proteins of EHEC and those of EPEC and *C. rodentium*, is that EPEC and *C. rodentium* contain tyrosine residues at positions 474 and 471 (see **Figure 2**) (Campellone et al., 2002; Gruenheid et al., 2001; Kenny, 1999), respectively, that are phosphorylated early in infection by host cell kinases (Phillips et al., 2004; Swimm et al., 2004b). This phosphorylation event recruits the host adapter protein, Nck, which binds and activates N-WASP (neuronal Wiskott–Aldrich Syndrome protein) (Campellone et al., 2002; Campellone et al., 2004a; Gruenheid et al., 2001). N-WASP, in turn, recruits and activates Arp-2/3, a heptameric complex that nucleates branched actin filament networks in eukaryotic cells (reviewed in (Goley and Welch, 2006; Stradal and Scita, 2006)), and leads to actin polymerization (Rivera et al., 2004; Rohatgi et al., 2001). Moreover, EPEC and *C. rodentium* possess an asparagine-proline-tyrosine (NPY) motif (Brady et al., 2007) and recruitment of IRTKS (insulin receptor tyrosine kinase substrate) to NPY454

of EPEC Tir or NPY451 of *C. rodentium* Tir, results in low level, Nck-independent actin polymerization (Campellone and Leong, 2005).

EHEC Tir also contains an NPY motif, but, unlike EPEC and *C. rodentium* Tir, it does not have a tyrosine residue that becomes phosphorylated upon intimin-Tir binding and therefore, does not recruit Nck. Instead, EHEC harbors an additional effector protein, $EspF_U$, encoded on the prophage CP-933U/Sp14 (Campellone et al., 2004b; Garmendia et al., 2004). $EspF_U$ binds Tir through IRTKS (insulin receptor tyrosine kinase substrate) and/or IRSp53 (insulin receptor substrate p53) (Vingadassalom et al., 2009; Weiss et al., 2009) and activates N-WASP by directly binding to its GTP-ase binding (GBD) region (Sallee *et al*., 2008; Campellone, 2010). Normally, N-WASP is in the autoinhibited state where the GBD is bound to the VCA (veroprolin homology, central hydrophobic, and acidic regions) domain, however, $EspF_U$ directly competes for the VCA binding site on the GBD and displaces it (Cheng et al., 2008), thereby allowing actin polymerization to occur.
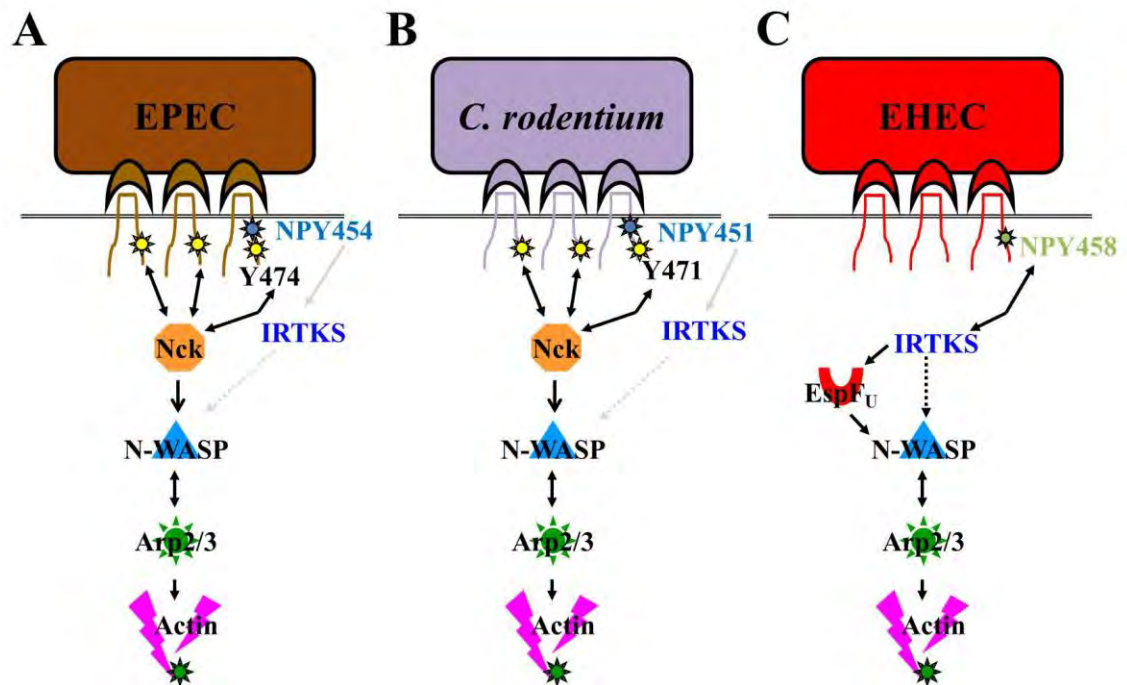
Figure 2. Mechanisms of actin pedestal formation in EPEC, *C. rodentium*, and EHEC.   (A-B) Tir of EPEC and *C. rodentium* possess a tyrosine motif (Y474 and Y471, respectively) that becomes phosphorylated upon Tir-intimin interaction and then recruits the adaptor protein, Nck. Nck recruits N-WASP, followed by Arp-2/3 and initiates a signaling cascade leading to actin polymerization. EPEC and *C. rodentium* Tir also contain an NPY motif (454 and 451, respectively) that upon phosphorylation, can lead to low-level actin polymerization through IRTKS. **(C)** Pedestal formation in EHEC requires EspF$_U$ which binds to Tir NPY458 through IRTKS. EspF$_U$ activates N-WASP, which activates Arp-2/3, leading to actin polymerization. IRTKS can also weakly activate N-WASP in the absence of EspF$_U$.

Significance of actin pedestal formation

AE lesions have proven to be important for infection and pathogens incapable of generating AE lesions display severe colonization defects and disease phenotypes (Deng et al., 2003; Donnenberg et al., 1993b; Marches et al., 2000; Ritchie et al., 2003; Tacket et al., 2000; Tzipori et al., 1995). The role of Tir-mediated actin assembly and pedestal formation in Stx-mediated disease, however, remains elusive. Some evidence suggests that the ability to generate actin pedestals aids in colonization, specifically at later time points in infection. Notably, Ritchie and colleagues found an EHEC mutant deficient in pedestal formation to be defective for colonization late in infection of infant rabbits (Ritchie et al., 2008). Additionally, this same pedestal-deficient mutant formed smaller than wild type bacterial aggregates on the intestine of gnotobiotic piglets (Ritchie et al., 2008). Recently, a study by Crepin and co-workers used a *C. rodentium* mutant unable to generate actin pedestals and found that it was out-competed by wild type bacteria in murine co-infection studies (Crepin et al., 2010). **Chapters III and IV** of this thesis will describe a novel murine model that we utilized to probe the function of Tir-mediated actin assembly in colonization and toxin-mediated disease.

III. EHEC Stx-mediated disease

Stx

EHEC elaborates a potent cytotoxin, Stx (for review, see (Tarr et al., 2005)), that is responsible for causing the extensive tissue damage that results during HUS (O'Brien et

al., 1992; Schuller et al., 2004; Tarr et al., 2005). Stx is encoded on a lambdoid prophage and toxin production is often increased upon phage induction (Muhldorfer et al., 1996; Schmidt, 2001; Waldor and Friedman, 2005). Stx is an AB toxin consisting of five B subunits and one enzymatically active A subunit (O'Brien et al., 1992). The B subunit binds to host cell surface globotriaosylceramide (Gb$_3$) receptors, allowing entry of the active A subunit to the cytosol via endocytosis and retrograde transport through the Golgi apparatus. The A subunit has N-glycosidase activity and cleaves 28S rRNA at a site specific adenine residue thereby directly inhibiting protein synthesis and inducing apoptosis of the host cell (Cohen et al., 1987; Endo et al., 1988; Lingwood et al., 1987; Romer et al., 2007).

Two main serotypes of Stx exist: Stx1 and Stx2, and EHEC strains that possess Stx2 are often associated with more severe disease and HUS (Donohue-Rolfe et al., 2000; Lindgren et al., 1993; Tesh et al., 1993). In fact, a large outbreak of diarrhea-associated HUS was recently documented in deaths in Northern Germany caused by an *E. coli* strain containing Stx2 (Bielaszewska et al., 2011; Frank et al., 2011). However, the strain was identified as enteroaggregative (EAEC) *E. coli* serotype O104:H4, as opposed to typical enterohemorrhagic (EHEC) *E. coli* O157:H7 usually responsible for diarrheal outbreaks resulting in HUS. It is thought that this EAEC strain acquired the *stx2* gene via horizontal gene transfer (Rasko et al., 2011). Nonetheless, the acquisition of *stx2* greatly enhanced the virulence of EAEC, and infection with this strain resulted in over 40 deaths (Bielaszewska et al., 2011; Frank et al., 2011).

Many variants of Stx1 and Stx2 exist including Stx1c, Stx1d, Stx2c, Stx2d, Stx2dact, Stx2e, and Stx2f. Interestingly, Stx2dact has been identified as a mucus-activatable toxin and in the presence of intestinal mucus, it becomes more cytotoxic following the cleavage of the two C-terminal amino acids of the A2 peptide in the context of the appropriate B subunit (Melton-Celsa et al., 2002). Interestingly, it has been hypothesized that toxin production by STEC and EHEC strains increases bacterial adherence to host cells and subsequent intestinal colonization (Robinson et al., 2006), possibly by increasing the expression of intimin-binding host cell receptors such as β_1-chain integrins (Liu et al., 2010) and/or nucleolin (Sinclair et al., 2006; Sinclair and O'Brien, 2002).

Stx translocation across intestinal epithelium

Upon intestinal colonization by EHEC, Stx translocates across intestinal epithelium by a mechanism not well known. While it has been shown that certain intestinal cell lines possess Gb_3 receptors (e.g. Caco-2) and Stx induces apoptosis and inhibits protein synthesis in these cell lines (Schuller et al., 2004), the majority of the intestinal epithelium is devoid of Gb_3 receptors. Therefore, the mechanism by which Stx traverses these cells differs from the retrograde transport pathway associated with endothelial cell intoxication. Early studies using immunoelectron microscopy confirmed that Stx passes through the intestinal epithelium via a transcellular pathway (Acheson et al., 1996; Philpott et al., 1997). It has been established that Stx induces secretion of the neutrophil chemoattractant, IL-8 (KC is the mouse homologue), from human colonic

epithelial cells (Thorpe et al., 1999), and there is evidence suggesting that neutrophil transmigration enhances Stx translocation across the intestinal epithelium (Hurley et al., 2001). Changes in the actin cytoskeleton have also been thought to facilitate transcytosis of Stx across monolayers (Maluykova et al., 2008). Both infiltration of neutrophils and changes in the actin cytoskeleton are believed to compromise the intestinal barrier and increase Stx uptake. Furthermore, evidence also exists suggesting that macropinocytosis facilitates and stimulates transcellular toxin translocation across Gb_3 negative intestinal epithelial cells (Malyukova et al., 2009). Finally, recent evidence suggests that outer membrane vesicles, which are naturally shed from gram negative bacteria, may play a possible role in toxin delivery into eukaryotic cells (Amano et al., 2010; Ellis and Kuehn, 2010). Interestingly, EHEC broth cultures have been shown to contain outer membrane vesicles containing Stx1 and Stx2 (Kolling and Matthews, 1999; Yokoyama et al., 2000).

Intestinal damage is a common finding in EHEC infection and has histological manifestations similar to colitis and inflammatory bowel disease (Bekassy et al., 2011; Moon, 1997). This damage is thought to be a direct result of Stx (although secondary intestinal damage may be due to ischemia and inflammation), despite the lack of Gb_3 receptors in most enterocytes. Therefore, the mechanism by which Stx-mediated intestinal damage occurs is not well known. Additionally, many small animal models of EHEC infection and HUS lack this important manifestation of disease, making it difficult to study. **Chapter III** of this thesis will describe a novel murine model of EHEC Stx-mediated disease that results in intestinal damage similar to that seen in human infection.

Once in the blood stream, Stx targets the vasculature and eventually reaches other organs expressing Gb_3 receptors. Endothelial cells, particularly those in the kidney, are exceptionally sensitive to Stx. One potential mechanism of Stx delivery to target cells is via binding to polymorphonuclear PMN's (for which it has relatively high affinity) and use of these cells for transport through the blood stream to target cells with Gb_3 receptors (which Stx binds with much higher affinity) (Brigotti et al., 2010; te Loo et al., 2000; Te Loo et al., 2001). In humans, Gb_3 receptors are predominantly found on glomerular vascular endothelial cells and cortical tubules of the kidney (Ergonul et al., 2003; Meyers and Kaplan, 2000). In mice however, they are found predominantly in the renal tubules (Psotka et al., 2009).

Systemic disease

Upon binding to cells, Stx induces the release of pro-inflammatory cytokines and activates transcription factors that encode them (O'Loughlin and Robins-Browne, 2001; Paton and Paton, 1998; Ray and Liu, 2001), leading to a systemic inflammatory response. Serum pro-inflammatory cytokines and chemokines are elevated in both humans suffering HUS and mice intoxicated with Stx (Keepers et al., 2007; Keepers et al., 2006; Proulx et al., 2001; Ray and Liu, 2001; Rovin and Phan, 1998; Sauter et al., 2008) and this inflammatory response seems crucial for development of the vascular damage observed in EHEC infection resulting in HUS. Indeed, circulating leukocytosis and increased neutrophil and macrophage counts are considered risk markers for developing HUS, and are associated with severity of renal failure (Bell et al., 1997; Buteau et al.,

2000; Coad et al., 1991; Walters et al., 1989; Wong et al., 2000). Moreover, monocyte chemoattractant protein (MCP-1) and granulocyte colony stimulating factor (G-CSF), have been shown to be elevated in the urine and serum of patients with HUS and this finding correlates to disease severity, further evidence suggesting that inflammation is an important contributor to the development of HUS (Murata et al., 1998; Proulx et al., 2002; van Setten et al., 1996; Vierzig et al., 1998).

The action of Stx on endothelial cells and subsequent inflammatory response also leads to thrombus formation in the vasculature, hemolytic anemia, and renal damage. Evidence of renal damage is often observed by elevated levels of serum blood urea nitrogen (BUN) and creatinine as well as the presence of proteinuria (Tarr et al., 2005). Histologically, renal disease is prominent in the glomeruli, the site of the majority of Gb_3 receptors in humans, and findings include glomerular capillary wall thickening, endothelial cell wall swelling, and detachment of the basement membrane with deposition of fibrin and thrombi in the capillary lumens (Richardson et al., 1988). Lastly, Stx can also target Gb_3 receptors in the CNS, and very severe cases of HUS can result in neurological complications (occurring in approximately 30 percent of patients with HUS) (Cimolai et al., 1992; Neild, 1994).

IV. Animal models of EHEC and EPEC pathogenesis

Many different animal models have been developed to study AE pathogenesis *in vivo*. These models include carriage models, EHEC and EPEC colonization models, models studying the effects of Stx *in vivo* (in the absence of bacteria), and EHEC

infection-like models studying bacterial colonization in the context of Stx-mediated disease. Animal species utilized in these studies (reviewed in (Wales et al., 2005)) include: chickens (Beery et al., 1985; Sueyoshi and Nakazawa, 1994), cows (Dean-Nystrom et al., 1997; Dean-Nystrom et al., 2008), macaques (Kang et al., 2001), baboons (Siegler et al., 2003; Taylor et al., 1999), lambs (Vlisidou et al., 2006a), ferrets (Woods et al., 2002), pigs (Tzipori et al., 1985; Tzipori et al., 1986), infant rabbits (Ritchie et al., 2003), Dutch Belted rabbits (Garcia et al., 2006; Garcia et al., 2002), and mice (for review, see (Mohawk and O'Brien, 2011)). Furthermore, animal models using murine, bovine, and ovine intestinal loops have been used to study EHEC and EPEC pathogenesis (Girard et al., 2008; Vlisidou et al., 2006a; Vlisidou et al., 2004; Wales et al., 2002).

Despite the abundance of animal models, no one model recapitulates the full spectrum of EHEC-related disease complete with oral infection followed by colonization with AE lesion formation, intestinal damage, and systemic disease including renal damage. Moreover, many of these models have limitations including high costs (e.g. non-human primates) and/or the requirement for complex animal facilities (e.g. gnotobiotic animals). This introduction will focus specifically on: (1) the animal models used to study allele- and Tir- dependent and independent functions of intimin (gnotobiotic piglets and mice) and (2) the animal models used to study EHEC colonization in the context of Stx-mediated disease (infant rabbits, Dutch Belted rabbits, and mice).

Gnotobiotic piglets

Gnotobiotic piglets have been used to study the pathogenesis of AE pathogens since the early 1980s. This model allows for study of the interaction of the bacterium and its toxins with the host intestinal epithelium without the influence of other bacteria. Animals are orally inoculated at one-to-two days of age and once colonized, they develop diarrhea and the formation of AE lesions on the small (distal ileum and colon) or large intestine when infected with EPEC and EHEC, respectively (Tzipori et al., 1985; Tzipori et al., 1986). Upon EHEC infection, animals occasionally develop signs of extraintestinal disease including CNS involvement (Tzipori et al., 1986). One drawback of this model is that renal disease is not a common finding, however, one study reports the presence of microangiopathy (small vessel disease) in the kidneys (Gunzer et al., 2002). Gnotobiotic piglets have been beneficial in studying the role of virulence factors, such as *eae*, *espF$_U$,* and Stx *in vivo* (McKee et al., 1995; Ritchie et al., 2008; Tzipori et al., 1995), and also for the development of potential vaccines and EHEC therapeutics (Sheoran et al., 2005; Zhang et al., 2009).

Infant rabbits

The infant rabbit model of EHEC infection was first described in 1983 (Farmer et al., 1983) and has been readily used since then to study EHEC pathogenesis (Elliott et al., 1994; Pai et al., 1986; Potter et al., 1985; Ritchie et al., 2003). This model is attractive because rabbits are less expensive than larger and germ-free animals, and they also become easily colonized without antibiotics. In this model, New Zealand white rabbits, approximately two-to-three days old, are intragastrically inoculated with EHEC (Ritchie

et al., 2003). Younger animals are normally used because the severity of disease declines

in infections of older animals (Pai et al., 1986). EHEC colonizes the rabbit large intestine

and infection results in diarrhea, intestinal inflammation (peaking approximately seven

days post-infection), and death, all of which are dependent on the T3SS, Tir, intimin, and

Stx (Ritchie et al., 2003; Ritchie and Waldor, 2005). Nevertheless, one main limitation

of this model is that these rabbits do not exhibit symptoms of toxigenic disease such as

microangiopathy and renal damage (Ritchie et al., 2003), which may be due to the lack of

Gb_3 receptor on the kidneys of these rabbits (Zoja et al., 1992). IV injection of Stx1 into

New Zealand white infant rabbits, however, can resemble some pathology of human HUS

including intestinal damage (with lesions specifically in the cecum), thrombotic

microangiopathy, and CNS involvement (Richardson et al., 1992).

Dutch Belted rabbits

Dutch Belted rabbits, which are susceptible to both natural and experimental

infection with EHEC, are also used to study EHEC pathogenesis. However, unlike in the

infant rabbit model, older rabbits, approximately five-to-ten weeks of age are typically

used. Garcia and co-workers initially identified these rabbits as a potential experimental

system for EHEC when they observed the development of bloody diarrhea and death in

rabbits bought from a commercial vendor (Garcia et al., 2002). Interestingly, these

rabbits had become infected naturally with an EHEC strain harboring both *eae* and Stx1,

which they characterized as EHEC O153:H-. Findings at necropsy revealed that these

rabbits had intestinal and renal pathology consistent with that of EHEC-induced HUS in

humans. Shortly after this observation, Garcia and Fox surveyed the prevalence of

naturally occurring EHEC in rabbits in several different environments and confirmed that

rabbits were indeed a new reservoir host for EHEC (Garcia and Fox, 2003). Further

characterization of Dutch Belted rabbits as an experimental model for EHEC revealed

that upon infection, rabbits develop similar symptoms to humans with HUS including

low hematocrit levels, thrombocytopenia, elevated BUN, fibrin thrombi formation, and

intestinal and kidney lesions, particularly in the glomeruli (Garcia et al., 2006; Tarr et al.,

2005). In addition to EHEC O153:H-, other EHEC strains have also been assessed in this

model and a recent study characterized the virulence of different strains in these rabbits

(Shringi et al., 2012). Moreover, Dutch belted rabbits injected with Stx2 via IV also

develop the extra-intestinal aspects of toxigenic disease, most notably, enteritis,

inflammation, thrombus formation, and renal disease (Garcia et al., 2008). While both

the infant rabbit and Dutch Belted rabbit intragastric inoculation models have proven

successful, the main difference between the two is the lack of renal damage in the infant

rabbit model (for a comparison of these two models, see (Panda et al., 2010)).

Mice

Murine models are preferable for general use due to their low costs and ease of

care, the availability of many genetic backgrounds and many different knockout animals,

and because large numbers are easily obtainable for experimentation. Several different

murine models of EPEC and EHEC pathogenesis exist. However, because EHEC and

EPEC are unable to efficiently colonize conventional mice, elimination of normal flora is

often necessary in order to establish an infection. Indeed, disruption of the normal flora by antibiotic pre-treatment, or its complete elimination by rearing the animals in a germ-free environment, sensitizes mice to lethal infection after relatively low dose oral inoculation (Eaton et al., 2008; Lindgren et al., 1993; Melton-Celsa et al., 1996). Additional manipulations have been made to enhance colonization by EHEC in mice (for review, see (Mohawk and O'Brien, 2011)) including treatment with mitomycin C or other toxin-inducing agents (Asahara et al., 2004; Fujii et al., 1994; Shimizu et al., 2003; Teel et al., 2002), and prolonged dietary restrictions such as protein calorie malnutrition (Kurioka et al., 1998).

Streptomycin treatment and gnotobiotic mice

Early studies of EHEC pathogenesis utilized streptomycin treatment or gnotobiotic animals in order study colonization and Stx-mediated disease. In the streptomycin treatment model, mice are given streptomycin in their drinking water prior to infection by EHEC (or both prior to infection and throughout infection with antibiotic-resistant EHEC) (Lindgren et al., 1993; Melton-Celsa et al., 1996; Wadolkowski et al., 1990a; Wadolkowski et al., 1990b). In both of these models, damage to the kidney, particularly to the renal tubules, which is the primary site of Gb_3 receptors in the mouse kidney (Psotka et al., 2009), is a consistent finding (Eaton et al., 2008; Melton-Celsa et al., 1996; Wadolkowski et al., 1990a; Wadolkowski et al., 1990b). However, only EHEC that produce the mucus-activatable type of Stx, Stx2dact, are consistently able to cause lethal infection in streptomycin-pretreated mice (Lindgren et al., 1993; Melton-Celsa et

al., 1996). Furthermore, EHEC infection of altered-flora mice does not result in well

documented AE lesions, nor have bacterial genes that promote AE lesion formation

proven required for intestinal colonization or disease (Eaton et al., 2008; Lindgren et al.,

1993; Melton-Celsa et al., 1996; Wadolkowski et al., 1990a; Wadolkowski et al., 1990b).

Indeed, a laboratory *E. coli* K12 strain that overproduces Stx2 but lacks Tir, intimin, and

the T3SS, is capable of lethal infection of streptomycin-pretreated mice (Wadolkowski et

al., 1990b).

Conventional mouse models

Although EHEC does not efficiently colonize conventional mice, recent models

have employed the use of large inoculums ($\sim 10^9$ CFU or greater) by pipette feeding or

gavage to obtain moderate levels of colonization (Mohawk et al., 2010a; Mohawk et al.,

2010b). In these models, colonization as measured in feces or tissue generally peaks at

approximately 10^6/gram and numbers diminish in the days following inoculation

(Mohawk et al., 2010a; Mohawk et al., 2010b). Mice display signs of Stx-mediated

disease including weight loss, tubular damage, increased BUN, and neutrophilia, and

lethal infection occurs approximately 30% of the time. Interestingly, although intestinal

damage and hemorrhagic colitis are prominent features of EHEC infection in humans,

intestinal damage has not been observed in this model (Mohawk et al., 2010b; Mohawk

and O'Brien, 2011).

Stx-injection models

Murine models of Stx-injection, using purified toxin in the presence or absence of lipopolysaccharide (LPS), have been used to study the development and pathogenesis of HUS. Injection of Stx into mice results in the induction of pro-inflammatory cytokines, vascular damage, hemolysis, and renal damage (Keepers et al., 2007; Keepers et al., 2006; Psotka et al., 2009; Sauter et al., 2008). However, in contrast to piglet, rabbit, and other mouse infection models (Garcia et al., 2006; Garcia et al., 2002; Mohawk and O'Brien, 2011; Panda et al., 2010; Tzipori et al., 1995), a major limitation of this model is that intestinal colonization and AE lesion formation are not required for disease.

C. rodentium

Due to its homology to other AE pathogens, *C. rodentium* is a commonly used infection model of EHEC and EPEC pathogenesis (Luperchio et al., 2000). Indeed, murine *C. rodentium* infection has been used to study the *in vivo* functions of intimin, effector proteins, and actin pedestal formation (Crepin et al., 2010; Deng et al., 2004; Deng et al., 2003; Frankel et al., 1996b; Girard et al., 2009b; Mundy et al., 2004; Nagai et al., 2005; Newman et al., 1999; Schauer and Falkow, 1993b). Upon infection, the cecum is colonized first, and it "seeds" the rest of the large intestine (Wiles et al., 2004). Similarly, bacterial clearance occurs first in the cecum, followed by the cecal patch, and then the colon (Wiles et al., 2004). Bacterial levels in the colon peak at ~10^9 organisms between post-infection day five-to-14 (Mundy et al., 2005), and while mice do not usually develop overt diarrhea, they have increased liquid accumulation in the colon. Approximately ten days to two weeks post-infection, mice develop significant epithelial

crypt hyperplasia in the descending colon (Luperchio and Schauer, 2001; Mundy et al.,
2005). Importantly, there is strain to strain variability in susceptibility to *C. rodentium*.
While C3H/HeJ are the most susceptible and usually die by ten days post-infection,
C57BL/6 mice are the most resistant and are able to clear infection (Vallance et al.,
2003).

IV. Summary and specific aims

The two most notable aspects of EHEC colonization and disease are pedestal
formation and Stx-mediated intestinal and systemic disease. There has been much insight
into the mechanism of intimin and Tir-mediated pedestal formation, as well as insight
into the mechanism of toxin actin and the resultant pathology in animals. However, we
lack insight into the role of intimin and pedestal formation in colonization, and have
virtually no insight into the relationship between pedestal formation and tissue damage.
Therefore, the following questions will be addressed here:

1. Does intimin have allele- and Tir-independent roles during infection?

2. Does Tir-mediated actin pedestal formation promote colonization and/or Stx-
   mediated disease?

The major limitation in addressing these questions is that no conventional murine model
exists to assess the function of different alleles of intimin or the role of Tir-mediated
pedestal formation in EHEC. Therefore, the AIMS of this thesis are as follows:

1. Gain insight into the critical allele- and Tir-independent functions of intimin
   during infection of EHEC, EPEC, and *Citrobacter*.

    i. Characterize these functions of intimin *in vitro*.

    ii. Develop animal models to assess these functions *in vivo*.

2. Develop an animal model to assess the function of Tir-mediated actin pedestal formation in Stx-mediated disease using *C. rodentium* (λstx_{2dact}).

    i. Characterize the model and determine if Tir is required for colonization and disease.

3. Using this new model, determine if Tir-mediated actin pedestal formation is required for colonization and disease.

    i. Identify the mechanism(s) by which actin pedestal formation facilitates colonization and disease.

CHAPTER II.

ALLELE- AND TIR-INDEPENDENT FUNCTIONS OF INTIMIN IN DIVERSE ANIMAL INFECTION MODELS

Abstract

Upon binding to intestinal epithelial cells, enterohemorrhagic *E. coli* (EHEC), enteropathogenic *E. coli* (EPEC), and *Citrobacter rodentium* trigger formation of actin pedestals beneath bound bacteria. Pedestal formation has been associated with enhanced colonization, and requires intimin, an adhesin that binds to the bacterial effector Tir, which is translocated to the host cell membrane and promotes bacterial adherence and pedestal formation. Intimin has been suggested to also promote cell adhesion by binding one or more host receptors, and allelic differences in intimin have been associated with differences in tissue and host specificity. We assessed the function of EHEC, EPEC, or *C. rodentium* intimin, or a set of intimin derivatives with varying Tir-binding abilities in animal models of infection. We found that EPEC and EHEC intimin were functionally indistinguishable during infection of gnotobiotic piglets by EHEC, and that EPEC, EHEC, and *C. rodentium* intimin were functionally indistinguishable during infection of C57BL/6 mice by *C. rodentium*. A derivative of EHEC intimin that bound Tir but did not promote robust pedestal formation on cultured cells was unable to promote *C. rodentium* colonization of conventional mice, indicating that the ability to trigger actin assembly, not simply to bind Tir, is required for intimin-mediated intestinal colonization. Interestingly, streptomycin pre-treatment of mice eliminated the requirement for Tir but not intimin during colonization, and intimin derivatives that were defective in Tir-binding

still promoted colonization of these mice. These results indicate that EPEC, EHEC, and

C. rodentium intimin are functionally interchangeable during infection of gnotobiotic

piglets or conventional C57BL/6 mice, and that whereas the ability to trigger Tir-

mediated pedestal formation is essential for colonization of conventional mice, intimin

provides a Tir-independent activity during colonization of streptomycin pre-treated mice.

Acknowledgements and contributions

This chapter has been previously published in Frontiers in Cellular and Infection

Microbiology (Mallick et al., 2012). The work is a result of several collaborations and I

would like to acknowledge people for their contribution to the work presented here:

Steve Luperchio and Hui Liu developed the majority of the plasmids used in this study
(see Table 2: Description of plasmids used in this study).

Mike Brady and Loranne Magoun constructed LM-1 and generated all the data in Figure
1: An EHEC strain containing EPEC intimin on the chromosome is functional for
pedestal formation.

The work in Table 4: An EHEC strain carrying a precise chromosomal replacement of
eae with EPEC *eae* displays piglet intestinal tropism indistinguishable from wild type
was done by Mike Brady, Saul Tzipori, and Art Donohue-Rolfe.

Steve Luperchio generated the data for Figure 4A.

The DERC Histology Core Facility at UMMS prepared intestinal samples for H&E (see
Figures 2B and 6B).

Vijay Vanguri assisted in viewing histological slides and taking pictures (see Figures 2B
and 6B).

Lara Strittmatter and Greg Hendricks of the UMASS Electron Microscopy Core Facility
assisted with the electron microscopy (see Figure 3).

Tim Blood (Master's student) helped generate the anti-EHEC Tir antibody used in Figure
5.

Introduction

The family of attaching and effacing (AE) pathogens consists of

enterohemorrhagic *Escherichia coli,* enteropathogenic *E. coli* (EPEC), and *Citrobacter*

rodentium. EHEC colonizes the large intestine and can result in diarrhea, hemorrhagic

colitis, and life-threatening hemolytic uremic syndrome (Kaper et al., 2004; Pennington,

2010). The highly related EPEC colonizes the small intestine and is a causative agent of

infantile diarrhea in the developing world (Chen and Frankel, 2005; Spears et al., 2006).

C. rodentium is a related murine pathogen that typically colonizes the large intestine and

causes transmissible murine colonic hyperplasia, characterized by colonic epithelial cell

proliferation and high rates of mortality in suckling animals (reviewed in (Luperchio and

Schauer, 2001; Mundy et al., 2005)).

The three pathogens are so-named AE pathogens because they each colonize the

intestinal epithelium by inducing in host cells "AE lesions", which consist of effacement

of brush border microvilli, intimate adherence of bacteria, and polymerization of actin

into a pedestal-like extension of the epithelial cell beneath the bound bacterium ((Moon

et al., 1983); for review, see (Kaper et al., 2004)). Bacteria entirely incapable of

generating AE lesions are severely defective for colonization and disease (Deng et al.,

2003; Donnenberg et al., 1993a; Donnenberg et al., 1993b; Ritchie et al., 2003; Schauer

and Falkow, 1993b; Tzipori et al., 1995), while bacteria still capable of intimate

attachment but defective selectively for pedestal formation are moderately attenuated

(Crepin et al., 2010; Ritchie et al., 2008).

The ability to generate the AE phenotype by these organisms requires the locus of

enterocyte effacement (LEE), a pathogenicity island that encodes a type III secretion system (T3SS) and several translocated effectors (Kenny and Finlay, 1995; McDaniel et al., 1995). Tir (translocated intimin receptor), a type III translocated effector critical for intimate bacterial attachment and actin pedestal formation, becomes localized in the host plasma membrane with the N- and C-terminal domains residing in the host cell cytoplasm (for review see, (Campellone, 2010; Frankel and Phillips, 2008; Lommel et al., 2004)). The central, extracellular domain is recognized by the outer membrane adhesin intimin, encoded by the *eae* gene (Donnenberg and Kaper, 1991; Jerse, 1990). The intimin N-terminus promotes outer membrane localization and multimerization, whereas the intimin C-terminus encodes its adhesive activities (Batchelor et al., 2000; Frankel et al., 1995; Liu et al., 1999; Luo et al., 2000; Yi et al., 2010).

It has been postulated that in addition to binding Tir, intimin possesses host receptor adhesive activities that also contribute to colonization. For instance, the intimin-related *Yersinia pseudotuberculosis* invasin protein binds to β_1-chain integrins (Isberg et al., 1987), and EPEC intimin was shown to be capable of recognizing β_1-chain integrins, albeit with apparently much lower affinity (Frankel et al., 1996a). Nucleolin is recognized by EHEC intimin (Sinclair and O'Brien, 2002) and localized beneath cell-associated EPEC during infection of cultured monolayers (Dean and Kenny, 2011). Finally, intimin but not Tir, contributes to the disruption of epithelial barrier function (Dean and Kenny, 2004), suggesting the existence of Tir-independent functions of intimin.

Although EPEC and EHEC intimin have been demonstrated to be interchangeable

for pedestal formation on cultured cells, intimin exhibits considerable allelic variation in the C-terminal domain responsible for adhesive activity (Frankel et al., 1994), and the intimin alleles from the canonical EHEC, EPEC, and *C. rodentium* strains are distinct and have been associated with differences in function. For example, although tissue tropism during infection of human intestinal explants is multifactorial, infection of intestinal tissue *ex vivo* suggests that intimin of EHEC O157:H7 (also known as intimin γ) promotes colonization of different epithelial types than intimin of canonical EPEC (intimin α) or *C. rodentium* (intimin β) (Fitzhenry et al., 2002; Girard et al., 2005; Mundy et al., 2007; Phillips and Frankel, 2000). In addition, whereas wild type EHEC colonizes the large bowel of gnotobiotic piglets, an EHEC strain harboring a plasmid expressing EPEC intimin acquired the additional ability to colonize the small intestine (Tzipori et al., 1995). Allelic differences may also contribute to differences in species host range, because whereas *C. rodentium* expressing EPEC intimin is able to efficiently colonize Swiss NIH and C3H/HeJ mice (Frankel et al., 1996b; Hartland et al., 2000; Schauer and Falkow, 1993b), *C. rodentium* expressing a derivative of EPEC intimin harboring the adhesive domain of EHEC intimin provided only poor colonization function in these animals (Hartland et al., 2000; Mundy et al., 2007).

To gain insight into the critical activities of intimin, we assessed the *in vivo* functionality of EHEC, EPEC, or *C. rodentium* intimin, or a set of EHEC intimin derivatives with varying Tir-binding abilities. Colonization was not detectably altered by allele-specific differences in intimin in two animal infection models. Notably, whereas the ability to trigger Tir-mediated pedestal formation was found to be essential for

colonization of conventional mice, intimin provided a Tir-independent function during

colonization of antibiotic pre-treated mice.

Materials and Methods

Media, bacterial strains, and growth conditions. Bacteria were stored in Luria-Bertani

(LB) broth (American Bioanalytical, Natick, MA, USA) with 50% glycerol at either -

80°C or -135°C. Bacteria were grown at 37°C in LB broth, in Antibiotic Medium 3

(Difco, Laboratories, Detroit, MI, USA), on LB agar (American Bioanalytical, Natick,

MA, USA), on MacConkey lactose agar, or on eosin-methylene blue agar (Difco

Laboratories, Lawrence, KS, USA). Where indicated, kanamycin, chloramphenicol,

gentamicin, ampicillin, and zeocin were added at final concentrations of 20 μg/ml, 10

μg/ml, 100 μg/ml, 100 or 750 μg/ml, and 75 μg/ml respectively. The bacterial strains

and plasmids used in this study are listed in **Tables 1 and 2**.

Construction of pCVD438 (pInt$_{EPEC}$) derivatives. Genomic DNA from EHEC

O157:H7 strain EDL933 and plasmid pInt$_{EPEC}$ were purified using standard

methodologies. All primers used to construct these pCVD438 derivatives are listed in

Table 3. To construct pHL69 (pInt$_{EHEC}$), a two-step amplification (fusion PCR) was

performed. First, the *Pfu* Turbo PCR system (Stratagene, La Jolla, CA, USA) was used

to generate three fragments: the region 5' of the *eae*$_{EPEC}$ open reading frame (ORF) in

pInt$_{EPEC}$ (from the *Hin*d III site to the *eae* start codon), the region 3' of the *eae*$_{EPEC}$ ORF

in pInt$_{EPEC}$ (from the *eae* stop codon to the *Sal* I site), and the coding region of the

eae$_{EHEC}$ gene from EDL933. To generate the first two fragments, pInt$_{EPEC}$ was restriction

enzyme digested with *Bst*E II to delete an internal 1,847-bp fragment (nucleotides 585 to

2432 of *eae*$_{EPEC}$) and used as the PCR template. The coding region of EDL933 *eae*$_{EHEC}$

was amplified from genomic DNA. Each primer at a junction point in the fusion PCR was tailed with a 9- to 15-bp overhanging sequence from the neighboring fragment. The amplification products were isolated using the QIAquick PCR purification kit (QIAgen Inc., Valencia, CA, USA), mixed, and subjected to a second round of amplification with the pACYC184 primers listed in **Table 3**. The fusion PCR product was confirmed by DNA sequencing and ligated into the corresponding *Hin*d III/*Sal* I site of pInt$_{EPEC}$, effectively replacing the *eae*$_{EPEC}$ ORF of pInt$_{EPEC}$ with that of EHEC EDL933. The ligation mix was introduced into laboratory strains of *E. coli* by high-voltage electroporation and chloramphenicol-resistant clones were isolated.

A similar methodology was used to generate pInv, pInv-Int395, pInv-Int181, and pInv-Int100 (**Table 2**). In the case of pInv, the coding region of the *Y. pseudotuberculosis inv* gene was amplified from pRI203. For the latter three plasmids, the hybrid invasin-intimin alleles had been previously generated and cloned into pT7-4 (Liu et al., 1999). These pT7-4 derivatives, pHL35, pHL49, and pHL55, respectively, were used as template DNA to amplify the coding region for pInv-Int395, pInv-Int181, and pInv-Int100, respectively.

Generation of *C. rodentium* strains. Plasmid DNA was isolated using the QIAprep Spin Miniprep Kit (QIAgen, Valencia, CA, USA) and quantified by UV spectrophotometry. Plasmids were introduced into the *C. rodentium*Δ*eae* strain by

chemical transformation using calcium chloride. Successful transformants were selected with chloramphenicol and were confirmed to be carrying the proper plasmid.

Generation of an EHEC strain encoding EPEC intimin. A three-way PCR was performed using templates encoding EHEC *cesT* with 3' tail encoding EPEC *eae* (~750 bp), EPEC *eae* (~2.8 kb) with 3' EHEC tail, and EHEC 3'UTR (~960 bp). The PCR product was cloned into pGEM7xf(+), linearized by *BamH* I and *Xba* I digestion, and transformed into KM48 harboring pTP223. Transformants were screened by sucrose resistance and chloramphenicol sensitivity. Candidates were confirmed by PCR sequencing.

Generation of *C. rodentium*Δ*tir*. The *C. rodentium tir* deletion mutant was made using a slightly modified version of the one-step PCR-based gene activation protocol (Datsenko and Wanner, 2000). Briefly, a tertiary PCR product containing the zeocin cassette and its promoter flanked by 576 bp homology upstream of the start of *tir* and 608 base pairs downstream of the stop of *tir* was generated using three template PCR products, A+B, C+D, and E+F. Product A+B was generated using primers F-A-Tir-KO and R-B-Tir-KO (**Table 3**) with genomic *C. rodentium* (DBS100) DNA (isolated using a kit by Promega, Madison, WI, USA) as a template. Primers F-C-Tir-KO-zeo and R-D-Tir-KO-zeo were used to amplify a *Mlu* I/*Eco*R I cut pDONORzeo fragment to generate the 504 bp PCR product C+D. Primers F-E-Tir-KO and R-F-Tir-KO were used to amplify genomic *C. rodentium* DNA to make PCR product E+F. This 1.65 kb was electroporated into *C.*

rodentium (DBS100) containing the lambda-red plasmid, pKD46 and recombinants were selected for by plating on LB plates supplemented with 750 μg/ml ampicillin. Replacement of *tir* with the zeocin cassette and its promoter was confirmed by PCR using the following primers: F-Tir-Ext, R-Tir-Ext, F-Tir-Int-323-342, R-Tir-Int-819-838, F-Tir-Int-590-610, R-Tir-Int-1049-1069, F-Zeo-Int, and R-Zeo-Int (see **Table 3**).

Purification of EHEC Tir and generation of an anti-EHEC Tir antibody. pDV205 (Amp^R) is a derivative of pET21 that contains EHEC *tir* with a histidine tag. For expression and purification of EHEC Tir, BL21 DE3+ pDV205 was cultured in 2xYT media at 37°C to an OD$_{600}$ of 0.6-0.7 then induced with 1 mM IPTG for three hours at 37°C. The culture was spun at 4,420 x g, 20 minutes at 4°C and the supernatant was discarded. The pellet was resuspended in 2.5 ml lysis buffer per gram wet weight. 4 mg lysozyme was added and the sample was sonicated (Branson Sonifier 450, Branson Ultrasonics Corporation, Danbury, CT, USA) Duty cycle 70, output 3, 10 second bursts X 6 cycles). The lysate was then centrifuged at 16,100 x g, 20 minutes at 4°C and the supernatant was run on a QIAgen Ni-NTA Agarose column (QIAgen, Valencia, CA, USA) and the resulting EHEC Tir was eluted and quantified using Bio-Rad Protein Assay kit (Bio-Rad Laboratories, Inc., Hercules, CA, USA).

For antibody production, all inoculations were completed subcutaneously with 30 ng of purified EHEC Tir in 50 μl with 50 μl of adjuvant for a total inoculation volume of 100 μl. Female BALB/c mice (Jackson Laboratories, Bar Harbor, ME, USA) were inoculated

with EHEC Tir supplemented with Imject Freund's Complete Adjuvant (Thermo

Scientific, Rockford, IL, USA). At days 14 and 28, mice were boosted with EHEC Tir

supplemented with Imject Freund's Incomplete Adjuvant (Thermo Scientific, Rockford,

IL, USA). Mice were sacrificed on day 38 and blood was harvested via cardiac bleed,

allowed to clot at room temperature for 30 minutes, and then was spun twice at 8,600 x g,

15 minutes at 4°C. Serum was then aliquoted and stored at -80°C.

Invasion assays. Entry into cultured cells was measured in a manner similar to that

described previously (Finlay and Falkow, 1988). Briefly, HEp-2 cells (ATCC CCL-23)

were seeded in 24-well plates and grown overnight at 37°C in 5% CO_2 and Dulbecco's

Modified Eagles medium supplemented with 10% heat inactivated calf serum and 2 mM

L-glutamine (DMEM). Bacteria were grown overnight in LB, diluted in fresh cell culture

medium, and inoculated at an approximate multiplicity of infection (MOI) of 100. The

cells were incubated for 3 hours at 37°C in 5% CO_2 and then washed with phosphate-

buffered saline (PBS). Fresh cell culture medium supplemented with gentamicin was

added to each well and the cells were incubated at 37°C in 5% CO_2 for 1 hour. The cells

were washed with PBS, lysed with 1% Triton X-100 in PBS, and diluted to 1 ml with LB

broth. Percent invasion for each well was determined by plating dilution series.

Infection of monolayers pre-infected with EPEC *eae*. The "prime and challenge"

assay is a modification of a previously described bacterial adherence assay (Liu et al.,

1999; Rosenshine et al., 1996) and was used to quantify intimin-Tir interactions *in vitro*.

Briefly, nearly confluent monolayers of HEp-2 cells were washed twice in PBS, and

RHFM (RPMI-1640 supplemented with 20 mM HEPES, pH 7.0, 2% FBS, 0.5% D-

mannose) was added to the monolayers. The monolayers were then mock-infected or

infected with the EPEC *eae*-mutant strain JPN15.96 at MOI of ~200 and incubated at

37°C in 5% CO_2 for 3 hours. JPN15.96 is capable of high efficiency translocation of Tir

into mammalian cells, but unable to form pedestals due to the absence of intimin. The

monolayers were washed twice with PBS and then incubated for 1 hour at 37°C in 5%

CO_2 with 100 µg/ml gentamicin in DMEM/HEPES to kill remaining bacteria. The

monolayers were washed three times in PBS and then infected with the appropriate

"challenge" bacterium, (i.e. *C. rodentium*, *C. rodentium∆eae*, or *C. rodentium∆eae*

expressing EPEC intimin, EHEC intimin, invasin, or an invasin-intimin hybrid) diluted in

fresh DMEM/HEPES at an MOI of 100 for 3 hours at 37° in 5% CO_2. At the conclusion

of the assay, monolayers were washed 6 times with PBS, lysed with 1% Triton X-100 in

PBS, and diluted to 1 ml with LB broth. Percent adherence for each well was determined

by plating dilution series.

The prime and challenge assay was also adapted to evaluate actin pedestal formation

mediated by intimin and its derivatives by seeding HEp-2 cells onto coverslips. At the

conclusion of the assay described above, coverslips were washed 6 times with PBS, fixed

with 2.5% paraformaldehyde, and permeabilized with 0.1% Triton X-100 in PBS.

Coverslips were then double fluorescently labeled for F-actin and bacteria and examined

on a Nikon Eclipse E600 microscope. F-actin was labeled with Texas red-conjugated

phalloidin (Molecular Probes, Eugene, OR, USA) and visualized with a 580-nm dichroic filter. *C. rodentium* were labeled with an anti-*C. rodentium* polyclonal rabbit antibody raised against *C. rodentium* strain DBS100 and visualized with a Cascade blue-conjugated goat anti-rabbit IgG antibody (Molecular Probes, Eugene, OR, USA) using a 400-nm dichroic filter. Coverslips labeled only with anti-*C. rodentium* primary antibody and the Cascade blue-conjugated secondary antibody showed no crossover when viewed with the 580-nm filter. Image acquisition was performed with the Spot program (Diagnostics Instruments, software version 3.0.4) and imported into Adobe Photoshop 5.0.

Pedestal, bacterial binding, and Tir focusing assays. The FAS assay of (Nicholls et al., 2000), as modified for *C. rodentium* (Newman et al., 1999) was the basis for this assay. A single colony from each strain was grown in 1 ml media (+/- antibiotic) for eight hours. Cultures were diluted 1:500 into 5 ml DMEM supplemented with 0.1 M HEPES (pH 7.0) (+/- antibiotic) and incubated at 37°C without agitation with 5% CO_2 for 12-15 hours. Cell monolayers were prepared by splitting 95-100% confluent mouse embryonic fibroblasts (MEFs) into 24-well culture plates containing sterile glass coverslips followed by overnight growth at 37°C with 5% CO_2. Prior to seeding onto culture plates, MEFs were maintained in MEF cell culture media (DMEM (hi glucose) + 10% fetal bovine serum (FBS) with penicillin, streptomycin, and glutamine) at 37°C, 5% CO_2. For infections, cell monolayers were washed twice with sterile PBS followed by addition of FAS media containing 25 μl of overnight cultured *C. rodentium* to each well.

Plates were spun at 700 g for 10 minutes then incubated at 37°C with 5% CO_2 for 3 hours. After 1.5 hours, plates were spun again at 700 g for an additional 10 minutes to insure proper bacterial binding to cells. After three hours, cells were washed twice with sterile PBS and 0.5 ml pre-warmed FAS media was added to each well and cells were then incubated for an additional three hours. Cells were then washed five times with sterile PBS, fixed with 4% PFA for 30 minutes, washed, permeabilized with 0.1% Triton-X 100, and stained with anti-EHEC Tir antibody (1:500) as a primary antibody for 30 minutes. The samples were washed and then stained for 30 minutes with anti-Mouse 488 secondary antibody (Invitrogen, Carlsbad, CA, USA) (1:200), phalloidin (Molecular Probes, Eugene, OR, USA) (1:100), and DAPI (1:500). After washing cells an additional three times with PBS, the coverslips were mounted on slides using ProLong® Gold anti-fade reagent (Invitrogen, Eugene, OR, USA). For binding assays, the number of bacteria per cell was counted for 25 random cells. Counting was done in triplicate and the mean, median, and maximum number of bacteria bound to cells was determined. The stratification of the number of cells with the given amount of bound bacteria in each interval (0, 1-5, 6-10, 11-15, 16-20, and >20) was also determined.

Immunoblotting. Preparation of bacterial cell lysates was performed as described previously (Brady et al., 2007; Campellone et al., 2002). Samples were resolved by 10% SDS PAGE and transferred to PVDF membrane. Membranes were blocked in PBS supplemented with 5% milk for 30 minutes prior to treatment with sheep anti-EHEC Intimin (1:500), goat anti-EPEC Intimin (1:2000), rabbit anti-OmpA, or rabbit anti-O157

antiserum (1:750, Difco Laboratories, Lawrence, KS, USA) for two hours, washed and treated with secondary antibody as previously described (Brady et al., 2007; Campellone and Leong, 2005; Campellone et al., 2004a).

Immunofluorescence microscopy of EHEC strains. To ensure an EHEC strain expressing EPEC intimin can generate actin pedestals and that the intimin plasmids used to overexpress EHEC and EPEC intimin were functional to complement a deletion of EHEC intimin by FAS, HeLa cell monolayers were infected with indicated strains, fixed, and permeabilized as described previously (Campellone et al., 2002). For each strain, qualitative scoring of F-actin pedestals was performed as indicated. Approximately equal numbers of actin pedestals were observed for EHECΔ*eae* expressing EHEC intimin (pHL6) or EPEC intimin (pHL4).

Mouse infection studies. Mice were purchased from Jackson Laboratories (Bar Harbor, ME, USA) and housed in the University of Massachusetts Medical School (UMMS) animal facility. All animal procedures were done in compliance with the UMMS IACUC. Female, eight-week-old C57BL/6J mice were gavaged with PBS or ~2 x 10^9 of overnight culture of *C. rodentium* strain specified in 100 μl PBS. Inoculum concentrations were confirmed by serial dilution plating. *C. rodentium* fecal shedding was determined by serial dilution plating of fecal slurries (10% w/v in PBS) on Maconkey agar or LB agar with selection for zeocin, kanamycin, chloramphenicol, or kanamycin and chloramphenicol. For streptomycin pre-treatment experiments, mice

were given 5 mg/ml streptomycin in their drinking water for 48 hours prior to infection.

Following inoculation, non-antibiotic treated water given to the mice.

Mouse tissue collection and histology. At necropsy the large intestine (colon through

cecum) was fixed in 10% buffered formalin, dehydrated and embedded in paraffin. Five-

micron sections stained with hematoxylin and eosin were evaluated and scored blindly by

a board-certified pathologist (V.V.). Assessment of mucosal hyperplasia was targeted to

areas of comparable muscularis propria thickness in order to reduce error from

differences in planes of section.

Transmission electron microscopy. Mouse intestinal tissue samples were taken at

various time points post infection and fixed in 2.5% gluteraldehyde in 0.05 M Sodium

Phosphate buffer, pH 7.2. Samples were processed and analyzed at the University of

Massachusetts Medical School Electron Microscopy core facility according to standard

procedures. Briefly, fixed samples were moved into fresh 2.5% gluteraldehyde in 0.05 M

Sodium Phosphate buffer and left overnight at $4^{o}C$. The samples were then rinsed twice

in the same fixation buffer and post-fixed with 1% osmium tetroxide for 1 hour at room

temperature. Samples were then washed twice with DH_2O for 20 minutes at $4^{o}C$ and then

dehydrated through a graded ethanol series of 20% increments, before two changes in

100% ethanol. Samples were then infiltrated first with two changes of 100% Propylene

Oxide and then with a 1:1 mix of propylene oxide:SPI-Pon 812 resin. The following day

three changes of fresh 100% SPI-Pon 812 resin were done before the samples were

polymerized at 68°C in plastic capsules. The samples were then reoriented and thin

sections were placed on copper support grids and stained with lead citrate and uranyl

acetate. Sections were examined using the FEI Tecani 12 BT with 80Kv accelerating

voltage, and images were captured using a Gatan TEM CCD camera.

Piglet infections. Gnotobiotic piglets were derived and infected orally with TUV93-0,

which is deficient for the expression of Stx, thus eliminating the potentially confounding

toxigenic effects on colonization (Tzipori et al., 1995), as described previously (Brady et

al., 2011; Campellone et al., 2007; Ritchie et al., 2008). To quantify bacteria in the small

intestine, the small intestine was divided into five parts and each section was viewed

individually for the presence of bacteria and AE lesions. If bacteria or AE lesions were

found in any of these sections, they were given the score of "+". The average score was

then determined for the small intestines of piglets in each group. A score of "+" indicates

the presence of bacteria and AE lesions in at least one of the five sections of the small

intestine in each of the piglets, a score of "+/-" indicates the presence of bacteria and AE

lesions in at least one of the five sections of the small intestine in at least half of the

piglets, and a score of "-" indicates that fewer than half of the piglets had bacteria and AE

lesions in at least one of the five sections of the small intestine and also includes piglets

that did not become colonized. To enumerate bacteria in the spiral colon and cecum,

each section was scored for the presence of bacteria and AE lesions. A score of "+"

indicates that every piglet in the group had bacteria and AE lesions present, a score of

"+/-" indicates that at least half of the piglets in the group had bacteria and AE lesions

present, and a score of "-" indicates that fewer than half of the piglets had bacteria and AE lesions present.

Statistical analysis. Data were analyzed using GraphPad Prism. Comparison of multiple groups was performed using one-way analysis of variance (ANOVA) with Tukey's multiple comparison post-tests or two-way ANOVA with Bonferroni's post-tests. Statistical significance of differences between two groups was evaluated using two tailed unpaired t tests. In all tests p values below 0.05 (*), 0.01 (**), and 0.001 (***) were considered statistically significant, unless indicated otherwise. In all graphs, error bars represent standard error of the mean (SEM), unless indicated otherwise.

Table 1. Bacterial strains used in this study.

Strain	Description or genotype	Source or reference
DBS100	*C. rodentium* (prototype TMCH isolate, ATCC 51459, original biotype 4280)	(Barthold et al., 1976; Schauer and Falkow, 1993b)
DBS255	*C. rodentium*Δ*eae*; Kan^R	(Schauer and Falkow, 1993a)
DBS434	*C. rodentium*Δ*eae*/pCVD438	(Frankel et al., 1996b)
SAL31	*C. rodentium* Δ*eae*/pHL69	This study
SAL32	*C. rodentium*Δ*eae*/pHL70	This study
SAL56	*C. rodentium*Δ*eae*/pHL76	This study
SAL57	*C. rodentium*Δ*eae*/pHL79	This study
SAL58	*C. rodentium*Δ*eae*/pHL80	This study
DH5α	F- ø80d*lac*ZΔM15 Δ(*lac*ZYA-*arg*F) U169 *end*A1 *rec*A1 *hsd*R17 (r$_K^-$ m$_K^+$) *deo*R *thi*-1 *pho*A *sup*E44 l⁻*gyr*A96 *rel*A1 *gal*⁻	Gibco BRL
SAL35	DH5α/pHL70F- ø80d*lac*ZΔM15 Δ(*lac*ZYA-*arg*F) U169 *end*A1 *rec*A1 *hsd*R17 (r$_K^-$ m$_K^+$) *deo*R *thi*-1 *pho*A *sup*E44 l⁻*gyr*A96 *rel*A1 *gal*⁻	This study
EDL933	EHEC O157:H7	(Riley et al., 1983)
JPN15.96	EPEC *eae*::Tn*phoA*	(Jerse, 1990)
BL21 DE3/ pDV205	BL21 DE3 containing EHEC Tir expression vector	(Vingadassalom et al., 2009)
EDL933	EHEC O157:H7 prototype	(Riley et al., 1983)
TUV93-0	Stx- derivative of EDL933	(Campellone et al., 2002)
KM60	EHEC TUV93-0 Δ*eae*	(Murphy and Campellone, 2003)
KM48	EHEC TUV93-0 Δ*eae::cat-sacB*	(Murphy and Campellone, 2003)
JPN15/pMAR7	Amp^R derivative of EPEC E2348/69 O127:H6 prototype	(Jerse, 1990)
LM1	KM46 derivative expressing EHEC *tir-cesT* and EPEC *eae*	This study
C. rodentium Δ*tir*	DBS100 with an in-frame deletion of *tir*; Zeo^R (i.e. zeocin resistance)	This study

Table 2. **Description of plasmids used in study.**

Plasmid	Protein	Description	Reference
pCVD438	Int$_{EPEC}$	pACYC184-derived plasmid encoding *eae* from E2348/69	(Donnenberg and Kaper, 1991)
pHL69	Int$_{EHEC}$	pCVD438 with *eae*$_{EPEC}$ ORF replaced by *eae*$_{EHEC}$ ORF	This study
pHL70	Inv	pCVD438 with *eae*$_{EPEC}$ ORF replaced by *inv* ORF	This study
pHL76	Inv-Int395	pCVD438 with *eae*$_{EPEC}$ ORF replaced by the 5' 489 codons of *inv* fused to the 3' 395 codons of *eae*$_{EHEC}$.	This study
pHL79	Inv-Int181	pCVD438 with *eae*$_{EPEC}$ ORF replaced by the 5' 793 codons of *inv* fused to the 3' 181 codons of *eae*$_{EHEC}$.	This study
pHL80	Inv-Int100	pCVD438 with *eae*$_{EPEC}$ ORF replaced by the 5' 878 codons of *inv* fused to the 3' 100 codons of *eae*$_{EHEC}$.	This study
pT7-4		Amp^R P$_{\phi10}$	(Tabor and Richardson, 1985)
pRI203		pT7-4 with *inv* from *Y. pseudotuberculosis*	(Isberg et al., 1987)
pACYC184		Cloning vector; Cam^R, Tet^R	(Rose, 1988)
pHL35		pT7-4 with *inv* (bp 1-1467)/*eae*$_{EHEC}$ (bp 1617-2802); produces the protein Inv-Int395	(Liu et al., 1999)
pHL49		pT7-4 with *inv* (bp 1-2379)/*eae*$_{EHEC}$ (bp 2260-2802) ; produces the protein Inv-Int181	(Liu et al., 1999)
pHL55		pT7-4 with *inv* (bp 1-2634)/*eae*$_{EHEC}$ (bp 2503-2802); produces the protein Inv-Int100	(Liu et al., 1999)
pDV205	EHEC Tir	pET21 containing EHEC *tir*	(Vingadassalom et al., 2009)
pUC19		High-copy cloning vector, Amp^R	(Yanisch-Perron et al., 1985)
pHL4	Int$_{EPEC}$	pUC19 derivative encoding EPEC *eae*	(Liu et al., 1999)
pHL6	Int$_{EHEC}$	pUC19 derivative encoding EHEC *eae*	(Liu et al., 1999)
pTP223		Produces λ-gam-bet-exa downstream of lac promoter	(Murphy and Campellone, 2003)
pKD46		Expresses lambda red recombinase, Amp^R	(Datsenko and Wanner, 2000)

Table 3. DNA sequences of oligonucleotides used in this study.

Primer[a]	Sequence
***eae*EPEC 5' region[b, c]**	
F-pACYC184	5' acc tga agt cag ccc cat acg ata 3'
R-*eae*EPEC	5' *agt aat cat* gtt tgg gct cca cca caa tg 3'
R-*eae*EPEC-2	5' *aac cat cat* gtt tgg gct cca cca caa tg 3'
***eae*EPEC 3' region[b, d]**	
F-*eae*EPEC	5' *gtt tgt gta gaa taa* att taa taa ata tct aat cat tgt ccg gct aa 3'
R-pACYC184	5' ccg <u>ctc gag</u> gct ctc cct tat gcg act cc 3'
F-*eae*EPEC-2	5' *gcg ctg tca ata taa* att taa taa ata tct aat cat tgt ccg gct aa 3'
R-pACYC184-2	5' tga ctg ggt tga agg ctc tca agg 3'
Open Reading Frames[b,e]	
F-*eae*EHEC	5' *agc cca aac* atg att act cat ggt tgt ta 3'
R-*eae*EHEC	5' *aga tat tta tta aat* tta ttc tac aca aac cgc at 3'
F-*inv*	5' *agc cca aac* atg atg gtt ttc cag cca at 3'
R-*inv*	5' *aga tat tta tta aat* tta tat tga cag cgc aca ga 3'
***C. rodentium tir* mutant[f, g]**	
F-A-Tir-KO	5' gtg cac aat cat caa tca gtc ac 3'
R-B-Tir-KO	5' *acc aaa atc cct taa cgt gag tta cgc gtc gtt cca ctg agc gtc aga cc*a cat ata tcc ttt tat tta atc gga aat ttt aca cta atc c 3'
F-C-Tir-KO-zeo	5' *ggt ctg acg ctc agt gga acg acg cgt aac tca cgt taa ggg att ttg gt* 3'
R-D-Tir-KO-zeo	5' *tca gtc ctg ctc ctc ggc cac gaa gtg cac gca gtt gcc ggc cgg gtc gc* 3'
F-E-Tir-KO	5' *gtg cac ttc gtg gcc gag gag cag gac tga* cgc tac aac acc ggg agt tga acg ttt cgt cta aat ata taa tgg gta ttt gtt ggg gga ggg gga g 3'
R-F-Tir-KO	5' ggc tcc acc aca atg agt tag 3'
F-Tir-Ext	5' gct tgc atca taa gtt aga ctg tg 3'
R-Tir-Ext	5' cgt cat tag tgt cag ata acg aga 3'
F-Tir-Int-323-342	5' ttc gtg ttg aac agc agc ca 3'
R-Tir-Int-819-838	5' tcg cag ctt ctg cag cat tt 3'
F-Tir-Int-590-610	5' ata cac gtt ctg ttg gtg tcg 3'
R-Tir-Int-1049-1069	5' cca att cct gct gac gtt tag 3'
F-Zeo-Int	5' *gag cgg tcg agt tct gg* 3'
R-Zeo-Int	5' *gcc acg aag tgc acg cag t* 3'

[a]F, forward (top strand) primer; R, reverse (bottom strand) primer.

[b]Underlined sequences represent the restriction enzyme sites used for cloning. Italicized sequences indicate the tails used for fusing eae_{EPEC} 5' and 3' sequences with eae_{EHEC}, inv, or hybrid allele coding regions.

[c]For pInt$_{EHEC}$, F-pACYC184 and R-eae_{EPEC} were used. For all others, F-pACYC184 and R-eae_{EPEC}-2 were used.

[d]For pInv, F-eae_{EPEC}-2 and R-pACYC184-2 were used. For all others, F-eae_{EPEC} and R-pACYC184 were used.

[e]For pInt$_{EHEC}$, F-eae_{EHEC} and R-eae_{EHEC} were used. For pInv, F-inv and R-inv were used. For all others, F-inv and R-eae_{EHEC} were used.

[f]Primers used to construct *C. rodentium*Δ*tir*. Italicized regions indicate homology to zeocin cassette.

[g]Numbers in primer name correspond to nucleotide positions primer is located within *tir* gene. Int represents screening primers internal to the gene (*tir* or *zeocin*) and Ext represents screening primers that are external to the gene.

Results

Precise chromosomal replacement of EHEC *eae* with EPEC *eae* does not alter tissue tropism in piglets.

Plasmid complementation of an EHEC *eae* mutant with EPEC *eae* results in a strain with altered tissue tropism that colonizes the small bowel of piglets (Tzipori et al., 1995). To determine if EPEC and EHEC intimin might be functionally interchangeable when expressed from the endogenous chromosomal locus, we precisely replaced the EHEC *eae* allele in EHEC TUV93-0 with the *eae* allele from EPEC strain JPN15/pMAR7 (**Figure 1A**). Immunoblotting confirmed that the resulting strain, LM-1, produced EPEC intimin (**Figure 1B**). As predicted from previous work demonstrating that EHEC and EPEC intimin are functionally interchangeable for *in vitro* pedestal formation (DeVinney et al., 1999b), LM-1 generated actin pedestals on cultured cells (**Figure 1C**).

To test the function of EPEC intimin during infection by EHEC, gnotobiotic piglets were infected orally with LM-1 and after 72 hours, infection was assessed by histological analysis of the small and large intestines. Upon infection with wild type EHEC, piglets suffered diarrheal illness and bacteria were associated with extensive segments of the cecal and colonic epithelium (**Table 4**). Wild type EHEC were only occasionally associated with the epithelium of the small intestine. In contrast, infection of gnotobiotic piglets with EHECΔ*eae* did not result in detectable bacterial association with epithelium of any intestinal segment, and correspondingly, the animals did not suffer
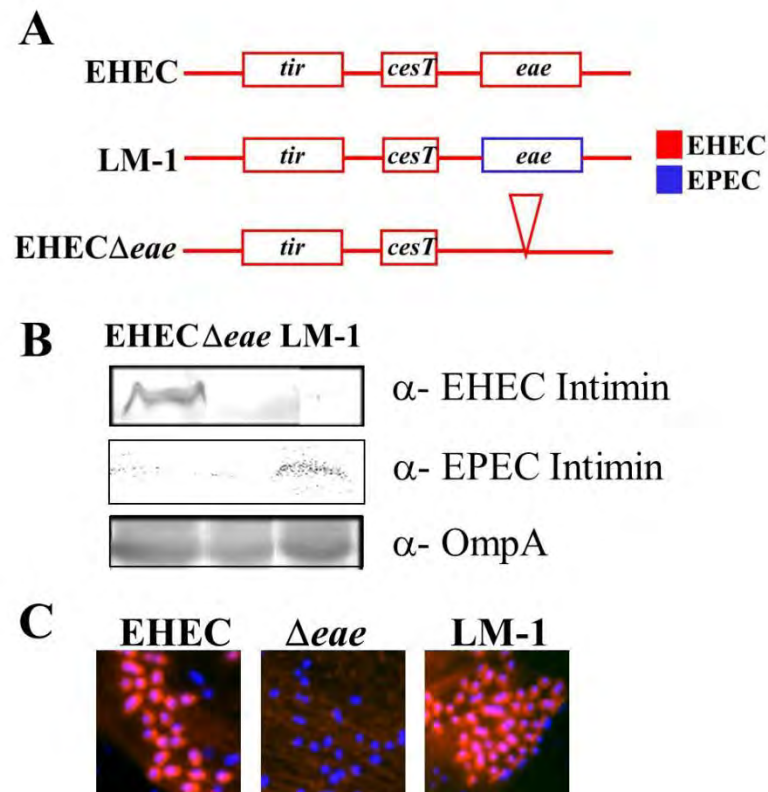
Figure 1. An EHEC strain containing EPEC intimin on the chromosome is functional for pedestal formation. (A) The endogenous EHEC *eae* gene was precisely replaced by EPEC *eae* to create LM-1. **(B)** Expression of EHEC and EPEC intimin in wild type EHEC, EHECΔ*eae*, and LM-1 was assessed by western blot. Blotting with anti-OmpA was included as a loading control. **(C)** HeLa cells were infected with the indicated strain and the monolayers were stained with DAPI (blue) to visualize bound bacteria and phalloidin (red) to visualize actin pedestals.

Table 4. An EHEC strain carrying a precise chromosomal replacement of *eae* with EPEC *eae* displays piglet intestinal tropism indistinguishable from wild type.

E. coli strain	No. of animals	No. of animals with diarrhea	AE lesions and colonization		
			Small intestine	Cecum	Spiral colon
WT EHEC	5	5	+/-	+	+
EHEC Δ*eae*	4	0	-	-	-
EHEC LM-1	4	4	+/-	+	+

Gnotobiotic piglets were infected orally with 5 x 10^9 EHEC, EHECΔ*eae*, or LM-1. Animals were sacrificed 72 hours after infection and the large intestines were removed, fixed, stained, and scored for colonization using a score adapted from Tzipori *et al*., 1995 (see **Materials and Methods**). "+" indicates bacteria and AE lesions present, "+/-" indicates minimal bacteria and AE lesions present, and "-" indicates no bacteria or AE lesions present. Values represent the average colonization score of all the piglets in the group.

from diarrhea. Notably, EHEC strain LM-1, which expresses EPEC intimin, colonized

the epithelium of the cecum and spiral colon at levels indistinguishable from that of wild

type EHEC, and like the wild type strain, induced diarrheal illness (**Table 4**). In contrast

to the previous finding that EHEC expressing EPEC intimin from a plasmid could

efficiently colonize the small intestine of gnotobiotic piglets (Tzipori et al., 1995),

bacteria were vanishingly sparse in the small intestine (**Table 4**). These results

demonstrate that EPEC intimin, when expressed in EHEC from the endogenous

chromosomal locus, can provide intimin function during intestinal infection of piglets,

but does not influence tissue tropism in this model.

EHEC intimin can promote murine colonization and disease by *C. rodentium*.

We further assessed ability of EHEC intimin to complement a *C. rodentium*Δ*eae*

mutant for colonization and intestinal disease in mice. Previous work demonstrated that

*C. rodentium*Δ*eae* harboring pCVD438, which encodes EPEC intimin, was fully virulent

in Swiss NIH and C3H/HeJ mice (Hartland et al., 2000; Mundy et al., 2007). In contrast,

*C. rodentium*Δ*eae* expressing an intimin hybrid carrying the N-terminal 554 residues of

EPEC intimin and the C-terminal 380 residues of EHEC intimin colonized mice 100-fold

less efficiently and did not cause the colonic hyperplasia that is characteristic of *C.*

rodentium infection (Hartland et al., 2000; Mundy et al., 2007).

To compare the colonization function of EPEC and EHEC intimin in mice, we

precisely replaced the EPEC *eae* coding sequence of pCVD438 (which for simplicity we

herein refer to as "pInt$_{EPEC}$") with the EHEC *eae* coding sequence to create pInt$_{EHEC}$ (i.e.,

pHL69; **Table 2**). C57BL/6 mice were infected with approximately 5 x 10^9 CFU of *C. rodentium*, *C. rodentium∆eae*, *C. rodentium∆eae/*pInt$_{EPEC}$, or *C. rodentium∆eae/*pInt$_{EHEC}$. Mice infected with *C. rodentium* reached peak colonization levels seven days post-infection with approximately 10^9 bacteria per gram of feces before being cleared from mice by approximately 15 to 20 days after inoculation, presumably due to the development of an adaptive immune response (Ghaem-Maghami et al., 2001; Simmons et al., 2003; Vallance et al., 2002) (**Figure 2A** and data not shown). In contrast, the number of *C. rodentium∆eae* in the stool peaked at three days post-infection, reaching less than 10^6 bacteria per gram of feces, and quickly diminished, never rising to more than 10^4 bacteria per gram of feces thereafter (**Figure 2A**). Similar to what was previously reported (Frankel et al., 1996b; Hartland et al., 2000; Mundy et al., 2007). EPEC intimin, when expressed in *C. rodentium∆eae* promoted high-level colonization with comparable kinetics to wild type *C. rodentium* (**Figure 2A**). Additionally, intestinal sections from rodents infected with *C. rodentium∆eae* expressing EPEC intimin showed colonic mucosal hyperplasia, goblet cell depletion, acute inflammation, erosions, and degenerative epithelial changes on the surface and in the crypts (**Figure 2B**). Interestingly, we also found that EHEC intimin, when expressed in *C. rodentium∆eae*, promoted colonization, colonic hyperplasia, and damage indistinguishable from wild type *C. rodentium* (**Figure 2**) and generated AE lesions morphologically identical to wild type *C. rodentium* (**Figure 3**). Thus, EHEC intimin, in spite of being significantly divergent in sequence from *C. rodentium* intimin, could provide complete intimin function in this model.
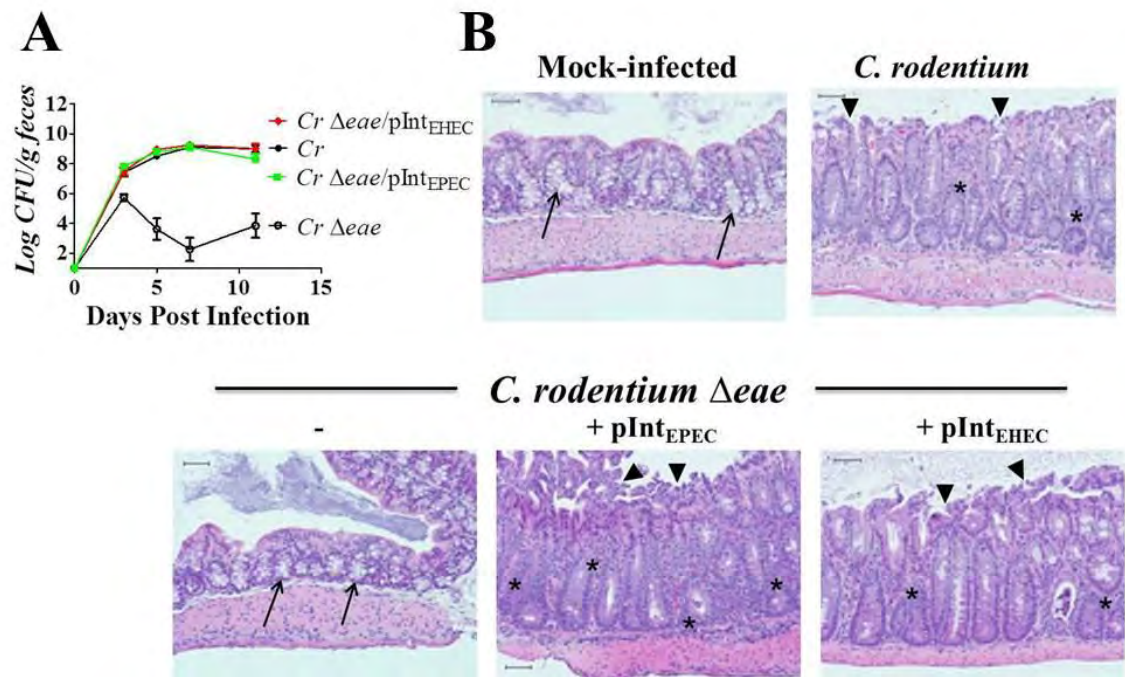
Figure 2. EHEC intimin is able to restore colonization and disease in a *C. rodentium eae* mutant. (A) Colonization of eight-week old C57BL/6 mice by *C. rodentium* ("*Cr*"), *C. rodentium∆eae*, *C. rodentium∆eae*/pInt$_{EPEC}$, or *C. rodentium∆eae*/pInt$_{EHEC}$ was determined by viable stool counts. Shown are the averages CFU (± SEM) of five mice. Data shown are representative of one of three independent experiments. **(B)** H&E-stained large intestinal sections from mock-infected mice or mice infected with indicated strain are shown under 100x magnification. Arrow heads point to ragged areas of the surface epithelium at sites of surface erosion. Arrows point to areas of many goblet cells. Asterisks indicate areas of active inflammation. Scale bars measure 50 µm.

0.5 μm

Figure 3. EHEC intimin can complement a *C. rodentium eae* mutant for AE lesion formation *in vivo*. Transmission electron micrograph showing AE pedestal formation on colonic epithelial cells from the distal colon of a mouse infected with *C. rodentium*Δ*eae*/pInt$_{EHEC}$. Original magnification, 25,000x. Bar, 0.5 μm.

EHEC intimin and Tir-binding invasin-intimin fusions can mediate host cell

adherence by *C. rodentium*.

We next characterized the ability of *C. rodentium*Δ*eae* expressing EHEC intimin

to attach to host cells that express high levels of Tir on their surface, which more

sensitively assesses Tir-intimin interactions compared to conventional infection assays

(Liu et al., 2002). Pre-infection (i.e. "priming") of cells with an EPECΔ*eae* mutant

permits efficient delivery of Tir to the eukaryotic cell (Liu et al., 1999; Rosenshine et al.,

1996). After gentamicin treatment and washing to kill and remove bound bacteria,

infection (i.e. "challenge") of these monolayers with intimin-expressing bacteria permits

sensitive assessment of bacterial binding mediated by Tir-intimin interaction (Liu et al.,

1999; Rosenshine et al., 1996). Utilizing this assay, *C. rodentium*Δ*eae*/pInt$_{EHEC}$ bound to

pre-infected monolayers indistinguishably from that of wild type *C. rodentium*, and

approximately 20-fold more efficiently than *C. rodentium*Δ*eae* (**Figure 4A**).

We next characterized the minimal region of EHEC intimin required for Tir-

mediated cell adherence when expressed in *C. rodenitum*. The intimin related protein *Y.*

pseudotuberculosis invasin, which binds to β_1-chain integrins (Frankel et al., 1996a;

Isberg and Leong, 1990), was previously used to deliver various portions of EHEC

intimin to the surface of the bacteria in the form of invasin-intimin hybrid proteins (Liu et

al., 1999). *C. rodentium*Δ*eae* expressing invasin was capable of high efficiency entry

into cultured epithelial cells, strongly suggesting that invasin can be expressed in a

functional form on the surface of *C. rodentium* (data not shown). Thus, we determined

the minimal region of EHEC intimin required for cell adherence by *C. rodentium* by

expression of invasin-intimin fusions in this bacterium. *C. rodentium*Δ*eae* producing Inv-Int395, a hybrid that contains the C-terminal 395 amino acids of intimin, bound to pre-infected monolayers at wild type levels, implying that this hybrid promotes Tir binding when expressed in *C. rodentium*Δ*eae*, as it does when expressed in *E. coli* K12 (**Figure 4A**; (Liu et al., 1999)). In contrast, Inv-Int181, which was previously shown to retain some Tir-binding activity when expressed in *E. coli* K12 (Liu et al., 1999), and Inv-Int100, bound poorly to monolayers pre-infected with the EPECΔ*eae* mutant (**Figure 4A**). These data suggest that the minimal functional domain of EHEC intimin that can confer high-level Tir binding on *C. rodentium* is located in the C-terminal 395 amino acids.

To determine if the functional Tir-binding domain defined by the more elaborate prime and challenge assay described above also functioned to promote cell attachment by *C. rodentium* during simple infection, we infected mouse embryonic fibroblasts (MEFs) with *C. rodentium*Δ*eae* expressing invasin or EHEC intimin derivatives and determined the number of bacteria bound to each of 25 randomly selected cells. Cells infected with wild type *C. rodentium* harbored an average of more than nine bacteria per cell, and fewer than five of the 25 cells were entirely free of bacteria (**Figure 4B**). Intimin was required for binding, because approximately 20 of the 25 cells infected with *C. rodentium*Δ*eae* were bacteria-free, and virtually no cells harbored more than five bacteria (**Figure 4B**). EHEC intimin, when expressed in *C. rodentium*Δ*eae*, was able to restore binding capabilities of the mutant strain, with an average of approximately six bacteria per cell (**Figure 4B**).
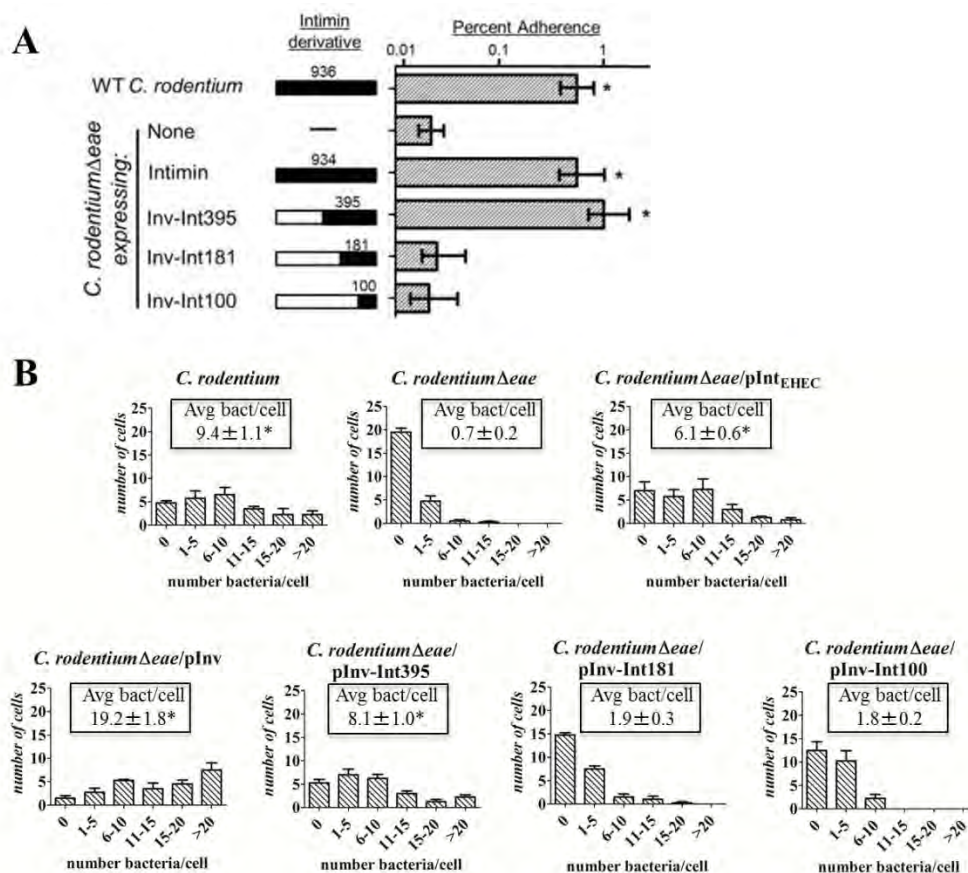
Figure 4. A hybrid containing the C-terminal 395 amino acids of EHEC intimin can complement a *C. rodentium eae* mutant for host cell attachment. (A) HEp-2 cells pre-infected with an EPECΔ*eae* strain were infected with wild type *C. rodentium*, *C. rodentium*Δ*eae*, or *C. rodentium*Δ*eae* strains expressing EHEC intimin, invasin, or the indicated invasin-EHEC intimin hybrids (Inv-Int395, Inv-Int181, and Inv-Int100), and stably bound bacteria were determined (**Materials and Methods**). Data are shown as the mean ± SEM and represent two independent assays with at least three replicates per assay. Asterisk indicates binding significantly (p<0.05) higher than *C. rodentium*Δ*eae* of *C. rodentium*Δ*eae* expressing pInv-Int181 or pInv-Int100, determined by two-tailed, unpaired t-test. **(B)** Mouse embryonic fibroblasts were infected with the indicated *C. rodentium* strains and the number of bound bacteria per cell was counted for four sets of 25 randomly selected cells. Shown are the number of cells with the given number (0, 1-5, 6-10, 11-15, 16-20, and >20) of bound bacteria. The experiment was performed in triplicate. Shown in box is the mean number of bacteria per cell ± SEM. Asterisk indicates a significant difference (p<0.05) compared to *C. rodentium*Δ*eae*, determined by one-way ANOVA.

We similarly tested the ability of the invasin-intimin hybrids to bind to cells. Invasin, when expressed on the surface of *C. rodentium*Δ*eae*, dramatically enhanced the ability of the bacteria to associate with cells (p<0.05), with an average of approximately 19 bacteria per cell, consistent with its ability to promote high-level host cell interaction (**Figure 4B**; (Isberg and Leong, 1990)). *C. rodentium*Δ*eae* expressing Inv-Int395, which mediated attachment of *C. rodentium* in the prime and challenge assay (**Figure 4A**), bound to mammalian cells statistically indistinguishably from wild type *C. rodentium*, with an average of approximately eight bacteria bound to each cell (**Figure 4B**). On average, fewer than five of the 25 cells were bacteria-free. In contrast, *C. rodentium* expressing Inv-Int181 and Inv-Int100 bound to cells indistinguishably from *C. rodentium*Δ*eae*, with an average of less than two bacteria per cell and the majority of cells harboring fewer than five bacteria (**Figure 4B**). These data indicate that EHEC intimin can complement a *C. rodentium*Δ*eae* mutant for cell attachment, and that the binding function of this protein is encompassed by the C-terminal 395 amino acids.

EHEC intimin, but not a Tir-binding invasin-intimin hybrid, promotes Tir clustering and pedestal formation by *C. rodentium*.

Given the ability of EHEC intimin and the hybrid Inv-Int395 to promote binding of *C. rodentium* to mammalian cells, we next tested their ability to promote Tir clustering and pedestal formation upon infection of mammalian cells. As expected, cells infected with *C. rodentium*Δ*eae* demonstrated virtually no bound bacteria and after staining monolayers with anti-EHEC Tir, only one quarter of the rare bound bacteria were

associated with somewhat diffuse foci of Tir (**Figure 5, column 2**; and data not shown).

In contrast, upon infection with wild type *C. rodentium,* 95% of bound bacteria were

associated with intensely stained Tir foci, and 98% of bacteria generated actin pedestals

(**Figure 5, "*Cr*"**). These defects in Tir clustering and pedestal formation were fully

complemented by a plasmid expressing EHEC intimin, as well as by a plasmid

expressing EPEC intimin, which was included as a positive control (**Figure 5,**

"pInt_{EHEC}" and "pInt_{EPEC}", respectively). Thus, EHEC intimin appears to provide full

function for cell binding, Tir clustering, and pedestal formation when expressed in *C.*

rodentium.

To define the region of EHEC intimin critical for Tir clustering and pedestal

formation, in parallel we infected monolayers with *C. rodentiumΔeae* expressing invasin-

intimin hybrids. *C. rodentiumΔeae* expressing invasin or either of the two fusion

proteins, Inv-Int181 or Inv-Int100, that were unable to promote Tir-mediated cellular

attachment by *C. rodentium*, resulted in detectable Tir foci no more frequently than was

found for *C. rodentiumΔeae* (**Figure 5, "pInv", "pInv-Int181", or "pInv-Int100"**). In

contrast, 59% of *C. rodentiumΔeae* expressing Inv-Int395, which promotes binding to *C.*

rodentium to mammalian cells (**Figure 4**), were associated with Tir foci (**Figure 5,**

"pInv-Int395"), a percentage that was both significantly higher than that of *C.*

rodentiumΔeae and significantly lower than that of wild type *C. rodentium* or *C.*

rodentiumΔeae expressing wild type EHEC intimin. The partial complementation of Tir

	Cr	—	pInt$_{EPEC}$	pInt$_{EHEC}$	pInv	pInv-Int395	pInv-Int181	pInv-Int100
				Cr Δeae				
% Tir foci[†]:	95±5%*	25±9%	97±3%*	100±0%*	23±5%	59±7%*,#	19±7%	17±4%
% Pedestals:	98±2%*	0±0%	91±6%*	91±1%*	0±0%	7±3%#	0±0%	0±0%
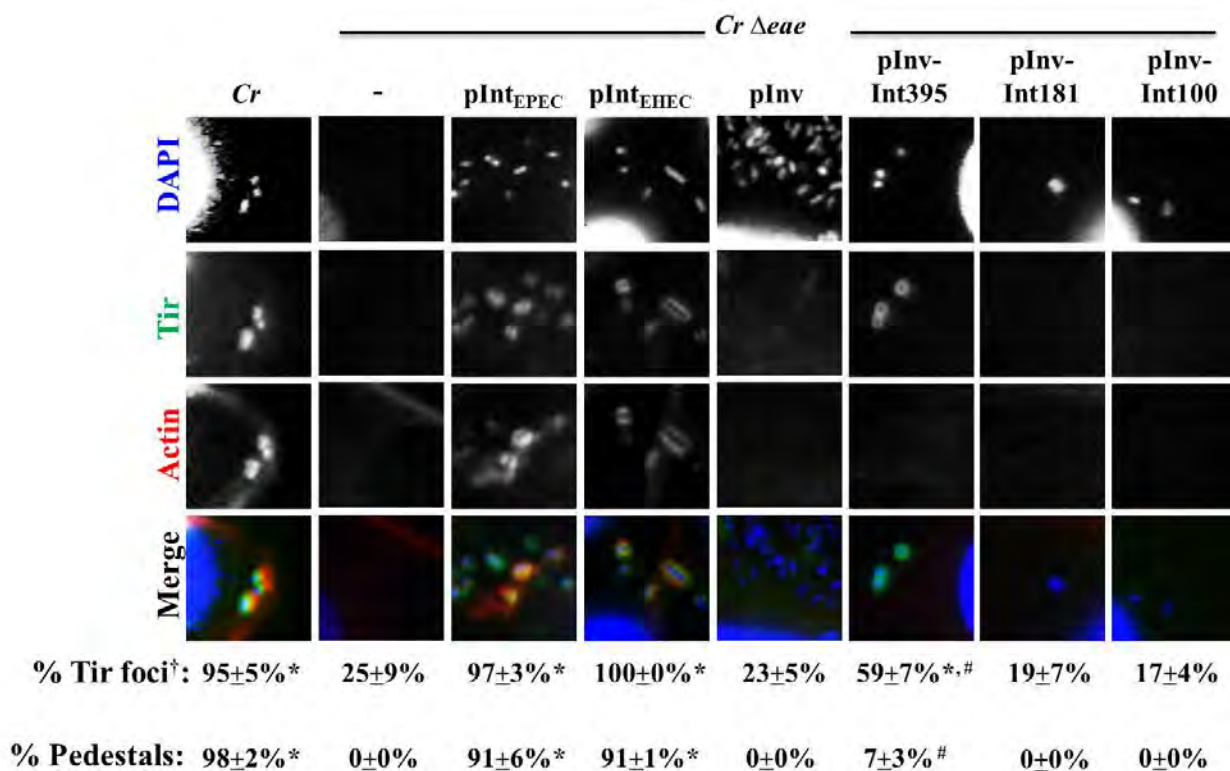
Figure 5. EHEC intimin, but not a Tir-binding invasin-intimin hybrid, promotes Tir clustering and pedestal formation by *C. rodentium*. Monolayers were infected with the indicated *C. rodentium* ("*Cr*") strains and stained with DAPI to visualize bacteria (blue), anti-EHEC Tir antibody (green), and fluorescent phalloidin (red) to detect F-actin. Twenty-five bound bacteria were scored for their association with Tir foci or pedestals. †Note that when quantifying the percentage of cells infected with *C. rodentium*Δ*eae* that had Tir foci and/or actin pedestals associated with bound bacteria, many more cells needed to be counted given the inability/lack of this strain to adhere efficiently to cells. Data represent quadruplicate samples. Asterisk indicates that percent positive bacteria is significantly ($p<0.05$) greater than that for *C. rodentium*Δ*eae*. "#" indicates that percent positive bacteria is significantly ($p<0.05$) lower than that for *C. rodentium*/pInt$_{EHEC}$.

clustering by pInv-Int395 was also reflected in the low (i.e. seven percent) frequency of pedestal formation (**Figure 5, "pInv-Int395"**). Thus, although the expression of Inv-Int395 in *C. rodentium* resulted in high-level Tir-mediated cell binding, it did not result in efficient Tir clustering or pedestal formation in cultured mammalian cells.

A Tir-binding invasin-intimin fusion protein does not promote murine colonization by *C. rodentium* and results in minimal colonic hyperplasia.

After characterizing the invasin-intimin hybrids *in vitro*, we next determined their ability to complement a *C. rodentium*Δ*eae* mutant for colonization and disease *in vivo*. As shown above (**Figure 2A**), after oral gavage of C57BL/6 mice with approximately 5 x 10^9 *C. rodentium*Δ*eae*/pInt$_{EHEC}$, *C. rodentium*Δ*eae* expressing EHEC intimin demonstrated wild type levels of colonization, colonic hyperplasia, goblet cell depletion, and abundant inflammation (**Figure 6A, B**). In contrast, in most instances *C. rodentium*Δ*eae*/pInv displayed colonization kinetics indistinguishable from *C. rodentium*Δ*eae* (**Figure 6A**) and did not trigger colitis (**Figure 6B**), showing that bacterial binding to β$_1$-chain integrins, even by a high affinity ligand such as invasin (Tran Van Nhieu and Isberg, 1993) is not sufficient to promote *C. rodentium* colonization. (Occasionally, *C. rodentium*Δ*eae*/pInv colonized mice somewhat better than *C. rodentium*Δ*eae*, but always at a level several orders of magnitude lower that wild type *C. rodentium* or *C. rodentium* expressing EHEC intimin and usually just above the limit of detection, i.e., 100 CFU/g feces; data not shown.)

As expected, *C. rodentium∆eae* expressing Inv-Int181 or Inv-Int100, neither of which mediated mammalian cell attachment, Tir clustering, or pedestal formation *in vitro*, colonized mice no better than *C. rodentium∆eae* and resulted in no detectable intestinal histopathology (**Figure 6A, B**). Notably, *C. rodentium∆eae* expressing Inv-Int395, which promoted Tir-mediated attachment to cultured monolayers but did not cluster Tir efficiently or trigger pedestal formation on cultured cells, was as defective as *C. rodentium∆eae* in colonization and triggered virtually no intestinal damage (**Figure 6A, B**). The inability of Inv-Int395 to demonstrate wild type intimin function during mammalian infection demonstrates that the ability of intimin to bind Tir, in the absence of efficiently clustering Tir and triggering pedestal formation, is insufficient to promote colonization and disease.
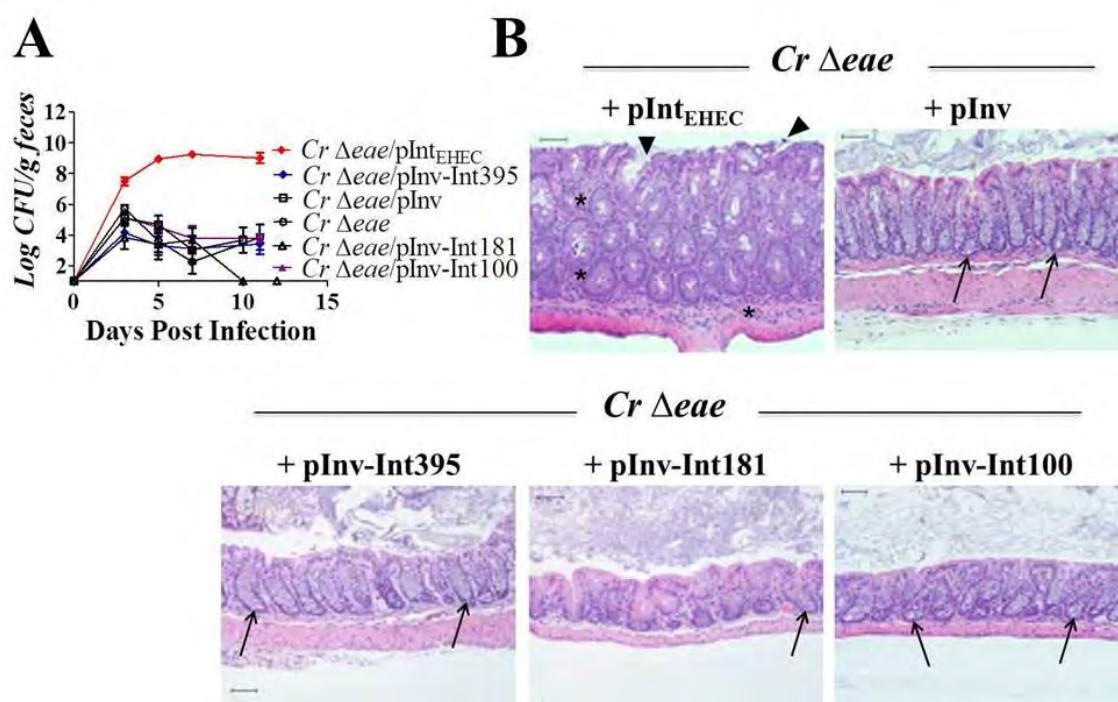
Figure 6. A Tir-binding invasin-intimin fusion protein does not promote murine colonization by *C. rodentium*. (A) Eight-week old C57BL/6 mice were inoculated with the indicated *C. rodentium* strains by oral gavage and colonization was determined by viable stool counts. Shown are the averages CFU (± SEM) of groups of five mice. Each strain was tested in at least three independent experiments. The data displayed includes data from two different experiments, one in which *C. rodentium*Δ*eae*/pInv and *C. rodentium*Δ*eae* were analyzed and another in which the remaining strains were tested. The combined results are overlaid on the graph for ease of comparison. **(B)** H&E stained large intestinal sections from mice infected with designated strain were analyzed at 100x magnification. Scale bars measure 50 μm. Arrow heads indicate foci of epithelial surface disruption. Arrows indicate areas of goblet cells and asterisks indicate foci of active inflammation.

Intimin but not Tir is required for *C. rodentium* colonization of mice pre-treated with streptomycin.

Streptomycin pre-treatment of mice permits EHEC, which is not normally an efficient mouse pathogen, to both colonize mice and cause toxigenic disease (Melton-Celsa et al., 1996; Mohawk and O'Brien, 2011; Wadolkowski et al., 1990a; Wadolkowski et al., 1990b). Pilot experiments indicated that brief streptomycin pre-treatment of outbred Swiss-Webster mice facilitated *C. rodentium* infection (D.S., Joseph Newman, and S.L., unpublished observations), so we pre-treated C57BL/6 mice with streptomycin for 48 hours prior to infection with *C. rodentium* strains that display different capacities to generate actin pedestals. Wild type *C. rodentium* colonized these mice with high efficiency, reaching $\sim 10^8$ to 10^9/g feces by day three after inoculation and persisting at that level for ~ 15 days (**Figure 7A, "*Cr*"**). Fecal colonization diminished after day 15 post-infection, but unlike infection of untreated mice, easily detectable CFU were present until the experiment was terminated at 31 days post-infection. Although *C. rodentiumΔeae* was present in the stool at high levels at three days post-infection, this strain was not capable of stable colonization (**Figure 7A, "*Cr Δeae*"**). Fecal colonization of *C. rodentiumΔeae* at five days post-infection and throughout the remainder of the experiment was significantly lower than colonization by *C. rodentium* (**Figure 7A, "*Cr Δeae*", p<0.05**). The colonization defect was fully complemented by plasmid-borne EHEC or EPEC intimin for at least the first 15 days post-infection (**Figure 7A, "*Cr Δeae*/pInt$_{EHEC}$" or "*Cr Δeae*/pInt$_{EPEC}$"**, respectively). Indeed, fecal colonization at seven to 18 was significantly higher (p<0.05) in mice infected with *C. rodentium*
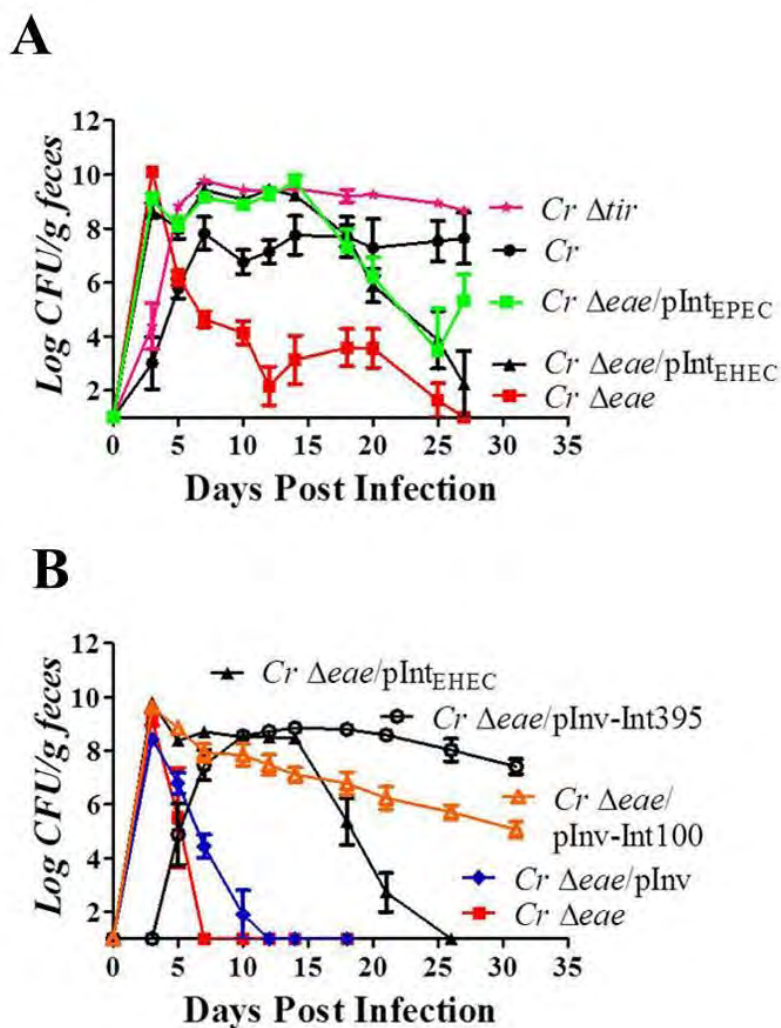
Figure 7. Intimin but not Tir is required for fecal colonization of streptomycin pre-treated mice by *C. rodentium*. (A, B) Eight-week old C57BL/6 mice were pre-treated with streptomycin in their drinking water for 48 hours prior to being inoculated with approximately 5×10^9 CFU of the indicated *C. rodentium* strains by oral gavage (see **Materials and Methods**), with the exception of *C. rodentium*Δ*tir* in panel **A**, in which approximately 10^6 CFU were inoculated. Fecal colonization was determined by viable stool counts, and shown are the averages CFU (± SEM) of three to five mice per group. (Note that the slightly lower level of colonization by *C. rodentium*Δ*tir* in panel **A** at three days post-infection was likely due to the lower inoculum used.) Each strain was tested in at least two independent experiments. Statistical testing was done using a two-way ANOVA followed by Bonferroni's post-tests.

expressing EHEC and EPEC intimin compared to mice infected with the *C. rodentium*

eae mutant. At later time points (after approximately 20 days post-infection),

complementation was not complete, as bacteria expressing either EPEC or EHEC intimin

were cleared somewhat more rapidly than wild type *C. rodentium*. These data indicate

that even when the flora is disrupted by antibiotic pre-treatment, intimin is required for

maximal murine colonization. In addition, the late time point differences

notwithstanding, EHEC or EPEC intimin were able to provide wild type colonization

function for the first two weeks of infection.

To determine whether the requirement for intimin was a reflection of its ability to

interact with Tir, we inoculated streptomycin pre-treated mice with a *C. rodentiumΔtir*

mutant. Notably, whereas Tir is essential for colonization by *C. rodentium* in

conventional mice (Deng et al., 2003), we found that Tir was dispensable in streptomycin

pre-treated mice. In fact, fecal counts of *C. rodentiumΔtir* reached approximately 10^{10}

CFU/gram of feces by six days post-infection and remained highly elevated thereafter

(**Figure 7A, "*Cr Δtir*"**). Clearly, intimin provides a Tir-independent colonization

function in this infection model.

To test whether the potential integrin-binding activity of intimin might be the Tir-

independent activity that provides this function, we infected streptomycin pre-treated

mice with *C. rodentiumΔeae* harboring pInv, which expresses the β_1-chain integrin ligand

invasin. *C. rodentiumΔeae*/pInv, like *C. rodentiumΔeae*, was present at high levels

transiently (at post-infection day three) in the stool of infected mice but was typically

unable to sustain infection, suggesting that integrin binding of intimin did not contribute

to colonization function (**Figure 7B, "*Cr* Δ*eae*/pInv"**). (As was the case for infection of untreated C57BL/6 mice, occasionally the expression of invasin promoted a level colonization several orders of magnitude lower than *C. rodentium* that expressed endogenous or EHEC intimin; data not shown.)

Finally, to determine what region of intimin was required to promote infection of antibiotic pre-treated mice, we infected mice with *C. rodentium*Δ*eae*/pInv-Int395 or *C. rodentium*Δ*eae*/pInv-Int100. We found that expression of either Inv-Int395, which binds Tir, or Inv-Int100, which does not, was sufficient to promote stable high-level colonization (**Figure 7B, "*Cr* Δ*eae*/pInv-Int395" and "*Cr* Δ*eae*/pInv-Int100"**). In some instances, the degree of colonization by *C. rodentium*Δ*eae*/pInv-Int100 was somewhat less than *C. rodentium*Δ*eae*/pInv-Int395 after ten days post-infection, but remained $\geq$ ~10^6/gram feces throughout the 25 to 31 days of infection (**Figure 7B** and data not shown). Thus, it appears that the C-terminal 100 residues of intimin contain the activity that promotes colonization of antibiotic pre-treated mice. The finding that this portion of intimin is incapable of binding to Tir is consistent with the hypothesis that a Tir-independent function of intimin provides a critical colonization activity in animals with altered flora.

Discussion

Intimin, encoded by *eae,* is an adhesin essential for colonization by AE pathogens (Dean-Nystrom et al., 1998; Donnenberg et al., 1993a; Ritchie et al., 2003; Schauer and Falkow, 1993b; Tzipori et al., 1995). Allelic variation of intimin has been associated with differences in colonization of intestinal samples *ex vivo* (Fitzhenry et al., 2002; Mundy et al., 2007), and inoculation of gnotobiotic piglets with an EHEC strain harboring a plasmid encoding EPEC intimin resulted in colonization of the small intestine, a property not possessed by the same strain harboring a plasmid encoding EHEC intimin (Tzipori et al., 1995). To avoid potential effects related solely to high copy number expression of intimin, in this study we precisely replaced the endogenous (chromosomal) *eae* coding sequence of EHEC with EPEC *eae*. In fact, we found that the recombinant strain was incapable of efficiently colonizing the small intestine and infected the piglet indistinguishably from its isogenic wild type EHEC parent. A previous study utilizing a newborn (not gnotobiotic) piglet model also failed to note differences in tissue tropism due to intimin allele, although that study was not designed to carefully assess tissue tropism (Donnenberg et al., 1993a). Preliminary findings suggest that neither overexpression of EHEC nor EPEC intimin is associated with clear change in EHEC tissue tropism in gnotobiotic piglets, suggesting that simple overexpression does not account for the previously described tropism differences (M.J.B. and S.T., unpublished observations).

To assess potential functional differences specific to intimin to particular alleles in a second animal model, we infected mice with *C. rodentium* strains expressing

endogenous intimin, or intimin of canonical EPEC or EHEC strains. We found that

EHEC intimin, like EPEC intimin, promoted efficient intestinal colonization and wild

type disease. Notably, previous studies indicated that *C. rodentium* expressing a chimeric

intimin composed of the 554 N-terminal residues of EPEC intimin fused to the 380 C-

terminal residues of EHEC intimin colonized the murine intestine approximately a

hundred-fold less efficiently than wild type *C. rodentium* and was entirely defective for

inducing disease (Hartland et al., 2000; Mundy et al., 2007). The N-terminal 554

residues of EPEC and EHEC intimin are 97 percent identical, and although we cannot

rule out the possibility that an important (perhaps Tir-binding) activity of EHEC intimin

is diminished by the exchange of its N-terminus for that of EPEC intimin, an alternative

hypothesis is that differences in the murine host strain contribute to the apparent

discrepant results; previous studies demonstrating allele-specific differences utilized

Swiss NIH or C3H/HeJ mice (Hartland et al., 2000; Mundy et al., 2007), whereas we

utilized C57BL/6 mice in the current study. Additionally, anecdotal evidence suggests

that the degree of murine infection by *C. rodentium* is dependent on the commercial

source of mice (M. McBee, personal communication), a factor that might influence the

composition of the intestinal microbiome (Littman and Pamer, 2011). Regardless, the

demonstration here that EHEC intimin can confer apparently full biological function in

this infection model provides a facile experimental system in which to assess either

EHEC intimin function or therapeutic strategies targeting this important virulence factor.

Intimin has the capacity to recognize mammalian proteins, such as β_1-chain

integrins or nucleolin, activities that have been postulated to facilitate colonization by

promoting initial bacterial attachment to mucosal surfaces (Frankel et al., 1996a; Sinclair and O'Brien, 2002). Expression of invasin, a high affinity β_1-chain integrin ligand, conferred on *C. rodentium* the ability to enter mammalian cells *in vitro*, indicating that the invasin integrin-binding domain was presented in a functional form on the bacterial surface. Invasin did not, however, provide consistent intimin function in promoting murine colonization by *C. rodentium*, indicating that the β_1-chain integrin binding activity is not the sole activity of intimin required for biological function.

The above finding is predicted from the demonstration that an essential receptor for intimin is the type III effector Tir, which becomes localized in the plasma membrane after translocation (Kenny et al., 1997). Tir binding by intimin is required for high-level attachment to cultured mammalian cells (Liu et al., 1999), and Tir-deficient mutants of AE pathogens, like intimin mutants, are incapable of intestinal colonization (Deng et al., 2003; Marches et al., 2000; Ritchie et al., 2003). We found that *C. rodentium* expressing EHEC intimin was capable of Tir-mediated binding to mammalian cells. A *C. rodentium* strain expressing the intimin-invasin chimera Inv-Int395, which contains three intimin immunoglobulin-like domains and the C type lectin-like domain (Frankel et al., 1995; Luo et al., 2000), also efficiently bound to mammalian cells. *C. rodentium* expressing Inv-Int181, which contains a region that is capable of binding Tir when expressed as a recombinant protein, did not bind primed cells or unmanipulated cells. Previous analysis of recombinant intimin derivatives revealed that sequences N-terminal to the minimal 181-residue Tir-recognition domain may influence binding (Liu et al., 1999). Interestingly however, a laboratory *E. coli* K12 strain expressing Inv-Int181, in contrast

to *C. rodentium* expressing this chimera, bound to mammalian cells that had been pre-infected with EPEC (Liu et al., 1999). LPS O antigen can sterically hinder the recognition of invasin in the outer membrane (Voorhis et al., 1991), and the strain-specific difference in the activity of Inv-Int181 may reflect differences in O antigen length and/or density.

Intimin-mediated clustering of Tir in the plasma membrane promotes the formation of an actin assembly complex beneath bound bacteria, leading to actin assembly (Campellone et al., 2004a; Touze et al., 2004). Indeed, *C. rodentium* expressing EHEC intimin not only bound to monolayers that were primed with EPECΔ*eae*, but also triggered robust actin assembly. In contrast, whereas *C. rodentium* expressing Inv-Int395 was capable of Tir-mediated binding to mammalian monolayers, this interaction did not trigger efficient pedestal formation. Given the extensive sequence differences between invasin and intimin, any number of factors may account for the partial function of Inv-Int395 in pedestal formation. However, multimeric interactions greatly facilitate the efficiency of actin assembly (Blasutig et al., 2008; Padrick et al., 2008; Sallee et al., 2008), and it is possible that Tir binding by *C. rodentium* producing Inv-Int395 did not result in the high-density membrane clustering of Tir that triggers efficient actin assembly. Consistent with this hypothesis, *C. rodentium* expressing Inv-Int395 generated foci of Tir in infected cells at a significantly lower efficiency did *C. rodentium* expressing full-length *C. rodentium*, EPEC or EHEC intimin. Indeed, whereas latex beads coated at high concentrations with C-terminal fragments of purified EHEC intimin stimulated robust actin assembly on monolayers pre-infected with EPECΔ*eae*, *E.*

coli K12 strains expressing invasin-intimin hybrids containing the equivalent regions of intimin did not (Liu et al., 1999).

The finding that *C. rodentium* expressing either EHEC intimin or Inv-Int395 both bound to Tir but only the former triggered actin pedestal formation *in vitro,* provided an opportunity to determine if pedestal formation correlated with intestinal colonization. Indeed, whereas *C. rodentium* expressing EHEC intimin was capable of colonizing mice to levels indistinguishable from levels attained by wild type *C. rodentium*, *C. rodentium* expressing Inv-Int395 colonized mice at levels a million-fold lower, barely above background, and were cleared from the mice by day five post-infection. *C. rodentiumΔeae* expressing Inv-Int395 also was not associated with any manifestations of disease. A correlation between the ability to generate robust pedestal *in vitro* and efficient colonization of the mammalian host has previously been described. First, an EHEC strain lacking a second translocated effector, $EspF_U$ (also known as TccP), remains capable of Tir translocation and intimin-mediated binding but is incapable of stimulating robust actin assembly (Campellone et al., 2004b; Garmendia et al., 2004), and is defective (albeit mildly) in late-stage colonization in infant rabbits (Ritchie et al., 2008). Second, a *C. rodentium* encoding a mutant Tir that binds intimin but is deficient in downstream actin signaling is out-competed late in infection by a wild type strain during co-infection experiments (Crepin et al., 2010). Thus, mutants of any of the three bacterial factors directly involved in pedestal formation, intimin, Tir, and $EspF_U$, that specifically diminish pedestal formation *in vitro* also diminish colonization *in vivo*. A genetically engineered *C. rodentium* strain that generates pedestals using an additional

mechanism did not display a competitive advantage over a wild type strain (Girard et al., 2009a), suggesting that even though inefficient pedestal formation is associated with diminished colonization, pedestal formation enhanced over wild type levels does not lead to enhanced colonization. The means by which a threshold pedestal formation activity may be required for maximal intestinal colonization is currently unclear, but the observation that the EHEC$\Delta espF_U$ mutant formed smaller than wild type aggregates on the intestinal epithelium of piglets and showed a late colonization defect in infant rabbits (Ritchie et al., 2008) suggests that pedestals may stabilize bacterial interaction with the mucosal surface or otherwise promote expansion of the infectious niche at that site.

Whereas Tir-mediated actin pedestal formation appears to contribute to colonization of gnotobiotic piglets and conventional mice, infection of streptomycin pre-treated mice revealed a Tir-independent function of intimin. Intimin function in this model was largely independent of intimin allele—*C. rodentium* expressing EPEC or EHEC intimin colonized these mice at high levels for at least two weeks, although they both showed somewhat diminished colonization relative to wild type *C. rodentium* beyond that time point. Most notably, whereas *C. rodentium*Δ*eae* was incapable of stably colonizing antibiotic-treated mice, *C. rodentium*Δ*tir* colonized these mice at least as well as wild type *C. rodentium*. The ability of intimin to bind host cells or components of host cells such as β_1-chain integrins or nucleolin has been previously mapped to C-terminal portions of intimin (Frankel et al., 1994; Frankel et al., 1996a; Sinclair and O'Brien, 2002, 2004). We found that the colonization activity of intimin in this infection model was retained by intimin derivatives harboring C-terminal regions of intimin, even

if such derivatives (e.g. Inv-Int100, containing only the C-terminal 100 residues of intimin) were incapable of binding Tir. Intimin also contributes to the disruption of epithelial barrier function *in vitro* in a Tir-independent manner (Dean and Kenny, 2004). Notably, the Tir-independent intimin activities in cell attachment or barrier disruption have been characterized entirely by *in vitro* assays, and the contribution of these activities to colonization and disease during mammalian infection has not been documented. A comparison of these Tir-independent intimin *in vitro* activities to intimin function in promoting colonization of streptomycin pre-treated mice might provide insight into novel activities of intimin relevant to colonization of a mammalian host.

CHAPTER III.

A NOVEL MURINE MODEL FOR SHIGA TOXIN-MEDIATED DISEASE BY ENTEROHEMORRHAGIC *ESCHERICHIA COLI*

Abstract

Upon attachment to intestinal epithelium, enterohemorrhagic *E. coli* (EHEC) generates 'attach and efface' (AE) lesions, characterized by intimate attachment, microvillar effacement, and actin pedestal formation beneath bound bacteria. AE lesion formation requires the type three-secreted effector Tir. Production of the phage-encoded cytotoxin, Shiga toxin (Stx), by EHEC contributes to hemorrhagic colitis and the triad of hemolytic anemia, thrombocytopenia, and renal failure. Conventional mice are not highly susceptible to infection with strains that produce Stx, and no mouse model clearly demonstrates AE lesions and intestinal damage after EHEC infection. We lysogenized *Citrobacter rodentium*, a murine AE pathogen lacking Stx, with a λ phage that produces Stx2dact, an allele of Stx that is highly toxic to mice. *C. rodentium* (λ*stx$_{2dact}$*) generated Stx2dact upon phage induction *in vitro*. Mice infected with *C. rodentium* (λ*stx$_{2dact}$*) formed AE lesions on the intestinal epithelium and developed Stx2dact-dependent intestinal inflammatory damage. In addition, renal proximal tubules were damaged, and mice suffered a lethal infection characterized by proteinuria, induction of serum and renal pro-inflammatory cytokines, and weight loss. A *C. rodentium* (λ*stx$_{2dact}$*) *tir* mutant failed to colonize or cause disease. Thus, *C. rodentium* (λ*stx$_{2dact}$*) provides a murine model for Stx-mediated intestinal and systemic disease by an AE pathogen.

Acknowledgments and contributions

This chapter is a result of several collaborations and has been submitted for publication in the Journal of Clinical Investigation. This work was supported by National Institutes of Health [R21 AI92009 and RO1 AI46454 to J.M.L. and R37 AI20148 to A.O.]; National Institutes of Health/New England Regional Center for Excellence, Biodefense and Emerging Infectious Diseases Cooperative Pilot Projects Program [RO1 DK59101 to J.R.B and D.S.]; National Institute of Allergy and Infectious Diseases [RO1 049842 PHS RO1 AI049842 to D.B.S.]; and National Cancer Institute [026731 PHS P01CA026731 to D.B.S]. I would like to acknowledge people for their contribution to the work presented here:

Angela Melton-Celsa performed the mucus activation assays shown in Table 1: Stx2d from *C. rodentium* (λstx_{2dact}) is mucus activatable. She also performed the alignment in Supplemental Figure 1: Amino acid alignment of Stx A and B subunits of φ1720a-02 from *C. rodentium* (λstx_{2dact}) with other Stx A and B subunits from various STEC strains.

Lara Strittmatter and Greg Hendricks of the UMASS Electron Microscopy Core Facility assisted with the electron microscopy (see Figure 3A).

The DERC Histology Core Facility at UMMS assisted prepared intestinal and kidney samples for H&E (see Supp. Fig 3, Figures 3B, 5B, and 6D-E).

Vijay Vanguri assisted in viewing histological slides and taking pictures (see Supp. Fig 3, Figures 3B, 5B, and 6D-E).

The UMMS Mouse Phenotyping Core Facility measured serum and renal cytokines and serum BUN (see Figures 4, 5A, and 5C).

<u>Introduction</u>

Enterohemorrhagic *E. coli* (EHEC), particularly serotype O157:H7, is an

important food-borne human pathogen responsible for both sporadic cases and epidemic

outbreaks of diarrheal illness (Kaper et al., 2004; Pennington, 2010). Human EHEC

infection can cause severe local disease such as hemorrhagic colitis, characterized by

damage to the intestinal epithelium, acute abdominal pain, and bloody diarrhea (Amirlak

and Amirlak, 2006; Karch et al., 2005; Karmali et al., 2009; Tarr et al., 2005). EHEC

infection may also result in life-threatening systemic disease, most notably hemolytic

uremic syndrome (HUS), characterized by the triad of hemolytic anemia,

thrombocytopenia, and renal failure (Scheiring et al., 2010; Tarr et al., 2005). In fact,

HUS is the leading cause of renal failure in children (Mead and Griffin, 1998; Scheiring

et al., 2008).

A characteristic pathogenic feature of EHEC, one that it shares with

enteropathogenic *E. coli* (EPEC), a cause of infantile diarrhea in the developing world,

and *Citrobacter rodentium,* a natural murine pathogen, is the ability to generate attach

and efface (AE) lesions (Kaper et al., 2004; Schauer and Falkow, 1993a). These

histopathological lesions are characterized by intimate adherence of the bacterium to the

host cell, effacement of brush border microvilli, and the formation of filamentous actin-

rich pedestals beneath bound bacteria ((Moon et al., 1983); for review see (Kaper et al.,

2004). The formation of AE lesions requires translocation of effector proteins into the

mammalian cell via a type three secretion system (Kenny and Finlay, 1995; McDaniel et

al., 1995). A critical type three effector protein is Tir, which localizes in the host plasma

membrane and acts as a receptor for the bacterial outer membrane protein intimin, promoting intimate adherence and filamentous actin assembly beneath bound bacteria (de Grado et al., 1999; Donnenberg and Kaper, 1991; Hartland et al., 1999; Jerse et al., 1990; Kenny et al., 2002). Both Tir and intimin are essential for colonization and virulence in several animal models of EHEC and *Citrobacter* infection (Deng et al., 2003; Donnenberg et al., 1993b; Marches et al., 2000; Ritchie et al., 2003; Schauer and Falkow, 1993b; Tzipori et al., 1995).

EHEC represent a subset of Shiga toxin-producing *E. coli* (STEC). Shiga toxin (Stx) is a potent inhibitor of protein synthesis that is largely responsible for the extensive tissue damage and systemic disease generated by EHEC (O'Brien et al., 1992; Schuller et al., 2004; Tarr et al., 2005). Stx is encoded by a lambdoid prophage and its production is often enhanced upon phage induction (Muhldorfer et al., 1996; Schmidt, 2001; Waldor and Friedman, 2005). Stx traverses the intestinal epithelium and targets the endothelium, leading to vascular damage, particularly in tissues such as the kidney and central nervous system because these tissues express high levels of the Stx receptor, the glycolipid globotriaosylceramide or Gb_3 (Obrig, 2010; Sandvig and van Deurs, 1996; Schuller, 2011). The action of Stx on endothelial cells leads to the induction of pro-inflammatory cytokines, thrombus formation in the vasculature, and renal damage (Nakao and Takeda, 2000; O'Loughlin and Robins-Browne, 2001; Sandvig, 2001; Tesh et al., 1994; Thorpe et al., 2001). Stx1 and Stx2 are the two major serotypes of Stx, and EHEC that express exclusively Stx2 are associated with a greater risk of HUS (Croxen and Finlay, 2010; Melton-Celsa et al., 2011; Ostroff et al., 1989). There are several variants of Stx2, of

which Stx2c and Stx2dact are particularly important in human disease (Eklund et al., 2002; Friedrich et al., 2002; Persson et al., 2007). In particular, Stx2dact is proteolytically activated in the intestinal mucus, and is associated with STEC that cause a toxigenic illness in humans despite the fact that they lack the ability to generate AE lesions (Ito et al., 1990; Melton-Celsa et al., 2002).

Injection of Stx into mice results in the induction of pro-inflammatory cytokines, vascular damage, hemolysis, and renal damage (Keepers et al., 2007; Keepers et al., 2006; Psotka et al., 2009; Sauter et al., 2008), but in contrast to piglet and rabbit infection models (Garcia et al., 2006; Garcia et al., 2002; Panda et al., 2010; Tzipori et al., 1995), murine models fail to recapitulate the efficient intestinal colonization via AE lesion formation (reviewed in (Mohawk and O'Brien, 2011)). For example, conventional mice suffer Stx-mediated mortality only after administration of large numbers of EHEC, numbers that diminish in the days following inoculation (Mohawk et al., 2010a; Mohawk et al., 2010b). Disruption of the normal flora by antibiotic pre-treatment, or its complete elimination by rearing the animals in a germ-free environment, sensitizes mice to lethal infection after relatively low dose oral inoculation (Eaton et al., 2008; Lindgren et al., 1993; Melton-Celsa et al., 1996). However, only STEC that produce a particular Stx2dact consistently cause lethal infection of streptomycin pre-treated mice (Lindgren et al., 1993; Melton-Celsa et al., 1996). Furthermore, EHEC or STEC infection of altered-flora mice does not result in well documented AE lesions, nor have bacterial genes that promote AE lesion formation been demonstrated to be required for intestinal colonization or disease (Eaton et al., 2008; Lindgren et al., 1993; Melton-Celsa et al., 1996;

Wadolkowski et al., 1990a; Wadolkowski et al., 1990b). Indeed, a laboratory *E. coli* K12 strain that overproduces Stx2 but lacks Tir, intimin, and the type III secretion apparatus, is capable of lethal infection of streptomycin pre-treated mice (Wadolkowski et al., 1990b). Interestingly, in spite of the fact that intestinal damage and hemorrhagic colitis are prominent features of EHEC infection in humans, intestinal damage is not a prominent feature of current models involving infection of mice (Mohawk et al., 2010b; Mohawk and O'Brien, 2011).

The AE pathogen *Citrobacter rodentium* has been used extensively as a murine model for EHEC and EPEC colonization (Barthold et al., 1978; Borenshtein et al., 2008; Deng et al., 2003; Luperchio and Schauer, 2001; Mundy et al., 2005), but does not express Stx. To establish an infection model that reflects both the characteristic mode of intestinal colonization and Stx-mediated disease, we constructed a *C. rodentium* strain lysogenized by an Stx2dact-producing phage. Administration of *C. rodentium* (λstx_{2dact}) to mice by gavage recapitulated Tir-dependent AE lesion formation, as well as essential aspects of systemic Stx-mediated disease, including intestinal and renal damage, accompanied by the induction of pro-inflammatory cytokines. Thus, *C. rodentium* (λstx_{2dact}) provides a model for EHEC colonization and toxin-mediated disease in conventional mice.

Materials and Methods

Plasmids, bacterial strains, and growth conditions. Bacterial strains and plasmids

used in this study are listed in **Supplemental Tables 1 and 2**. All bacteria were cultured

in Luria-Bertani broth (LB) (Miller) at 37°C, unless otherwise stated. Antibiotics were

used in the following concentrations kanamycin (25 µg/ml), zeocin (75 µg/ml), and

chloramphenicol (10 µg/ml).

Sequencing of Φ1720a-02 from Gobius EC1720. Sequencing of the newly identified

Φ1720a-02 from EC1720a, a strain originally isolated from retail ground beef (Gobius et

al., 2003) was performed using the panhandle PCR technique as previously described

(Jones and Winistorfer, 1993; Siebert et al., 1995), and Egan, PH.D. Thesis). The adaptor

sequences used were F-Adaptor 1 (see **Supplemental Table 3**) and R-Adaptor 2 (see

Supplemental Table 3). Primers F-AP1 and R-AP2 (see **Supplemental Table 3**) were

used for the PCR reaction and sequencing of the PCR reaction, respectively. Reactions

for restriction digests and ligation of adaptors to genomic Φ1720a-02 DNA were as

follows: 1 µg genomic Φ1720a-02 DNA, 10 pmol F-Adapter 1, 10 pmol R-Adapter 2, 10

units blunt-end restriction enzyme (EcoRV, PvuII, RsaI, SspI, XmnI, DraI, HincII, HpaI,

ScaI), 2.5 units T4 DNA ligase, 2 µl 20mM ATP, 4 µl of 10x One-Phor-All buffer PLUS

(Amersham-Pharmacia, Piscataway, NJ, USA), and up to 20 µl water. Reactions were

then incubated at 20°C for 16 hours. Next, enzymes were deactivated by heating at 68°C

for 10 minutes and reactions were ethanol precipitated and resuspended in 50 µl sterile

water. The panhandle PCR reaction was then performed using 1 µl of the ethanol

precipitated template DNA, 2 µl Taq 10x reaction buffer containing 20 mM MgCl$_2$, 1 µl

10 mM dNTP mix, 10 pmol F-AP1 primer, 10 pmol gene specific primer, 1 unit Taq

polymerase, and up to 20 µl water. The PCR cycle parameters were as follows: (1) 95°C

for 1 minute, (2) 95°C for 30 sec, (3) 68°C for 7 minutes, and steps 2-3 were repeated 25

times. PCR reactions were then cleaned up using a QIAgen (Valencia, CA, USA) spin

kit and sequenced at Tufts Core Sequencing Facility.

To confirm the nucleotide and protein sequences of StxA and StxB from the newly

identified Φ1720a-02 (λ*stx$_{2dact}$*), fragments of both genes, the predicted promoter region,

and the region upstream of *stxA* were amplified by PCR and TA cloned into JM109 high

efficiency competent cells (Promega, Madison, WI, USA). The following primers (see

Supplemental Table 3 for sequences) were used to clone each fragment: F-Oli218+R-

Oli219 (593 bp), F-Oli224+R-Oli210 (1.490 kb), R-Oli220+F-Oli221 (1.647 kb), F-

Oli222+R-Oli220 (~2 kb), R-Oli223+F-Oli222 (1.159 kb), F-Oli224+R-Oli223 (1.3 kb),

F-Oli221+R-Oli210 (918 bp), F-Oli224+R-Oli219 (1.2 kb), R-Oli219+F-Oli226 (~2.1

kb), and F-Oli228+R-Oli219 (~2 kb) (see **Supplemental Table 3**). The clones were

screened by colony PCR and restriction digestion. Correct clones were sequenced at

Tufts Core Sequencing Facility. Fragments were aligned using BioEdit software and/or

MacVector. Nucleotide sequences of *stxA* and *stxB* were submitted to Genbank and were

assigned the following accession numbers: JN194203 and JN194204.

Alignment of Φ 1720a-02 StxA2 and StxB2 from with other Stxs. The predicted

amino acid sequence of the A and B subunits of from the Φ1720a-02 from *C. rodentium*

(λstx_{2dact}) were aligned with the A and B subunits of Stx2 from EDL933 (Genbank

accession number X078655), Stx2c from E32511 (Genbank accession number M59432),

Stx2d from EH250 (Genbank accession number AF043627), Stx2d$_{act}$ (formerly called

Stx2vhb) from B2F1 (Genbank accession number AF479829), and Stx2e from S1191

(Genbank accession number M21534). The sequences were aligned using the Align Plus

5 program, version 5.03 (Scientific & Educational Software, Durham, NC, USA)

following the global-ref alignment procedure (Myers and Miller, 1988) and the scoring

matrix BLOSUM 62 (Henikoff and Henikoff, 1992).

Antibiotic marking Φ1720a-02. To create an antibiotic-marked Stx2-expressing

Φ1720a-02 bacteriophage, a chloramphenicol resistance marker (*cat*, Cm^{R}) was inserted

into the nonessential gene, *Rz* (Hernandez et al., 1985) using lambda red recombination.

Briefly, a 707-bp fragment containing sequence upstream of the *Rz* gene was amplified

from EC1720a genomic DNA using primers F-425 and R-426, flanked by *Sph* I and

BamH I sites. A 692-bp fragment containing sequence downstream of the *Rz* gene was

amplified by PCR using primers F-259 and R-427 with *BamH* I and *Sac* I sites. A 900 bp

cat cassette was then amplified from pBR328 with flanking *BamH* I sites using primers

F-265 and R-266. A tertiary PCR reaction was done using the three PCR fragments with

primers F-425 and R-427. This tertiary PCR fragment was then inserted between the *Sph*

I and *Sac* I sites of pUC to create pBJK5. This plasmid was digested with *Sph* I and *Sac* I

to release a 2.3 kb fragment containing the *cat* cassette flanked by regions of the *Rz* gene. This fragment was electroporated into arabinose-induced EC1720a containing the lambda red recombinase plasmid pKD46. The culture was recovered in 1 ml SOC for 1.5 hours at $37^{o}C$, and then plated on LB plates supplemented with chloramphenicol to select for recombinants. Recombinants were screened by PCR using primer pairs F-425/R-427 and F-265/R-266.

Creation of an *stx*-deletion within EC1720aΔ*Rz::cat*. Chimeric PCR was used to produce a fragment containing the Km^{R} cassette within an in-frame deletion of *stxAB*. Three PCR reactions were done as follows: 1- template pUC18K with primers F-2dH1/R-2dH2, 2-template EC1720a genomic DNA with primers F-498/R-2dH1AP, and 3- template EC1720a genomic DNA with primers F-2dH2AP/R-499. A tertiary PCR was then done using these three PCR reactions as templates and the resulting PCR product was then electroporated into EC1720aΔ*Rz::cat* containing the lambda red recombinase plasmid, pKD46 and induced to recombine. Recombinants were selected on LB plates supplemented with chloramphenicol and kanamycin and then screened by PCR using the following primer pairs: F-498/R-499, F-2dH1/R-2dH2, F-316/R-2dH2, F-316/R-398, and F-2dH1/R-398. The loss of pKD46 from the resulting strain, EC1720aΔ*stx₂dactAB::kan* Δ*Rz::cat* was confirmed by plating the strain on both kanamycin and ampicillin.

Isolation of Φ1720aΔ*Rz::cat* and Φ1720aΔ*stx2d::kan* Δ*Rz::cat*. Recombinant Stx bacteriophages Φ1720aΔ*Rz::cat* and Φ1720aΔ*Rz::cat* Δ*stx₂dactAB::kan* were isolated from

the newly modified genetically manipulated EHEC strains JB-13-06 and JB-13-28 (see

Supplemental Table 1), respectively, as previously described (Gobius et al., 2003; Teel

et al., 2002). Briefly, EHEC isolates were treated with mitomycin C (0.5 μg/ml) to

induce the bacteriophage lytic cycle and production of phage. The cells were treated with

0.5 ml of chloroform per 3.0 ml of broth culture and were filtered through a 0.45 μm pore

size filter to ensure a cell-free lysate.

Construction of *C. rodentium* (λ*stx$_{2dact}$*) and *C. rodentium* (λ*stx$_{2dact}$::kan^R*). The

genetically engineered Stx2dact bacteriophages Φ1720a-02Δ*Rz::cat* which has a

chloramphenicol resistance cassette inserted into *Rz*, and Φ1720a-02Δ*Rz::cat*

Δ*stx2d::kan*, which has a chloramphenicol resistance cassette inserted into *Rz* and a

kanamycin resistance cassette inserted into Stx2dactAB, were isolated from genetically

modified EHEC strains EC1720aΔ*Rz::cat* and EC1720aΔ*Rz::cat* Δ*stx2d::kan*,

respectively. *C. rodentium* DBS100 (Schauer and Falkow, 1993a) was provided with cell

surface receptor for bacteriophage Stx2d by transformation of plasmid pTROY9 which

contains the *E. coli lamB* gene and a tetracycline resistance marker (de Vries et al., 1984;

Wehmeier et al., 1989). The lambda phage receptor was put into DBS100, creating

DBS100/pTROY9 and induced by growing overnight at 37°C in lambda broth with 0.2%

maltose and 10 mM MgSO$_4$. This strain was then lysogenized with the antibiotic-marked

bacteriophages as described (McDonough and Butterton, 1999), resulting in DBS770 (*C.*

rodentium (λ*stx$_{2dact}$*)) or DBS771 ((*C. rodentium* (λ*stx$_{2dact}$::kan^R*)).

Generation of *C. rodentium* (λ*stx₂dact*)Δ*tir*. The *C. rodentium* (λ*stx₂dact*) *tir* deletion

mutant was made as previously described (Mallick et al., 2012) using a slightly modified

version of the one-step PCR-based gene activation protocol (Datsenko and Wanner,

2000).

Construction of a plasmid expressing *C. rodentium Tir*. Isolation of all plasmid DNA

was done by the Miniprep procedure (QIAgen, Valencia, CA, USA). Oligonucleotides

were ordered from Invitrogen. The *C. rodentium* complementation vector, pEM129

(pTir), was created using a modified version of pMB46, pEM123, containing the

additional unique restriction sites *Mlu* I and *Sac* II between *Kpn* I and *Hind* III. *C.*

rodentium tir – cesT was then amplified with using F-MluI-Cr-tirU and R-SacII-Cr-tirL

and ligated into *Mlu* I and *Sac* II site of pEM123 to create pEM129. Sequencing was

performed at the DNA Sequencing Core Facility at Tufts Medical School.

ELISA quantification of Stx. Overnight bacterial cultures with antibiotic were diluted

into a 5 ml culture with new medium and antibiotic. The cultures were grown to OD_{600} =

0.5-0.7. Mitomycin C (5 μl of 0.5 ng/ml) was added to cultures and they were grown

overnight with agitation. Cultures were spun at 14,000 rpm for 5 minutes at room

temperature. Supernatants were collected for analysis. To prepare pellets for ELISA,

pellets were washed with 1M Tris pH8 on ice, frozen at -70°C for 30 minutes,

resuspended in 1 ml ice cold 1M Tris pH8, and sonicated (20 second bursts 3 times) and

prepared for Stx2 ELISAs. 96-well plates (Corning Maxisorb) were coated with 4D1

Stx2 antibody (a gift from Cheleste Thorpe, M.D., Tufts University) 1:1000 in coating

buffer, pH 9.6 overnight at 4°C. The plate was then blocked with 2% BSA in PBS or

coating buffer for 1 hour at room temperature. Plates were washed 5 times with

PBS/Tween 20 (0.05%). Samples of bacterial supernatants or lysed pellets were added to

wells then incubated 1 hour at room temperature. The primary antibody, rabbit anti-Stx2

203αCT69 (a gift from Cheleste Thorpe, M.D., Tufts University), was added to the wells

for 30 minutes followed by secondary antibody, anti-rabbit IgG Fc AP conjugate

(Promega, Madison, WI, USA) for 30 minutes. Freshly prepared para-nitro phenyl

phosphate (Sigma, St Louis, MO, USA) was used as substrate. ODs were read at 405

nm.

Mucus activation assays. Activation assays were performed as previously described

(Melton-Celsa et al., 1996; Melton-Celsa et al., 2002). Briefly, culture supernatants were

incubated with intestinal mucus from the small intestine of a mouse at a final

concentration of 1 mg/ml for 2 hours at 37°C. As a control, a separate sample of each

preparation was treated with HEPES buffer and incubated in the same manner.

Following incubation with mucus or HEPES, protease inhibitor was added and samples

were frozen at -20°C until ready to assay. The cytotoxicity of the samples was then

determined on Vero cells (as previously described in (Melton-Celsa et al., 1996; Melton-

Celsa et al., 2002)). The level of activation was determined by dividing the cytotoxicity

of the mucus-treated sample by the cytotoxicity of the HEPES-treated sample. Data

shown are the averages (±SEM) of at least two activation assays.

Analysis of pedestal formation by *C. rodentium* on cultured cells. Filamentous staining assays (FAS) using *C. rodentium* were done as previously described (Mallick et al., 2012). Briefly, a single colony from each strain was grown in 1 ml media (+/- antibiotic) for 8 hours. Cultures were diluted 1:500 into 5 ml DMEM supplemented with 0.1M HEPES (pH 7.0) (+/- antibiotic) and incubated at 37°C without agitation with 5% CO_2 for 12-15 hours. Cell monolayers were prepared by splitting 95-100% confluent MEFs into 24-well culture plates containing sterile glass coverslips followed by overnight growth at 37°C with 5% CO_2. Prior to seeding onto culture plates, MEFs were maintained in MEF cell culture media (DMEM (hi glucose) + 10% fetal bovine serum (FBS) with penicillin, streptomycin, and glutamine) at 37°C, 5% CO_2. For infections, cell monolayers were washed twice with sterile PBS followed by addition of FAS media containing 25 μl of overnight cultured *C. rodentium* to each well. Plates were spun at 700 g for 10 minutes then incubated at 37°C with 5% CO_2 for 3 hours. After 1.5 hours, plates were spun again at 700 g for an additional 10 minutes then to insure proper bacterial binding to cells. After 3 hours, cells were washed twice with sterile PBS and 0.5 ml pre-warmed FAS media was added to each well followed by an additional 3 hour incubation. Cells were washed 5 times with sterile PBS, fixed with 4% PFA for 30 minutes, washed, permeabilized with 0.1% Triton-X 100, and then stained with Phalloidin (Molecular Probes, Eugene, OR, USA) (1:100) and DAPI (1:500). After washing cells an additional three times with PBS, the coverslips were mounted on slides using ProLong® Gold antifade reagent (Invitrogen, Eugene, OR, USA).

Mouse infections. Mice were purchased from Jackson Laboratories (Bar Harbor, ME, USA) and housed in the UMMS animal facility and protocols were approved by the department of animal medicine. Female, five to eight-week old C57BL/6J mice were gavaged with PBS or ~5 x 10^9 of overnight culture of *C. rodentium* in 100 µl PBS. This dose is used to minimize the potential variability in colonization kinetics observed using lower inoculums (Mallick et al., 2012). Inoculum concentrations were confirmed by serial dilution plating. *C. rodentium* fecal shedding was determined by serial dilution plating of fecal slurries (10% w/v in PBS) on LB or Maconkey agar with selection for kanamycin, chloramphenicol, or kanamycin and chloramphenicol, as appropriate. When using complemented strains containing antibiotics, feces were plated on plates containing both antibiotics. Previously we have tested the rate of plasmid loss by plating on only one antibiotic and determined it was minimal. Fecal water content was evaluated as previously described (Borenshtein et al., 2009). Water content in stool was expressed as the percentage of wet-weight minus dry-weight divided by wet-weight. Fecal occult blood was assessed by Sure-Vue[TM] Fecal Occult Blood Test (Fisher Healthcare, Houston, TX, USA). Fecal occult scores were as follows: 0=no occult blood, 0.5=trace amounts of fecal occult blood, 1=presence of fecal occult blood. Body weights were monitored daily and mice were euthanized if they lost >20% of their body weight. Some mice became moribund or died prior to the scheduled necropsy date, and these mice were necropsied early. Mouse urinalysis was performed by collecting urine into a 1.5 ml conical tube. The urine in the tube was thoroughly mixed and a 2 µl aliquot was pipetted

onto a Chemstrip 4MD urinalysis test strip (Roche Diagnostics, Laval, Quebec). After 60 seconds, the color change on the strip was compared to a supplied color scale. The range of protein measured was 0 – 500 mg/dl, with the scale 0 indicating undetectable protein, 0.5 indicating trace, 1.0 indicating ~30 mg/dl, 2.0 indicating ~100 mg/dl, and 3.0 indicating ~500 mg/dl. The range of hematuria measured was 0, trace, ~50 erythrocytes/µl, and ~250 erythrocytes/ µl. The amount of Kidney injury molecule-1 (KIM-1) in mouse urine was measured using a KIM-1 ELISA kit (Adipo Bioscience, Santa Clara, CA, USA) according to manufacturer's protocols. All experimental groups contained at least five mice. All animal experiments complied with the UMASS IACUC protocols.

Tissue collection and histology. At necropsy distal colon (~0.5 cm) and one kidney were snap frozen in liquid nitrogen and stored at -80°C until RNA or protein isolation. Remaining colon, cecum, longitudinally divided kidneys, spleen, heart, lung, liver, and nasal turbinates were fixed in 10% buffered formalin, dehydrated and embedded in paraffin. Five-micron tissue sections were cut and stained with hematoxylin and eosin (H&E) and/or period acid-Schiff (PAS). Tissue sections were evaluated and scored blindly by a board-certified pathologist (V.V.).

Tissue protein isolation and cytokine analysis. Tissues were homogenized and protein was extracted using the Bio-Plex Cell Lysis Kit (Bio-Rad, Hercules, CA, USA) following manufacturer's instructions. Briefly, 200-500 µl lysis solution was added to sample.

Sample was ground on ice using disposable Kontes tubes and disposable pestle and frozen at -80°C. Sample was then thawed and sonicated (Duty cycle 40, output 6, pulse 18x). Sample was then centrifuged at 4,500 x g for 20 minutes at 4°C. Protein concentration of sample was then determined by BCA assay (Thermo Scientific, Rockford, IL, USA) and protein concentration was adjusted to 2 μg/ml with lysing solution. Cytokine analysis was performed by UMASS mouse phenotyping core facility using the cytokine mouse 23-plex Bio-plex kit (Bio-Rad, Hercules, CA, USA) and Bioplex 200 Luminex machine.

Serum BUN and cytokine analysis. Blood was collected via cardiac puncture at necropsy and allowed to clot on ice for 30 minutes. Blood was spun at 10,000 x g for 15 minutes at 4°C and serum was collected. Serum was spun at 10,000 x g for an additional 15 minutes at 4°C and the remaining serum was collected and frozen at -80°C until analysis. Serum BUN and cytokine (mouse 23-plex Bio-plex kit [Bio-Rad, Hercules, CA, USA]) analysis was performed by UMASS mouse phenotyping core facility using a Cobas analyzer or Bioplex 200 Luminex, respectively.

Transmission electron microscopy. Mouse intestinal tissue samples were taken at various time points post infection and fixed in 2.5% gluteraldehyde in 0.05 M Sodium Phosphate buffer, pH 7.2. Samples were processed and analyzed at the University of Massachusetts Medical School Electron Microscopy core facility according to standard procedures. Briefly, fixed samples were moved into fresh 2.5% gluteraldehyde in 0.05 M

Sodium Phosphate buffer and left overnight at 4°C. The samples were then rinsed twice

in the same fixation buffer and post-fixed with 1% osmium tetroxide for 1 hour at room

temperature. Samples were then washed twice with DH_2O for 20 minutes at 4°C and then

dehydrated through a graded ethanol series of 20% increments, before two changes in

100% ethanol. Subsequently, samples were infiltrated first with two changes of 100%

Propylene Oxide and then with a 1:1 mix of propylene oxide:SPI-Pon 812 resin. The

following day three changes of fresh 100% SPI-Pon 812 resin were done before the

samples were polymerized at 68°C in plastic capsules. The samples were then reoriented

and thin sections were placed on copper support grids and stained with Lead citrate and

Uranyl acetate. Sections were examined using the FEI Tecani 12 BT with 80Kv

accelerating voltage, and images were captured using a Gatan TEM CCD camera.

Statistical analysis. Data were analyzed using GraphPad Prism software. Comparison

of multiple groups was performed using one-way analysis of variance (ANOVA) with

Tukey's multiple comparison post-tests or by using a two-way ANOVA with

Bonferroni's multiple comparison post-tests. Statistical significance of differences

between two groups was evaluated using two tailed unpaired *t* tests. In all tests p values

below 0.05 (*), 0.01 (**), and 0.001 (***) were considered statistically significant. In all

graphs error bars represent standard error of the mean (SEM), unless otherwise indicated.

Nucleotide sequence and accession numbers

stxA from Phage 1720a02: BankIt1463613 Seq1 JN194203

stxB from Phage 1720a02: BankIt1463613 Seq2 JN194204

Supplemental Table 1. Strains used in this study.

Strain	Description and relevant phenotype	Reference
DBS100	*Citrobacter rodentium* wild type strain (prototype TMCH isolate, ATTC 51459, original biotype 4280)	(Barthold et al., 1976; Schauer and Falkow, 1993a)
DBS132	DBS100/pTROY09,Nal^R	(de Vries et al., 1984; Wehmeier et al., 1989)
EC1720a	EC1720a containing Φ1720a-01 and Φ1720a-02.	(Gobius et al., 2003)
JB-13-06	EC1720a containing Φ1720a-02 Δ*Rz*::*cat*, Cm^R	This study
JB-13-28	Φ1720a Δ*Rz*::*cat* Δ*stx$_{2dact}$AB*::*kan*, Cm^R, Km^R	This study
DBS770	DBS100 lysogenized with Φ1720a-02 Δ*Rz*::*cat*, Cm^R	This study
DBS771	DBS100 lysogenized with Φ 1720a-02 Δ*Rz*::*cat* Δ*stx$_{2dact}$AB*::*kan*, Cm^R, Km^R	This study
EDL933	EHEC O157:H7 strain encoding *stx$_1$* and *stx$_2$*	(Riley et al., 1983)
TUV93-0	EDL933 cured of Stx1 and 2-producing phages	(Campellone et al., 2002)
B2F1	O91:H21 serotype containing 2 copies of Stx2d	(Teel et al., 2002)
EH250	EHEC strain containing non-activatable Stx2d toxin	(Pierard et al., 1998)

Nal^R, nalidixic acid resistant
Cm^R, chloramphenicol resistant
Km^R, kanamycin resistant

Supplemental Table 2. Plasmids used in this study.

Plasmids	Description	Reference
pTROY9	expresses LamB, Nal^R, Tet^R	(de Vries et al., 1984; Wehmeier et al., 1989)
pKD46	Expresses lambda Red recombinase; Amp^R	(Datsenko and Wanner, 2000)
pK184	Cloning vector, Km^R	(Jobling and Holmes, 1990)
pMB46	pK184 containing EPEC *tir* promoter - EHEC *tir* - EHEC *cesT*, Km^R in the KpnI and HindIII sites.	This study
pEM123	pMB46ΔEHEC *tir - cesT* with new restriction sites (MluI and SacII), Km^R	This study
pEM129 (pTir)	pEM123 containing *C. rodentium tir – cesT*, Km^R	This study
pDONRzeo	Contains zeocin gene	Invitrogen
pBJK5	pUC-based plasmid containing *cat* cassette flanked by 707 bp upstream and 692 bp downstream of *Rz* in EC1720a in the SphI and SacI site; Cm^R	This study
pBR328	Cloning vector; Amp^R	(Soberon et al., 1980)
pUC18K	Cloning vector; Km^R	(Menard et al., 1993)

Nal^R, nalidixic acid resistant
Tet^R, tetracycline resistant
Amp^R, ampicillin resistant
Km^R, kanamycin resistant
Cm^R, chloramphenicol resistant

Supplemental Table 3. Oligonucleotide sequences used in this study.

Primer	Nucleotide sequence (from 5' to 3')[a]
PanHandle PCR	
F-Adaptor1	CTA ATA CGA CTC ACT ATA GGG CTC GAG CGG CCG CCC GGG CAG GT
R-Adaptor2	/5Phos/ACCTGCCCGG/3AmMC7/
F-AP1 primer	GGA TCC TAA TAC GAC TCA CTA TAG GG
R-AP2 primer	AAT AGG GCT CGA GCG GC
Sequencing of Φ1720a-02 (λ*stx$_{2dact}$*)	
R-Oli210	TGT ACC GTT CAT GCA TGG TG
F-Oli218	ACT GTC TGA AAC TGC TCC TGT G
R-Oli219	CAA ATC CTG AAC CTG ACG CAC AGG
R-Oli220	TTC GGA TGG TTA GGG CGG CT
F-Oli221	CGC TTC AGG CAG ATA CAG AG
F-Oli222	ACG GAC AGA GAT ATC GAC CC
R-Oli223	CTG TAA CTA CAT TGC TGC AC
F-Oli224	ATG AAG TGT ATA TTA TTT AAA TGG GTA CTG TGC CTG
F-Oli226	GGT GCT GAT TAC TTC AGC CAA
F-Oli228	GAA TCC AGT ACA ACG CGC CAC A
Antibiotic marking of Φ1720a-02	
F-425	AAAAAA<u>GCATGC</u>CTGCTGACATATCTGACGAAC
R-426	AAAAAA<u>GGATCC</u>TTTGTAGGTGATGGCGTTATC
R-427	AAAAAA<u>GAGCTC</u>ATATCAATAACTTACACTGGT
F-259	AAAAAA<u>GGATCC</u>GCGCAGCGCGATAAAAAAGCC
F-265	AAAAA<u>GGATCC</u>TTCGAATAAATACCTGTGACGGAAGATCAC
R-266	AAAAA<u>GGATCC</u>TTCGAATTTCTGCCATTCATCCGCTTATTA
Stx-deletion within Φ1720a-02Δ*Rz*::*cat*	
F-2dH1	CGT CAC TCA CTG GTT TCA TCA TAT CTG GCG TCC GGG GTG ACT AAC TAG GAG GAA TAA ATG
F-498	GGC GCG TTT TGA CCA TTT CGT TTG ATT
R-2dH2	TGA TTT GAT TGT TAC CGT CAT TCC TGT TAA TCC CCG GGT CAT TAT TCC CTC CAG GTA CTA
R-2dH1AP	CAT TTA TTC CTC CTA GTT AGT CAC CCG GAC GCC AGA TAT GAT GAA ACC AGT GAG TGA CG
F-2dH2AP	TAG TAC CTG GAG GGA ATA ATG ACC GGG GGA TTA ACA GGA ATG ACG GTA ACA ATC AAA TCA
R-499	CTG TGA CGC TGA TAT GCC CCG CCG CTC
F-316	CTC AGG GGA CCA CAT CGG
R-398	GCC GCC CTG ACC ACA TCG
Generation of pTir	

F-MluI-Cr-tirU	CAT CAT <u>ACG CGT</u> ATG CCT ATT GGT AAT CTT GGT AAT AAT AAT ATA AGT AAC
R-SacII-Cr-tirL	CAT CAT <u>CCG CGG</u> GTT ATA GGC TCC ACC ACA ATG AGT TAG AAT GAG TAG TAA

[a]F, forward (top strand) primer; R, reverse (bottom strand) primer. Restriction sites are underlined.

[b]Primers used to construct *C. rodentium*Δ*tir*. Italicized regions indicate homology to zeocin cassette. Numbers in primer name correspond to nucleotide positions primer is located within *tir* gene. Int represents screening primers internal to the gene (*tir* or *zeocin*) and Ext represents screening primers that are external to the gene.

Results

Cultured *C. rodentium* (λ*stx$_{2dact}$*), a *C. rodentium* strain lysogenized with a λ Stx phage, produces mucus-activatable Stx2dact at levels comparable to STEC.

EC1720a, a STEC strain originally isolated from ground beef, has previously been shown to contain an Stx2dact-producing phage, Φ1720a-01 (Gobius et al., 2003). We identified and isolated an additional phage in this strain, Φ1720a-02. The sequences of *stxA* and *stxB* of Φ1720a-02 were determined and the inferred protein sequences of the StxA and StxB subunits of Φ1720a-02 were aligned with other Stx2-producing bacteriophages isolated from *E. coli* strains (**Supplementary Figure 1A and B**). The predicted amino acid sequences of *stx$_2$A* and *stx$_2$B* of Φ1720a-02 aligned well with non-mucus activatable Stx2d (Pierard et al., 1998) (**Supplementary Figure 1A and B**) and contained the C-terminal glutamic acid necessary for activation of Stx2dact (Melton-Celsa et al., 2002).

In order to facilitate the generation of lysogens of Φ1720a-02, a chloramphenicol resistance cassette (*cat*, Cm^R) was inserted into the *Rz* locus of Φ1720a-02. *C. rodentium* DBS100 (Schauer and Falkow, 1993a) (referred herein as "*C. rodentium*") was lysogenized with Φ1720a-02 *Rz*::*cat* to create *C. rodentium* DBS100 (Φ1720a-02 *Rz*::*cat*), which, for simplicity, we herein refer to as "*C. rodentium* (λ*stx$_{2dact}$*)". In addition, a *C. rodentium* lysogen of an Stx-deficient control phage, λ*stx$_{2dact}$*::*kan^R* was also generated (see **Materials and Methods**).

To test if *C. rodentium* (λ*stx$_{2dact}$*) was able to produce Stx2 upon *in vitro* growth, the level of Stx2 was quantified by enzyme-linked immunosorbent assay (ELISA).

A

```
              10        20        30        40        50        60        70        80        90       100
               *         *         *         *         *         *         *         *         *         *
Stx2       MKCILFKWVLCLLLGFSSVSYSREFTIDFSTQQSYVSSLNSIRTEISTPLEHISQGTTSVSVINHTPPGSYFAVDIRGLDVYQARFDHLRLIIEQNNLYV
Stx2c      ....................................................................................................
Stx2d      .....L.....................................C........................................................
Stx2d_act  ....................................................................................................
Stx2e      .....L..I...........Q....................A..........A...............IS.G........E.............R.....
Φ1729a-02  .......................M............................................................................

              110       120       130       140       150       160       170       180       190       200
               *         *         *         *         *         *         *         *         *         *
Stx2       AGFVNTATNTFYRFSDFTHISVPGVTTVSMTTDSSYTTLQRVAALERSGMQISRHSLVSSYLALMEFSGNTMTRDASRAVLRFVTVTAEALRFRQIQREF
Stx2c      ....................................................................................................
Stx2d      ...............A.................................................................A...................
Stx2d_act  ....................................................................................................
Stx2e      ......T..........A...L....I.........................................................................
Φ1729a-02  ....................................................................................................

              210       220       230       240       250       260       270       280       290       300
               *         *         *         *         *         *         *         *         *         *
Stx2       RQALSETAPVYTMTPGDVDLTLNWGRISNVLPEYRGEDGVRVGRISFNNISAILGTVAVILNCHHQGARSVRAVNEESQPECQITGDRPVIKINNTLWES
Stx2c      ....................................................................................................
Stx2d      .L...............EE................F...G.................................S....I................RL......
Stx2d_act  ....................................................................................................
Stx2e      .L...............E................A.................................................................
Φ1729a-02  .................EE................F................................................................

              310
               *
Stx2       NTAAAFLNRKSQFLYTTGK
Stx2c      ..................
Stx2d      .........RAHS.N.S.E
Stx2d_act  ............S.....E
Stx2e      ............S.....E
Φ1729a-02  .........RAHS.N.S.E
```

B

```
                10        20        30        40        50        60        70        80
                 *         *         *         *         *         *         *         *
Stx2        MKKMFMAVLFALASVNAMAADCAKGKIEFSKYNEDDTFTVKVDGKEYWTSRWNLQPLLQSAQLTGMTVTIKSSTCESGSGFAEVQFNND
Stx2c       ...........V.......................N.....A...................................................
Stx2d       ...I.V.A...FV......................N.....A.....N.....................N..A...........--
Stx2d_act   ...........V.......................N.....A...................................................
Stx2e       .....I.....V......................N.....S.R....N....................I.N..S......Q.K..--
Φ1720a-02   ...I.V.A...FV......................N.....A.....N.....................N..A...........—
```

Supplementary Figure 1. Amino acid alignment of Stx A and B subunits of φ1720a-02 from *C. rodentium* (λ*stx2dact*) with other Stx A and B subunits from various STEC strains. The A **(A)** or B **(B)** subunits of Φ1720a-02 (for simplicity termed "λ*stx2dact*" in this study) were aligned with the corresponding subunits of Stx2 from EDL933 (Genbank accession number X078655), Stx2c from E32511 (Genbank accession number M59432), Stx2d from EH250 (Genbank accession number AF043627), Stx2dact (formerly called Stx2vhb) from B2F1 (Genbank accession number AF479829), and Stx2e from S1191 (Genbank accession number M21534). The sequences were aligned using the Align Plus 5 program, version 5.03 (Scientific & Educational Software, Durham, NC, USA) following the global-ref alignment procedure (Myers and Miller, 1988) and the scoring matrix BLOSUM 62 (Henikoff and Henikoff, 1992). The underlined regions indicate the processed signal sequence, dots depict identical residues, green or red letters highlight conserved or non-conserved residues respectively, and a red dash indicates a gap in the alignment.

Spontaneous prophage induction is predicted to release toxin into culture supernatants, so supernatants and bacterial pellets were analyzed separately. EDL933, an EHEC O157:H7 strain that harbors both stx_1 and stx_2 (Riley et al., 1983), produced high levels of Stx2 in both the supernatant and pellet (**Figure 1, solid bars**). In contrast, TUV93-0, the stx_1- and stx_2-deficient derivative of EDL933 (Campellone et al., 2002) was completely unable to produce Stx2 (**Figure 1**). EC1720a, which harbors Φ1720a-01 and Φ1720a-02, produced easily detectable levels of Stx2 in both supernatant and pellet, albeit several orders of magnitude lower than those found for EDL933, suggesting that baseline expression and/or prophage induction is lower in EC1720a compared to EDL933 (**Figure 1, solid bars**). Importantly, *C. rodentium* (λstx_{2dact}) produced high levels of Stx2, the vast majority of which was present in the culture supernatant (**Figure 1, solid bars**). *C. rodentium* ($\lambda stx_{2dact}::kan^R$) did not produce detectable toxin, a finding that indicates that, as predicted, Stx production by this strain required an intact stx_{2dact} gene (**Figure 1**).

Induction of the Stx-producing prophage often promotes high-level production of Stx by EHEC strains (Muhldorfer et al., 1996; Schmidt, 2001; Waldor and Friedman, 2005), so each of the above bacterial strains were treated with mitomycin C to induce lysogenic phage. Compared to uninduced samples, cultures of EDL933, EC1720a, and *C. rodentium* (λstx_{2dact}) treated with mitomycin C produced several orders of magnitude more Stx2, particularly in the supernatant, consistent with lytic induction of the *stx*-encoding prophage (**Figure 1, open bars**). Strain TV93-0 and *C. rodentium* ($\lambda stx_{2dact}::kan^R$) did not produce any Stx upon mitomycin C treatment, a finding that indicates the predicted requirement of phage-encoded Stx for toxin production. Notably,
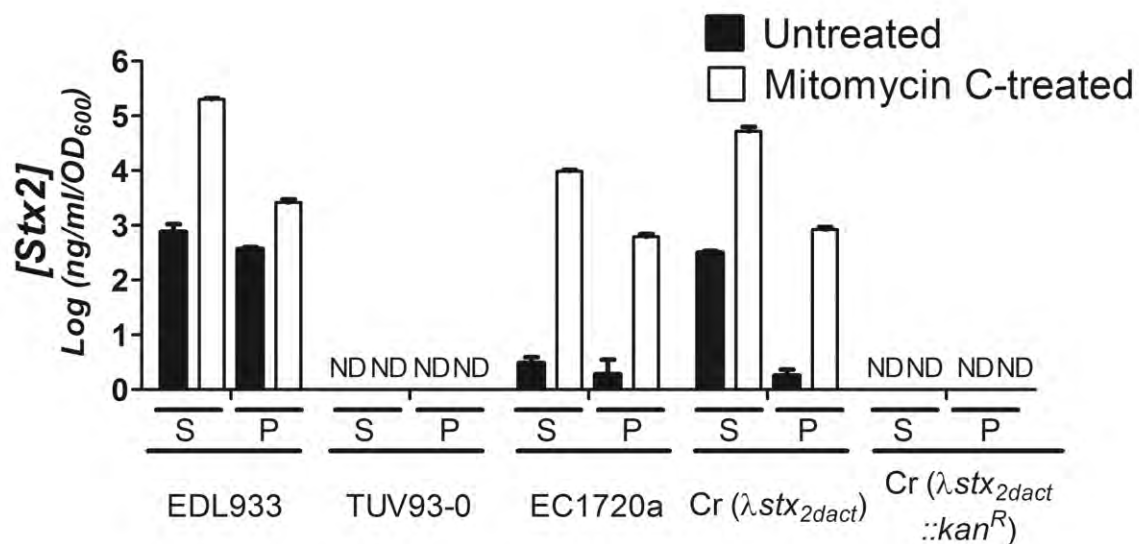
Figure 1. *C. rodentium* (λ*stx_{2dact}*) **produces high levels of Shiga toxin upon prophage induction at levels comparable to EHEC isolates.** Stx2 in supernatants ("S") or pellets ("P") of untreated (filled bars) or mitomycin C-treated (open bars) cultures of the indicated strains was measured by capture ELISA and is expressed relative to bacterial number (see **Materials and Methods**). Shown are the averages ± SEM of quadruplicate samples. ND, not detected. Data are representative of one of three independent experiments.

the levels of Stx produced by *C. rodentium* (λ*stx₂dact*) were comparable to or higher than the levels generated by the EHEC or STEC strains EC1720a and EDL933, suggesting that this strain might produce Stx-mediated disease upon animal infection.

Because λ*stx₂dact* encodes an Stx allele that contains the C-terminal glutamic acid necessary for activation of Stx2dact (Melton-Celsa et al., 2002), we tested the capacity of the toxin produced by *C. rodentium* (λ*stx₂dact*) to be activated in the presence of intestinal mucus. Strains B2F1, which encodes the mucus-activatable toxin Stx2dact, and EH250 which encodes the non-activatable Stx2d were used in parallel assays as positive and negative controls, respectively (Melton-Celsa et al., 2002; Pierard et al., 1998; Teel et al., 2002). Culture supernatants from each strain were incubated with murine intestinal mucus or with buffer alone, and the Vero cell cytotoxicity of serially diluted samples was determined. Toxin activity in culture supernatants from *E. coli* strain B2F1 increased ~15-fold upon incubation with murine mucus (**Table 1**). In contrast, there was minimal increase in the presence of the mucus in toxin activity of EH250, which does not contain mucus-activatable toxin (**Table 1**). Toxin activity in the culture supernatant of *C. rodentium* (λ*stx₂dact*) increased approximately ~18-fold, comparable to the activity of *E. coli* B2F1, upon incubation with mucus indicating that the Stx produced by λ*stx₂dact* is indeed mucus-activatable (**Table 1**).

Table 1. Stx2d from *C. rodentium* (λstx_{2dact}) is mucus activatable.

Strain	Fold activation	Range	n
Cr (λstx_{2dact})	17.9 ($\pm$ 5.3)*	5.4-31	4
B2F1	15.2 ($\pm$ 2.9)*	11.7-21	3
EH250	1.2 ($\pm$ 0.1)	1.1-1.3	2

Supernatant from *C. rodentium* (λstx_{2dact}), B2F1 (as a positive control), and EH250 (as a negative control) were tested for Vero Cell cytotoxicity in the presence or absence of mouse intestinal mucus. Shown here are the average fold-increases in cytotoxicity ($\pm$ SEM) with the addition of mouse intestinal mucus compared to supernatants incubated with buffer alone. n represents the number of replicates performed for each strain tested. Statistical significance was determined using a one-way ANOVA. "*" ($p<0.05$) indicates a statistically significant difference compared to the increase in activation of EH250 in the presence of intestinal mucus.

C. rodentium (λ*stx_{2dact}*) causes lethal infection in mice.

To determine whether *C. rodentium* (λ*stx_{2dact}*) would provide an Stx-mediated disease model, five-to-eight-week old C57BL/6 mice were infected with approximately 1 x 10^9 CFU of this strain via oral gavage. As controls, the Stx-deficient derivative *C. rodentium* (λ*stx_{2dact}::kan^R*) and the parental nonlysogen *C. rodentium* DBS100 were inoculated in parallel. Fecal shedding of *C. rodentium* DBS100 and *C. rodentium* (λ*stx_{2dact}::kan^R*) reached approximately 10^9 CFU per gram of feces at day six post-infection and remained relatively constant to the end of monitoring, ten days post-infection (**Figure 2A**). *C. rodentium* (λ*stx_{2dact}*) colonized the feces with similar kinetics, reaching a peak of ~10^{10} CFU per gram, which was not significantly higher than the two non-toxigenic strains (**Figure 2A**).

To test whether mice infected with *C. rodentium* (λ*stx_{2dact}*) suffer Stx-mediated intestinal disease, we monitored fecal water content. As expected, feces from uninfected mice contained 45-60% water throughout the course of infection (**Figure 2B**). Feces from mice infected with *C. rodentium* DBS100 or *C. rodentium* (λ*stx_{2dact}::kan^R*) contained similar values of water content through approximately day four post-infection, but demonstrated elevated and progressively increasing levels of water after maximal bacterial burden was reached on day four post-infection, as previously observed (Borenshtein et al., 2009). In contrast, water content of feces from mice infected with *C. rodentium* (λ*stx_{2dact}*) was significantly elevated (>70%) at four days post-infection (**Figure 2B**), indicating that the production of Stx was associated with an early increase in fecal water content. By eight days post-infection, fecal water content declined to
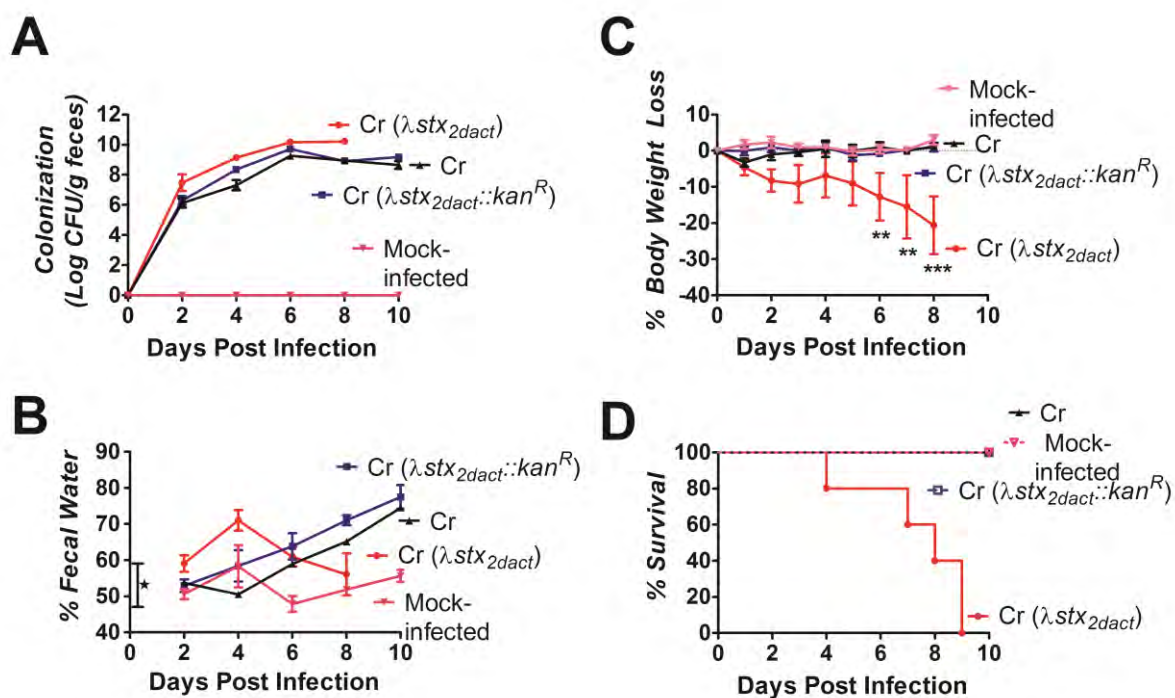
Figure 2. *C. rodentium* (λ*stx₂dact*) **causes a lethal infection in mice.** **(A)** Colonization of five-week old C57BL/6 mice by *C. rodentium* (λ*stx₂dact*), *C. rodentium* (λ*stx₂dact::kanᴿ*), and *C. rodentium* (DBS100) was determined by viable stool counts. Shown are the averages CFU (± SEM) of five mice. **(B)** Fecal water content of mock-infected five-week old mice or mice infected with *C. rodentium* (λ*stx₂dact*), *C. rodentium* (λ*stx₂dact::kanᴿ*), or *C. rodentium* (DBS100). Shown are the averages (±SEM) of groups of five mice. Range of average fecal water content of uninfected mice is represented by vertical bar at zero days post-infection. "*" ($p<0.05$) indicates a statistically significant difference from all other groups as determined by two-way ANOVA followed by Bonferroni post-tests. **(C)** Body weight during infection of eight-week old mice, expressed as percent change from day zero body weight. Shown are the averages (±SEM) of five mice per group. "**" ($p<0.01$) and "***" ($p<0.001$) indicate a statistically significant difference from all other groups as determined by two-way ANOVA followed by Bonferroni post-tests. **(D)** Percent survival of groups of five eight-week old mice that were mock-infected or infected with *C. rodentium* (λ*stx₂dact*), *C. rodentium* (λ*stx₂dact::kanᴿ*), or *C. rodentium* (i.e., DBS100). Statistical significance was determined using a Chi squared test and in this panel, *C. rodentium* (λ*stx₂dact*) is significantly different from all other groups ($p<0.05$). For all panels, results are representative of one of at least five independent experiments.

normal values, which could be due to the putative increasing dehydration and concomitant water reabsorption that may occur in these mice during later stages of infection (see **Figure 2C**).

Weight loss is a notable feature in mice after Stx injection or infection in mice with an intact commensal flora with high doses of STEC (Keepers et al., 2006; Mohawk and O'Brien, 2011; Sauter et al., 2008). We found that mock-infected mice, as well as mice infected with *C. rodentium* DBS100 or *C. rodentium* ($\lambda stx_{2dact}::kan^R$), maintained body weight, indicating that infection with *C. rodentium* strains that do not produce Stx were not associated with weight loss (**Figure 2C**). In contrast, mice infected with *C. rodentium* (λstx_{2dact}) lost >10% of their starting weight by six days post-infection and >20% by eight days post-infection.

Finally, the severe weight loss in mice infected with *C. rodentium* (λstx_{2dact}) corresponded temporally with mortality or severe disease warranting euthanasia (**Figure 2D**). Mock-infected mice, or mice infected with *C. rodentium* DBS100 or *C. rodentium* ($\lambda stx_{2dact}::kan^R$), suffered no mortality. In contrast, mortality was observed in mice infected with *C. rodentium* (λstx_{2dact}) starting at day four post-infection, and no mice survived past day nine. Consistent with the previous correlation between weight loss and serious systemic disease (Keepers et al., 2006; Mohawk and O'Brien, 2011; Sauter et al., 2008), nearly all (~95%) of mice that died or were euthanized had lost >20% body weight at the preceding weight assessment (data not shown).

Stx-mediated intestinal damage during murine infection with *C. rodentium* (λ*stx₂dact*).

Although EHEC infection of humans is associated with hemorrhagic colitis, EHEC infection of streptomycin pre-treated or gnotobiotic mice does not typically result in obvious AE lesion formation or striking intestinal damage (Eaton et al., 2008; Lindgren et al., 1993), A.M. unpublished observations). To assess the presence of hemorrhagic colitis in mice infected with *C. rodentium* (λ*stx₂dact*), we collected feces throughout infection and assessed for the presence of occult blood (see **Materials and Methods**). Interestingly, we observed occult blood in mice infected with either *C. rodentium* (λ*stx₂dact*) or the non-toxigenic control strain *C. rodentium* (λ*stx₂dact*::kan^R) from approximately three-to-four days post-infection and throughout the remaining infection until the mice either succumbed to lethal disease (those infected with *C. rodentium* (λ*stx₂dact*)) or cleared infection (those infected with *C. rodentium* (λ*stx₂dact*::kan^R)) (**Supplementary Figure 2**).

To assess the presence of AE lesions in mice infected with *C. rodentium* (λ*stx₂dact*), we examined colonic tissue by transmission electron microscopy (TEM) at six days post-infection. Indeed, intimate bacterial attachment, microvillar effacement, and robust actin pedestals were produced on the intestinal epithelium of mice infected with *C. rodentium* (λ*stx₂dact*) in contrast to the normal intestinal architecture observed in mock-infected mice (**Figure 3A**). To investigate intestinal disease caused by infection with *C. rodentium* (λ*stx₂dact*), the large intestines of mice infected with *C. rodentium* (λ*stx₂dact*) for seven-to-ten days were examined histologically. In accordance with previous studies, we
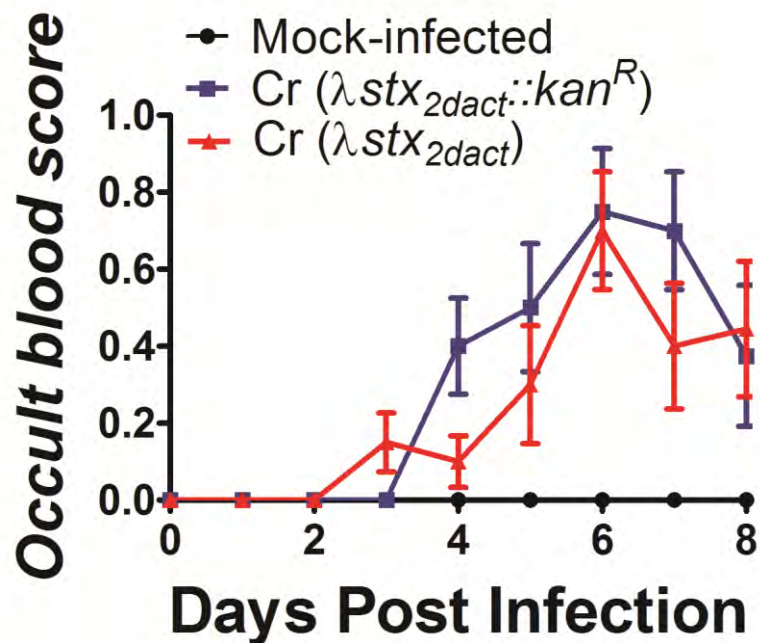
Supplementary Figure 2. Infection by *C. rodentium* (λ*stx₂dact*) and *C. rodentium* (λ*stx₂dact*::*kan^R*) results in the presence of fecal occult blood. Fecal samples were collected from mice daily throughout infection and assessed for the presence of occult blood. Occult blood scores were assigned as follows: 0=no occult blood, 0.5=trace amounts of occult blood, and 1=presence of occult blood. Data are representative of the average fecal occult blood scores (±SEM) of groups of ten mice infected with either *C. rodentium* (λ*stx₂dact*) or *C. rodentium* (λ*stx₂dact*::*kan^R*) or mock-infected.
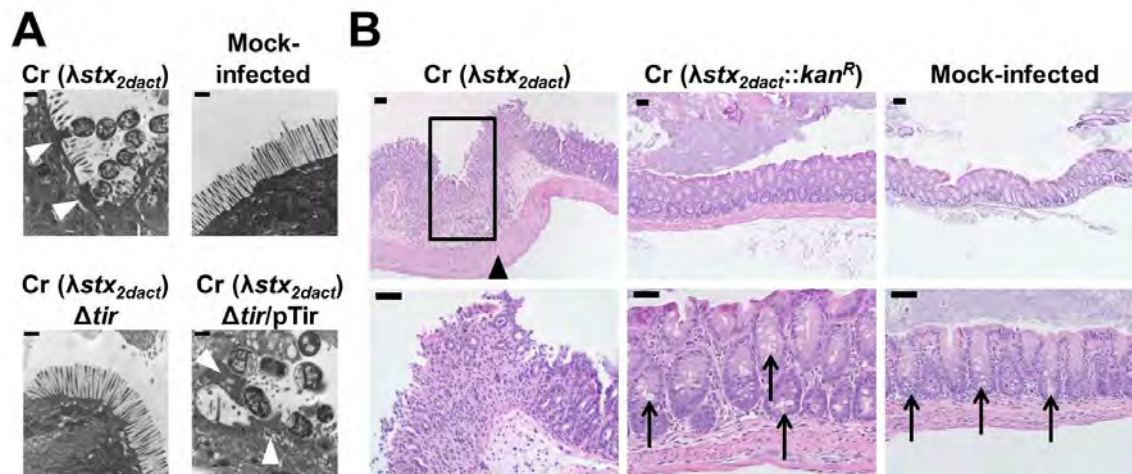
Figure 3. Stx-mediated intestinal damage during murine infection with *C. rodentium* (λ*stx₂dact*). **(A)** Transmission electron microscopy of the proximal large intestine of C57BL/6 mice six days after mock-infection or infection by the indicated strain. White arrowheads indicate the presence of actin-rich pedestals. Scale bars measure 0.5 μm. **(B)** H&E-stained large intestinal sections of mock-infected mice or mice infected with designated strain are shown under 100x (top row) or 400x (bottom row) magnification. Scale bars measure 50 μm. Black box indicates area of complete crypt loss and abscess formation. Black arrows depict goblet cells that are prominent in normal intestinal tissue and diminished in mice infected with *C. rodentium* (λ*stx₂dact*). Arrow head indicates infiltration of inflammatory cells into the mucscularis mucosa and muscularis propria layers.

observed that at seven-to-ten days post-infection, mice infected with *C. rodentium*

DBS100 or *C. rodentium* ($\lambda stx_{2dact}::kan^R$) showed limited intestinal pathology, with only

minimal hyperplasia and inflammatory infiltrates compared with mock-infected mice

(data not shown and **Figure 3B, middle and right panels**). *C. rodentium* infection

results in colonic hyperplasia, but this manifestation typically is observed only after

approximately 14 days of infection ((Luperchio and Schauer, 2001; McBee et al., 2008),

and was not observed here). In contrast, gross evaluation of intestines from mice infected

for seven-to-ten days with *C. rodentium* (λstx_{2dact}) showed severe destruction of the

intestinal mucosa, colitis, and acute ischemic injury, with neutrophil infiltration into the

muscularis layer and lamina propria, and intestinal abscesses (**Figure 3B, left panels**).

Also present were areas of necrosis and degenerative changes in the epithelial cells, with

crypt withering, and an overall loss of goblet cells (**Figure 3B, left panels**). These data

show that *C. rodentium* (λstx_{2dact}) infection is associated with AE lesion formation and

severe Stx-mediated intestinal damage.

Stx-mediated systemic induction of pro-inflammatory cytokines during murine

infection with *C. rodentium* (λstx_{2dact}).

Serum pro-inflammatory cytokines and chemokines are elevated in both humans

suffering HUS and mice intoxicated with Stx (Keepers et al., 2007; Keepers et al., 2006;

Proulx et al., 2001; Ray and Liu, 2001; Rovin and Phan, 1998; Sauter et al., 2008). We

measured 23 cytokines in the sera of mice infected with *C. rodentium* (λstx_{2dact}) between

seven and ten days post-infection (see **Materials and Methods**). We found that
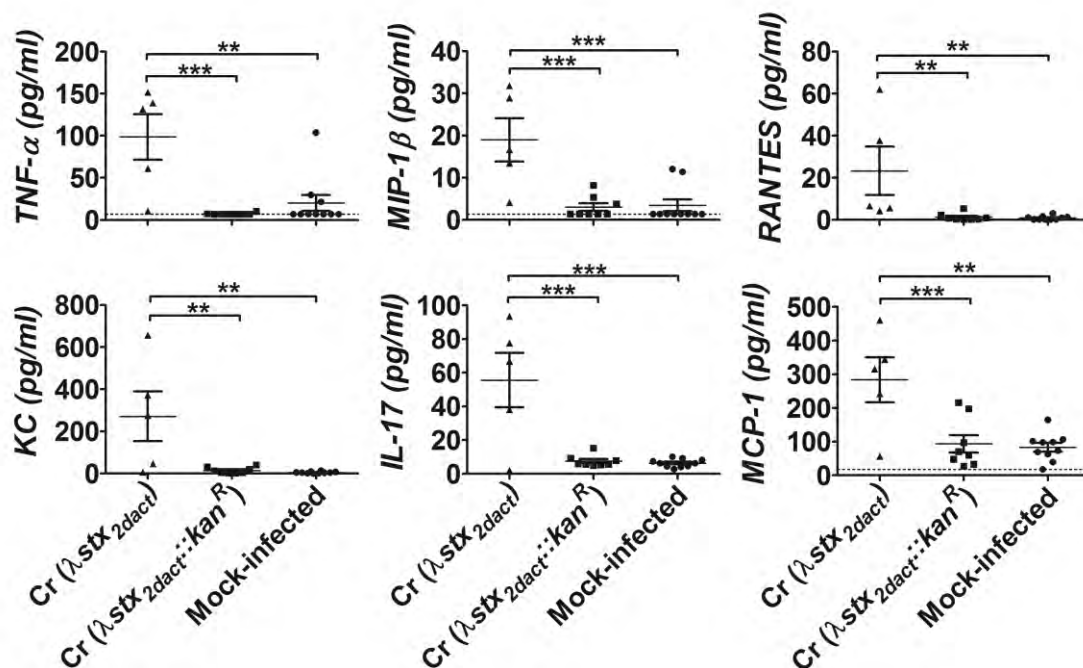
Figure 4. Stx-mediated systemic induction of proinflammatory cytokines during murine infection with _C. rodentium_ (λ*stx₂dact*). The concentrations of TNF-α, IL-17, KC, RANTES, MCP-1, and MIP-1β in serum at seven-to-ten days post-infection in mock-infected mice or mice infected with the indicated strain was determined by Luminex (see **Materials and Methods**). Data are pooled from two independent experiments, each using three- to eight-week old female mice and five to ten mice per group. (Note: many of the mice infected with _C. rodentium_ (λ*stx₂dact*) that had extremely elevated levels of serum cytokines were those on the verge of death (e.g. had >15% body weight loss, high-level colonization, ruffled fur, and needed to be sacrifice because of severe disease.) Statistical significance was determined by one-way ANOVA and Tukey's Multiple Comparison Tests. "*" ($p<0.05$), "**" ($p<0.01$), and "***" ($p<0.001$) indicate statistically significant differences between the two groups. Dotted line in the graphs represents the limit of detection.

cytokines commonly associated with disease in humans and animal models of HUS were reproducibly elevated relative to mock-infected mice. Serum levels of the pro-inflammatory cytokine TNF-α were elevated, as were the neutrophil chemoattractants IL-17 and KC (**Figure 4**). Additionally, macrophage/monocyte chemoattractants RANTES, MCP-1, and MIP-1β were elevated two- to five-fold in serum from *C. rodentium* (λstx_{2dact}) infected mice relative to mock-infected mice (**Figure 4**). In all instances, the cytokine or chemokine levels of mice infected with *C. rodentium* (λstx_{2dact}) were significantly higher than those of mice infected with *C. rodentium* ($\lambda stx_{2dact}::kan^{R}$) (**Figure 4**), indicating that induction of the cytokines/chemokines was attributable to the production of Stx2dact rather than to simple colonization by *C. rodentium*.

Stx-mediated renal damage during murine infection with *C. rodentium* (λstx_{2dact}).

Kidney damage is a hallmark of HUS and Stx causes renal pathology in mice after direct injection or upon absorption from intestinal STEC (Keepers et al., 2006; Lindgren et al., 1993; Mohawk and O'Brien, 2011; Sauter et al., 2008). Renal cytokines and chemokines are elevated in murine models of Stx intoxication, therefore we measured cytokine and chemokine levels in the kidneys of mice infected with *C. rodentium* (λstx_{2dact}) at seven-to-ten days post-infection. Although the levels of the cytokines IL-6 and G-CSF varied considerably from mouse to mouse, they were significantly increased in the kidneys of mice infected with *C. rodentium* (λstx_{2dact}) compared to mock-infected controls, as were the chemokines RANTES and KC (**Figure 5A**). In all cases, the increase in levels with respect to mock-infected mice was strictly associated with the

production of Stx2dact, because infection by *C. rodentium* ($\lambda stx_{2dact}::kan^R$) was not associated with any significant elevation of cytokine/chemokine levels (**Figure 5A**). Furthermore, the increase in renal IL-6 and RANTES was at least in part a reflection of increased transcription of the corresponding genes, because RT-PCR analysis of kidney mRNA revealed increased levels of IL-6 and RANTES mRNA relative to mock infected mice or mice infected with by *C. rodentium* ($\lambda stx_{2dact}::kan^R$) (data not shown).

Stx intoxication of mice results in damage to the renal distal tubules (Keepers et al., 2006; Psotka et al., 2009; Sauter et al., 2008). To evaluate renal pathology associated with the *C. rodentium* (λstx_{2dact}) infection model, kidney sections were taken between seven and ten days post-infection from mice infected with *C. rodentium* (λstx_{2dact}) and were stained with hematoxylin/eosin (H&E) and Periodic acid-Schiff (PAS) stain. Whereas the kidneys of mice infected with *C. rodentium* ($\lambda stx_{2dact}::kan^R$) or mock-infected showed no signs of damage (**Figure 5B, middle and lower panel**), kidneys of mice infected with *C. rodentium* (λstx_{2dact}) showed proximal tubule damage (**Figure 5B, upper panel**). The epithelial lining of the tubules were attenuated or flattened, with prominent pyknotic nuclear material, loss of luminal brush border, and sloughing of dead cells in the tubular lumen (**Figure 5B, upper panel, arrow heads**). Mitotic activity, indicating regenerative repopulation of the proximal tubules, was also observed in some mice (data not shown).

To assess renal function in mice infected with *C. rodentium* (λstx_{2dact}) in our model of HUS, we measured blood urea nitrogen (BUN). To assess BUN during the
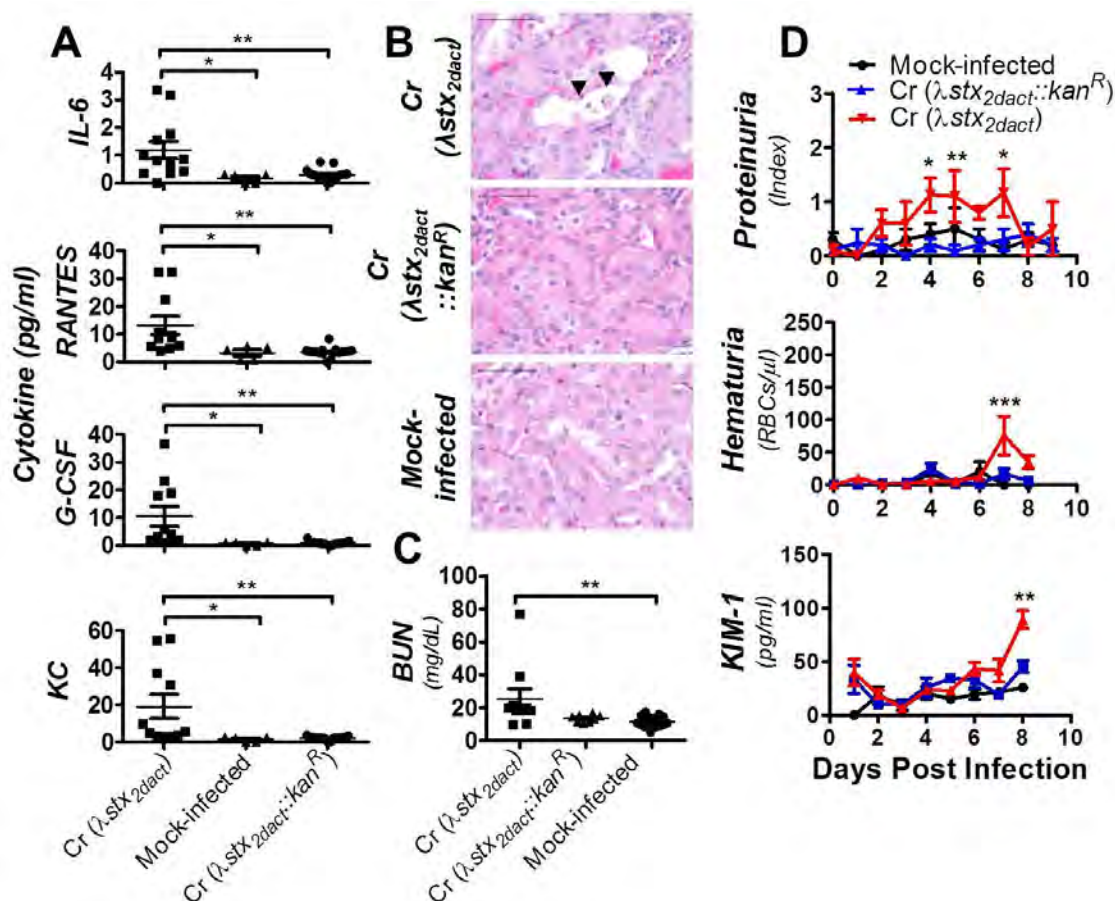
Figure 5. Stx-mediated renal damage during murine infection with *C. rodentium* (λ*stx$_{2dact}$*). (A) Renal cytokines were measured in mock-infected eight-week old female mice or mice infected with the indicated strain. Data are pooled from three independent experiments. Statistical significance was determined by one-way ANOVA followed by Tukey's Multiple Comparison Test; "*" ($p<0.05$) and "**" ($p<0.01$). **(B)** 600x micrograph of H&E staining of kidney sections taken from mock-infected mice or mice infected with the indicated strain at seven-to-ten days post-infection. Arrowheads indicate attenuation and sloughing of epithelial cells within the proximal tubules. Scale bars measure 50 μm. **(C)** Blood urea nitrogen (BUN) of eight-week old, female mice infected with indicated strain or mock-infected mice at day of necropsy, between seven and ten days post-infection. Each data point represents BUN from a single mouse, and shown is the pool of four independent experiments using five eight-week old mice per group. Statistical significance was determined using a one-way ANOVA followed by Tukey's Multiple Comparison Test (**$p<0.01$). **(D)** Urine protein content was measured daily in mock-infected eight-week old, female mice or mice infected with the indicated strain. Data shown are average protein indices (see **Materials and Methods**) ± SEM of five mice per group. Data shown represents one independent experiment that was repeated five times. Statistical significance was determined using a two-way ANOVA and Bonferroni post-tests; "*" ($p<0.05$) and "**" ($p<0.01$) indicate a statistically

significant difference compared to *C. rodentium* (λ*stx$_{2dact}$::kan^R*). Hematuria was measured (see **Materials and Methods**) in mock-infected mice or mice infected with *C. rodentium* (λstx$_{2dact}$) or *C. rodentium* (λ*stx$_{2dact}$::kan^R*) and data are represented as the averages ($\pm$SEM) amounts of erythrocytes/µl urine in groups of ten mice. Statistical significance was measured using a two-way ANOVA and Bonferroni's post-tests. "***" (p<0.001) indicates a statistically significant difference compared to the other groups. Urine Kim-1 concentrations were measured in mock-infected mice or mice infected with *C. rodentium* (λstx$_{2dact}$) or *C. rodentium* (λ*stx$_{2dact}$::kan^R*) and data are represented as the averages ($\pm$SEM) pg/ml of Kim-1 urine in groups of three-to-six mice. Statistical significance was measured using a two-way ANOVA and Bonferroni's post-tests. "**" (p<0.01) indicates a statistically significant difference compared to the other groups.

phase of terminal illness, we euthanized individual mice when they demonstrated signs of serious disease (see **Materials and Methods**), which occurred seven-to-ten days post-infection. In cases where mice were euthanized prior to ten days post-infection (due to severe disease), a mouse from the mock-infected group and *C. rodentium* ($\lambda stx_{2dact}::kan^R$) group were euthanized and analyzed in parallel. The mean BUN of mice infected with *C. rodentium* (λstx_{2dact}) was significantly (p<0.01) elevated relative to mock-infected mice, and was also elevated relative to mice infected with *C. rodentium* ($\lambda stx_{2dact}::kan^R$), although the latter comparison did not reach statistical significance (**Figure 5C**). Renal tubular damage, with both leakage of protein and sloughing of cells into the lumen, may result in proteinuria, which we measured using a colorimetric assay (see **Materials and Methods**). Whereas the urine of mock-infected mice or mice infected with *C. rodentium* ($\lambda stx_{2dact}::kan^R$) contained no or only trace levels of protein (protein index of 0-0.5 indicating <50 mg/dl) and was not statistically different from protein content of urine from mock-infected mice, the urine of mice infected with *C. rodentium* (λstx_{2dact}) contained significantly elevated protein indices as early as two days post-infection (**Figure 5D**). Between four and seven days post-infection, average urine protein indices were as high 1 to 1.5 (corresponding to approximately 50-100 mg/dl), indicating that infection by *C. rodentium* (λstx_{2dact}) results in functional renal compromise. Additional renal compromise in mice infected with *C. rodentium* (λstx_{2dact}) was evident from the presence of hematuria and increased levels of a renal tubule-specific biomarker, Kidney injury molecule-1 (Kim-1) specifically late in infection compared to mock-infected mice or mice infected with *C. rodentium* ($\lambda stx_{2dact}::kan^R$) (**Figure 5D**).

Given the presence of systemic disease, including specific intestinal and renal damage, we next evaluated histology of other tissues to investigate their involvement with disease upon infection by *C. rodentium* (λstx_{2dact}). Mice were either mock-infected or infected with *C. rodentium* (λstx_{2dact}) or *C. rodentium* ($\lambda stx_{2dact}::kan^R$), and spleen, heart, lung, liver, and nasal turbinates were evaluated histologically. The spleens of mice infected with *C. rodentium* (λstx_{2dact}) or *C. rodentium* ($\lambda stx_{2dact}::kan^R$) both showed reactive germinal center formation and germinal center hyperplasia with large follicles (**Supplemental Figure 3A**). More germinal center activity, depicted by evident cell turnover was observed in the spleens of mice infected with *C. rodentium* (λstx_{2dact}), consistent with a shift to a state of reactive extramedullary hematopoiesis (EMH) (**Supplemental Figure 3A**). A more robust germinal center hyperplasia was observed in mice infected with *C. rodentium* ($\lambda stx_{2dact}::kan^R$), which is consistent with evidence of gross splenomegaly (~30% increase in size compared to mice infected with *C. rodentium* (λstx_{2dact}) (**Supplemental Figure 3A**). Histological examination of both the lungs and the heart revealed no abnormal pathology in mice infected with either *C. rodentium* (λstx_{2dact}) or *C. rodentium* ($\lambda stx_{2dact}::kan^R$) (**Supplementary Figure 3B, C**). In contrast, the livers of mice infected with *C. rodentium* (λstx_{2dact}) or *C. rodentium* ($\lambda stx_{2dact}::kan^R$) revealed foci of neutrophilic and lymphocytic inflammation as well as scattered hepatocellular death (**Supplementary Figure 3D**). The liver injury was slightly worse in mice infected with *C. rodentium* (λstx_{2dact}) compared to mice infected with *C. rodentium* ($\lambda stx_{2dact}::kan^R$) in the representative livers examined. Lastly, nasal turbinates which
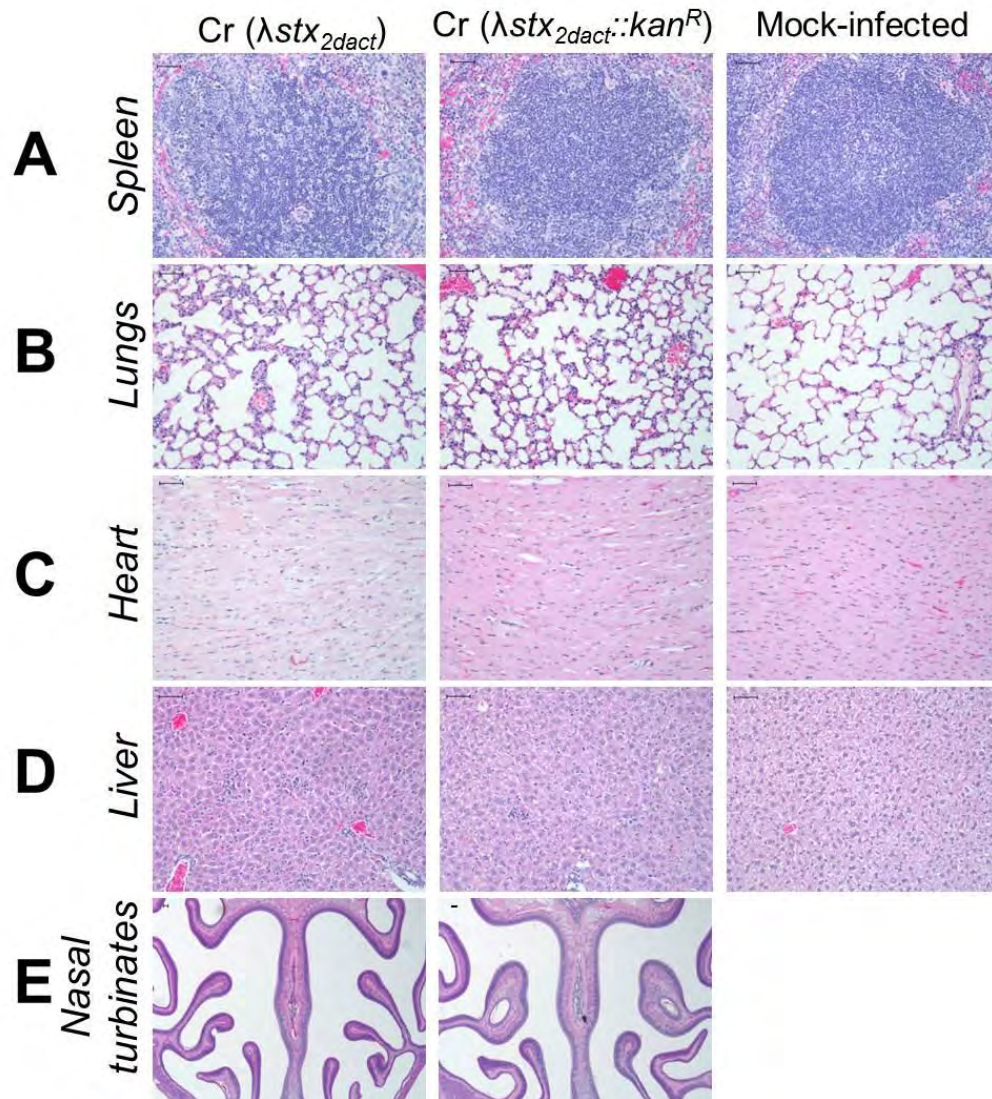
Supplementary Figure 3. Infection by *C. rodentium* (λ*stx$_{2dact}$*) does not result in significant histological damage to the spleen, heart, lung, liver, or nasal turbinates. Tissue sections of the spleen (A), heart (B), lung (C), liver (D), and nasal turbinates (E) were taken from mock-infected mice or mice infected with *C. rodentium* (λ*stx$_{2dact}$*) or *C. rodentium* (λ*stx$_{2dact}$::kan^{R}*) at seven days post-infection, stained with H&E, and analyzed histologically by a board certified pathologist. The magnification of spleen, lungs, heart, and liver samples is 200x and the magnification of the nasal turbinate samples is 40x. Scale bars measure 50 μm. For spleen, heart, lung, and liver samples, data are representative of one mock-infected mouse, four mice infected with *C. rodentium* (λ*stx$_{2dact}$*) and two mice infected with *C. rodentium* (λ*stx$_{2dact}$::kan^{R}*). For nasal turbinate samples, data are representative of five mice infected with *C. rodentium* (λ*stx$_{2dact}$*) and five mice infected with *C. rodentium* (λ*stx$_{2dact}$::kan^{R}*).

have been shown to express Gb_3 receptors (Rutjes et al., 2002) were evaluated in mice

infected with *C. rodentium* (λstx_{2dact}) or *C. rodentium* (λstx_{2dact}::*kan^R*). There was no

evidence of tissue damage to the nasal turbinates in mice infected with either *C.

rodentium* (λstx_{2dact}) or *C. rodentium* (λstx_{2dact}::*kan^R*) (**Supplementary Figure 3E**).

Tir is required for colonization and disease in the *C. rodentium* (λstx_{2dact}) infection

model.

The ability to generate of AE lesions is a well-established virulence attribute of

EHEC, but STEC strains that produce Stx2dact are capable of causing disease in humans

(and mice) in the absence of AE lesion formation (Ito et al., 1990; Lindgren et al., 1993;

Melton-Celsa et al., 1996). To test whether murine infection with *C. rodentium* (λstx_{2dact})

provided a disease model that was dependent on AE lesion formation, we determined if a

C. rodentium (λstx_{2dact}) defective for Tir production was also defective for colonization

and disease. Whereas *C. rodentium* (λstx_{2dact}) and *C. rodentium* (λstx_{2dact}::*kan^R*) were

capable of generating actin pedestals indistinguishable from those formed by wild type *C.

rodentium* DBS100 on monolayers of mouse embryonic fibroblasts, *C. rodentium*

(λstx_{2dact})Δtir was impaired in cell binding and unable to form pedestals (data not shown).

Pedestal formation was restored to this strain by pTir (pEM129), a Tir-expressing

plasmid (data not shown; see **Supplementary Table 2** and **Materials and Methods**). To

confirm that Tir was also required for AE lesion formation during infection, we compared

the intestinal epithelia of mice infected with *C. rodentium* (λstx_{2dact})Δtir or the parental

strain *C. rodentium* (λstx_{2dact}) by transmission electron microscopy (TEM) six days post-

infection. Whereas infection by *C. rodentium* (λstx_{2dact}) resulted in effacement of the intestinal brush-border microvilli and the formation of robust pedestals (**Figure 3A, top left panel, arrowhead**), *C. rodentium* (λstx_{2dact})Δtir left the epithelial cytoskeletal architecture indistinguishable from mock-infected controls (**Figure 3A, lower left panel**). When *tir* was introduced in *trans* on pTir, the intestines of mice infected with *C. rodentium* (λstx_{2dact})Δtir/pTir showed many bound bacteria elevated on actin pedestals (**Figure 3A, lower right panel, arrowhead**) with concomitant destruction of microvilli, indicating that, as expected, Tir is required for AE lesion formation.

The lack of *C. rodentium* (λstx_{2dact})Δtir detected by TEM reflected a significant colonization defect when assessed quantitatively, because mice infected with *C. rodentium* (λstx_{2dact})Δtir had vastly fewer fecal bacteria than mice infected with *C. rodentium* (λstx_{2dact}) (**Figure 6A**). At three days post-infection, fecal counts of mice infected with *C. rodentium* (λstx_{2dact})Δtir were approximately three orders of magnitude lower than mice infected with *C. rodentium* (λstx_{2dact}), and this difference grew to approximately seven orders of magnitude four days later. In contrast, *C. rodentium* (λstx_{2dact})Δtir/pTir was capable of efficiently colonizing mice, with peak bacterial burdens reaching almost 10^{10} CFU per gram of stool (**Figure 6A**). Notably, the kinetics of colonization by *C. rodentium* (λstx_{2dact})Δtir/pTir were somewhat delayed relative to *C. rodentium* (λstx_{2dact}), consistent with previous reports that plasmid complementation of a *C. rodentium tir* mutant is incomplete (Deng et al., 2003; Mundy et al., 2004).
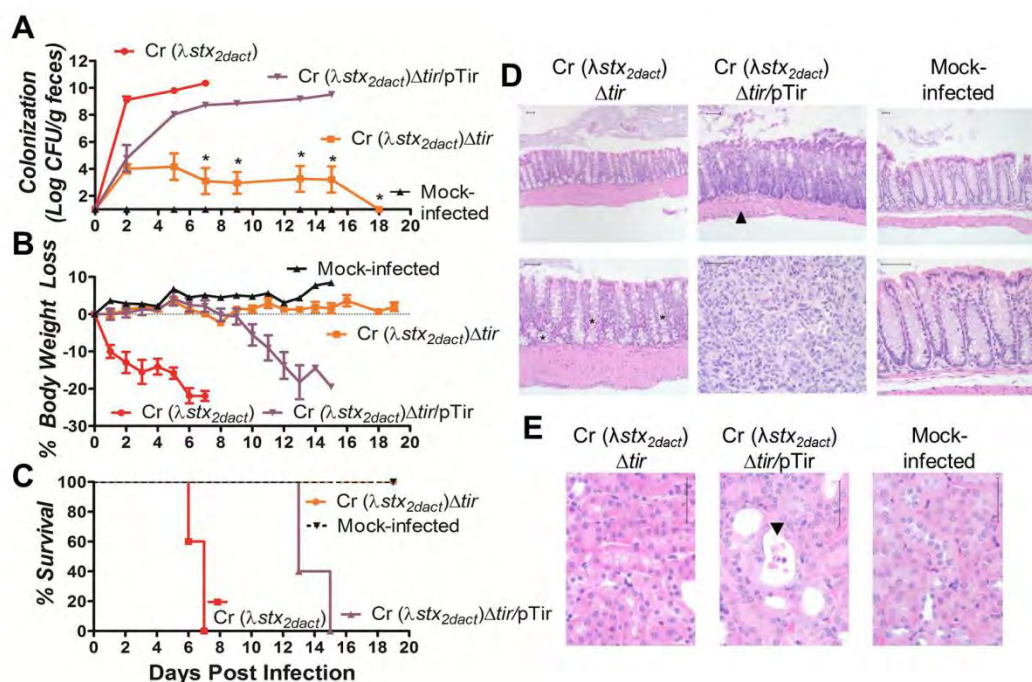
Figure 6. Tir is required for colonization and disease upon *C. rodentium* (λ*stx₂dact*) infection of mice. (A) Colonization of eight-week old C57BL/6 mock-infected mice, or infected with the indicated strain, was determined by plating stool for viable counts. Shown are the averages CFU (± SEM) of five mice. Data are representative of four independent experiments. Statistical significance was determined using two-way ANOVA and Bonferroni post-tests indicates that *C. rodentium* (λ*stx₂dact*)Δ*tir* colonized mice significantly (*p<0.05) less efficiently than *C. rodentium* (λ*stx₂dact*) and *C. rodentium* (λ*stx₂dact*)Δ*tir*/pTir). **(B)** Body weight during infection of eight-week old mice was determined and is expressed as percent change from day zero weight. Shown are the averages (±SEM) of five mice per group. Data are representative of four independent experiments. **(C)** Percent survival of mock-infected eight-week old mice or mice infected with *C. rodentium* (λ*stx₂dact*), *C. rodentium* (λ*stx₂dact*)Δ*tir*, or *C. rodentium* (λ*stx₂dact*)Δ*tir*/pTir. Groups of five mice were analyzed. Data are representative of five independent experiments. **(D)** H&E-stained large intestinal sections of mock-infected mice or mice infected with the indicated strain are shown under 100x (top row) or 400x (bottom row) magnification. Scale bars measure 50 μm. Asterisks (*) depict goblet cells that are prominent in normal intestinal tissue. Arrowheads indicate infiltration of inflammatory cells into the mucscularis mucosa and muscularis propria layers. **(E)** H&E-stained 600x micrograph of kidney sections from mock-infected mice or mice infected with the indicated strain. Arrowheads indicate attenuation and sloughing of epithelial cells within the proximal tubules. Scale bars measure 50 μm.

The defect of *C. rodentium* (λstx_{2dact})Δtir in intestinal colonization was reflected in all aspects of Stx-mediated disease. Histological analyses of the intestines of mice infected with *C. rodentium* (λstx_{2dact})Δtir were indistinguishable from those of mock-infected mice, in contrast to those of mice infected with *C. rodentium* (λstx_{2dact})Δtir/pTir, which showed areas of necrosis, inflammatory infiltrates, and the loss of goblet cells (**Figure 6D**). Renal damage was associated only with infection by *C. rodentium* (λstx_{2dact})Δtir/pTir, not with the Tir-deficient mutant (**Figure 6E**). These histological assessments of disease correlated with weight loss, because mice infected with *C. rodentium* (λstx_{2dact})Δtir maintained weight throughout infection (**Figure 6B**). In contrast, mice infected with *C. rodentium* (λstx_{2dact})Δtir/pTir lost on average 18% body weight by 15 days post-infection. The kinetics of weight loss by mice infected with the Tir-complemented strain, similar to the kinetics of colonization, were delayed several days relative to mice infected with *C. rodentium* (λstx_{2dact}), but once weight began to decrease at approximately ten days post-infection, it declined steadily (**Figure 6B**). Finally, whereas infection by *C. rodentium* (λstx_{2dact})Δtir caused no mortality, infection by *C. rodentium* (λstx_{2dact})Δtir/pTir, like that of *C. rodentium* (λstx_{2dact}), was uniformly fatal, with the predicted temporal delay (**Figure 6C**). Thus, Tir is an essential virulence factor during lethal infection by *C. rodentium* (λstx_{2dact}).

<u>Discussion</u>

EHEC infection features high-level intestinal colonization accompanied by the formation of AE lesions and the production of Stx. Some rabbit and piglet models mimic these two central aspects of EHEC infection (Garcia et al., 2006; Panda et al., 2010; Ritchie et al., 2003; Ritchie and Waldor, 2005; Tzipori et al., 1995), but no analogous model has yet been developed in conventional mice. We show here that *C. rodentium* lysogenized with λ*stx*$_{2\text{dact}}$ provides a model that features prototypic AE lesions during intestinal colonization, weight loss, and death, and recapitulates many manifestations of Stx-mediated disease observed in human EHEC infection and murine toxin injection models (Amirlak and Amirlak, 2006; Mohawk and O'Brien, 2011).

Human HUS is associated with the induction of inflammatory cytokines (Caprioli et al., 2005b; Ray and Liu, 2001), and patients with a preponderance of pro-inflammatory cytokines often have more severe disease (Litalien et al., 1999). Indeed, one model of Stx-mediated disease in mice requires the co-administration of LPS and Stx (Keepers et al., 2007). Several means by which inflammatory cytokines may promote systemic disease have been proposed, including induction of the Gb$_3$ glycolipid Stx receptor on host cells (Simon et al., 1998; van de Kar et al., 1992; van Setten et al., 1997), alteration of fibrinolysis and anticoagulation, or recruitment of inflammatory cells into damaged tissues (Ray and Liu, 2001). In response to Stx, cultured monocytes secrete TNF-α and IL-6 (Foster et al., 2000; van Setten et al., 1996; van Setten et al., 1997), and we found that these cytokines were elevated in the serum or kidneys of mice infected with *C. rodentium* (λ*stx*$_{2dact}$). This response was dependent on Stx production, because neither

TNF-α nor IL-6 was elevated in mice infected with *C. rodentium* ($\lambda stx_{2dact}::kan^R$). MCP-1 and KC were also elevated in *C. rodentium* (λstx_{2dact})-infected mice in an Stx-dependent manner. Notably, MCP-1 and IL-8, a functional human analog of KC, are found at elevated levels in the urine of children with HUS (van Setten et al., 1998). Interestingly, some mice infected with *C. rodentium* (λstx_{2dact}) displayed much higher levels of all serum cytokines than others infected with the same strain. Upon further analysis, we found that the mice on the verge of death (exhibiting >15% body weight loss, ruffled fur, high-level colonization, and were seizing) had consistently elevated serum cytokines throughout the panel of cytokines tested. It is possible that the remainder of the mice infected with *C. rodentium* (λstx_{2dact}) that had lower levels of serum cytokines would have had higher serum cytokine levels if testing were done at a later time point when these mice were moribund.

Renal damage is central to human HUS (Scheiring et al., 2008), and the induction of kidney cytokines in the *C. rodentium* (λstx_{2dact}) model was accompanied by renal compromise. Glomerulonephritis is a prominent feature of human HUS, a manifestation that correlates with the relative abundance of Gb_3 receptors on glomerular endothelium (Richardson et al., 1988). In mice however, Gb_3 is enriched in the renal tubules (Psotka et al., 2009), and the tubular damage we observed in infected mice likely reflects this localization. Consistent with this hypothesis, tubular damage is also typically observed in EHEC-infected germ-free or streptomycin-treated mice (Eaton et al., 2008; Lindgren et al., 1993; Melton-Celsa et al., 1996; Psotka et al., 2009). The histopathological findings were reflected in functional compromise, because mice infected with *C. rodentium*

(λstx_{2dact}), but not *C. rodentium* ($\lambda stx_{2dact}::kan^R$), demonstrated elevated BUN and proteinuria, consistent with other murine models of HUS (Eaton et al., 2008; Keepers et al., 2006; Lindgren et al., 1993; Mohawk and O'Brien, 2011; Sauter et al., 2008). Elevated serum creatinine, another indicator of renal dysfunction, has been observed in some other murine models for Stx-mediated disease (Keepers et al., 2006; Lindgren et al., 1993; Sauter et al., 2008). In contrast, we found that, although serum creatinine was somewhat elevated in mice infected with *C. rodentium* (λstx_{2dact}), the increase did not reach statistical significance (E.M. unpublished data), similar to the serum creatinine levels observed upon infection of BALB/c mice by EHEC (Mohawk et al., 2010b).

Although our model resembles many aspects of murine Stx-mediated disease, several manifestations of human HUS are not recapitulated in the *C. rodentium* (λstx_{2dact}) murine model. For example, neurological damage is associated with HUS, and cerebral hemorrhage and edema have been reported in EHEC-infected, streptomycin pre-treated mice (Fujii et al., 1994; Kurioka et al., 1998). Although mice infected with *C. rodentium* (λstx_{2dact}) occasionally displayed tremors and seizures, we did not observe consistent pathological changes in the brain (E.M., M. McBee, and V.V., unpublished observations). In addition, contrary to what has been observed in human disease (Scheiring et al., 2010; Tarr et al., 2005) and Stx administration models (Karpman et al., 1997; Keepers et al., 2006; Psotka et al., 2009; Roche et al., 2007; Sauter et al., 2008), mice infected with *C. rodentium* (λstx_{2dact}) did not display renal platelet aggregation, red cell congestion, or fibrin deposition, and did not suffer thrombocytopenia or anemia. Given that it has been hypothesized that erythrocytes are ruptured upon passage through damaged renal

glomeruli (Bull et al., 1967), it is tempting to speculate that the lack of

glomerulonephritis in our model partially explains the lack of observable anemia. We

also found no hematological evidence of thrombotic disease, such as prolonged clotting

time, fibrin D-dimer formation, or complement activation determined by measuring

serum levels of Bb, C3, and sC5b-9 (E.M. unpublished observations).

Given that a central goal of this study was to test whether *C. rodentium* (λstx_{2dact})

could recapitulate EHEC toxin-mediated disease, an important finding was the

requirement for Tir in promoting Stx-mediated disease in this model. Colonization by a

Tir-deficient derivative of *C. rodentium* (λstx_{2dact}) was many orders of magnitude lower

than colonization by the parental strain. A Tir-encoding plasmid complemented the

mutant for the ability to colonize mice and cause disease, although the kinetics of

colonization, weight loss and death were somewhat slower than that by *C. rodentium*

(λstx_{2dact}). The apparent partial complementation is consistent with previous studies

indicating that plasmid-based expression in *C. rodentium* is often unable to completely

restore wild type phenotypes (Deng et al., 2003; Mundy et al., 2004).

Interestingly, in spite of the reports that the Stx receptor Gb_3 is expressed on cells

in the distal colon of the mouse (Imai et al., 2003; Schuller, 2011), the streptomycin pre-

treatment and gnotobiotic mouse models of EHEC infection models do not typically

result in obvious intestinal damage ((Eaton et al., 2008; Lindgren et al., 1993), A.M

unpublished observations). Mild inflammatory cell infiltration, goblet cell depletion, and

intestinal epithelial necrosis have been reported in a few studies (Isogai et al., 1998;

Kurioka et al., 1998; Shimizu et al., 2003; Taguchi et al., 2002). In contrast, we found

here dramatic intestinal damage in mice infected with *C. rodentium* (λstx_{2dact}); indeed,

these pathological changes were similar to those commonly observed in human infection

by EHEC, which in some cases can mimic inflammatory bowel disease or ischemic

colitis (Griffin et al., 1988; Moon, 1997; Sebbag et al., 1999; Siegler, 1994). It is

tempting to speculate that AE lesion formation, a prominent feature of this murine

infection model, is critical to facilitating Stx-mediated intestinal epithelial damage. The

development of a murine model that encompasses both AE lesion formation and severe

Stx-mediated tissue damage provides an opportunity to more fully explore the

relationship between the dramatic alteration in host cytoskeletal structure and subsequent

systemic disease.

CHAPTER IV.

ACTIN PEDESTAL FORMATION BY AE PATHOGENS PROMOTES SYSTEMIC SHIGA TOXIN-MEDIATED DISEASE.

Abstract

Enterohemorrhagic *E. coli* (EHEC) colonizes the intestine and produces the phage-encoded Shiga toxin (Stx), which is absorbed systemically and can cause life-threatening hemolytic uremic syndrome (HUS) consisting of the triad of hemolytic anemia, thrombocytopenia, and renal failure. EHEC is an attaching and effacing (AE) pathogen that intimately adheres to epithelial cells and forms actin-rich "pedestals" beneath bound bacteria. To generate AE lesions, EHEC translocates the type III effector, Tir, into mammalian cells, which functions as a receptor for the EHEC adhesin intimin. Tir-intimin binding triggers a signaling cascade leading to pedestal formation through the N-WASP-Arp-2/3 pathway. The ability to generate pedestals has been associated with moderately enhanced colonization, particularly late in infection; however, dramatic phenotypes associated with pedestal-defective mutants have yet to be identified. Using our previously described murine model of Stx-mediated disease by *C. rodentium* (λstx_{2dact}), we assessed the role of Tir-mediated actin assembly in colonization and disease. First, conditional, intestinal, N-WASP$^{-/-}$ (iNWKO) mice were infected with *C. rodentium* (λstx_{2dact}). Interestingly, iNWKO mice were less colonized and exhibited less disease and mortality compared to littermate controls. Next, wild type mice were infected with *C. rodentium* (λstx_{2dact}) expressing a point mutant of Tir that promotes intimate bacterial attachment but not actin assembly. *C. rodentium* expressing the mutant

Tir colonized mice almost as efficiently as *C. rodentium* expressing wild type Tir.

Nevertheless, *C. rodentium* expressing wild type Tir caused lethal infection, while *C. rodentium* expressing the Tir point mutant was almost entirely incapable of lethality. The

expression of wild type Tir, but not the Tir mutant was associated with the ability to

stably colonize the colonic mucosal surface. These studies suggest that Tir-mediated

actin pedestal formation may promote systemic Stx-mediated disease by stably localizing

Stx-producing bacteria on the mucosal surface, thereby increasing delivery of the toxin

across the mucosal barrier.

Acknowledgements and contributions

This chapter is a result of collaborations between Emily M. Mallick, John Garber, Tim Blood, Vijay K. Vanguri, Didier Vingadassalom, David B. Schauer, Scott B. Snapper, and John M. Leong. A subset of this manuscript will be submitted for publication. This work was supported by NIH R21 AI AI092009 and R01 AI46454. I would like to acknowledge people for their contribution to the work presented here:

Introduction

Enterohemorrhagic *Escherichia coli* (EHEC) particularly serotype O157:H7 is an important food-borne human pathogen responsible for both sporadic and epidemic outbreaks of diarrheal disease (Kaper et al., 2004; Pennington, 2010). Human EHEC infection can result in local, intestinal disease such as diarrhea or hemorrhagic colitis, characterized by bloody diarrhea and severe abdominal pain or manifest in a life-threatening, systemic disease known as hemolytic uremic syndrome (HUS) characterized by the triad of hemolytic anemia, thrombocytopenia, and renal failure (Karmali et al., 2009; Tarr et al., 2005). Notably, HUS is the leading cause of renal failure in children (Mead and Griffin, 1998; Scheiring et al., 2008).

Systemic disease resulting from EHEC infection requires the phage-encoded cytotoxin Shiga toxin (Stx), and toxin expression is often enhanced upon phage induction (Muhldorfer et al., 1996; Schmidt, 2001; Waldor and Friedman, 2005). Stx produced in the gut traverses the intestinal epithelium, enters the blood stream, and targets organs possessing the globotriasosylceramide Gb_3 receptor, such as the vasculature, kidney, and central nervous system (CNS) (Obrig, 2010; Sandvig and van Deurs, 1996; Schuller, 2011), where it inhibits protein synthesis. Of the two major serotypes of Stx, Stx1 and Stx2, EHEC strains that express exclusively Stx2 are associated with a greater risk of HUS (Croxen and Finlay, 2010; Melton-Celsa et al., 2011; Ostroff et al., 1989).

A characteristic colonization feature of EHEC that it shares with enteropathogenic *E. coli*, a cause of infantile diarrhea in the developing world, and *Citrobacter rodentium*, a murine pathogen that causes transmissible colonic hyperplasia, is the ability to form

attaching and effacing (AE) lesions on the intestinal epithelium (Kaper et al., 2004; Schauer and Falkow, 1993a). These lesions are characterized by the degeneration of brush border microvilli, intimate attachment of bacteria to the host cell, and the formation of actin-rich pedestals beneath bound bacteria ((Moon et al., 1983), for review see (Kaper et al., 2004)). Upon animal infection with EHEC or *C. rodentium*, mucosally adhered bacteria and AE lesions have been observed in the cecum, colon, and rectum (Dean-Nystrom et al., 1999; Nagano et al., 2003; Nart et al., 2008; Schauer and Falkow, 1993a; Wales et al., 2001). Interestingly, the cecum is the primary site of colonization of mice with *C. rodentium* (Wiles et al., 2004).

The formation of AE lesions is dependent on a type III secretion system (T3SS) that translocates bacterial effectors directly into host cells (Garmendia et al., 2005; Kenny and Finlay, 1995; McDaniel et al., 1995). An effector that is essential for pedestal formation is the translocated intimin receptor (Tir), which localizes in the host cell plasma membrane in a hair loop conformation with N- and C-terminal cytoplasmic domains and a central extracellular domain. The extracellular domain binds to the outer membrane protein intimin (de Grado et al., 1999; Hartland et al., 1999; Kenny et al., 1997), and membrane clustering of Tir by intimin induces a signaling cascade within the host cell resulting in the formation of filamentous (F)-actin-rich pedestals (reviewed in (Campellone, 2010; Caron et al., 2006; Hayward et al., 2006)).

To generate actin pedestals, EPEC and *C. rodentium* utilize the Tir-Nck-N-WASP pathway (Campellone et al., 2002; Gruenheid et al., 2001; Kenny, 1999). The Tir proteins of these two pathogens contain a critical tyrosine residue (TirY471 in *C.*

rodentium or its equivalent TirY474 in EPEC) that after translocation becomes

phosphorylated by mammalian cell kinases (Phillips et al., 2004; Swimm et al., 2004a) to

create a docking site for the SH-2 (src homology 2) domain of the host cell adaptor

protein Nck (Campellone et al., 2002; Campellone et al., 2004a; Gruenheid et al., 2001).

Nck then recruits all the components necessary for actin polymerization via the N-WASP

and Arp-2/3 pathway ((Rivera et al., 2004; Rohatgi et al., 2001); for review see (Frankel

and Phillips, 2008)). Although canonical EHEC strains also produce Tir and intimin,

EHEC Tir lacks a Nck binding sequence and instead produces an additional bacterial

factor, $EspF_U$ (aka TccP) (Campellone et al., 2004b; Garmendia et al., 2004), absent in

EPEC and *C. rodentium*, that vastly increases the efficiency of actin assembly via a Nck-

independent pathway (Brady et al., 2007; Campellone and Leong, 2005).

While there is extensive evidence that intimin and Tir are required for

colonization in a variety of animal models (Deng et al., 2003; Marches et al., 2000;

Ritchie et al., 2003; Schauer and Falkow, 1993b; Tzipori et al., 1995), the importance of

Tir-mediated actin rearrangement is less defined. Some studies have indicated that the

ability to generate actin pedestals is dispensable for colonization (Deng et al., 2003;

Schuller et al., 2007; Vlisidou et al., 2006a), while other findings suggest that Tir-

mediated actin assembly enhances colonization (Crepin et al., 2010; Ritchie et al., 2008).

For example, murine infection with a *C. rodentium tir* mutant harboring a plasmid

containing a Tir deficient in pedestal formation *in vitro* ($pTir_{Y471F}$) was not significantly

down for colonization compared to infection by a pedestal-proficient strain (*C.

rodentium∆tir*/$pTir_{WT}$) (Deng et al., 2003). Similarly, intestinal colonization in calves

and lambs was unaltered upon infection with an EHEC *espF$_U$* mutant (Vlisidou et al., 2006a), nor was colonization of intestinal explants altered by infection with EPEC, Tir phosphorylation-deficient mutants (Schuller et al., 2007). In contrast, an EHEC strain deficient for pedestal formation displayed a mild colonization defect late in infection of infant rabbits and generated smaller than wild type bacterial aggregates on the intestinal mucosa of infected piglets (Ritchie et al., 2008). In addition, a *C. rodentium* pedestal-deficient mutant was outcompeted by wild type *C. rodentium* in a dual infection (Crepin et al., 2010).

The above experiments were not performed in experimental systems that prominently manifest Stx-mediated systemic disease, a central aspect of EHEC infection. To assess the consequence of pedestal formation in an animal model that features Stx-mediated intestinal and renal damage, we utilized *C. rodentium* lysogenized with an Stx-producing phage. Infection of mice with *C. rodentium* (λ*stx$_{2dact}$*) recapitulates many aspects of EHEC toxin-mediated disease, including high-level colonization, intestinal damage, and renal compromise (**Chapter III**). We found that pedestal formation promotes colonization of the colonic but not the cecal mucosa, and that dramatically enhanced colonic colonization was required to cause severe systemic disease.

Materials and Methods

Plasmids, bacterial strains, and growth conditions. All bacteria were cultured in Luria-Bertani broth (LB) (Miller) at 37°C, unless indicated otherwise. Antibiotics were used in the following concentrations kanamycin (25 µg/ml), zeocin (75 µg/ml), chloramphenicol (10 µg/ml), and tetracycline (5 µg/ml). For recombination using pKD46 in *C. rodentium* (λstx_{2dact}) strains, 750 µg/ml of ampicillin was used to select for transformants because of the presence of a chromosomal β-lactamase in *C. rodentium* (λstx_{2dact}). The bacterial strains and plasmids used in this study are listed in **Tables 1 and 2**.

Plasmid isolation, primers, and sequencing. Isolation of all plasmid DNA was done using the QIAprep Spin Miniprep Kit (QIAgen, Valencia, CA, USA). All primers were purchased from Invitrogen (Grand Island, NY, USA) and are listed in **Table 3**. Sequencing was performed at Tufts University Core Sequencing Facility (Boston, MA, USA). Sequences were analyzed using BioEdit and MacVector software.

Construction of a plasmid expressing *C. rodentium* TirY471F. The pTir$_{Y471F}$ plasmid was constructed using SLIM as previously described (Chiu et al., 2004) using the following primers: R-Oli178, F-Oli179, R-Oli180, and F-Oli181. Plasmid sequence was confirmed by sequencing and pedestal formation was tested in a FAS assay.

Generation of an anti-*Citrobacter* antibody. To generate the *C. rodentium* Tir

expressing plasmid pCrTirExp, primers F-190 and R-191 were used to amplify *C.*

rodentium tir with *Nde* I and *Sal* I flanking restriction sites (1.644 kb) from pEM129

"pTir$_{WT}$". This PCR fragment was cloned into the *Nde* I and *Sal* I sites of pET21b ligated

and transformed into CaCl$_2$ competent DH5α *E. coli*. Transformants were selected on

plates containing ampicillin. Candidate clones were then verified by restriction digestion,

PCR with primers R-iTirL and F-iTirU (480 bp), and sequencing. Sequences were

analyzed using BioEdit software (Ibis Therapeutics, Carlsbad, CA, USA). pCrTirExp

was then transformed into BL21 DE3.

For expression and protein purification of *C. rodentium* Tir, BL21 DE3+pCrTirExp was

cultured in 2xYT media at 37°C to an OD$_{600}$ of 0.6- 0.7 then induced with 1 mM IPTG

for three hours at 37°C. The culture was spun at 4,420 x g, 20 minutes at 4°C and the

supernatant was discarded. The pellet was resuspended in 2.5 ml lysis buffer per gram

wet weight. 4 mg lysozyme was added and the sample was sonicated ([Branson Sonifier

450, Branson Ultrasonics Corporation, Danbury, CT, USA] Duty cycle 70, output 3, 10

second bursts X 6 cycles). The lysate was then centrifuged at 16,100 x g, 20 minutes at

4°C. The supernatant was run on a QIAgen Ni-NTA Agarose column (QIAgen,

Valencia, CA, USA) and resulting *C. rodentium* Tir was eluted and quantified using Bio-

Rad Protein Assay kit (Bio-Rad Laboratories, Inc., Hercules, CA, USA).

For *C. rodentium* antibody production, all inoculations were completed subcutaneously with 30 ng of purified *C. rodentium* Tir in 50 μl with 50 μl of adjuvant for a total inoculation volume of 100 μl. Eight-week old, female BALB/c mice (Jackson Laboratories, Bar Harbor, ME, USA) were inoculated with *C. rodentium* Tir supplemented with Imject Freund's Complete Adjuvant (Thermo Scientific, Rockford, IL, USA). At days 14 and 28 mice were boosted with *C. rodentium* Tir supplemented with Imject Freund's Incomplete Adjuvant (Thermo Scientific, Rockford, IL, USA). Mice were sacrificed on day 38 and blood was harvested via cardiac bleed. Blood was allowed to clot at room temperature for 30 minutes, and then was spun twice at 8,600 x g, 15 minutes at 4°C, aliquoted and stored at -80°C.

Tir immunoblotting. *C. rodentium* strains were cultured in DMEM + 0.1 M HEPES at 37°C, 5% CO_2 for 4.5 hours. After centrifuging at 22,000 x g for 10 minutes at room temperature, media was decanted and trichloroacetic acid was added in a 1:1 volume and incubated overnight at -20°C. After incubation, sample was centrifuged at 22,000 x g for 10 minutes at 4°C. Supernatant was decanted and pellet was resuspended in acetone and centrifuged at 20,800 x g at 4°C for 10 minutes. The acetone was decanted and the pellet was allowed to air dry for 10 minutes and was then resuspended in glass-distilled water. Loading of sodium dodecyl sulfate polyacrylamide gel (SDS-PAGE) was standardized to either final protein concentration quantified by Nanodrop (Thermo Fisher Scientific Inc., Wilmington, DE, USA) or final OD_{600}.

Infection analysis of *C. rodentium* (λstx_{2da}ct) and mutants on cultured cells. The filamentous actin staining assay was done as previously described (Mallick et al., 2012). Briefly, a single colony from each strain was grown in 1 ml media (+/- antibiotic) for eight hours. Cultures were diluted 1:500 into 5 ml DMEM supplemented with 0.1M HEPES (pH 7.0) (+/- antibiotic) and incubated at 37°C without agitation with 5% CO_2 for 12-15 hours. Cell monolayers were prepared by splitting 95-100% confluent mouse embryonic fibroblasts (MEFs) into 24-well culture plates containing sterile glass coverslips followed by overnight growth at 37°C with 5% CO_2. For infections, cell monolayers were washed twice with sterile PBS followed by addition of FAS media containing 25 μl of overnight cultured *C. rodentium* to each well. Plates were spun at 700g for 10 minutes then incubated at 37°C with 5% CO_2 for 3 hours. After 1.5 hours, plates were spun again at 700 g for an additional 10 minutes then to insure proper bacterial binding to cells. After 3 hours, cells were washed twice with sterile PBS and 0.5 ml pre-warmed FAS media was added to each well and plates were incubated for 3 hours. Cells were washed 5 times with sterile PBS, fixed with 4% PFA for 30 minutes, washed, permeabilized with 0.1% Triton-X 100, and then stained with Phalloidin (Molecular Probes, Eugene, OR, USA) (1:100) and DAPI (1:500). After washing cells an additional three times with PBS, the coverslips were mounted on slides using ProLong® Gold antifade reagent (Invitrogen, Eugene, OR, USA).

Mouse infections. Mice were purchased from Jackson Laboratories (Bar Harbor, ME, USA) and housed in the UMMS animal facility. Protocols were approved by the

department of animal medicine and complied with the UMMS IACUC protocols. Female

five-to-eight week old C57BL/6J mice were gavaged with PBS or ~5 x 10^9 of overnight

culture of *C. rodentium* in 100 μl PBS. Inoculum concentrations were confirmed by

serial dilution plating. *C. rodentium* fecal shedding was determined by serial dilution

plating of fecal slurries (10% w/v in PBS) on LB or Maconkey agar with selection for

kanamycin, chloramphenicol, or kanamycin and chloramphenicol, as appropriate. When

using complemented strains containing antibiotics, feces were plated on plates containing

both antibiotics. Previously we have tested the rate of plasmid loss by plating on only

one antibiotic and determined it was minimal. Body weights were monitored daily and

mice were euthanized if they lost >20% of their body weight. Some mice became

moribund or died prior to the scheduled necropsy date, and these mice were necropsied

early. Mouse urinalysis was performed by collecting urine into a 1.5 ml conical tube.

The urine in the tube was thoroughly mixed and a 2 μl aliquot was pipetted onto a

Chemstrip 4MD urinalysis test strip (Roche Diagnostics, Laval, Quebec). After 60

seconds, the color change on the strip was compared to a supplied color scale. The range

of protein measured was 0 – 500 mg/dl, with the scale 0 indicating undetectable protein,

0.5 indicating trace, 1.0 indicating ~30 mg/dl, 2 indicating ~100 mg/dl, and 3.0 indicating

~500 mg/dl. All experimental groups contained at least five mice unless otherwise

stated.

Tissue Collection and Histology. At necropsy, the distal colon and cecum were taken

along with longitudinally divided kidneys and were fixed in 10% buffered formalin,

dehydrated and embedded in paraffin. Five-micron intestinal and kidney sections were

cut and stained with hematoxylin and eosin (H&E). Tissue sections were evaluated by a

board-certified pathologist (V.V.) with a subspecialty expertise in renal pathology.

Assessment of intestinal mucosal hyperplasia was targeted to areas of comparable

muscularis propria thickness in order to reduce error from differences in planes of

section. For immunofluorescence staining, histological sections of the intestine were

stained with an anti-*Citrobacter* antibody (a gift from the lab of David Schauer, MIT)

used at 1:1600, DAPI, and phalloidin (1:100) (Invitrogen, Grand Island, NY, USA) by

the DERC Histology Core Facility at UMMS.

Determination of CFU associated with different intestinal segments. Mice were

gavaged with approximately 5×10^9 bacteria and fecal colonization and body weight was

monitored throughout infection. At day of necropsy, the large intestine (cecum through

rectum) was removed and after removal of fecal contents, the large intestine was flushed

with 1 ml sterile PBS and to remove any loosely bound bacteria. The contents of the

flush ("output" or "luminal contents") were then collected and serial dilutions of the flush

("output" or "luminal contents") were plated on the LB with the appropriate antibiotic.

The intestine was then divided into two parts: cecum and colon, homogenized, and serial

dilutions of the tissue homogenate were plated on the appropriate antibiotic to determine

the amount of bacteria per mg of tissue.

Generation and characterization of conditional, intestinal, N-WASP$^{-/-}$ mice.   It has

previously been shown that germline deletion of N-WASP results in early embryonic

lethality in association with severe neural tube defects and cardiac abnormalities

(Lommel et al., 2001; Snapper et al., 2001). Therefore, a conditional, intestinal, N-

WASP knockout mouse (iNWKO) was generated using the Cre-Lox system, where Cre

expression was driven by a villin-specific promoter. Breeders to generate conditional,

intestinal N-WASP knockout mice were obtained from Scott Snapper (Children's

Hospital, Boston, MA) and bred at UMMS. The breeding scheme was as follows: a

female mouse homozygous for LoxP-flanked N-WASP alleles and Cre- (L2L/L2L, Cre-)

was bred with a male heterozygous for LoxP-flanked N-WASP alleles and Cre+ (L2L/+,

Cre+). iNWKO knockout offspring were the pups that were homozygous for LoxP-

flanked N-WASP and Cre+ (L2L/L2L, Cre+). This breeding resulted in approximately

15% of the desired genotype. Genotyping was performed by Transnetyx (Cordovia, TN,

USA) using a specific genotyping assay designed for the iNWKO mouse. Western blot

analysis was performed on the colon, ileum, jejunum, and duodenum of correctly

genotyped mice using an anti-N-WASP antibody. Body weight of iNWKO and

littermate controls was measured daily after birth. The colons of iNWKO mice were

analyzed grossly, by H&E, and by Transmission Electron Microscopy (TEM). The

colonic mucosa and distribution of colonic goblet cells of iNWKO mice appeared grossly

normal. The ileum of the iNWKO mice exhibited uncondensed nuclei compared to

littermate controls. Additionally, iNWKO mice displayed normal ultrastructural

intestinal architecture, with prominent microvilli, however the microvilli were shorter in

length than those of the littermate controls. To assess intestinal permeability in iNWKO

mice, mice were given 100 μl of 10 mg/ml solution of FITC-dextran (Sigma, St. Louis,

MI, USA) and four hours later were sacrificed. Blood was collected via cardiac bleed,

allowed to clot, and then centrifuged for 30 minutes. The serum was separated and

fluorescence intensity was measured in undiluted serum using SpectraMax Gemini XS at

an excitation wavelength of 483 and emission wavelength of 517. All infection

experiments using the iNWKO mouse were completed as described above (Mouse

Infections, Tissue Collection and Histology, and Determination of CFU associated with

different intestinal segments) and included age and sex matched littermate controls.

Transmission Electron Microscopy. Mouse intestinal tissue samples were taken at

various time points post infection and fixed in 2.5% gluteraldehyde in 0.05 M Sodium

Phosphate buffer, pH 7.2. Samples were processed and analyzed at the UMMS Electron

Microscopy core facility according to standard procedures. Briefly, fixed samples were

moved into fresh 2.5% gluteraldehyde in 0.05 M sodium phosphate buffer and left

overnight at 4^oC. The samples were then rinsed twice in the same fixation buffer and

post-fixed with 1% osmium tetroxide for 1 hour at room temperature. Samples were then

washed twice with DH_2O for 20 minutes at 4^oC and then dehydrated through a graded

ethanol series of 20% increments, before two changes in 100% ethanol. Samples were

then infiltrated first with two changes of 100% propylene oxide and then with a 1:1 mix

of propylene oxide:SPI-Pon 812 resin. The following day three changes of fresh 100%

SPI-Pon 812 resin were done before the samples were polymerized at 68^oC in plastic

capsules. The samples were then reoriented and thin sections were placed on copper

support grids and stained with lead citrate and uranyl acetate. Sections were examined

using the FEI Tecani 12 BT with 80Kv accelerating voltage, and images were captured

using a Gatan TEM CCD camera.

Statistical analysis. Data were analyzed using GraphPad Prism software. Comparison

of multiple groups was performed using one-way analysis of variance (ANOVA) with

Tukey's multiple comparison post-tests or using a two-way ANOVA with Bonferroni's

post-tests. Statistical significance of differences between two groups was evaluated using

two tailed unpaired t tests. In all tests p values below 0.05 (*), 0.01 (**), and 0.001 (***)

were considered statistically significant. In all graphs error bars represent standard error

of the mean (SEM), unless indicated otherwise. Logistic analysis was performed by

Stephen Baker at the UMMS.

Table 1. Strains used in this study.

Strain	Description and relevant phenotype	Reference
DBS100	*Citrobacter rodentium* wild type strain (prototype TMCH isolate, ATTC 51459, original biotype 4280)	(Barthold et al., 1976; Schauer and Falkow, 1993a)
DBS770	DBS100 lysogenized with Φ1720a-02 ΔRz::*cat*, Cm^R	**Chapter III**
DBS771	DBS100 lysogenized with Φ 1720a-02 ΔRz::*cat* $\Delta stx_{2dact}AB$::*kan*, Cm^R, Km^R	**Chapter III**
DH5α BL21DE3	Protein expression *E. coli* strain	Invitrogen

Cm^R, chloramphenicol resistant

Km^R, kanamycin resistant

Table 2. Plasmids used in this study.

Plasmids	Description	Reference
pK184	Cloning vector, Km^R	(Jobling and Holmes, 1990)
pEM129 (pTir$_{WT}$)	pEM123 containing *C. rodentium tir – cesT*, Km^R	**Chapter III**
pTir$_{Y471F}$	pK184 based plasmid containing Y471F *C. rodentium* Tir point mutant; Km^R	This study
pCrTirExp	pET21b containing *C. rodentium tir*, Amp^R	This study
PET21b	Expression vector with T7 promoter, Amp^R	EMD Biosciences, San Diego, CA

Amp^R, ampicillin resistant
Km^R, kanamycin resistant
Cm^R, chloramphenicol resistant

Table 3. Oligonucleotide sequences used in this study.

Primer[a]	Nucleotide sequence (from 5' to 3')[b]
R-Oli178	cga ctt cat caa aaa tag gct ctt ctg gag cga gaa gcg atg gat t
F-Oli179	aga gcc tat ttt tga tga agt cgc tcc gga tcc taa cta tag cgt t
R-Oli180	tct gga gcg aga agc gat gga tt
F-Oli181	ctc cgg atc cta act ata gcg tt
F-190	cat cat cat <u>cat atg </u>atg cct att ggt aat ctt ggt
R-191	cat cat cat <u>gtc gac </u>gac gaa acg ttc aac t
R-iTirL	cca att cct gct gac gtt tag
F-iTirU	ata cac gtt ctg ttg gtg tcg

[a]F indicates forward (top-strand) primer and R indicates reverse (bottom-strand) primer.
[b]Restriction sites are underlined

Results

Characterization of a conditional, intestinal, N-WASP$^{-/-}$ mouse.

iNWKO mice were generated as described in **Materials and Methods**. To confirm the absence of N-WASP, western blot analysis was performed. As expected, littermate control mice (designated "LMC" in figures) produced high levels of N-WASP in the colon, ileum, jejunum, and duodenum, while N-WASP was absent in iNWKO mice (**Figure 1A**). iNWKO mice were viable but gained weight less rapidly than their littermate controls (**Figure 1B, C**). As depicted in **Figure 1B**, wild type mice (LoxP-NW$^{-/-}$, Vil-Cre-) and littermate control mice homozygous for LoxP-flanked N-WASP alleles and negative for Cre (LoxP-NW$^{+/+}$, Vil-Cre-) appeared larger than iNWKO mice (LoxP-NW$^{+/+}$, Vil-Cre +). Notably, between eight and 15 weeks of age, iNWKO mice gained significantly less ($p<0.05$) weight than their littermate controls (**Figure 1C**). Histologically, the colons of iNWKO were grossly normal, but ultrastructural analysis revealed that their intestinal microvilli and apical junction complexes (AJC) were significantly shorter compared to littermate controls (**Figure 1D, E**). Because of this abnormal ultrastructure, we assessed barrier function by measuring intestinal permeability (see **Materials and Methods**). Interestingly, iNWKO mice had increased gut permeability compared to controls, suggesting that elimination of intestinal N-WASP decreases barrier function (**Figure 1F**).
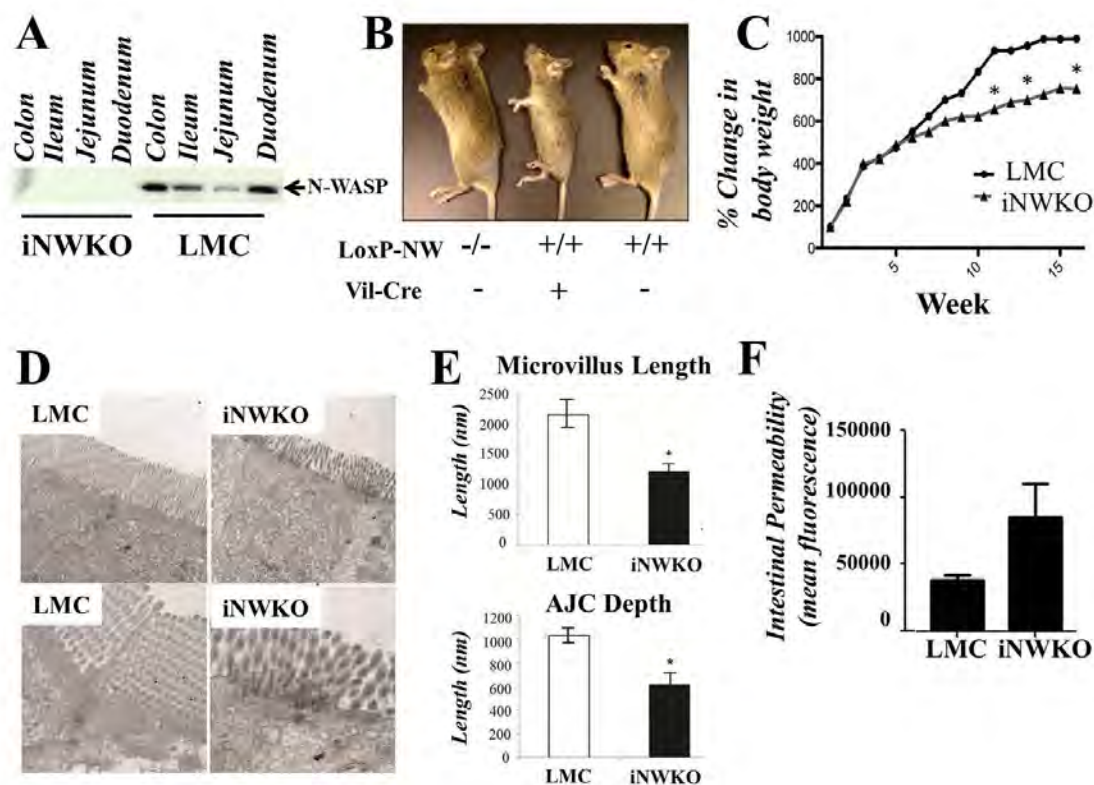
Figure 1. Characterization of a conditional, intestinal, N-WASP knockout mouse.
(A) Western blotting showing complete deletion of N-WASP in iNWKO mice. **(B)**
Overall appearance of wild type (LoxP-NW^{-/-}, Vil-Cre-) or littermate controls (NW^{+/+},
Vil-Cre-), and iNWKO (NW^{+/+}, Vil-Cre+) mice. iNWKO mice (middle animal) are
smaller than wild type mice and their littermate controls (left and right animals). **(C)**
Change in body weight of iNWKO and littermate controls over time. Littermate controls
are depicted by black circles and iNWKO mice are depicted by black triangles. Asterisk
(*) indicates that iNWKO is statistically different from littermate controls (p<0.05). **(D)**
Transmission electron microscopy of the intestines of iNWKO mice and littermate
control mice. **(E)** Microvillus length and apical junction complex depth were measured
in iNWKO mice and littermate controls. Shown are the average lengths (± SEM). **(F)**
Intestinal permeability of iNWKO mice compared to littermate controls measured as
mean fluorescence. Data are representative of one experiment using two-three mice per
group.

N-WASP promotes high-level colonization and systemic disease during *C. rodentium* (λ*stx$_{2dact}$*) infection.

In order to determine whether the N-WASP pathway of actin pedestal formation was required for colonization, iNWKO and littermate control mice were infected with approximately 1×10^9 CFU *C. rodentium* (λ*stx$_{2dact}$*) by oral gavage and intestinal colonization was monitored by viable stool counts throughout infection. Peak colonization in littermate controls occurred between 11 and 14 days post-infection and reached approximately 10^9 CFU/g stool. Colonization slowly diminished thereafter, and by 30 days post-infection, bacteria were no longer detected in the stool (**Figure 2**), presumably reflecting clearance by an adaptive immune response (Ghaem-Maghami et al., 2001; Simmons et al., 2003; Vallance et al., 2002). In comparison to littermate controls, colonization of iNWKO mice by *C. rodentium* (λ*stx$_{2dact}$*) was diminished ten- to 1000-fold, depending on the particular experiment, a difference that was statistically significant in two of four independently performed experiments (**Figure 2**). By 30 days post-infection, no bacteria were detected in the stool of iNWKO mice, presumably reflecting clearance by an adaptive immune response (Ghaem-Maghami et al., 2001; Simmons et al., 2003; Vallance et al., 2002). Tissue colonization was also measured in iNWKO and littermate control mice and, similar to fecal colonization, at 11 days post-infection colonization of the cecum and colon was significantly (1000-fold, $p<0.05$) attenuated in iNWKO mice compared to littermate controls (data not shown).

Weight loss is a common finding in murine models of HUS including infection of C57BL/6 mice with *C. rodentium* (λ*stx$_{2dact}$*) (**Chapter III**), infection of conventional
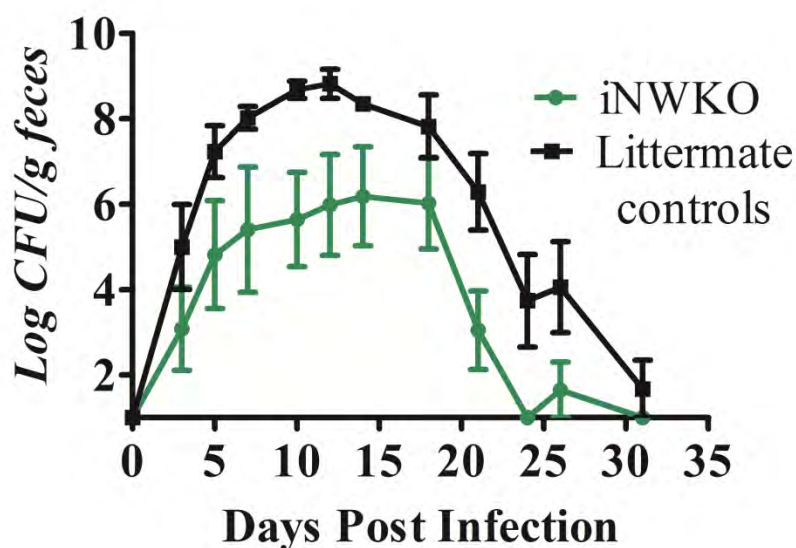
Figure 2. N-WASP promotes high-level colonization during *C. rodentium* (λstx_{2dact}) infection. (A) Colonization of iNWKO (green) or littermate controls (black) mice infected with *C. rodentium* (λstx_{2dact}) was determined by viable counts in stool samples. Shown are the average CFU (± SEM) of three iNWKO and two littermate controls. Data are representative of one of four single experiments using two-to-seven mice per group. Statistically significant differences between the two groups were determined by two-way ANOVA and Bonferroni's post-tests and in the experiment shown, no statistically significant differences were identified.

mice by EHEC, and injection of mice with Stx (mouse models of HUS are reviewed in (Mohawk and O'Brien, 2011)). Therefore, body weight loss was monitored throughout infection of iNWKO mice and littermate controls by *C. rodentium* (λ*stx$_{2dact}$*). Body weight remained constant (similar to day zero body weight) in littermate controls through nine days post-infection, however, by day ten post-infection, mice began losing weight (**Figure 3A**). Notably, the moderate weight loss displayed by the littermate controls during this time correlated not only with peak colonization, but also with mortality (in 40% of littermate control mice) (**Figure 3B**). The mice that survived infection re-gained lost weight as the infection started to be cleared at approximately 25 days post-infection (**Figure 3A**). In contrast, body weight of iNWKO mice remained constant throughout the course of infection (~30 days) and none of the iNWKO mice succumbed to lethal disease. These data indicate that N-WASP is required for weight loss and mortality upon murine infection by *C. rodentium* (λ*stx$_{2dact}$*).

Given that intestinal damage is often observed in patients with HUS and in murine infection by *C. rodentium* (λ*stx$_{2dact}$*) (**Chapter III**), intestinal sections of iNWKO mice and littermate control mice infected with *C. rodentium* (λ*stx$_{2dact}$*) were examined histologically. The intestines of littermate control mice displayed severe damage to the mucosal surface of the intestine (**Figure 4, left hand panel, asterisks**), infiltration of inflammatory cells (**Figure 4, left hand panel, arrowheads**), crypt withering, and depletion of goblet cells, all of which are evidence of acute injury. In contrast, the intestines of iNWKO mice appeared histologically normal with an intact mucosal surface and abundance of goblet cells (**Figure 4, right hand panel, arrows**). These data suggest
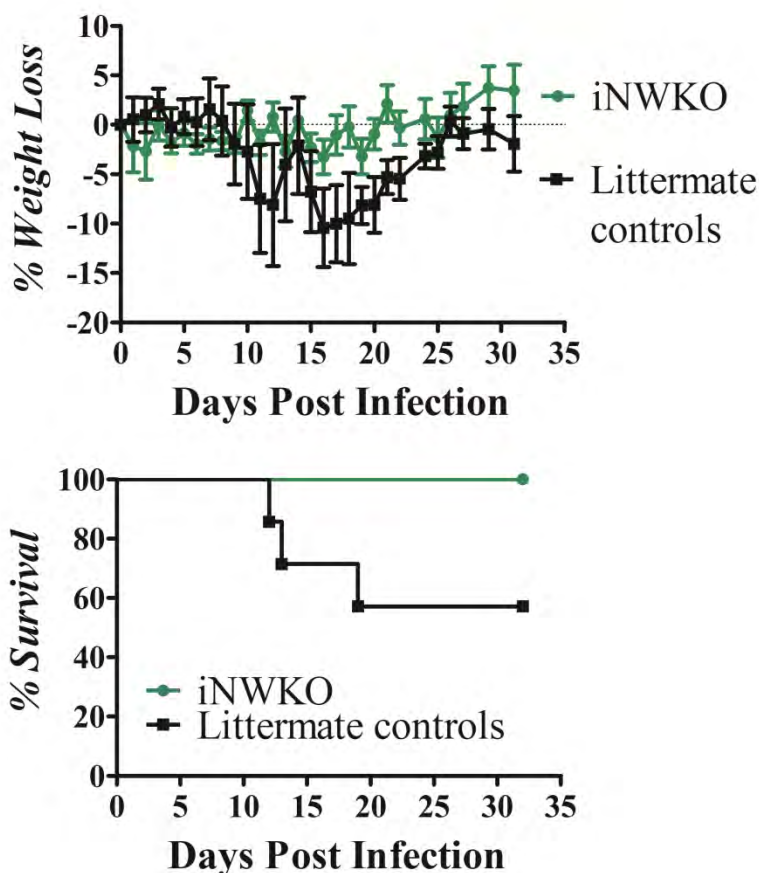
Figure 3. N-WASP is required for weight loss and mortality during *C. rodentium* (λ*stx*$_{2dact}$) infection. (A) Percent body weight during infection of iNWKO (green) or littermate controls (black) mice infected with *C. rodentium* (λ*stx*$_{2dact}$) was determined. Shown are the averages (±SEM) of six iNWKO and seven littermate control mice per group. Data are one representative of four independent experiments using two-to-seven mice per group. Statistically significant differences between the two groups were determined by two-way ANOVA and Bonferroni's post-tests and in the experiment shown, no statistically significant differences were identified. **(B)** Percent survival of iNWKO (green) or littermate control (black) mice infected with *C. rodentium* (λ*stx*$_{2dact}$). Statistical significance was determined using a Chi squared test and in the data presented there is not a statistically significant difference between the two groups. Data are one representative of four independent experiments using two-to-seven mice per group. Note that while the mortality rate for littermate controls was typically 40-50%, in one of the four experiments performed, none of the littermate controls suffered a lethal infection.
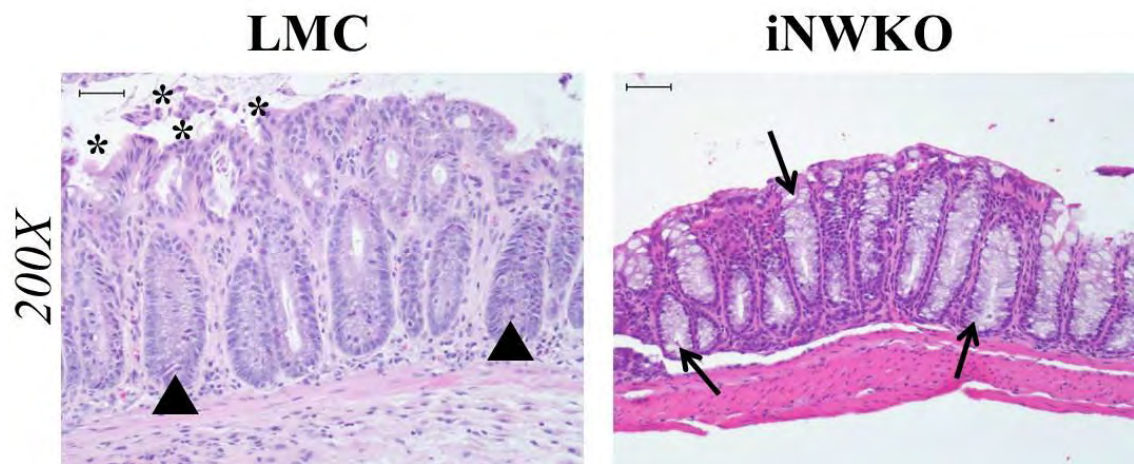
Figure 4. N-WASP promotes intestinal damage upon infection with *C. rodentium* (λ*stx₂dact*). H&E stained intestinal sections of iNWKO and littermate control mice infected with *C. rodentium* (λ*stx₂dact*) at 11 days post-infection are shown at 100x. Asterisks indicate areas where the integrity of the mucosal surface of the intestine has been destroyed. Arrow heads represent areas of inflammation and arrows represent areas of goblet cells. Scale bars measure 50 μm.

that intestinal N-WASP, and presumably the presence of a functional pathway to polymerize actin, is required for Stx-mediated intestinal damage.

HUS is known to manifest in renal disease during human EHEC infection as well as in murine models of HUS (Keepers et al., 2006; Lindgren et al., 1993; Mohawk and O'Brien, 2011; Sauter et al., 2008; Tarr et al., 2005) (**Chapter III**). Therefore, we assessed renal impairment by measuring protein content in urine of iNWKO mice or littermate controls infected with *C. rodentium* (λstx_{2dact}) (see **Materials and Methods**). Whereas the urine of iNWKO mice infected with *C. rodentium* (λstx_{2dact}) contained no protein or only trace levels, i.e. a protein index of 0-0.5 indicating <50 mg/dl, the urine of littermate control mice infected with *C. rodentium* (λstx_{2dact}) contained significantly elevated protein indices as early as one day post-infection (**Figure 5A**). Between one and 12 days post-infection, average urine protein indices were as high as 1 to 1.5, corresponding to approximately 50-100 mg/dl, indicating that infection by *C. rodentium* (λstx_{2dact}) results in renal compromise only in mice that express intestinal N-WASP. The compromise in renal function corresponded to severe damage to the proximal tubules, with cells sloughing into the lumen (**Figure 5B, left hand panel, arrows**) and flattening of proximal tubule cells (**Figure 5B, left hand panel, arrowheads**). Mitotic activity was observed in some proximal tubule cells, presumably reflecting regeneration of damaged cells (V.V. and E.M. unpublished observations). In contrast, the kidneys of iNWKO mice, which did not suffer proteinuria upon infection with *C. rodentium* (λstx_{2dact}), were structurally normal, and showed no evidence of renal damage (**Figure 5B, right hand**
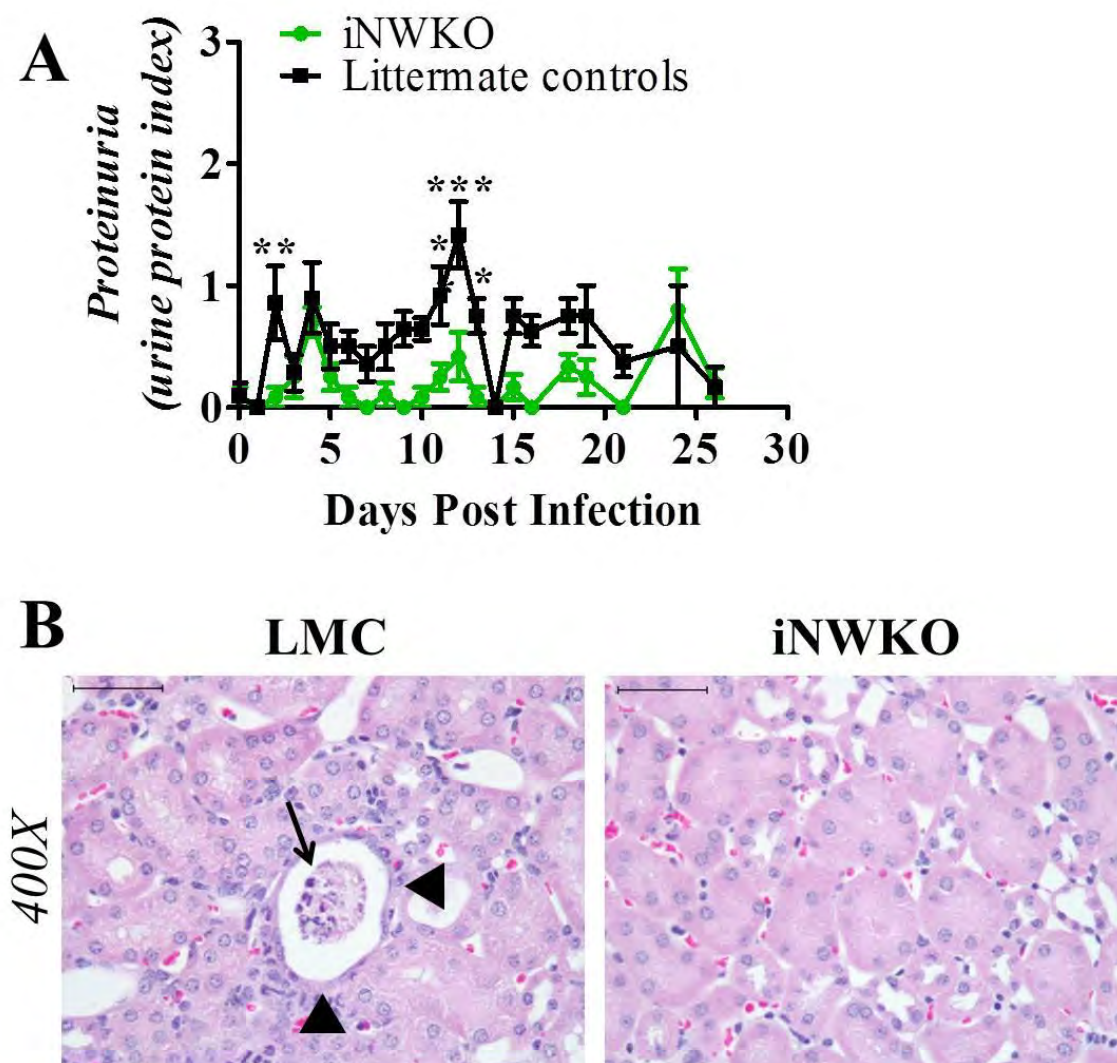
Figure 5. N-WASP promotes renal damage upon infection with *C. rodentium* (λ*stx₂dact*). **(A)** Urine protein content was monitored daily in iNWKO (green) or littermate control (black) mice infected with *C. rodentium* (λ*stx₂dact*) and is represented as average protein index (see **Materials and Methods**) (±SEM). Statistical significance was determined using a two-way ANOVA and Bonferroni post-tests; "*" (p<0.05), "**" (p<0.01), "***" (p<0.001) indicate a statistically significant difference between the two groups. Data are representative of one of three experiments using four-to-seven mice per group. **(B)** H&E-stained 400x micrograph of kidney sections from iNWKO or littermate control mice infected with *C. rodentium* (λ*stx₂dact*) at 11 days post-infection. Arrowheads indicate flattening of the lining of the tubules and arrows indicate sloughed tubules and necrotic tissue. Scale bars measure 50 μm.

panel). These data suggest that the presence of intestinal N-WASP is required for renal tubule damage upon infection by *C. rodentium* (λstx_{2dact}).

Tir-mediated actin pedestal formation is required for high-level fecal colonization by *C. rodentium* (λstx_{2dact}).

To further assess the requirement for Tir-mediated actin pedestal formation in colonization and Stx-mediated disease, we next infected wild type mice with a bacterial strain that is specifically defective in generating actin pedestals. We previously established that murine infection with *C. rodentium* (λstx_{2dact}) results in Tir-dependent colonization and Stx-mediated disease and that the defect in colonization and disease displayed by the *tir* mutant could be rescued in *trans* by a plasmid expressing wild type Tir ("pTir$_{WT}$") (**Chapter III**). Therefore, to abolish the ability of *C. rodentium* to generate actin pedestals, we generated a plasmid, pTir$_{Y471F}$, that expressed the Tir phenylalanine substitution mutant TirY471F, which is incapable of recruiting Nck and generating robust pedestals on cultured cells (Deng et al., 2003) (see **Materials and Methods**).

To ensure the Tir plasmids expressed similar levels of protein, a western blot was performed on bacterial lysates and TCA (trichloroacetic acid) precipitated bacterial proteins secreted into the culture media (**Supplementary Figure 1A and B**, respectively). *C. rodentium* (λstx_{2dact}) bacterial lysates produced a strong protein band that migrated at ~70 kD that reacted specifically with the anti-*C. rodentium* Tir antibody, while the same band was missing from the *tir* mutant. Plasmid expression of either
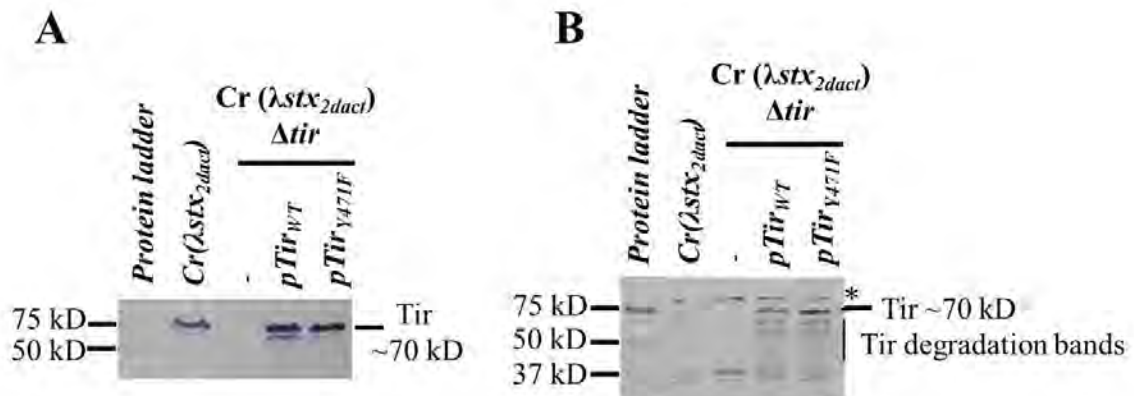
Supplementary Figure 1. Wild type Tir and Tir point mutants are expressed at similar levels. Western blot of Tir from isogenic strains of *C. rodentium* (λ*stx_{2dact}*) and representative *C. rodentium* (λ*stx_{2dact}*)Δ*tir, C. rodentium* (λ*stx_{2dact}*)Δ*tir*/pTir$_{WT}$, and *C. rodentium* (λ*stx_{2dact}*)Δ*tir*/pTir$_{Y471F}$ mutants. Note that although the predicted molecular weight of *C. rodentium* Tir is 56.2 kD, Deng and co-workers have previously shown that *C. rodentium* Tir migrates on SDS-PAGE at approximately 68 kDa (Deng et al., 2003) due to proposed post-translational modifications (DeVinney et al., 1999a; Kenny et al., 1997). **(A)** Bacterial lysates of isogenic strains of *C. rodentium* (λ*stx_{2dact}*) and representative *C. rodentium* (λ*stx_{2dact}*)Δ*tir, C. rodentium* (λ*stx_{2dact}*)Δ*tir*/pTir$_{WT}$, and *C. rodentium* (λ*stx_{2dact}*)Δ*tir*/pTir$_{Y471F}$ mutants. SDS-PAGE loading was standardized to culture OD$_{600}$ reading. Asterisk "*" designates Tir degradation bands. Membranes were blotted with anti-*C. rodentium* Tir antibody. **(B)** TCA precipitated culture supernatant from isogenic strains of *C. rodentium* (λ*stx_{2dact}*) and representative *C. rodentium* (λ*stx_{2dact}*)Δ*tir, C. rodentium* (λ*stx_{2dact}*)Δ*tir*/pTir$_{WT}$, and *C. rodentium* (λ*stx_{2dact}*)Δ*tir*/pTir$_{Y471F}$. SDS-PAGE loading was standardized to protein concentration. Membranes were blotted with anti-*C. rodentium* Tir antibody. Asterisk ("*") indicates an unknown band that cross-reacted with the anti- *C. rodentium* Tir antibody.

pTir$_{WT}$ or pTir$_{Y471F}$, was able to restore (or even increase to greater than endogenous levels) Tir expression the *tir* mutant in bacterial lysates (**Supplementary Figure 1A**). Similar to *C. rodentium* (λ*stx$_{2dact}$*), *C. rodentium* (λ*stx$_{2dact}$*)Δ*tir* expressing either pTir$_{WT}$ or pTir$_{Y471F}$ also generated several Tir-degradation bands <70 kD that reacted with the anti-*C. rodentium* Tir antibody. These results indicate that Tir is being expressed to similar levels in bacterial lysates of each of our strains.

To ensure Tir expressed from a plasmid was being secreted from the bacteria, and that type III secretion was functional in each of our strains, we measured the amount of Tir produced in bacterial culture supernatants of each of our strains. As shown in **Supplementary Figure 1B**, a ~70 kD band was present in culture supernatant from *C. rodentium* (λ*stx$_{2dact}$*) that was absent in the *tir* mutant. Expression of pTir$_{WT}$ or pTir$_{Y471F}$ generated a more intense band at 70 kD than seen in *C. rodentium* (λ*stx$_{2dact}$*), indicating that plasmid-based Tir is overexpressed in culture supernatants (**Supplementary Figure 1B**). These data demonstrate that Tir is indeed being expressed from the plasmid constructs and that the amount of Tir being produced is often greater than that produced from wild type *C. rodentium* (λ*stx$_{2dact}$*).

Next, we tested the ability of pTir$_{WT}$ and pTir$_{Y471F}$ to generate actin pedestals on mouse embryonic fibroblasts (MEFs) in a filamentous actin staining assay (FAS). As previously described, *C. rodentium* (λ*stx$_{2dact}$*) generated robust actin pedestals beneath bound bacteria (**Chapter III**, **Supplementary Figure 2, row 1**), while the *tir* mutant bound very poorly to cells and failed to generate any actin pedestals (**Supplementary Figure 2, row 2**) similar to the *tir* mutant complemented with the empty vector (pVector)
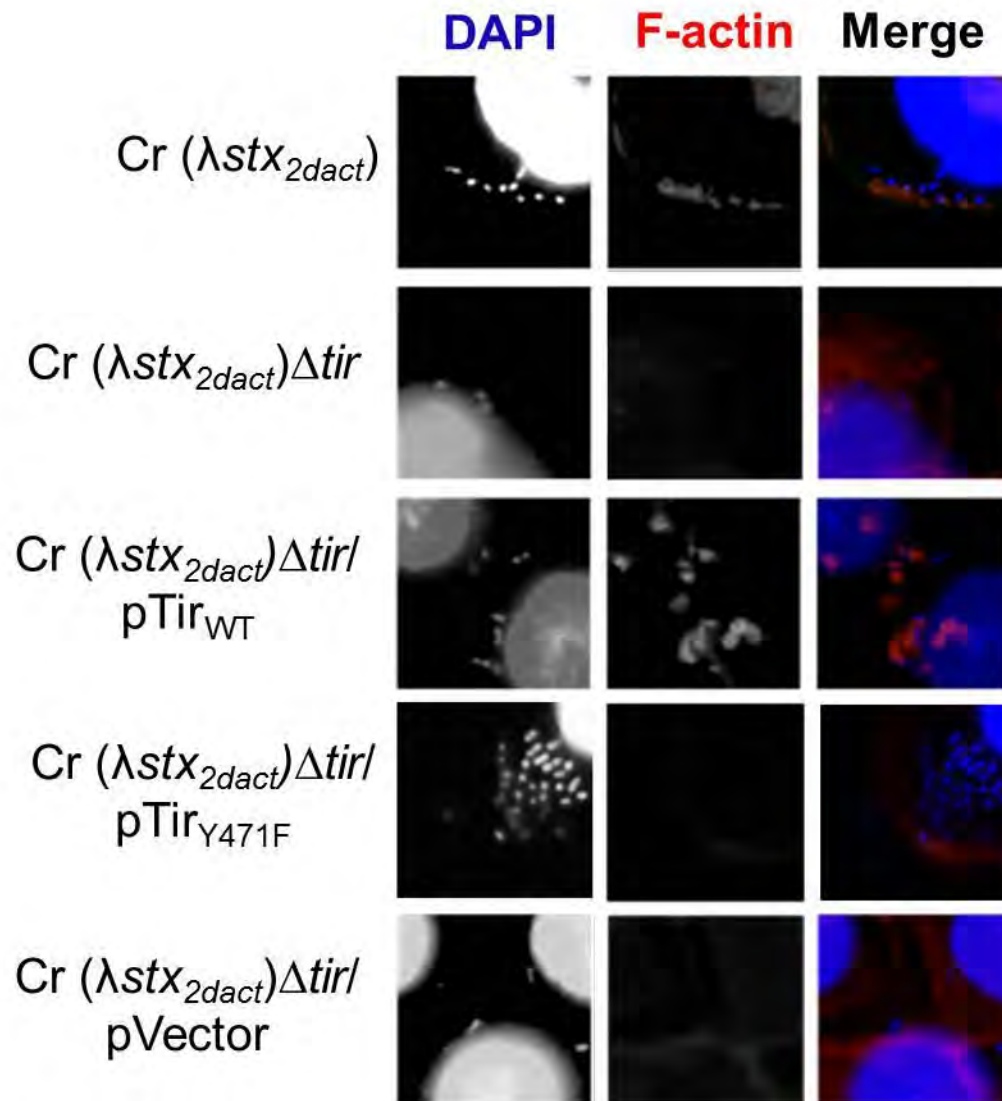
Supplementary Figure 2. TirY471F does not promote *C. rodentium* (λ*stx*$_{2dact}$) pedestal formation on cultured cells. Mouse embryonic fibroblasts (MEFs) were infected with isogenic strains of *C. rodentium* in a FAS assay. Bacteria and MEF cell nuclei were stained with DAPI (blue) and F-actin was stained with phalloidin (red).

(**Supplementary Figure 2, row 5**). In contrast, expression of pTir$_{WT}$ in *C. rodentium* (λ*stx$_{2dact}$*)Δ*tir* restored bacterial binding and pedestal formation on cultured cells (**Supplementary Figure 2, row 3**). Conversely, although the *C. rodentium* (λ*stx$_{2dact}$*)Δ*tir*/pTir$_{Y471F}$ was able to bind to cells, none of these bacteria were associated with actin pedestals (**Supplementary Figure 2, row 4**), verifying that the TirY471F mutant could promote bacterial binding to mammalian cells but was deficient in pedestal formation.

We subsequently utilized murine infection to assess the function of TirY471 when expressed in *C. rodentium* either expressing or not expressing Stx using the toxigenic, cell-binding, pedestal-deficient mutant (*C. rodentium* (λ*stx$_{2dact}$*)Δ*tir*/pTir$_{Y471F}$) and the non-toxigenic cell-binding, pedestal-deficient mutant (*C. rodentium*Δ*tir*/pTir$_{Y471F}$) to colonize C57BL/6 mice. Mice were infected with approximately $5x10^9$ CFU of the designated *C. rodentium* strain and fecal colonization was monitored every two-to-three days post-infection. We confirmed that infection with *C. rodentium* (λ*stx$_{2dact}$*) resulted in high-level colonization that peaked approximately seven days post-infection (**Chapter III; Figure 6**). In contrast, *C. rodentium* (λ*stx$_{2dact}$*)Δ*tir* was unable to detectably (>100 CFU/gram feces) colonize mice. Complementation of *C. rodentium* (λ*stx$_{2dact}$*)Δ*tir* with pTir$_{WT}$ restored colonization to near wild type levels (**Figure 6** and **Chapter III**). Infection with *C. rodentium* (λ*stx$_{2dact}$*)Δ*tir*/pTir$_{Y471F}$ resulted in a moderate (10- to 100-fold) defect in colonization, particularly late (>seven days) in infection, a defect that was statistically different from colonization by *C. rodentium* (λ*stx$_{2dact}$*)Δ*tir*/pTir$_{WT}$ in five out of the seven independently performed experiments (**Figure 6** and data not shown).
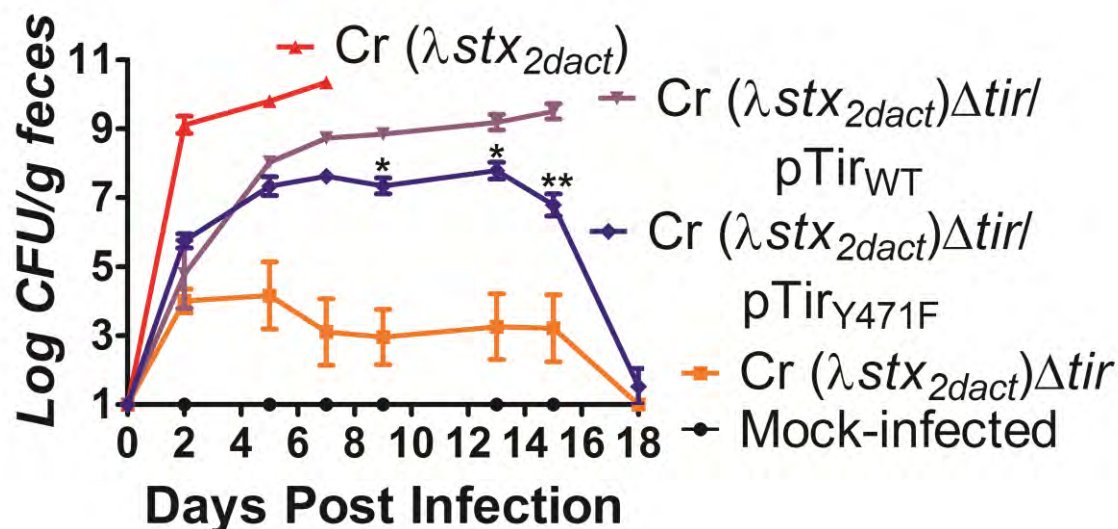
Figure 6. Tir-mediated actin pedestal formation is required for maximal intestinal colonization by *C. rodentium* (λ*stx2dact*). Colonization of eight-week old C57BL/6 mice infected with *C. rodentium* (λ*stx2dact*), *C. rodentium* (λ*stx2dact*)Δ*tir*, *C. rodentium* (λ*stx2dact*)Δ*tir*/pTir$_{WT}$, and *C. rodentium* (λ*stx2dact*)Δ*tir*/pTir$_{Y471F}$ was determined by viable counts in stool samples. Shown are the average CFU (± SEM) of five mice. Statistical significance was determined using two-way ANOVA and Bonferroni post-tests. "*" ($p < 0.05$) indicates that *C. rodentium* (λ*stx2dact*)Δ*tir*/pTir$_{WT}$ is significantly different from *C. rodentium* (λ*stx2dact*)Δ*tir*/pTir$_{Y471F}$. Data are representative of one of five single experiments. The results for *C. rodentium* (λ*stx2dact*), *C. rodentium* (λ*stx2dact*)Δ*tir*, and *C. rodentium* (λ*stx2dact*)Δ*tir*/pTir$_{WT}$ have been previously described and are included here for ease of comparison (see **Chapter III**).

The colonization defect was independent of Stx production because *C. rodentium*Δ*tir*/pTir_{Y471F}, which does not produce Stx, also typically colonized mice late in infection significantly less efficiently than the pedestal-proficient strains *C. rodentium* and *C. rodentium*Δ*tir*/pTir_{WT} (**Supplementary Figure 3**). These results suggest that Tir-mediated actin pedestal formation promotes late colonization by *C. rodentium* independently of Stx production.

Tir-mediated actin assembly and Stx-mediated disease by *C. rodentium* (λ*stx_{2dact}*).

Given that EHEC-induced HUS results in intestinal and renal damage, we next assessed intestinal and renal pathology in mice infected with either *C. rodentium* (λ*stx_{2dact}*)Δ*tir*, *C. rodentium* (λ*stx_{2dact}*)Δ*tir*/pTir_{WT}, or *C. rodentium* (λ*stx_{2dact}*)Δ*tir*/pTir_{Y471F} between ten and 13 days post-infection. Similar to our previous study (**Chapter III**), mice infected with the *tir* mutant had virtually no intestinal damage and an abundance of goblet cells (**Figure 7, left column, arrows**). In contrast, the intestines of mice infected with *C. rodentium* (λ*stx_{2dact}*)Δ*tir*/pTir_{WT} showed severe destruction of the intestinal mucosa, colitis, and acute ischemic injury with infiltration of inflammatory cells into the muscularis layer and lamina propria (**Figure 7, middle column, arrowheads**). Also present were areas of necrosis and degenerative changes in the epithelial cells with crypt withering (**Figure 7, middle column**). Interestingly, despite the fact that *C. rodentium* (λ*stx_{2dact}*)Δ*tir*/pTir_{Y471F} was able to colonize mice, infection was not associated with colonic damage (**Figure 7, right column**).
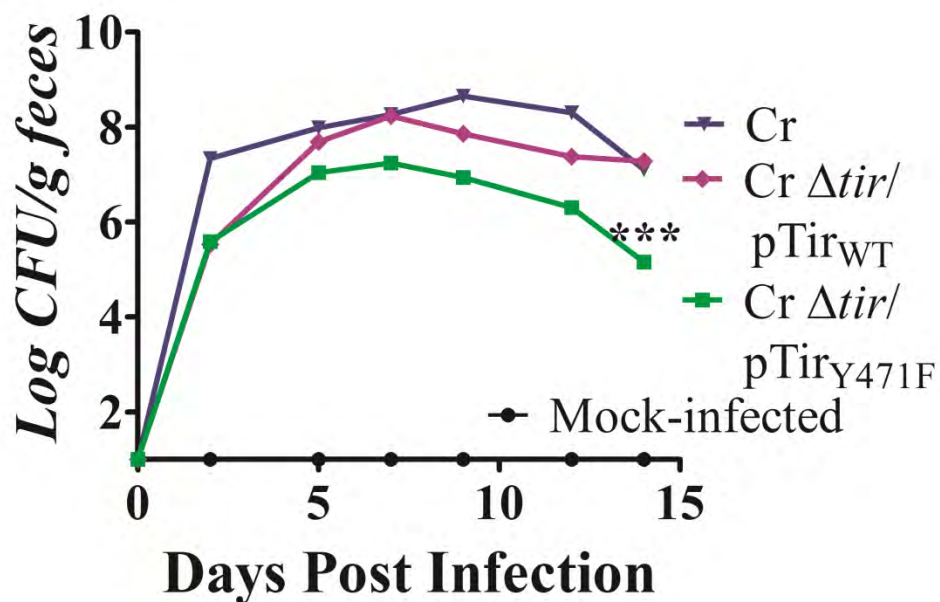
Supplementary Figure 3. Pedestal formation promotes colonization by *C. rodentium* that does not produce Shiga toxin. Fecal CFUs of mice infected with *C. rodentium, C. rodentium*Δtir, *C. rodentium*Δtir/pTir$_{WT}$, and *C. rodentium*Δtir/pTir$_{Y471F}$ were determined at indicated times post-infection. Shown are the average CFU ($\pm$ SEM) from groups of five eight-week old mice. Statistical significance was determined using two-way ANOVA and Bonferroni post-tests. "***" indicates a statistically significant difference from *C. rodentium* or *C. rodentium*Δtir/pTir$_{WT}$. Data shown are representative of one of three independent experiments.
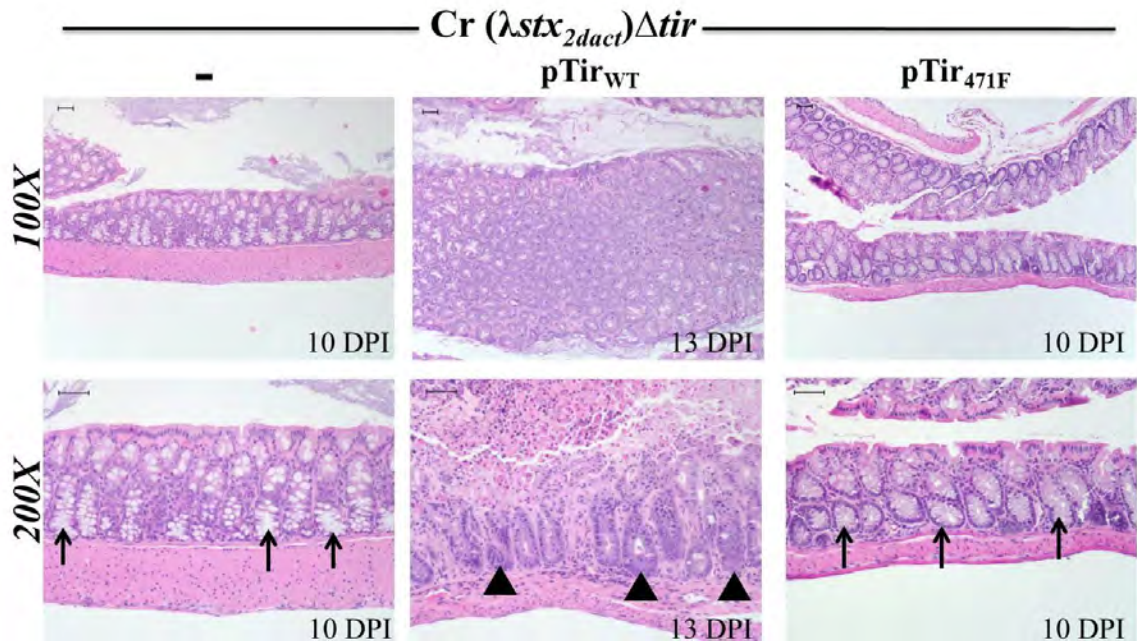
Figure 7. Tir-mediated actin assembly by *C. rodentium* (λ*stx₂dact*) promotes intestinal damage. H&E stained intestinal sections of mice infected with *C. rodentium* (λ*stx₂dact*)Δ*tir, C. rodentium* (λ*stx₂dact*)Δ*tir/*pTir$_{WT}$, and *C. rodentium* (λ*stx₂dact*)Δ*tir/*pTir$_{Y471F}$ at ten-to-13 days post-infection are shown at 100x (top) and 200x (bottom). Arrowheads indicate areas of inflammation/inflammatory infiltrates and arrows indicate areas of goblet cells. Scale bars measure 50 μm.

The majority of mouse Gb_3 receptors are present on the renal tubules (Psotka et al., 2009), therefore, much of renal destruction that resulting from infection with *C. rodentium* (λstx_{2dact}) occurs here. As previously shown (**Chapter III**), infection by *C. rodentium* (λstx_{2dact})Δtir/pTir$_{WT}$ resulted in extensive damage to the proximal tubules depicted by an attenuated or flattened epithelial lining, pyknotic nuclear material, and sloughing of dead cells in the tubular lumen (**Figure 8A, middle panel, arrowheads**). Mitotic activity, indicating regenerative repopulation of the proximal tubules, was also observed in some mice (data not shown). Similar to infection with *C. rodentium* (λstx_{2dact})Δtir, infection with *C. rodentium* (λstx_{2dact})Δtir/pTir$_{Y471F}$ did not result in damage to the proximal renal tubules (**Chapter III**; **Figure 8A, right panel**). Additionally, we observed significant increases ($p<0.001$) in proteinuria at five, six, and ten days post-infection in mice infected with *C. rodentium* (λstx_{2dact})Δtir/pTir$_{WT}$, compared to zero-to-trace levels of protein in mice infected with *C. rodentium* (λstx_{2dact})Δtir/pTir$_{Y471F}$ (**Figure 8B**). These findings provide evidence that actin pedestal formation, not simply Tir binding, is required for intestinal and renal tubule damage upon infection with *C. rodentium* (λstx_{2dact}).

Weight loss and death are consistent findings in murine models of Stx intoxication (Keepers et al., 2006; Mohawk and O'Brien, 2011; Sauter et al., 2008) and we have previously shown that Tir is required for weight loss and death upon murine infection by *C. rodentium* (λstx_{2dact}) (**Chapter III**). Therefore, we determined the requirement of TirY471 in systemic disease caused by *C. rodentium* (λstx_{2dact}). Similar to our previous study (**Chapter III**), mice infected with either *C. rodentium* (λstx_{2dact}) or *C.*
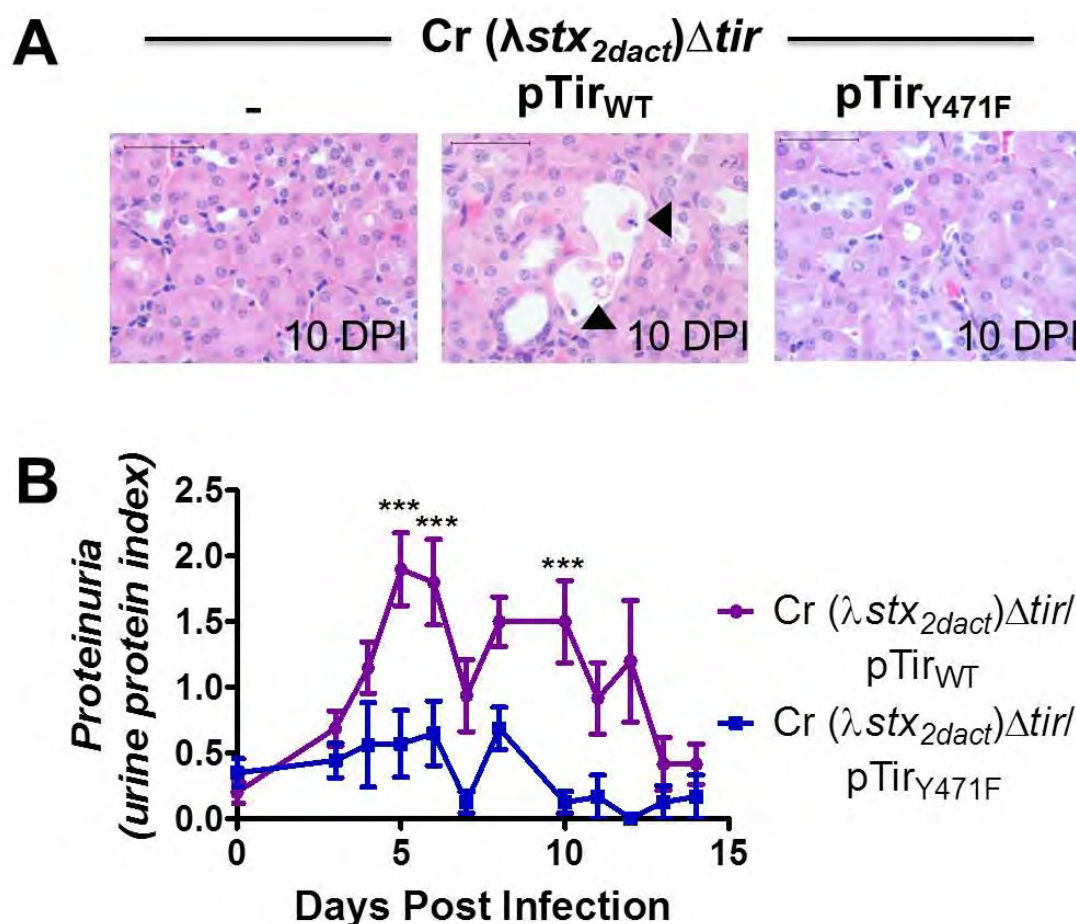
Figure 8. Tir-mediated actin assembly by *C. rodentium* (λ*stx₂dact*) promotes renal damage. (A) H&E-stained 600x micrograph of kidney sections from mice infected with *C. rodentium* (λ*stx₂dact*)Δ*tir* and *C. rodentium* (λ*stx₂dact*)Δ*tir*/pTir_{WT}, and *C. rodentium* (λ*stx₂dact*)Δ*tir*/pTir_{Y471F} at ten days post-infection. Sloughing and attenuation of epithelial cells within the proximal tubules is indicated by arrow head. Scale bars measure 50 μm. **(B)** Urine protein content was monitored daily in mice infected with *C. rodentium* (λ*stx₂dact*)Δ*tir*/pTir_{WT} (purple) and *C. rodentium* (λ*stx₂dact*)Δ*tir*/pTir_{Y471F} (blue) and is represented as average proteinuria index (see **Materials and Methods**) (±SEM). Statistical significance was determined using a two-way ANOVA and Bonferroni posttests; "***" ($p<0.001$) indicates a statistically significant difference between the two groups. Data are representative of one of two independent experiments using five-to-ten mice per group.
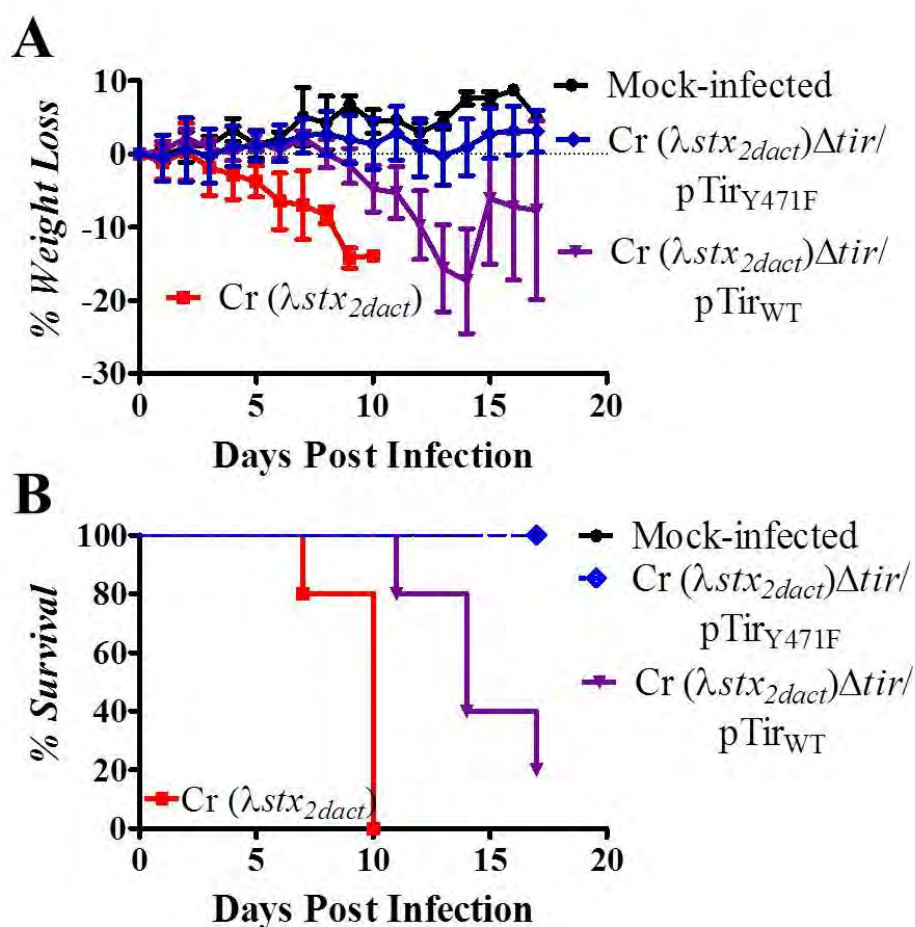
Figure 9. Tir-mediated actin assembly is required for weight loss and death by *C. rodentium* (λstx_{2dact}). (A) Body weight during infection of mock-infected eight-week-old C57BL/6 mice or mice infected with *C. rodentium* (λstx_{2dact}), *C. rodentium* (λstx_{2dact})Δtir/pTir$_{WT}$, or *C. rodentium* (λstx_{2dact})Δtir/pTir$_{Y471F}$ was determined and is expressed as percent change from day zero weight. Shown are the averages ($\pm$SEM) of five mice per group. Data are representative of one of six independent experiments. Statistical significance was determined using a two-way ANOVA and Bonferroni's Post Tests. **(B)** Percent survival of mock-infected eight-week old mice or mice infected with *C. rodentium* ($\lambda stx2_{dact}$), *C. rodentium* (λstx_{2dact})Δtir/pTir$_{WT}$, or *C. rodentium* (λstx_{2dact})Δtir/pTir$_{Y471F}$. Groups of six mice were analyzed. Data shown are representative of one of five independent experiments using six to eight mice per group. Statistical significance was determined using a Log-rank (Mantel-Cox) Test.

rodentium (λ*stx₂dact*)Δ*tir*/pTir_WT lost a significant amount [(mice infected with *C.*

rodentium (λ*stx₂dact*) lost significantly (p<0.05) more weight than mice infected with

other strains at six to ten days post infection; mice infected with *C. rodentium*

(λ*stx₂dact*)Δ*tir*/pTir_WT lost significantly more body weight than mice infected with *C.*

rodentium (λ*stx₂dact*)Δ*tir*/pTir_Y471F at 13 and 14 days post-infection (p<0.05) and (p<0.01),

respectively)] of body weight after approximately six and 11 days post-infection,

respectively (**Figure 9A**) and succumbed to lethal infection (infection by *C. rodentium*

(λ*stx₂dact*)Δ*tir*/pTir_WT resulted in significantly more death (p<0.05) than infection by *C.*

rodentium (λ*stx₂dact*)Δ*tir*/pTir_Y471F) (**Figure 9B**). In contrast, mock-infected mice and

mice infected with the *tir* mutant maintained day zero body weight or gained weight

throughout the course of infection (**Figure 9A**) and survived (**Figure 9B**). Interestingly,

mice infected with *C. rodentium* (λ*stx₂dact*)Δ*tir*/pTir_Y471F also maintained body weight

throughout infection and survived, implying that weight loss and death caused by *C.*

rodentium (λ*stx₂dact*) is dependent on the ability of the bacterium to generate actin

pedestals.

Actin pedestal formation promotes lethal infection independent of level of fecal

colonization.

We next assessed whether high-level colonization correlated with mortality by

analyzing peak fecal colonization levels of mice infected with each of our strains in a

total of seven independent experiments and whether the mouse survived or succumbed to

lethal infection. Peak colonization of mice infected with *C. rodentium* (λ*stx₂dact*) was

approximately 6.3×10^9 CFU/gram stool and infection always resulted in 100% mortality (**Figure 10, green**). The majority of mice infected with *C. rodentium* (λstx_{2dact})Δtir/pTir$_{WT}$ (62%) succumbed to lethal infection and peak colonization of these mice was 1.5×10^9 CFU/gram stool (**Figure 10, red**). In contrast, the peak colonization level of mice that survived infection by *C. rodentium* (λstx_{2dact})Δtir/pTir$_{WT}$ (38%) was much lower (5.0×10^7 CFU/gram stool) (**Figure 10, red**). The majority of mice infected with *C. rodentium* (λstx_{2dact})Δtir/pTir$_{Y471F}$ (95%) had lower peak colonization levels than mice infected with *C. rodentium* (λstx_{2dact})Δtir/pTir$_{WT}$ (7.9×10^7 CFU/gram stool), and survived infection (**Figure 10, black**). Interestingly, only one mouse (1/20) infected with *C. rodentium* (λstx_{2dact})Δtir/pTir$_{Y471F}$ succumbed to lethal infection and was very highly colonized (2.5×10^9 CFU/gram feces) (**Figure 10, black**). These data demonstrate that high-level colonization ($\geq 2.5 \times 10^9$ CFU/gram feces) regardless of the ability to generate actin pedestals, results in mortality. Indeed, logistic analysis of these data revealed that the relative risk factor for death increased approximately 11 times for every one-log unit of increase in fecal colonization (with a 95% confidence interval of 4.383-25.656), regardless of the strain of bacteria the mice were infected with.

We next determined whether infection with a strain able to generate actin pedestals resulted in more lethality at lower levels of colonization by comparing similar peak colonization levels of mice infected with *C. rodentium* (λstx_{2dact})Δtir/pTir$_{WT}$ and *C. rodentium* (λstx_{2dact})Δtir/pTir$_{Y471F}$ in conjunction with the outcome of infection. We stratified peak colonization levels into five intervals (<7.7 Log CFU/gram feces, 8.3-9.1 Log CFU/gram feces, 9.1-9.7 Log CFU/gram feces, and 9.7-10.7 Log CFU/gram feces)
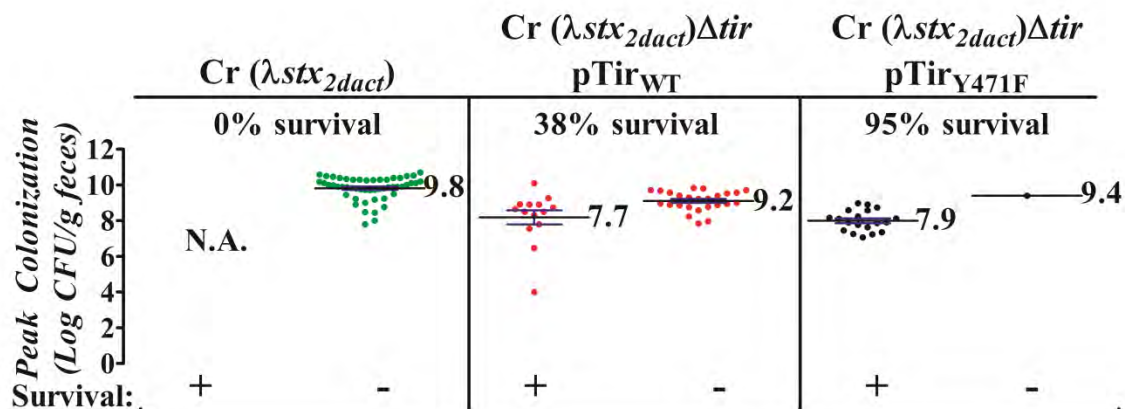
Figure 10. Actin assembly by *C. rodentium* (λ*stx₂dact*) promotes lethal infection independent of level of fecal colonization. Fecal CFUs of mice infected with *C. rodentium* (λ*stx₂dact*) (green), *C. rodentium* (λ*stx₂dact*)Δ*tir*/pTir$_{WT}$ (red), and *C. rodentium* (λ*stx₂dact*)Δ*tir*/pTir$_{Y471F}$ (black) were determined daily, and shown are the peak fecal CFU in each mouse. Black horizontal lines and the number next to the line represent the mean peak CFU for the designated group of mice. Error bars represent ± SEM. Data are representative of a compilation of seven independent experiments using groups of five eight-week old mice per group. Each dot represents one mouse. A total of 51, 40, and 20 mice were infected with *C. rodentium* (λ*stx₂dact*), *C. rodentium* (λ*stx₂dact*)Δ*tir*/pTir$_{WT}$, and *C. rodentium* (λ*stx₂dact*)Δ*tir*/pTir$_{Y471F}$, respectively. Whether the mouse survived or succumbed to lethal infection is depicted by "survival" at the top of the graph and by "+" or "-" on the x axis. N.A., not applicable.

Table 4. Actin pedestal formation promotes lethal infection independent of level of fecal colonization.

Range of fecal counts (log)	Cr (λstx_{2dact})Δtir/pTir		Cr (λstx_{2dact})Δtir/pTir$_{Y471F}$	
	Average log fecal colonization	% Lethality (#dead/total)	Average log fecal colonization	% Lethality (#dead/total)
9.7-10.7	9.8	80% (4/5)	na	na
9.1-9.7	9.3	91% (10/11)	9.4	100% (1/1)
8.3-9.1	8.8	**53%*** (8/15)	8.8	**0%** (0/5)
7.7-8.3	8.0	**60%*** (3/5)	8.0	**0%** (0/8)
Below 7.7	4.8	0% (0/4)	7.4	0% (0/6)

Average fecal counts were determined in each colonization interval for mice infected with the designated strain and are represented as Log(10) CFU/g feces. Data are compiled from seven independent experiments using groups of five eight-week old mice per group. Number in parentheses represents the number of mice that succumbed to lethal infection over the total number of mice colonized by the indicated strain at the indicated level. Asterisk (*) represents a statistically significant difference compared to mice infected with Cr (λstx_{2dact})Δtir/pTir$_{Y471F}$ (p<0.05). na, not applicable. Note: stratification of fecal colonization levels were grouped such that there was an approximately even distribution of mice within each interval and the average fecal colonization level of each interval was the same for mice infected with Cr (λstx_{2dact})Δtir/pTir and Cr (λstx_{2dact})Δtir/pTir$_{Y471F}$.

and determined the average peak colonization and percent lethality in each interval (**Table 4**). Both *C. rodentium* (λstx_{2dact})Δtir/pTir$_{WT}$ and *C. rodentium* (λstx_{2dact})Δtir/pTir$_{Y471F}$ were capable of colonizing mice to 1.9×10^8 to 1.2×10^9 CFU/gram stool, however, significantly more mice infected with *C. rodentium* (λstx_{2dact})Δtir/pTir$_{WT}$ succumbed to lethal infection (53% and 0%, respectively; p<0.05) (**Figure 10, Table 4**). Similarly, infection by *C. rodentium* (λstx_{2dact})Δtir/pTir$_{WT}$ resulted in significantly (p<0.05) more death (60%) at even lower levels of peak colonization (5.0×10^7 to 1.9×10^8 CFU/gram stool) compared to no death in mice infected with *C. rodentium* (λstx_{2dact})Δtir/pTir$_{Y471F}$ colonized to the same amount (**Figure 10, Table 4**).

In addition to the stratification analysis, a logistic regression analysis was also performed on these data. We determined that even when the levels of fecal colonization are normalized, mice infected with *C. rodentium* (λstx_{2dact})Δtir/pTir$_{WT}$ have a 16-times greater relative risk (with a 95% confidence interval of 1.712-147.345) of succumbing to lethal infection compared to mice infected with the pedestal-deficient *C. rodentium* (λstx_{2dact})Δtir/pTir$_{Y471F}$ strain. Taken together, these data indicate that Tir-mediated actin pedestal formation facilitates in Stx-mediated killing at any level of colonization.

Tir-mediated actin pedestal formation facilitates efficient colonization of the colonic mucosa by *C. rodentium* (λstx_{2dact}).

Fecal counts of mice infected with *C. rodentium* (λstx_{2dact})Δtir/pTir$_{Y471F}$ were somewhat diminished relative to *C. rodentium* (λstx_{2dact})Δtir/pTir$_{WT}$ late in infection, so we determined bacterial counts that were closely associated with different segments of

the intestine. Mice infected with *C. rodentium* (λstx_{2dact})Δtir/pTir$_{WT}$ or *C. rodentium* (λstx_{2dact})Δtir/pTir$_{Y471F}$ were sacrificed at six days post-infection, the cecum and the colon were isolated and fecal contents were removed. In addition, the lumen was flushed with PBS. The number of *C. rodentium* associated with the feces, the luminal washings, or cecal or colonic homogenates were determined by plating for viable counts (see **Materials and Methods**). Cecal and colonic colonization were then compared to fecal and luminal colonization. (Note: fecal and luminal colonization are often highly related and therefore, are usually equivalent). As expected, fecal colonization was similar (and not statistically different) between mice infected with the *tir* mutant expressing pTir$_{WT}$ and mice infected with the *tir* mutant expressing pTir$_{Y471F}$, with mean fecal counts of 3.1×10^8 and 3.1×10^7 CFU/gram, respectively (**Figure 11A**, **far left panel**), similar to what was observed previously (**Figure 6**). Likewise, there was no difference in luminal colonization between mice infected with *C. rodentium* (λstx_{2dact})Δtir/pTir$_{WT}$ or *C. rodentium* (λstx_{2dact})Δtir/pTir$_{Y471F}$ (**Figure 11A, middle left panel, "luminal washings"**), suggesting that the ability to generate actin pedestals does not influence the ability of the bacterium to colonize the lumen of the intestine. We next quantified bacterial colonization of the cecum, which is the first site of colonization in *C. rodentium* infection (Wiles et al., 2004), in the pedestal-proficient and pedestal-deficient mutant. Cecal colonization of mice infected with *C. rodentium* (λstx_{2dact})Δtir/pTir$_{WT}$ was comparable to mice infected with *C. rodentium* (λstx_{2dact})Δtir/pTir$_{Y471F}$ (**Figure 11A, middle right panel**). Surprisingly, however, the colons of mice infected with *C. rodentium* (λstx_{2dact})Δtir/pTir$_{WT}$ were significantly ($p<0.01$) more colonized than those of
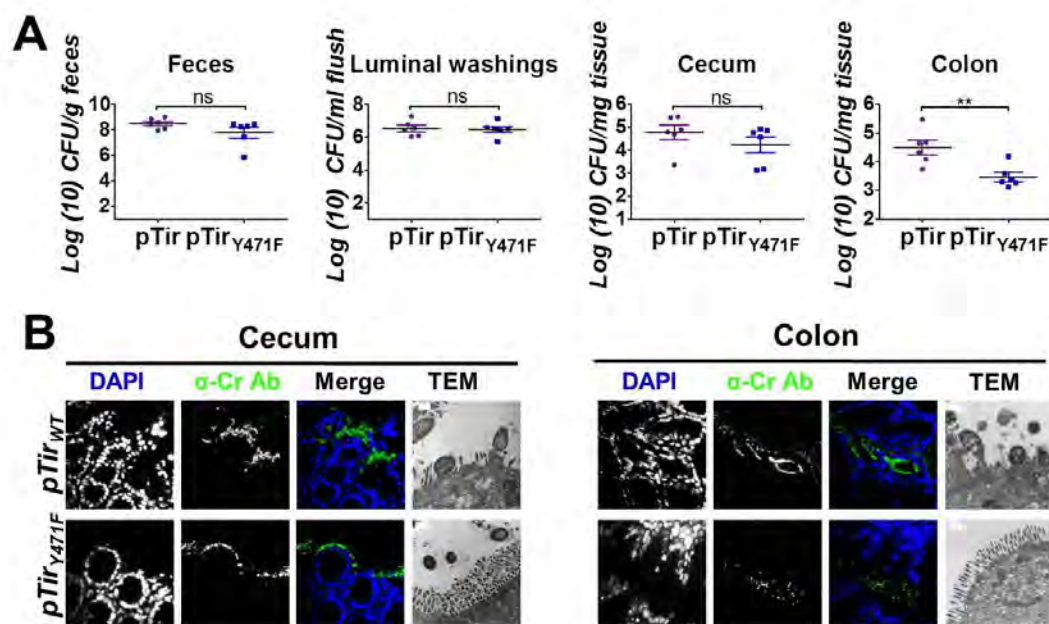
Figure 11. Tir-mediated actin assembly by C. *rodentium* (λ*stx₂dact*) promotes colonization of the mucosal surface. (A) Fecal colonization of eight-week old C57BL/6 mice infected with *C. rodentium* (λ*stx₂dact*)Δ*tir*/pTir$_{WT}$ and *C. rodentium* (λ*stx₂dact*)Δ*tir*/pTir$_{Y471F}$ was determined by viable stool counts at six days post-infection (left panel). Luminal colonization at six days post-infection was determined by plating serial dilutions of luminal contents and determining CFU/ml flush (see **Materials and Methods**) (middle left panel). Intestinal colonization [cecum (middle right panel) and colonic (right panel)] was determined by harvesting intestines at six days post-infection, homogenizing, and plating for CFU (See **Materials and Methods**). Data are a compilation of two experiments using three mice per group. Each data point represents a different mouse and horizontal line indicates the mean. Error bars indicate ± SEM. Statistical significance was determined using an unpaired *t*-test. "**" ($p<0.01$) indicates a statistically significant difference between the two groups. **(B)** Cecal (left) and colonic (right) sections of mice infected with *C. rodentium* (λ*stx₂dact*)Δ*tir*/pTir$_{WT}$ or *C. rodentium* (λ*stx₂dact*)Δ*tir*/pTir$_{Y471F}$ at ten days post-infection were either stained with DAPI (blue) and anti-*Citrobacter* antibody to visualize bacteria adhered to the intestinal surface (green) or processed for TEM (Note: colonic tissue was taken at six days post-infection and processed for TEM). Fecal counts of mice infected with each strain were equivalent. For the immunofluorescence and cecal TEM experiment, at ten days post-infection mice infected with *C. rodentium* (λ*stx₂dact*)Δ*tir*/pTir$_{WT}$ and *C. rodentium* (λ*stx₂dact*)Δ*tir*/pTir$_{Y471F}$ were colonized in the stool to 4.8×10^7 CFU/g and 3.6×10^7 CFU/g for, respectively. In the colonic TEM experiment at five days post-infection, fecal colonization levels were 1.1×10^7 CFU/g, 1.6×10^7 CFU/g for *C. rodentium* (λ*stx₂dact*)Δ*tir*/pTir$_{WT}$ and *C. rodentium* (λ*stx₂dact*)Δ*tir*/pTir$_{Y471F}$, respectively. White scale bars in TEM images measure 0.5 μm, magnification 20,500x.

mice infected with *C. rodentium* (λstx_{2dact})Δtir/pTir$_{Y471F}$ (~10^5 CFU/mg colon and 10^3 CFU/mg colon, respectively). These data provide evidence that the ability to generate actin pedestals aids in colonization of the colon (**Figure 11A, far right panel**).

We next utilized immunofluorescence staining to assess mucosal colonization of the cecum and colon in greater detail. At ten days post-infection intestinal sections of mice infected with *C. rodentium* (λstx_{2dact})Δtir/pTir$_{WT}$ or *C. rodentium* (λstx_{2dact})Δtir/pTir$_{Y471F}$ with similar levels of fecal colonization (4.8×10^7 and 3.6×10^7 CFU/gram stool, respectively) were stained with anti-*Citrobacter* antibody and DAPI and evaluated microscopically. The cecum of mice infected with *C. rodentium* (λstx_{2dact})Δtir/pTir$_{WT}$ contained bacteria adhered to the mucosal surface that penetrated into the intestinal crypts (**Figure 11B, left panel, top row**). Similarly, bacteria were closely adhered to the surface of cecal enterocytes mice infected with *C. rodentium* (λstx_{2dact})Δtir/pTir$_{Y471F}$ (**Figure 11B, left panel, bottom row**). These data indicate that actin pedestal formation is dispensable for colonization of the cecal mucosa.

In the colon, bacteria were closely adhered to the mucosal surface and penetrated deep into the intestinal crypts of mice infected with *C. rodentium* (λstx_{2dact})Δtir/pTir$_{WT}$ (**Figure 11B, right panel, top row**). In contrast, despite high-level fecal colonization comparable to fecal colonization levels in mice infected with *C. rodentium* (λstx_{2dact})Δtir/pTir$_{WT}$, few bacteria were closely associated with the colonic surface on mice infected with *C. rodentium* (λstx_{2dact})Δtir/pTir$_{Y471F}$, and the majority of the bacteria were located within the intestinal lumen (**Figure 11B, right panel, bottom row**).

To determine if the mucosal colonization observed for *C. rodentium* (λstx_{2dact}) derivatives expressing wild type Tir reflected *bona fide* AE lesion formation, cecal and colonic tissue were collected (see **Materials and Methods**) at six (colonic) and ten (cecal) days post-infection to assess surface colonization by transmission electron microscopy. The cecum of mice infected with *C. rodentium* (λstx_{2dact})Δtir/pTir formed distinct AE lesions on the intestinal surface (**Figure 11B, left panel, top row**). Infection by *C. rodentium* (λstx_{2dact})Δtir/pTir$_{Y471F}$ resulted in close attachment of bacteria to the mucosal surface, as seen by immunofluorescence, however, no distinct AE lesions were identified (**Figure 11B, left panel, bottom row**). Actin pedestals were also present on the colons of mice infected *C. rodentium* (λstx_{2dact})Δtir/pTir$_{WT}$ (**Figure 11B, right panel, top row**). Interestingly, and contrary to what was previously seen by Deng and co-workers (Deng et al., 2003), the majority of the colons of mice infected with *C. rodentium* (λstx_{2dact})Δtir/pTir$_{Y471F}$ were devoid of bacteria (**Figure 11B, right panel, bottom row**). Extensive examination of samples revealed rare bacteria associated with the intestinal colonic surface and evidence of actin accumulation beneath these few bound bacteria was lacking (data not shown). These results suggest that pedestal formation is required for mucosal colonization of colonic but not cecal epithelium.

Discussion

While the requirement for Tir in colonization is well documented (Deng et al., 2003; Marches et al., 2000; Ritchie et al., 2003; Schauer and Falkow, 1993b; Tzipori et al., 1995), the ability of Tir-mediated actin pedestal formation has been associated with either no or only a modest colonization defect in several animal models (Crepin et al., 2010; Deng et al., 2003; Vlisidou et al., 2006a). We addressed the role of Tir-promoted actin assembly in a murine model for Stx-mediated disease (**Chapter III**). *C. rodentium* (λstx_{2dact}) was incapable of maximal colonization of mice deficient in intestinal N-WASP, a host nucleation promoting factor that is required for pedestal formation by *C. rodentium*. N-WASP has been previously shown to be required for efficient type III secretion (Vingadassalom et al., 2010), raising the possibility that the colonization defect observed may in part be due to diminished type III secretion, a process required for efficient colonization (Deng et al., 2004; Ritchie and Waldor, 2005).

Thus, we also evaluated colonization by *C. rodentium* (λstx_{2dact}) expressing the mutant TirY471, which lacks the ability to recruit the host adaptor Nck that promotes robust actin assembly (Campellone et al., 2002; Gruenheid et al., 2001). This mutant was incapable of actin pedestal formation *in vitro*, consistent with previous results (Campellone et al., 2002; Deng et al., 2003; Gruenheid et al., 2001). In contrast to several previous findings in which AE strains incapable of pedestal formation *in vitro* nevertheless appeared to efficiently generate AE lesions during infection of animals (Crepin et al., 2010; Deng et al., 2003; Vlisidou et al., 2006a) or intestinal explants (Schuller et al., 2007), we found that *C. rodentium* (λstx_{2dact}) expressing TirY471 was

only very rarely intimately associated with intestinal epithelium (**Figure 11B** and data not shown). Numerous differences in methodology, such as the choice of host animal, infecting bacterium or intestinal segment(s) examined (see below) may account for the discrepant findings.

We found that the actin pedestal formation by *C. rodentium* (λstx_{2dact}) was not required for colonization of the cecal mucosa. Localization of *C. rodentium* on the epithelial surface by immunofluorescence microscopy and quantitation of viable bacteria in cecal homogenates revealed no differences between *C. rodentium* (λstx_{2dact}) expressing TirY471F or wild type Tir. TEM analysis showed that *C. rodentium* expressing TirY471F was closely associated with the cecal epithelium, although bacteria did not form canonical AE lesions, suggesting that, as is the case in the colon, Nck-mediated actin assembly is required for pedestal formation in this intestinal segment. Apparently, translocation of Tir to the plasma membrane of cecal epithelial cells, followed by intimin-mediated attachment, is sufficient to promote bacterial infection of the cecal mucosa even without subsequent robust actin assembly.

In contrast, colonization of the colonic epithelium was largely dependent on the ability of Tir to trigger robust pedestal formation. Although *C. rodentium* (λstx_{2dact}) expressing TirY471F was found in high numbers in feces and luminal washings, analysis of bacterial-mucosal interaction by TEM and immunofluorescence microscopy, and assessment of living bacteria plating for viable counts, indicated that the mutant was severely defective in colonization of the colonic mucosa (**Figure 11**). Analysis of infection by non-toxigenic *C. rodentium* strains suggested that the colonization defect

associated with TirY471F is independent of Stx (**Supplementary Figure 3**). In addition, a non-toxigenic derivative of an EHEC mutant lacking $EspF_U$, a type III translocated effector that generates pedestals in concert with EHEC Tir, similarly displayed a defect in mucosal colonization (Ritchie et al., 2008), suggesting that a defect in pedestal formation, regardless of its underlying etiology or the presence or absence of Stx, compromises epithelial colonization.

The critical colonic colonization function provided by pedestal formation is not known. Pedestal formation, by promoting (indirect) attachment of the bacterium to the host cytoskeleton, may stabilize bacteria at the cell surface. Indeed, the ability to generate actin assembly is associated with enhanced intimin binding by Tir localized in the plasma membrane of cultured mammalian cells (M. Brady, S. Battle, P. Kailasan, and G. Hecht, personal communication). Alternatively, both EHEC and EPEC have been demonstrated to be propelled on the surface of cultured mammalian cells in an actin-dependent manner (Sanger et al., 1996; Shaner et al., 2005). One can speculate that, similar to actin-based cell-to-cell spread by *Vaccinia* virus (Goldberg, 2001), pedestal formation may promote movement of AE pathogens on the intestinal epithelium, perhaps resulting in lateral spread and the formation of bacterial aggregates that occupy relatively large patches of intestinal mucosa (Ritchie et al., 2008).

Regardless of the mechanism of pedestal-mediated enhancement of epithelial colonization, apparently this function is required in the colon more so than in the cecum. The differential requirement for pedestal formation may be related to the observation that blind pouches or cul de sacs, of which the cecum is an example, are more efficiently

colonized by AE pathogens on the basis of their anatomy (Sherman and Boedeker, 1987).

In addition, the cecum is the initial site of *C. rodentium* colonization in mice (Wiles et al.,

2004) and EHEC colonization in lambs, calves, and chickens (Beery et al., 1985; Dean-

Nystrom et al., 1999; Wales et al., 2001; Wiles et al., 2004), indicating that it may

provide AE pathogens with an environment in which to establish an initial intestinal

infection. Apparently, this environment is "hospitable" enough to support mucosal

colonization in the absence of robust pedestal formation. Nevertheless, the observation

that a *C. rodentium* TirY471A/Y451A double mutant, which is defective in both the

TirY451-mediated, Nck-independent actin assembly pathway and the TirY471-mediated,

Nck-dependent pathway, is severely defective during murine co-infection studies with

wild type *C. rodentium*, whereas either single tyrosine substitution alone is not, suggests

that efficient colonization of even the cecum may require some level of Tir-mediated

actin assembly.

A striking feature was that although we found that colonic colonization by *C.

rodentium* (λstx_{2dact}) expressing TirY471F was diminished dramatically (i.e.

approximately 50-fold) when assessed by viable counts, colonization of the feces or of

luminal washings revealed no or only a moderate (approximately five-fold) colonization

defect. Similarly, during infant rabbit infection, the fecal colonization defect of an

EspF$_U$- (and pedestal-) deficient EHEC strain was muted compared to its defect in tissue

colonization (Ritchie et al., 2008). We speculate that the efficient colonization of the

cecum by *C. rodentium* (λstx_{2dact}) expressing TirY471F provides an abundant source of

these bacteria in the feces, but that, lacking the ability to form pedestals, these bacteria

are unable to stably localize to the colonic epithelium. Interestingly, fecal counts are routinely used to follow colonization by AE pathogens (Crepin et al., 2010; Deng et al., 2003; Girard et al., 2009a; Marches et al., 2005; Mundy et al., 2004; Ritchie and Waldor, 2005; Vlisidou et al., 2006a), and the failure of this method to accurately reflect more severe segment-specific mucosal colonization defects may contribute to the inability of many studies to detect epithelial colonization defects of pedestal-defective AE pathogens.

The ability to generate actin pedestals had a dramatic effect on toxin-mediated disease. Mice lacking intestinal N-WASP uniformly survived infection by *C. rodentium* (λstx_{2dact}), whereas littermate controls lost weight and exhibited 50% lethality. Consistent with the hypothesis that the protection afforded by N-WASP-deficiency was due to the role of N-WASP in pedestal formation, C57BL/6 mice infected with *C. rodentium* (λstx_{2dact}) expressing TirY471F routinely survived, whereas 62% of mice infected with *C. rodentium* (λstx_{2dact}) expressing wild type suffered lethal infection. Lethal disease was likely a function of Stx production, because wild type-infected mice exhibited manifestations of toxemia, including weight loss, proteinuria, renal damage, and intestinal damage. Although *C. rodentium* (λstx_{2dact}) expressing TirY471F did not, on average, colonize to the same degree as wild type *C. rodentium* (λstx_{2dact}), mice infected with wild type *C. rodentium* (λstx_{2dact}) were still dramatically more likely to suffer lethal consequences of infection even after normalizing for fecal colonization (**Table 4, Figure 10**).

The association of actin pedestal formation with lethal toxigenic disease may be multifactorial. First, it is tempting to speculate that the production of Stx by bacteria in

intimate proximity to the mucosal surface facilitates toxin uptake across the epithelium and into the bloodstream, where it may readily access endothelium, its major target. In addition, the barrier function of epithelium may be compromised by pedestal formation, which alters the apical actin network that promotes tight junction integrity, or by an inflammatory response to the simple proximity of bacteria (and their proinflammatory components) to the epithelial surface. Interestingly, infection by the recently emerged *E. coli* O1O4:H4, a Stx-producing strain that is related to the highly adherent enteroaggregative *E. coli* (EAEC) (Rasko et al., 2011), is associated with a high rate of rapidly progressing Stx-mediated disease and HUS, giving rise to speculation that the combination of tight bacterial adherence and Stx production is particularly effective at triggering severe disease (Bielaszewska et al., 2011). Thus, the analysis of how Tir-mediated pedestal formation, a virulence attribute that facilitates tissue-specific mucosal colonization, promotes lethality during infection by *C. rodentium* (λstx_{2dact}) may provide general insight into the pathogenesis of toxigenic mucosal pathogens.

CHAPTER V.

DISCUSSION

The striking AE lesion was first described in the early 1980's (Riley et al., 1983) and much has been learned about the mechanism of AE lesion formation. However, nearly all the work has been done using biochemical or cell culture approaches. To examine the biological significance of properties of EHEC or purified EHEC proteins characterized *in vitro* one must be able to assay their function during infection of mammalian hosts. Several animal models exist to study the pathogenesis of EHEC (for review, see (Mohawk and O'Brien, 2011; Wales et al., 2005)), yet no single model recapitulates all aspects of colonization and Stx-mediated disease.

The bacterial adhesin intimin has been shown to promote tight attachment and pedestal formation via Tir binding ((Hartland et al., 1999; Kenny et al., 1997), for review, see (Campellone, 2010; Caron et al., 2006; Hayward et al., 2006)), and to promote colonization (Marches et al., 2000; Schauer and Falkow, 1993b; Tzipori et al., 1995). Some alleles of intimin, including EHEC intimin, cannot be easily tested for function because of the lack of a murine model. In addition, Tir-independent functions of intimin have been demonstrated *in vitro*, but the *in vivo* significance of these functions remains unknown. Finally, Tir has been shown to be critical for actin assembly (for review, see (Campellone, 2010; Caron et al., 2006)), and despite the fact that the mechanisms of pedestal formation have been well characterized, the significance of pedestal formation has not been clearly defined.

In this thesis we first addressed the allele- and Tir-dependent and independent roles of intimin during infection using two animal infection models. Next, we developed a novel murine model of EHEC Stx-mediated disease. Finally, using this model, we addressed the role of Tir-mediated actin pedestal formation in colonization and Stx-mediated disease.

Allele- and Tir-independent functions of intimin

Efficient attachment to mammalian cells is an essential step in bacterial pathogenesis. Indeed, the AE pathogens EHEC, EPEC, and *C. rodentium* employ a multitude of ways to attach to host cells. Initial attachment is mediated by fimbriae, pili, curli, surface proteins, outer-membrane proteins, and flagella (for review, see (Bardiau et al., 2010; Nougayrede et al., 2003; Torres et al., 2005)). The most well characterized bacterial adhesin for AE pathogens, however, is intimin, which binds to the bacterial type III secreted effector Tir, initiating intimate attachment.

In addition to binding Tir, intimin may also provide Tir-independent functions. For example, intimin has been shown to bind mammalian proteins *in vitro* including β_1-chain integrins and nucleolin (Frankel et al., 1996a; Sinclair and O'Brien, 2002). In addition, intimin contributes to disruption of epithelial barrier function *in vitro* in a Tir-independent manner (Dean and Kenny, 2004). Despite these *in vitro* findings, little is known about the Tir-independent functions of intimin *in vivo*.

Based on differences in the C-terminus of intimin, several alleles of intimin exist, and these allelic differences have been associated with variations in tissue tropism and

host species range (Fitzhenry et al., 2002; Girard et al., 2005; Mundy et al., 2007; Phillips and Frankel, 2000). For instance, whereas wild type EHEC colonizes the large intestine of gnotobiotic piglets, an EHEC strain harboring a plasmid expressing EPEC intimin gained the ability to colonize the small intestine (Tzipori et al., 1995). Additionally, while *C. rodentium* expressing EPEC intimin is able to efficiently colonize Swiss NIH and C3H/HeJ mice (Frankel et al., 1996b; Hartland et al., 2000; Schauer and Falkow, 1993b), *C. rodentium* expressing a derivative of EPEC intimin containing the adhesive domain of EHEC intimin provided poor colonization function in these animals (Hartland et al., 2000; Mundy et al., 2007). In **Chapter II**, we addressed the following questions (1) do allelic differences in intimin contribute to tissue tropism and host species range? and (2) do allele- and Tir-independent functions of intimin exist *in vivo*?

To gain insight into the critical allele- and Tir-independent functions *in vivo*, we used gnotobiotic piglet and murine infection models. For the gnotobiotic piglet model, we replaced the EHEC chromosomal *eae* gene with EPEC *eae* and found that the two alleles were functionally homologous in infection (**Chapter II**), in disagreement with previous results (Tzpiori et al., 1995). The fact that Tzipori and co-workers used plasmid complementation, while we used chromosomal replacement may explain the discrepant results. Next, we tested whether full-length EHEC intimin could complement a *C. rodentium eae* mutant for colonization and disease in C57BL/6 mice. In contrast to previous studies (Hartland et al., 2000; Mundy et al., 2007), we established that *C. rodentium* expressing EHEC intimin was fully functional for colonization as well as induction of colonic hyperplasia (**Chapter II**). The inconsistent findings may be due to

the use of an EHEC-EPEC hybrid plasmid in previous work that exchanged the N-terminus of EHEC intimin for that of EPEC intimin which may have diminished an important (possibly Tir-binding) activity of EHEC intimin. Alternatively, the inconsistency may be explained by differences in murine host strain. Indeed, strain-strain variability in susceptibility to *C. rodentium* has been documented (Vallance et al., 2003), and we have observed variations in the kinetics of colonization and disease when using animals purchased from different vendors or with different genetic backgrounds (E.M. and M. McBee unpublished observations).

We next tested whether Tir-intimin binding (in the absence of actin pedestal formation) was sufficient for murine colonization of *C. rodentium* and determined that the Tir binding domain of EHEC intimin (expressed from pInv-Int395) could not restore colonization by *C. rodentiumΔeae* (**Chapter II**). These results indicate that the ability to trigger actin assembly, not simply to bind Tir, is required for intimin-mediated intestinal colonization. One caveat, however, is that, due to lack of a suitable assay, we do not know how well the fusion containing the Tir-binding domain (Inv-Int395) expressed in *C. rodentium* is able to bind to Tir. Nonetheless, it has been established that Inv-Int395 expressed in *E. coli* K12 binds Tir with less efficiency than full length intimin (Liu et al., 1999). Similarly, our data suggests that Inv-Int395, when expressed in *C. rodentium*, also displays a binding defect because pedestal formation by this strain was not as robust as *C. rodentium* expressing full length intimin (**Chapter II**). This finding may be due to inefficient Tir clustering by Inv-Int395.

To assess the Tir-independent functions of intimin *in vivo*, we developed an experimental system using streptomycin pre-treated mice. In contrast to previous studies using conventional mice (Deng et al., 2003), we found that streptomycin pre-treated mice infected with a *C. rodentium tir* mutant became colonized to high levels and remained colonized throughout the course of ~30 days (**Chapter II**). Additionally, we observed that intimin was required for this Tir-independent function. We mapped the region of intimin responsible for this activity and found that the C-terminal 100 amino acids of EHEC intimin were sufficient for colonization. Biochemical approaches could be used to determine the host cell receptor these 100 amino acids of intimin are binding to. For instance, the C-terminal 100 amino acids of intimin could be purified and used in pull-down experiments with uninfected cell membrane fractions to identify potential binding partners. Similarly, one could use the yeast two-hybrid system or Biacore^{TM} to identify potential host cell receptors for this region of intimin.

The above results are consistent with the hypothesis that in addition to Tir, intimin binds a host cell receptor. Two potential candidates are β_1-chain integrins and nucleolin, both of which have been shown to bind intimin *in vitro* but have not been identified as receptors *in vivo* (Frankel et al., 1996a; Sinclair and O'Brien, 2002). Nucleolin knockout mice are currently being generated (at KOMP repository) and may prove to be useful reagent for future studies. Similarly, the newly developed conditional, β_1-chain integrin-deficient mice (which have β_1-chain integrins knocked out in collagen 1-producing cells) (Riopel et al., 2011) have been generated, and a strategy to specifically eliminate β_1-chain integrins in the intestine could be of use for future experiments. Streptomycin pre-

treatment of mice reveals a Tir-independent function of intimin *in vivo*, and may be used in mice deficient in β_1-chain integrins or nucleolin to determine if either of these two molecules functions as a host cell receptor for intimin.

Elucidating the role of actin pedestal formation in colonization and Stx-mediated disease

EHEC, EPEC, and *C. rodentium* all generate distinctive AE lesions on the intestinal epithelium consisting of the intimate attachment of bacteria, effacement of brush border microvilli, and the formation of actin-rich pedestals beneath bound bacteria. Actin pedestal formation is dependent on the adhesin intimin and the type III secreted effector Tir, and the mechanisms of pedestal formation by these three AE pathogens have been studied in great detail (for review, see (Caron et al., 2006)). While several previous studies have been unable to detect a requirement for actin polymerization during colonization (Schuller et al., 2007; Vlisidou et al., 2006;Deng et al., 2003), three groups have shown that actin assembly enhances colonization (Bai et al., 2008; Crepin et al., 2010; Ritchie et al., 2008). Unfortunately, the phenotypes linking actin pedestal formation and colonization have been modest and the mechanism by which this occurs is unknown. To generate a small animal model to study Stx-mediated disease that requires colonization and the presence of normal flora, we developed a model where wild type C57BL/6 mice were infected with *C. rodentium* (λstx_{2dact}) (**Chapter III**). Infection resulted in high-level colonization, significant weight loss, renal damage, intestinal damage, and mortality, consistent with many features of human HUS caused by EHEC

infection. Interestingly, in our model, colonization and disease were dependent on Tir, in contrast to other models of Stx-mediated disease utilizing streptomycin-treated or gnotobiotic mice (Eaton et al., 2008; Lindgren et al., 1993; Melton-Celsa et al., 1996; Wadolkowski et al., 1990a; Wadolkowski et al., 1990b). Therefore, we were able to use this model to assess whether Tir-mediated actin pedestal formation promotes colonization and/or Stx-mediated disease.

We began by using EHEC effectors (Tir and EspF$_U$) expressed from a single plasmid or dual plasmids to complement a *C. rodentium* (λ*stx$_{2dact}$*)Δ*tir* mutant (see **Appendix C**). We hypothesized that *C. rodentium* (λ*stx$_{2dact}$*) expressing EHEC Tir but not EspF$_U$ would be able to bind cells but not generate actin pedestals, while *C. rodentium* (λ*stx$_{2dact}$*) expressing both EHEC Tir and EspF$_U$ would be able to generate actin pedestals via the Nck-independent pathway (Brady et al., 2007; Campellone and Leong, 2005). Our hypothesis held true in cell culture (both when EHEC Tir and EspF$_U$ were expressed from dual plasmids and when expressed from a single plasmid; data not shown), consistent with results showing that EspF$_U$ is able to cooperate with *C. rodentium* to generate actin pedestals in a Nck-independent pathway (Girard et al., 2009a).

Given that these *C. rodentium* strains carrying EHEC alleles in *trans* behaved appropriately *in vitro*, we assessed the function of actin pedestal formation in colonization and Stx-mediated disease *in vivo* by comparing infection with pedestal-proficient (*C. rodentium* (λ*stx$_{2dact}$*) expressing EHEC Tir and EspF$_U$) and pedestal-deficient bacteria (*C. rodentium* (λ*stx$_{2dact}$*) expressing EHEC Tir). Mice infected with *C.*

rodentium (λstx_{2dact}) expressing EHEC Tir became colonized to an intermediate level, (i.e. peak levels of ~10^4-10^7 CFU/g between six and eight days post-infection) (**Appendix C**), several logs lower than peak colonization by wild type *C. rodentium* (λstx_{2dact}) (see **Chapter III**). Consistent with the intermediate colonization phenotype, very little weight loss and mortality was observed in these mice. Colonization by *C. rodentium* (λstx_{2dact}) expressing EspF$_U$ in addition to EHEC Tir expressed from two individual plasmids resulted in similar levels of peak colonization (~10^4-10^7 CFU/g feces) as *C. rodentium* expressing EHEC Tir alone (**Appendix C**). Interestingly, in one out of three experiments, *C. rodentium* (λstx_{2dact}) expressing EspF$_U$ and EHEC Tir from two plasmids resulted in more severe disease than *C. rodentium* (λstx_{2dact}) expressing EHEC Tir alone, with approximately 60% vs. 0% mortality. These data suggest that actin pedestal formation does not augment colonization but possibly enhances Stx-mediated disease and mortality. Unfortunately, this phenotype was not consistently reproducible, perhaps due to the inadequacies of plasmid complementation (e.g. plasmid loss or variable expression).

We then hypothesized that a single plasmid containing both EHEC Tir and EspF$_U$ may eliminate some of the confounding issues of plasmid complementation and yield a consistent phenotype. Despite our efforts, murine infection by *C. rodentium* (λstx_{2dact}) expressing a single plasmid containing both EHEC Tir and EspF$_U$ resulted in no difference in colonization, weight loss, or death compared to mice infected with *C. rodentium* (λstx_{2dact}) expressing EHEC Tir (**Appendix C**). These data suggest that while EHEC effectors have the ability to function in *C. rodentium*, expression of these effectors

from a plasmid results in variability in their effectiveness. Future experiments may include incorporation of EHEC effectors onto the chromosome of *C. rodentium*. Nonetheless, this initial data provides very weak evidence that actin pedestal formation contributes to Stx-mediated disease.

Using alternative experimental systems: (1) iNWKO mice and (2) infection by *C. rodentium* (λ*stx₂dact*) expressing a pedestal-deficient mutant (**Chapter IV**), we determined that Tir-mediated actin pedestal formation was required for maximal colonization, similar to previous findings (Bai et al., 2008; Crepin et al., 2010; Ritchie et al., 2008). We also demonstrated that FAS activity *in vitro* correlated with FAS activity *in vivo*—a question that has remained ambiguous for many years (Crepin et al., 2010; Deng et al., 2003; Girard et al., 2008; Schuller et al., 2007; Vlisidou et al., 2006a). In addition, we found that the ability to generate actin pedestals promoted Stx-mediated disease including weight loss, renal damage, intestinal damage, and death (**Chapter IV**). Finally, we provided strong evidence that actin pedestal formation facilitates colonization of the colonic, but not cecal, mucosa (**Chapter IV**).

It has been established that *C. rodentium* undergoes weak actin polymerization via a Nck-independent pathway in the absence of TirY471 phosphorylation, utilizing TirY451 (Brady et al., 2007; Campellone and Leong, 2005). To assess the contribution of this alternative pathway to colonization and Stx-mediated disease in our model, we constructed Tir complementation vectors expressing the single TirY451A mutant or the double TirY471F/Y451A mutant. Murine infection by *C. rodentium* (λ*stx₂dact*) expressing TirY471F/Y451A was identical to infection with *C. rodentium* (λ*stx₂dact*)

expressing TirY471F, resulting in a mild colonization defect in stool late in infection, less disease, and less mortality compared to infection with *C. rodentium* (λstx_{2dact}) expressing TirWT or TirY451A (see **Appendix C**). Our observations are consistent with a previous study using a non-toxigenic *C. rodentium* strain expressing a TirY451A point mutation on the chromosome revealing that TirY451 is dispensable for colonization (Crepin et al., 2010). Contrary to our previously described results, however, this same group observed no defect in colonization by *C. rodentium* expressing TirY471F/Y451A or TirY471F on the chromosome in single infection experiments (Crepin et al., 2010). In dual infection experiments, on the other hand, the double TirY471F/Y451A mutant was outcompeted by wild type *C. rodentium* (Crepin et al., 2010).

One aspect of colonization that was not addressed in our studies was the contribution of TirY451A to mucosal colonization of the cecum. We speculate that the low-level actin polymerization via the Nck-independent pathway may be sufficient to colonize the cecal mucosa (which would presumably allow for some luminal colonization and the presence of bacteria in the stool) in the absence of TirY471-mediated actin assembly. To test this, one could infect mice with *C. rodentium* (λstx_{2dact}) expressing TirY471F/Y451A and assay for mucosal colonization by immunofluorescence and TEM. If TirY451 was contributing to cecal colonization, we would expect to see a lack of mucosal colonization upon infection with the TirY471A point mutant. However, since we have not observed a defect in fecal colonization during infection with the double TirY471F/Y451A mutant (see **Appendix C**), it is likely that it colonizes the cecum. *C. rodentium* (λstx_{2dact})Δtir should be included in the experiment and we would predict that

it would be unable to colonize the cecal mucosa, given that infection results in fecal colonization at or below the limit of detection.

Because plasmid complementation by TirWT only partially restored colonization and disease in *C. rodentium* (λstx_{2dact})Δtir (see **Chapter III**), we cannot ignore the fact that subtle phenotypes observed by complementing *C. rodentium* (λstx_{2dact})Δtir with Tir point mutants on a plasmid might be very difficult to discern, especially with the TirY451A mutant. Generation of chromosomal point mutants as done by Crepin and co-workers (Crepin et al., 2010) could resolve this. One might predict that *C. rodentium* (λstx_{2dact}) expressing TirY451A from the chromosome may display a phenotype that would have been missed using the plasmid complementation system.

Expression of the TirY471F, TirY451A, and TirY471F/Y451A point mutants from the chromosome of *C. rodentium* (λstx_{2dact}) may also provide an experimental system to test the role of multiple actin polymerization pathways on colonization and Stx-mediated disease, a question that remains ambiguous due to conflicting results. Notably, one study suggested that additional actin polymerization pathways to EHEC enhances colonization in human intestinal *in vitro* organ cultures (Bai et al., 2008), while another study using *C. rodentium* expressing EspF$_U$ on the chromosome revealed that the enhanced actin polymerization capabilities offered no competitive advantage to the bacteria during murine infection (Girard et al., 2009). One way to explain this discrepancy is that one group used *in vitro* organ cultures as their experimental system, while the other group used an animal infection model.

Insights into the mechanism(s) of how actin pedestal formation facilitates

colonization and Stx-mediated disease

Even though defects in colonization and disease resulted from abolition of actin

pedestal formation, the question of whether these phenotypes are really due to the

inability to generate actin pedestals per se remains. Other alternatives to the actin

pedestals themselves affecting colonization and disease include the fact that simple

disruption of the host cytoskeleton may result in higher level colonization and/or disease

or that simply higher levels of bacteria produce more toxin and therefore, cause lethal

disease. To address this, we attempted to restore colonization and disease in mice

infected with *C. rodentium* (λstx_{2dact}) expressing TirY417F by adding EspF$_U$ to the strain

(either on its own plasmid or on the same plasmid as TirY471F, see **Appendix C**). The

expression of EspF$_U$ in the mutant expressing TirY471F restored its ability to generate

actin pedestals *in vitro* but resulted in no evident increase in murine colonization, weight

loss, or death (see **Appendix C**). There was a slight increase, however, in colonic

colonization upon addition of EspF$_U$, suggesting that actin pedestal formation facilitates

the association of bacteria with the colonic mucosa and presumably, subsequent lethal

disease. Chromosomal expression of EspF$_U$ in *C. rodentium* (λstx_{2dact}) expressing

TirY417F may more fully recapitulate infection by pedestal-proficient bacteria.

Our effector knockout studies (see **Appendix A**) provide additional support for

the hypothesis that toxigenic bacteria cause lethal disease via pedestal formation, rather

than by simply causing alterations in the host cell cytoskeleton. No defects in

colonization or disease resulted from infection with *C. rodentium* (λstx_{2dact})Δ*espH, C.*

rodentium (λ*stx$_{2dact}$*)Δ*espG, C. rodentium* (λ*stx$_{2dact}$*)Δ*espF,* or *C. rodentium* (λ*stx$_{2dact}$*)Δ*espK* even though these effectors are known to disrupt the actin cytoskeleton (see **Appendix A**). Taken together, our findings support that pedestal formation itself, or some specific actin rearrangement that is closely associated with pedestal formation, is responsible for increased colonization of the colonic mucosa and lethal disease upon infection by *C. rodentium* (λ*stx$_{2dact}$*).

Evidence from our lab suggests that actin assembly promotes bacterial binding *in vitro*, and paired with the findings in this thesis, strong bacterial binding via pedestal formation may promote lethal Stx-mediated disease. Previous studies examined the Tir-intimin adhesion pathway in absence of potentially redundant pathways by infecting mammalian cells with EPEC or EHEC intimin mutants that deliver Tir but cannot stably attach to host cells and challenged the "pre-infected" monolayers with a lab strain of *E. coli* that expresses intimin but cannot otherwise attach to mammalian cells. These studies revealed that intimin-mediated bacterial attachment was decreased by point mutations (i.e. EHEC TirY458A) in the cytoplasmic domain of Tir that diminish actin pedestal formation, and by chemical inhibitors of actin assembly (M. Brady Thesis).

An additional study measured the ability of EHEC and EPEC mutants to bind to intimin coated plates and revealed that EHEC TUV bound significantly better than an EHEC pedestal-deficient mutant (Δ*espF$_U$*) (P.K. unpublished data). Similarly, the TirY454F/TirY474F double mutant of EPEC bound to intimin at significantly lower levels compared to wild type EPEC. On the other hand, EPEC containing either the

chromosomal point mutant TirY454F or TirY474F bound less than wild type EPEC but the differences were not statistically significant (P.K. unpublished data).

Several hypotheses can explain how actin polymerization enhances bacterial binding. One possible mechanism could be that actin polymerization may enhance type III secretion. However, preliminary data makes this hypothesis unlikely as EHEC expressing TirY458A is translocated with wild type efficiency into mammalian cells (M. Brady Thesis). A more likely hypothesis is that actin assembly increases the affinity or avidity of Tir and intimin and therefore augments bacterial binding to the mucosal surface. For example, it is possible that initiation of actin assembly induces a conformational change in the intimin binding region of Tir resulting in a higher affinity for intimin. Alternatively, actin assembly may increase the avidity of intimin-Tir interactions by assisting the movement of Tir from the cytoplasm to the membrane. To test this, one could measure surface expression of Tir by FLOW cytometry using anti-Tir. It is also possible that actin polymerization blocks endocytosis of Tir and therefore allows for more Tir to be retained in the host cell membrane. Preliminary data from our lab is consistent with this model, as EHEC Tir mutants deficient in actin polymerization generate fewer Tir foci than wild type EHEC (M. Brady Thesis). Similarly, Tir foci are diminished upon treatment with the actin polymerization inhibitor, cytochalasin D (M. Brady Thesis).

One can imagine that actin polymerization may "anchor" a rather weak binding interaction by physically linking the extracellular pathogen with the cytoskeletal network of the host cell. Consistent with this model is the fact that pedestal-deficient bacteria are

rarely found in close association with the colonic mucosa as opposed to pedestal-proficient bacteria. We hypothesize that the mechanical force of washing the intestines prior to analysis breaks the bonds between the weakly adherent bacteria and the colonic surface, allowing only bacteria bound by actin pedestals to remain. To test this hypothesis *in vitro*, one could utilize optical/laser tweezers to quantitate the degree of binding and see if bacteria bound to cells via actin pedestals bind more tightly to cells than bacteria unable to generate actin pedestals.

Actin pedestal formation may also increase bacterial motility on the epithelial surface, leading to expansion of the infectious niche on the mucosal surface. Indeed, this phenomenon of hijacking host cell actin machinery as a means of bacterial motility to spread from host cell to host cell has been observed for several intracellular bacterial and viral pathogens (e.g. *Shigella*, *Listeria*, *Rickettsia*, and *Vaccinia*) (Goldberg, 2001). Furthermore, it has been established that extracellular EPEC and EHEC move along the surface of cultured epithelial cells in an actin polymerization-dependent fashion, suggesting that pedestal formation is important for bacterial movement (Sanger et al., 1996; Shaner et al., 2005). Finally, two studies revealed that bacterial aggregates on the intestinal epithelium were much smaller upon infection pedestal-deficient mutants in infection of gnotobiotic piglets (Ritchie et al., 2008) and human intestinal explants (Schuller et al., 2007), suggesting that this actin-based motility allows for aggregation of bacteria and expansion beyond the initial infectious niche. It is also possible that actin polymerization-based surface motility may help the bacteria to move into and occupy the intestinal crypts.

A corollary of the observation that pedestal formation is associated with mucosal colonization is that bacteria localized on the mucosal surface promote systemic disease. A simple hypothesis is that Stx production in direct apposition to the epithelium has the most serious consequence. Data from **Chapter IV** supports this hypothesis because even when bacteria maintain the ability to colonize the feces, lumen, and cecum, but are unable to colonize the colonic mucosal surface, they are unable to cause lethal disease, as seen with mice infected with *C. rodentium* (λstx_{2dact})Δtir expressing TirY471F. Additionally, streptomycin pre-treated mice infected with non-pedestal-producing *C. rodentium* (λstx_{2dact})Δtir became colonized to high levels (i.e. >10^9 CFU/g through the duration of the ~30 day experiment), and did not experience weight loss or lethal disease (data not shown). We hypothesize that infection by *C. rodentium* (λstx_{2dact})Δtir in streptomycin pre-treated mice results in lethal disease because the bacteria were unable to efficiently colonize the colonic mucosa, similar to non-streptomycin pre-treated mice infected with *C. rodentium* (λstx_{2dact}) expressing TirY471F (**Chapter IV**). We predict that in both instances, bacteria are able to colonize the cecum, but cannot produce Stx in sufficient quantity or in close enough proximity to the colonic mucosa to deliver lethal quantities of toxin into the bloodstream. To test this hypothesis, we could infect streptomycin pre-treated mice with *C. rodentium* (λstx_{2dact})Δtir and evaluate cecal and colonic adherence by immunofluorescence and TEM. In addition, we could also measure Stx in the blood of mice infected with toxigenic pedestal-proficient and pedestal-deficient bacteria or in streptomycin pre-treated mice infected with *C. rodentium* (λstx_{2dact})Δtir. An alternative approach would be to treat mice infected with a pedestal-deficient strain

with a toxin-inducing agent (e.g. mitomycin C or Cipro) and assess whether toxin induction and presumably increased toxin concentration now is able to result in lethal disease. Lastly, we could reassess both cecal and colonic TEM sections of mice infected with pedestal-proficient and pedestal-deficient strains by immuno-EM using an anti-Stx antibody and determine if more Stx is present under bacteria attached via actin pedestals as opposed to simply "sitting" on the mucosal surface.

Further data supporting the hypothesis that localization of mucosal-associated bacteria is responsible for lethal disease comes from our results of *C. rodentium* (λstx_{2dact}) infection in immunodeficient mice. We determined that MyD88 was necessary to protect mice against pedestal-deficient bacteria (**Appendix B**). One might predict that in the absence of MyD88, more bacteria (regardless of their ability to generate actin pedestals) would be located at the mucosal surface of the intestine due to poor recognition of PAMPs (pattern associated molecular patterns). These putative PAMPs presumably are not restricted to LPS because TLR4 is not required for protecting against pedestal-deficient bacteria (**Appendix B**).

Another reason why localization may promote lethality is that normal flora [the apparent implication is that normal flora is located more closely to the mucosa] and/or close contact with host cells may promote phage induction, resulting in more toxin production, and more disease. Interestingly, there is evidence that *stx2* expression is highly dependent on the lytic cycle and is induced by DNA-damaging agents (Wagner et al., 2001b). Furthermore, while *in vitro* and *in vivo* studies reveal that administration of probiotic bacteria (i.e. *Lactobacillus* and *Bifidobacterium*) inhibits Stx1 and Stx2

production (Asahara et al., 2004; Carey et al., 2008), other studies have discovered that the presence of commensal *E. coli* susceptible to Stx2 phage infection leads to increased Stx2 production (Gamage et al., 2003). Finally, exposure to human neutrophils and macrophages has also has been shown to lead to increases in *stx2* expression and toxin production (Poirier et al., 2008; Shimizu et al., 2011; Wagner et al., 2001a).

We tested the hypothesis of whether toxin production is increased by bacteria that are in close proximity to mammalian cells by growing *C. rodentium* (λstx_{2dact}) in the presence or absence of MEFs in a 96-well plate. The bacteria were grown for three hours (in an empty well or in a well with a confluent layer of MEF's), after which, the media was changed and mitomycin C was added to induce phage induction. After an additional three hour incubation, the wells were washed and culture supernatant was assayed for Stx2 production via ELISA (see **Chapter III Materials and Methods**). The amount of bacteria in each well was enumerated by plating serial dilutions, and toxin production was normalized to total bacteria in the well. We found that toxin production was increased when bacteria were in the presence of mammalian cells (E.M. unpublished observations). Given this finding, another interesting experiment would be to determine if pedestal-proficient bacteria generate greater quantities of toxin in the presence of mammalian cells compared to pedestal-deficient bacteria. Preliminary data from our lab, however, suggests that both *C. rodentium* (λstx_{2dact})Δtir/pTir$_{WT}$ and *C. rodentium* (λstx_{2dact})Δtir/pTir$_{Y471F}$ produce similar amounts of Stx in the presence of mammalian cells (E.M. unpublished data).

An additional mechanism for how actin pedestal formation facilitates lethal disease may be that actin polymerization results in better toxin translocation across epithelium. There is evidence that Stx1 uptake and transcytosis is actin dependent (Malyukova et al., 2008; Mettlen et al., 2006) and it has also been shown that Stx1 can be taken up by the cell via macropinocytosis, a fluid-phase uptake pathway that uses actin turnover (Malyukova et al., 2009). Furthermore, it has been established that neutrophil migration enhances toxin translocation across polarized epithelial cell monolayers (Hurley et al., 2001). Therefore, to test whether inhibition of neutrophil migration has any effect on toxigenic disease *in vivo*, we infected 12-LOX$^{-/-}$ mice, which are deficient in the pathway to generate the neutrophil chemoattractant hepoxilin A_3 (McCormick, 2007) with *C. rodentium* (λstx_{2dact}) (see **Appendix B**). We found that infection by *C. rodentium* (λstx_{2dact}) in these mice was no different than infection of wild type mice in regards to colonization, weight loss, mortality, and renal and intestinal pathology (**Appendix B** and data not shown). However, this does not rule out the hypothesis that neutrophil migration enhances toxin translocation completely, because the absence of 12-LOX may have little impact on neutrophil migration across the intestinal epithelium, which was not tested in these experiments.

The hypothesis that close bacterial association with the mucosal surface facilitates toxin translocation is consistent with the pathogenesis of the recently described EHEC-EAEC hybrid bacterium responsible for the outbreak of HUS in Germany in the spring of 2011. This strain, *E. coli* O14:H4, contains Stx2 from EHEC, is *eae* negative, and possesses the adhesive properties of EAEC, most notably the ability to adhere to

epithelial cells in a stacked-brick conformation. Researchers hypothesize that the augmented adherence of this strain, coupled with the presence of the Stx2 toxin, facilitated toxin translocation and systemic absorption of toxin, explaining the high progression to HUS (Bielaszewska et al., 2011).

To further test the hypothesis that actin pedestal formation facilitates toxin translocation, one could measure amount of Stx in serum of C57BL/6 mice infected with pedestal-proficient and pedestal-deficient strains of *C. rodentium* (λstx_{2dact}) or in iNWKO and littermate control mice infected with *C. rodentium* (λstx_{2dact}). If actin pedestal formation promotes toxin translocation, we would expect there to be more Stx in the blood of C57BL/6 mice infected with pedestal-producing strains of *C. rodentium* (λstx_{2dact}) and in littermate control mice infected with *C. rodentium* (λstx_{2dact}). Other experiments to address the hypothesis could assess toxin translocation across the intestinal epithelium with polarized cells. Potential problems may result from using *C. rodentium* in these experiments because of *C. rodentium*'s preference to attach to and infect murine cells (E.M. unpublished observations; D.B.S. and B. McCormick personal comm.). Use of murine epithelial cells such as CT26 (colorectal carcinoma cells) would remedy this problem. Alternatively, one might quantitate toxin translocation across polarized monolayers (e.g. T84, CaCo2) using EHEC in the presence and absence of EspFu. Finally, one could treat cells with inhibitors of actin polymerization (e.g. cytochalasin D) and examine the effects on toxin translocation.

Final conclusions

For the first time, a clearly defined a role of Tir-mediated actin polymerization in colonization and toxin-mediated disease has been identified. We have shown that actin pedestal formation is required for colonization of the colonic but not cecal mucosa. While we have discussed many hypotheses for how actin pedestal formation facilitates lethal disease, future research needs to be conducted to determine the exact mechanism. These studies will give insight into the long-standing questions of EHEC pathogenesis and offer suggestions for future treatment options.

APPENDIX

The following data is from other work I conducted while I was in the lab that was not an integral component to the stories presented in this thesis and will not be submitted for publication at this time. However, it represents initial forays into research avenues that may have impact on future work conducted in the lab.

A. *C. RODENTIUM* (λ*STX*$_{2DACT}$) EFFECTOR KNOCKOUT STUDIES

Summary

Many type III secreted effectors injected into host cells are implicated in disruption of the host cell cytoskeleton. Some of these effector proteins include: EspF, EspG, EspK, and EspH. One well known function of EspF is to disrupt epithelial barrier function, presumably by altering the distribution of tight junction proteins and modulating the architecture of intermediate filament networks within cells (Guttman et al., 2006a; McNamara et al., 2001; Viswanathan et al., 2004a). Additionally, it has been suggested that EspF promotes colonization of *C. rodentium* in mice early in infection and appears to control EHEC-induced inflammation in infant rabbits (Deng et al., 2004; Mundy et al., 2004; Ritchie and Waldor, 2005). EspG has been shown to destabilize microtubule networks, induce the formation of stress fibers, and cause damage to the Golgi apparatus (Clements et al., 2011; Matsuzawa et al., 2004). Previous data also suggests that EspG contributes to colonization and colonic hyperplasia in murine infection with *C. rodentium* (Hardwidge et al., 2005; Mundy et al., 2004) and colonization of the small intestine of infant rabbits by EHEC (Ritchie and Waldor, 2005). While EspK has no apparent effect on actin nucleation in HeLa cells *in vitro*, it has been shown to promote persistence in an orally infected calf model (Vlisidou et al., 2006b). On the other hand, there is evidence that EspH diminishes filopodium formation, enhances actin pedestal formation, and plays a role in brush border microvilli remodeling (Shaw et al., 2005a; Tu et al., 2003). Furthermore, while the role of EspH in murine infection by *C. rodentium* has been controversial (Deng et al., 2004; Mundy et al., 2004),

EspH has been suggested to promote colonization and diarrhea in infant rabbits (Ritchie and Waldor, 2005).

To assess the function of these cytoskeletal modulating effector proteins in our model of EHEC toxin-mediated disease, we generated complete, in-frame deletions in *C. rodentium* (λ*stx₂dact*) strain using lambda red recombination (Datsenko and Wanner, 2000). We first assessed the ability of each of these mutants to form actin pedestals *in vitro*. Mouse embryonic fibroblasts infected with either *C. rodentium* (λ*stx₂dact*)Δ*espF*, *C. rodentium* (λ*stx₂dact*)Δ*espG*, *C. rodentium* (λ*stx₂dact*)Δ*espK*, or *C. rodentium* (λ*stx₂dact*)Δ*espH* all generated actin pedestals indistinguishable from wild type *C. rodentium* (λ*stx₂dact*) (data not shown), indicating that EspF, EspG, EspK, and EspH are not required for actin pedestal formation *in vitro*.

Because alterations in the host cell cytoskeleton are thought to facilitate toxin translocation, we next assessed the function of these effector proteins on colonization and weight loss, a common finding in murine intoxication with Stx (Keepers et al., 2006; Mohawk and O'Brien, 2011; Sauter et al., 2008). C57BL/6 mice were inoculated with approximately 5×10^9 CFU of each mutant *C. rodentium* (λ*stx₂dact*) strain and fecal colonization was monitored every other day throughout infection. *C. rodentium* (λ*stx₂dact*)Δ*espF*, *C. rodentium* (λ*stx₂dact*)Δ*espG*, *C. rodentium* (λ*stx₂dact*)Δ*espK*, and *C. rodentium* (λ*stx₂dact*)Δ*espH* colonized mice to levels comparable to colonization by *C. rodentium* (λ*stx₂dact*), indicating that EspF, EspG, EspK, and EspH are dispensable for colonization by *C. rodentium* (λ*stx₂dact*) (**Figure 1A**). Likewise, each of these cytoskeletal modulating effector proteins were dispensable for weight loss in mice

infected with *C. rodentium* (λ*stx$_{2dact}$*) (**Figure 1B**). These results indicate that EspF,

EspG, EspK, and EspH are not required for colonization and Stx-mediated disease in

murine infection with *C. rodentium* (λ*stx$_{2dact}$*).
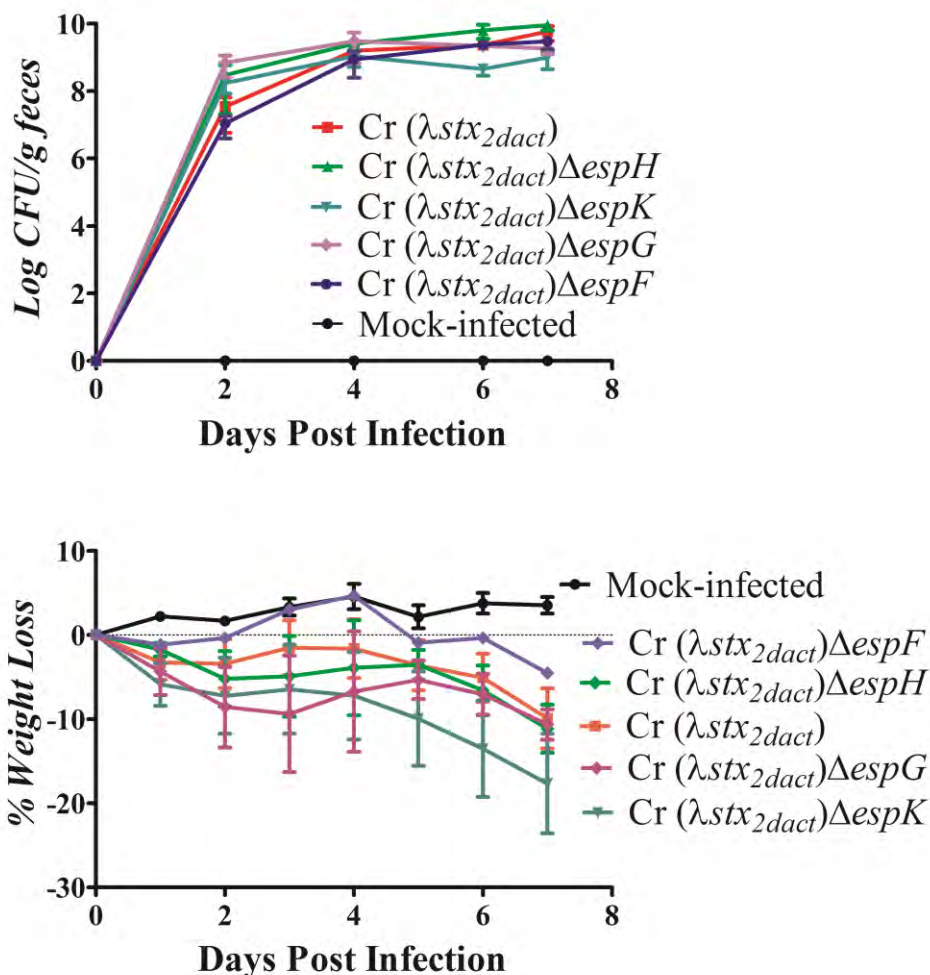
Figure 1. T3SS cytoskeletal modulating effector proteins are not required for colonization or weight loss upon colonization by *C. rodentium* (λ*stx₂dact*).   (A) Colonization of eight-week-old female C57BL/6 mice by *C. rodentium* (λ*stx₂dact*), *C. rodentium* (λ*stx₂dact*)Δ*espF*, *C. rodentium* (λ*stx₂dact*)Δ*espG*, *C. rodentium* (λ*stx₂dact*)Δ*espK*, and *C. rodentium* (λ*stx₂dact*)Δ*espH* was determined by viable stool counts. Shown are the averages CFU (± SEM) of five mice. **(B)** Body weight during infection of C57BL/6 mice by *C. rodentium* (λ*stx₂dact*), *C. rodentium* (λ*stx₂dact*)Δ*espF*, *C. rodentium* (λ*stx₂dact*)Δ*espG*, *C. rodentium* (λ*stx₂dact*)Δ*espK,* and *C. rodentium* (λ*stx₂dact*)Δ*espH* expressed as percent change from day zero body weight. Shown are the averages (±SEM) of five mice per group. Data are representative of a single experiment that was performed in triplicate.

B. IMMUNE STUDIES WITH *C. RODENTIUM* (λSTX_{2DACT})

Summary

The innate immune system is a non-specific first line of defense against microbial pathogens. It is comprised of natural anatomic barriers (e.g. normal flora), non-specific immune cells (e.g. neutrophils, mast cells, and macrophages), inflammation, the complement system, and Toll signaling through Toll-like receptors (TLRs). TLRs are pattern recognition receptors that identify molecules associated with microbial pathogens (Takeda and Akira, 2004). One of the main adapter molecules for all TLRs except TLR3 is MyD88 (Adachi et al., 1998). Signaling through MyD88 is important for protection against microbial pathogens as mice deficient in MyD88 are more susceptible to infection (Gibson et al., 2008; LaRosa et al., 2008). TLR4, which signals through MyD88, is an innate signaling molecule responsible for sensing lipopolysaccharide, the main component in the outer bacterial membrane of gram negative bacteria. Additionally, TLR4 signaling has been implicated in mediating much of the inflammation during murine infection of *C. rodentium* (Khan et al., 2006).

Given the importance of MyD88 and TLR4 in defense against microbial pathogens, we tested their requirement for colonization and disease by *C. rodentium* (λstx_{2dact}). Since *C. rodentium* (λstx_{2dact}) infection of wild type C57BL/6 mice always results in lethal infection, infection with *C. rodentium* (λstx_{2dact})Δtir/pTir$_{Y471F}$ only results in 5% mortality, and *C. rodentium* (λstx_{2dact})Δtir results in virtually no mortality (see **Chapters III and IV**), we used these three strains in our experiments in order to measure severity of disease.

C. rodentium (λ*stx₂ₐₐₐ*) and *C. rodentium* (λ*stx₂ₐₐₐ*)Δ*tir*/pTir$_{Y471F}$ infected MyD88$^{-/-}$ mice became colonized, lost weight, and succumbed to lethal infection to similar levels (**Figure 2**). This is in contrast to infection of wild type mice where *C. rodentium* (λ*stx₂ₐₐₐ*)Δ*tir*/pTir$_{Y471F}$ caused only 5% mortality (**Chapter IV**). On the other hand, MyD88$^{-/-}$ mice infected with *C. rodentium* (λ*stx₂ₐₐₐ*)Δ*tir* did not become colonized, lose weight, or succumb to lethal infection, similar to wild type C57BL/6 mice infected with this strain (**Figure 2,** see **Chapters III and IV**). These results suggest that the MyD88 pathway plays a critical role in the recognition and clearance of pedestal-deficient *C. rodentium* (λ*stx₂ₐₐₐ*)Δ*tir*/pTir$_{Y471F}$ bacteria.

We next assessed the function of TLR4-mediated signaling in our model of toxigenic disease by infecting TLR4$^{-/-}$ mice with *C. rodentium* (λ*stx₂ₐₐₐ*). In order to evaluate the severity or attenuation of disease, we infected TLR4$^{-/-}$ mice with *C. rodentium* (λ*stx₂ₐₐₐ*)Δ*tir*/pTir$_{Y471F}$ and *C. rodentium* (λ*stx₂ₐₐₐ*)Δ*tir*. We found that TLR4$^{-/-}$ mice infected with *C. rodentium* (λ*stx₂ₐₐₐ*) became highly colonized, lost weight, and succumbed to lethal infection (**Figure 3**), similar to wild type C57BL/6 mice infected with this strain. TLR4$^{-/-}$ mice infected with the pedestal-deficient mutant (*C. rodentium* (λ*stx₂ₐₐₐ*)Δ*tir*/pTir$_{Y471F}$) became less colonized, did not lose weight, and survived infection, similar to C57BL/6 mice infected with the same strain (**Figure 3**). Finally, TLR4$^{-/-}$ mice infected with the *tir* mutant failed to become colonized, did not lose weight and survived infection (**Figure 3**). These data suggest that TLR-mediated signaling is dispensable for defense against pedestal-deficient *C. rodentium* (λ*stx₂ₐₐₐ*) in contrast to MyD88 signaling.
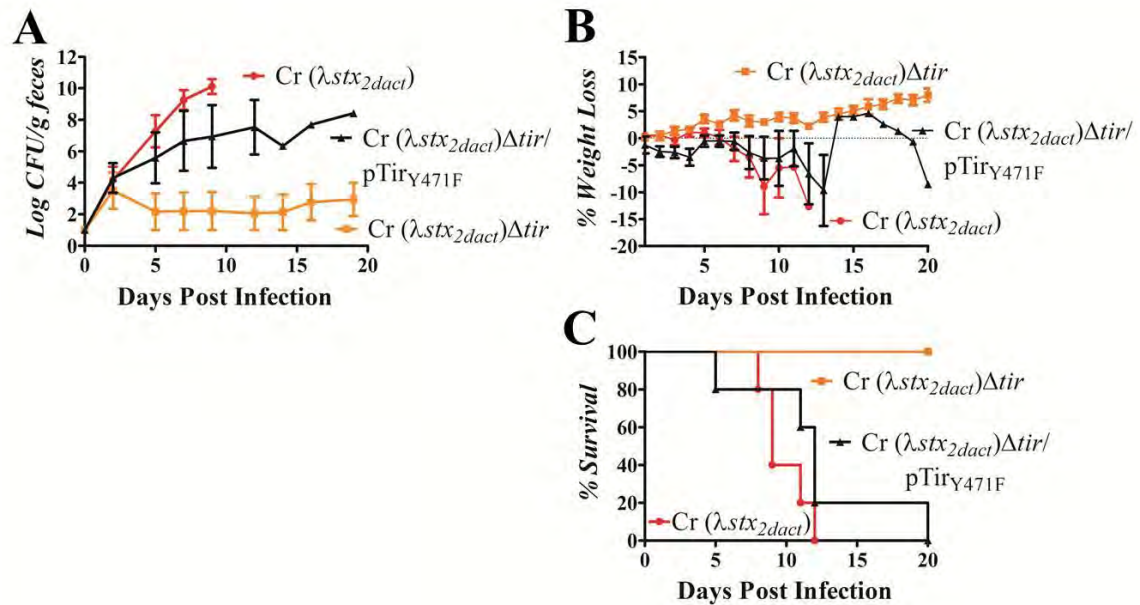
Figure 2. MyD88 protects mice against pedestal-deficient bacteria. (A) Colonization of MyD88$^{-/-}$ mice by *C. rodentium* (λ*stx$_{2dact}$*), *C. rodentium* (λ*stx$_{2dact}$*)Δ*tir*/pTir$_{Y471F}$, and *C. rodentium* (λ*stx$_{2dact}$*)Δ*tir* was determined by viable stool counts. Shown are the averages CFU (± SEM) of five mice. **(B)** Body weight during infection of MyD88$^{-/-}$ mice by *C. rodentium* (λ*stx$_{2dact}$*), *C. rodentium* (λ*stx$_{2dact}$*)Δ*tir*/pTir$_{Y471F}$, and *C. rodentium* (λ*stx$_{2dact}$*)Δ*tir* expressed as percent change from day zero body weight. Shown are the averages (±SEM) of five mice per group. **(C)** Percent survival of MyD88$^{-/-}$ mice that were infected with *C. rodentium* (λ*stx$_{2dact}$*), *C. rodentium* (λ*stx$_{2dact}$*)Δ*tir*/pTir$_{Y471F}$, and *C. rodentium* (λ*stx$_{2dact}$*)Δ*tir*. For all panels, data are representative of one experiment that was performed twice using strains *C. rodentium* (λ*stx$_{2dact}$*) and *C. rodentium* (λ*stx$_{2dact}$*)Δ*tir*/pTir$_{Y471F}$, and once using *C. rodentium* (λ*stx$_{2dact}$*)Δ*tir*.
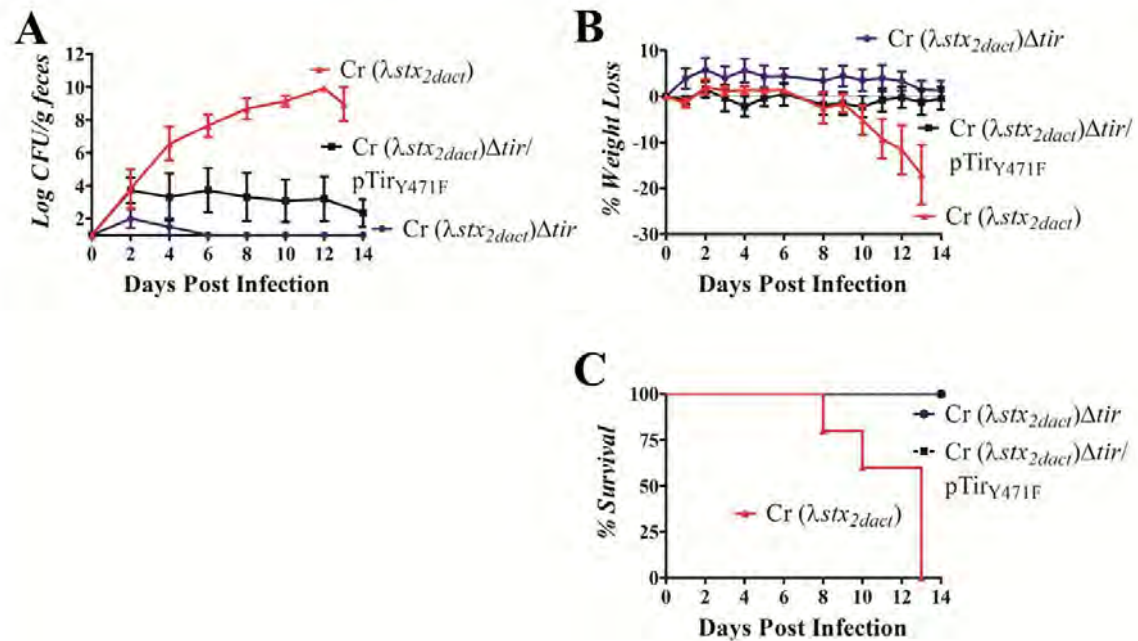
Figure 3. Stx-mediated colonization and mortality in TLR4$^{-/-}$ requires pedestal formation. (A) Colonization of TLR4$^{-/-}$ mice by *C. rodentium* (λ*stx$_{2dact}$*), *C. rodentium* (λ*stx$_{2dact}$*)Δ*tir*/pTir$_{Y471F}$, and *C. rodentium* (λ*stx$_{2dact}$*)Δ*tir* was determined by viable stool counts. Shown are the averages CFU (± SEM) of five mice. **(B)** Body weight during infection of TLR4 KO mice by *C. rodentium* (λ*stx$_{2dact}$*), *C. rodentium* (λ*stx$_{2dact}$*)Δ*tir*/pTir$_{Y471F}$, and *C. rodentium* (λ*stx$_{2dact}$*)Δ*tir* expressed as percent change from day zero body weight. Shown are the averages (±SEM) of five mice per group. **(C)** Percent survival of TLR4 KO mice that were infected with *C. rodentium* (λ*stx$_{2dact}$*), *C. rodentium* (λ*stx$_{2dact}$*)Δ*tir*/pTir$_{Y471F}$, and *C. rodentium* (λ*stx$_{2dact}$*)Δ*tir*. For all panels, data are representative of one experiment that was performed twice using strains *C. rodentium* (λ*stx$_{2dact}$*) and *C. rodentium* (λ*stx$_{2dact}$*)Δ*tir*/pTir$_{Y471F}$, and once using *C. rodentium* (λ*stx$_{2dact}$*)Δ*tir*.

Not only is the innate immune system is the first line of defense against bacterial pathogens, but the actions of the innate immune systems are also implicated in the pathogenesis of HUS. For instance, it has been established that Stx induces secretion of the neutrophil chemoattractant, IL-8, from human colonic epithelial cells (Thorpe et al., 1999) and evidence suggests that neutrophil transmigration enhances Stx translocation across the intestinal epithelium (Hurley et al., 2001). To test this hypothesis *in vivo*, we infected 12-lypoxygenase (12-LOX) knockout mice, which are deficient in the pathway to generate the neutrophil chemoattractant hepoxilin A_3 (McCormick, 2007), and therefore do not promote efficient neutrophil migration, with *C. rodentium* (λstx_{2dact}) and compared the outcome of infection to C57BL/6 mice infected with *C. rodentium* (λstx_{2dact}). We found that elimination of the 12-LOX pathway did not influence Stx-mediated colonization or disease. Both wild type C57BL/6 mice and 12-LOX$^{-/-}$ mice became highly colonized, exhibited significant weight loss, and succumbed to lethal infection (**Figure 4**). Moreover, there were no significant differences in renal and intestinal histology upon infection between the two strains of mice (data not shown).
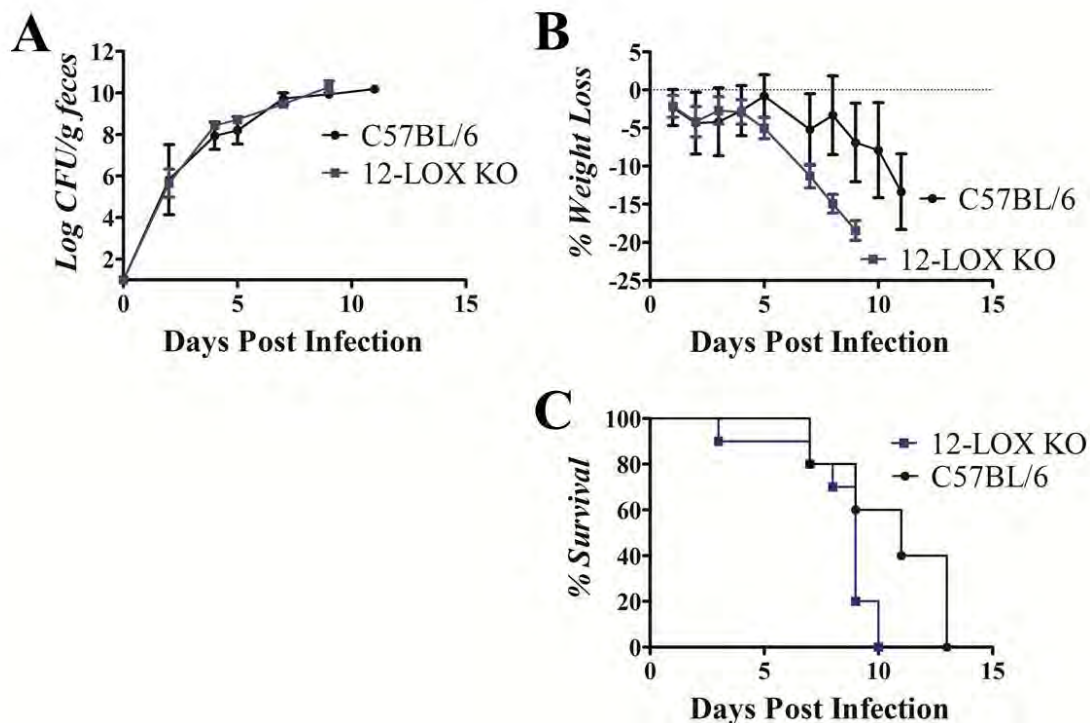
Figure 4. The 12-LOX pathway does not influence Stx-mediated colonization and disease by *C. rodentium* (λ*stx₂dact*). **(A)** Colonization of 12-LOX KO (blue) and C57BL/6 (black) mice by *C. rodentium* (λ*stx₂dact*) was determined by viable stool counts. Shown are the averages CFU (± SEM) of five mice. **(B)** Body weight during infection of 12-LOX KO (blue) and C57BL/6 (black), expressed as percent change from day zero body weight. Shown are the averages (±SEM) of five mice per group. **(C)** Percent survival of 12-LOX KO (blue) and C57BL/6 (black) mice that were infected with *C. rodentium* (λ*stx₂dact*). For all panels, results are representative of one experiment.

C. OTHER ATTEMPTS AT ASSESSING THE FUNCTION OF ACTIN

PEDESTAL FORMATION

Table 1. Attempts at assessing the function of actin pedestals *in vivo*.

Experiment	Objective	Results	Repetitions
EHEC$\Delta espF$ $\Delta espF_U$	To assess whether the residual pedestal formation in an $espF_U$ mutant is due to EspF. This mutant was tested in an infant rabbit infection (J. Ritchie).	In a FAS assay, EHEC$\Delta espF$ $\Delta espF_U$ has some, residual pedestal formation similar to an $espF_U$ mutant. Pedestal formation was restored by providing EspF$_U$ in *trans*. There was no phenotype in infant rabbit model in single or competition experiments (J. Ritchie).	FAS (3); rabbit infection-2 single infections and 2 competition experiments)
Murine infection with *C. rodentium* (λstx_{2dact})Δtir/pTir$_{EHEC}$ OR pTir$_{CR}$ (L. Magoun and K. Schlieper)	To test whether Tir is required for infection by *C. rodentium* (λstx_{2dact}).	None of these strains were able to colonize wild type mice, most likely because these complementation vectors were pBR322-derived.	1
Murine infection with *C. rodentium* (λstx_{2dact})Δtir/pTir$_{EHEC}$	To test whether EHEC Tir can complement a *C. rodentium* (λstx_{2dact}) *tir* mutant.	Infection resulted in intermediate colonization that peaked at levels of ~10^4-10^7 CFU/g six-to-eight days post-infection. There was very little weight loss and no mortality.	5
Murine infection with *C. rodentium* (λstx_{2dact})Δtir/pTir$_{EHEC}$ + pEspF$_U$ (2 plasmids)	To test whether EHEC Tir and EspF$_U$ can rescue a *tir* mutant for high-level colonization, weight loss, and death.	Colonization peaked at ~10^4-10^7 CFU/g six-to-eight days post-infection. In one experiment mice infected *C. rodentium* (λstx_{2dact})Δtir/pEHEC Tir + pEspF$_U$ appeared sicker and experienced more death (60% vs. 0%) than mice infected with *C. rodentium* (λstx_{2dact})Δtir complemented with only EHEC Tir. Infection resulted in	3

		incomplete complementation of colonization, weight loss, and lethality (e.g. <60% mortality) in the other two experiments.	
Murine infection with *C. rodentium* (λstx_{2dact})Δtir/pTir$_{EHEC}$ + EspF$_U$ (1 plasmid)	To test whether EHEC Tir and EspF$_U$ can rescue a *tir* mutant for high-level colonization, weight loss, and death.	There was no difference in colonization, weight loss, and death compared to mice infected with *C. rodentium* (λstx_{2dact})Δtir expressing EHEC Tir alone.	3
Murine infection with *C. rodentium* (λstx_{2dact})Δtir/pCr Tir$_{Y471F}$ + pEspF$_U$ (2 plasmids)	To test whether the addition of EspF$_U$ can rescue a TirY471F mutant for high-level colonization, weight loss, and death.	This strain did not colonize well and did not complement for weight loss, fecal water phenotype (see **Chapter III**), or mortality.	2
Murine infection with *C. rodentium* (λstx_{2dact})Δtir/pCr Tir$_{Y471F}$ + EspF$_U$ (1 plasmid)	To test whether the addition of EspF$_U$ can rescue a TirY471F mutant for high-level colonization, weight loss, and death.	This strain did not colonize well or clearly complement for weight loss, fecal water phenotype, or mortality. However, there was some evidence of better colonization with the addition of EspF$_U$, specifically in an *in vivo* binding study (done once) where the addition of EspF$_U$ allowed for higher (but not statistically significant) colonization of the colon compared to *C. rodentium* (λstx_{2dact})Δtir expressing TirY471F alone.	3
Infection of iNWKO mice with *C. rodentium* (λstx_{2dact})	To test if the defect in colonization	Not all mice became colonized with each strain and therefore, it was difficult to evaluate results.	1

+ pEspF$_U$ (1 plasmid)	observed in iNWKO mice infected with *C. rodentium* (λ*stx$_{2dact}$*) (see **Chapter IV**) could be rescued by the addition of EspF$_U$. To assess the N-WASP independent pathway of pedestal formation *in vivo*.	It may be best to repeat experiment using chromosomal copy of EspF$_U$. This strain is available with EspF$_U$ inserted into the XylE gene.	
Murine infection with *C. rodentium* (λ*stx$_{2dact}$*)Δ*tir*/pCr Tir$_{Y451A}$ and murine infection with *C. rodentium* (λ*stx$_{2dact}$*)Δ*tir*/pCr Tir$_{Y471F/Y451A}$	To assess the function of both actin polymerization pathways in the context of Stx-mediated disease (also assessed in the non-toxigenic strain and results were similar).	Infection with *C. rodentium* (λ*stx$_{2dact}$*)Δ*tir*/pCr Tir$_{Y451A}$ was not different than infection with *C. rodentium* (λ*stx$_{2dact}$*)Δ*tir*/pCr Tir. Infection with *C. rodentium* (λ*stx$_{2dact}$*)Δ*tir*/pCr Tir$_{Y471F/Y451A}$ was the same as infection with *C. rodentium* (λ*stx$_{2dact}$*)Δ*tir*/pCr Tir$_{Y471F}$. Histology and mucosal colonization of colon and cecum were not assessed in these experiments.	1

REFERENCES

Acheson, D.W., Moore, R., De Breucker, S., Lincicome, L., Jacewicz, M., Skutelsky, E., and Keusch, G.T. (1996). Translocation of Shiga toxin across polarized intestinal cells in tissue culture. Infect Immun *64*, 3294-3300.

Adachi, O., Kawai, T., Takeda, K., Matsumoto, M., Tsutsui, H., Sakagami, M., Nakanishi, K., and Akira, S. (1998). Targeted disruption of the MyD88 gene results in loss of IL-1- and IL-18-mediated function. Immunity *9*, 143-150.

Adams, L.M., Simmons, C.P., Rezmann, L., Strugnell, R.A., and Robins-Browne, R.M. (1997). Identification and characterization of a K88- and CS31A-like operon of a rabbit enteropathogenic *Escherichia coli* strain which encodes fimbriae involved in the colonization of rabbit intestine. Infection and immunity *65*, 5222-5230.

Adu-Bobie, J., Frankel, G., Bain, C., Goncalves, A.G., Trabulsi, L.R., Douce, G., Knutton, S., and Dougan, G. (1998). Detection of intimins alpha, beta, gamma, and delta, four intimin derivatives expressed by attaching and effacing microbial pathogens. J Clin Microbiol *36*, 662-668.

Alto, N.M., Shao, F., Lazar, C.S., Brost, R.L., Chua, G., Mattoo, S., McMahon, S.A., Ghosh, P., Hughes, T.R., Boone, C.*, et al.* (2006). Identification of a bacterial type III effector family with G protein mimicry functions. Cell *124*, 133-145.

Amano, A., Takeuchi, H., and Furuta, N. (2010). Outer membrane vesicles function as offensive weapons in host-parasite interactions. Microbes and infection / Institut Pasteur *12*, 791-798.

Amirlak, I., and Amirlak, B. (2006). Haemolytic uraemic syndrome: an overview. Nephrology (Carlton) *11*, 213-218.

Arbeloa, A., Blanco, M., Moreira, F.C., Bulgin, R., Lopez, C., Dahbi, G., Blanco, J.E., Mora, A., Alonso, M.P., Mamani, R.C.*, et al.* (2009). Distribution of *espM* and *espT* among enteropathogenic and enterohaemorrhagic *Escherichia coli*. Journal of medical microbiology *58*, 988-995.

Arbeloa, A., Bulgin, R.R., MacKenzie, G., Shaw, R.K., Pallen, M.J., Crepin, V.F., Berger, C.N., and Frankel, G. (2008). Subversion of actin dynamics by EspM effectors of attaching and effacing bacterial pathogens. Cellular microbiology *10*, 1429-1441.

Asahara, T., Shimizu, K., Nomoto, K., Hamabata, T., Ozawa, A., and Takeda, Y. (2004). Probiotic bifidobacteria protect mice from lethal infection with Shiga toxin-producing *Escherichia coli* O157:H7. Infection and immunity *72*, 2240-2247.

Bai, L., Schuller, S., Whale, A., Mousnier, A., Marches, O., Wang, L., Ooka, T., Heuschkel, R., Torrente, F., Kaper, J.B.*, et al.* (2008). Enteropathogenic *Escherichia coli* O125:H6 triggers attaching and effacing lesions on human intestinal biopsy specimens independently of Nck and TccP/TccP2. Infection and immunity *76*, 361-368.

Barba, J., Bustamante, V.H., Flores-Valdez, M.A., Deng, W., Finlay, B.B., and Puente, J.L. (2005). A positive regulatory loop controls expression of the locus of enterocyte effacement-encoded regulators Ler and GrlA. Journal of bacteriology *187*, 7918-7930.

Bardiau, M., Szalo, M., and Mainil, J.G. (2010). Initial adherence of EPEC, EHEC and VTEC to host cells. Vet Res *41*, 57.

Barthold, S.W., Coleman, G.L., Bhatt, P.N., Osbaldiston, G.W., and Jonas, A.M. (1976). The etiology of transmissible murine colonic hyperplasia. Lab Anim Sci *26*, 889-894.

Barthold, S.W., Coleman, G.L., Jacoby, R.O., Livestone, E.M., and Jonas, A.M. (1978). Transmissible murine colonic hyperplasia. Vet Pathol *15*, 223-236.

Batchelor, M., Prasannan, S., Daniell, S., Reece, S., Connerton, I., Bloomberg, G., Dougan, G., Frankel, G., and Matthews, S. (2000). Structural basis for recognition of the translocated intimin receptor (Tir) by intimin from enteropathogenic *Escherichia coli*. EMBO J *19*, 2452-2464.

Beery, J.T., Doyle, M.P., and Schoeni, J.L. (1985). Colonization of chicken cecae by *Escherichia coli* associated with hemorrhagic colitis. Applied and environmental microbiology *49*, 310-315.

Bekassy, Z.D., Calderon Toledo, C., Leoj, G., Kristoffersson, A., Leopold, S.R., Perez, M.T., and Karpman, D. (2011). Intestinal damage in enterohemorrhagic *Escherichia coli* infection. Pediatric nephrology *26*, 2059-2071.

Bell, B.P., Griffin, P.M., Lozano, P., Christie, D.L., Kobayashi, J.M., and Tarr, P.I. (1997). Predictors of hemolytic uremic syndrome in children during a large outbreak of Escherichia coli O157:H7 infections. Pediatrics *100*, E12.

Bieber, D., Ramer, S.W., Wu, C.Y., Murray, W.J., Tobe, T., Fernandez, R., and Schoolnik, G.K. (1998). Type IV pili, transient bacterial aggregates, and virulence of enteropathogenic *Escherichia coli*. Science *280*, 2114-2118.

Bielaszewska, M., Mellmann, A., Zhang, W., Kock, R., Fruth, A., Bauwens, A., Peters, G., and Karch, H. (2011). Characterisation of the *Escherichia coli* strain associated with an outbreak of haemolytic uraemic syndrome in Germany, 2011: a microbiological study. Lancet Infect Dis *11*, 671-676.

Blasutig, I.M., New, L.A., Thanabalasuriar, A., Dayarathna, T.K., Goudreault, M., Quaggin, S.E., Li, S.S., Gruenheid, S., Jones, N., and Pawson, T. (2008). Phosphorylated YDXV motifs and Nck SH2/SH3 adaptors act cooperatively to induce actin reorganization. Mol Cell Biol *28*, 2035-2046.

Borczyk, A.A., Karmali, M.A., Lior, H., and Duncan, L.M. (1987). Bovine reservoir for verotoxin-producing *Escherichia coli* O157:H7. Lancet *1*, 98.

Borenshtein, D., McBee, M.E., and Schauer, D.B. (2008). Utility of the *Citrobacter rodentium* infection model in laboratory mice. Curr Opin Gastroenterol *24*, 32-37.

Borenshtein, D., Schlieper, K.A., Rickman, B.H., Chapman, J.M., Schweinfest, C.W., Fox, J.G., and Schauer, D.B. (2009). Decreased expression of colonic Slc26a3 and carbonic anhydrase iv as a cause of fatal infectious diarrhea in mice. Infection and immunity *77*, 3639-3650.

Brady, M.J., Campellone, K.G., Ghildiyal, M., and Leong, J.M. (2007). Enterohaemorrhagic and enteropathogenic *Escherichia coli* Tir proteins trigger a common Nck-independent actin assembly pathway. Cell Microbiol *9*, 2242-2253.

Brady, M.J., Radhakrishnan, P., Liu, H., Magoun, L., Murphy, K.C., Mukherjee, J., Donohue-Rolfe, A., Tzipori, S., and Leong, J.M. (2011). Enhanced Actin Pedestal Formation by Enterohemorrhagic *Escherichia coli* O157:H7 Adapted to the Mammalian Host. Front Microbiol *2*, 226.

Brigotti, M., Tazzari, P.L., Ravanelli, E., Carnicelli, D., Barbieri, S., Rocchi, L., Arfilli, V., Scavia, G., Ricci, F., Bontadini, A.*, et al.* (2010). Endothelial damage induced by Shiga toxins delivered by neutrophils during transmigration. J Leukoc Biol *88*, 201-210.

Bulgin, R.R., Arbeloa, A., Chung, J.C., and Frankel, G. (2009). EspT triggers formation of lamellipodia and membrane ruffles through activation of Rac-1 and Cdc42. Cellular microbiology *11*, 217-229.

Bull, B.S., Rubenberg, M.L., Dacie, J.V., and Brain, M.C. (1967). Red-blood-cell fragmentation in microangiopathic haemolytic anaemia: *in vitro* studies. Lancet *2*, 1123-1125.

Buteau, C., Proulx, F., Chaibou, M., Raymond, D., Clermont, M.J., Mariscalco, M.M., Lebel, M.H., and Seidman, E. (2000). Leukocytosis in children with Escherichia coli O157:H7 enteritis developing the hemolytic-uremic syndrome. Pediatr Infect Dis J *19*, 642-647.

Callebaut, C., Blanco, J., Benkirane, N., Krust, B., Jacotot, E., Guichard, G., Seddiki, N., Svab, J., Dam, E., Muller, S.*, et al.* (1998). Identification of V3 loop-binding proteins as

potential receptors implicated in the binding of HIV particles to CD4(+) cells. The Journal of biological chemistry *273*, 21988-21997.

Campellone, K.G. (2010). Cytoskeleton-modulating effectors of enteropathogenic and enterohaemorrhagic *Escherichia coli*: Tir, EspFu and actin pedestal assembly. FEBS J *277*, 2390-2402.

Campellone, K.G., Brady, M.J., Alamares, J.G., Rowe, D.C., Skehan, B.M., Tipper, D.J., and Leong, J.M. (2006). Enterohaemorrhagic *Escherichia coli* Tir requires a C-terminal 12-residue peptide to initiate EspF$_U$-mediated actin assembly and harbours N-terminal sequences that influence pedestal length. Cell Microbiol *8*, 1488-1503.

Campellone, K.G., Giese, A., Tipper, D.J., and Leong, J.M. (2002). A tyrosine-phosphorylated 12-amino-acid sequence of enteropathogenic *Escherichia coli* Tir binds the host adaptor protein Nck and is required for Nck localization to actin pedestals. Mol Microbiol *43*, 1227-1241.

Campellone, K.G., and Leong, J.M. (2005). Nck-independent actin assembly is mediated by two phosphorylated tyrosines within enteropathogenic *Escherichia coli* Tir. Mol Microbiol *56*, 416-432.

Campellone, K.G., Rankin, S., Pawson, T., Kirschner, M.W., Tipper, D.J., and Leong, J.M. (2004a). Clustering of Nck by a 12-residue Tir phosphopeptide is sufficient to trigger localized actin assembly. J Cell Biol *164*, 407-416.

Campellone, K.G., Robbins, D., and Leong, J.M. (2004b). EspF$_U$ is a translocated EHEC effector that interacts with Tir and N-WASP and promotes Nck-independent actin assembly. Dev Cell *7*, 217-228.

Campellone, K.G., Roe, A.J., Lobner-Olesen, A., Murphy, K.C., Magoun, L., Brady, M.J., Donohue-Rolfe, A., Tzipori, S., Gally, D.L., Leong, J.M.*, et al.* (2007). Increased adherence and actin pedestal formation by dam-deficient enterohaemorrhagic *Escherichia coli* O157:H7. Mol Microbiol *63*, 1468-1481.

Canil, C., Rosenshine, I., Ruschkowski, S., Donnenberg, M.S., Kaper, J.B., and Finlay, B.B. (1993). Enteropathogenic *Escherichia coli* decreases the transepithelial electrical resistance of polarized epithelial monolayers. Infect Immun *61*, 2755-2762.

Cantarelli, V.V., Takahashi, A., Yanagihara, I., Akeda, Y., Imura, K., Kodama, T., Kono, G., Sato, Y., Iida, T., and Honda, T. (2002). Cortactin is necessary for F-actin accumulation in pedestal structures induced by enteropathogenic *Escherichia coli* infection. Infection and immunity *70*, 2206-2209.

Caprioli, A., Morabito, S., Brugere, H., and Oswald, E. (2005a). Enterohaemorrhagic *Escherichia coli*: emerging issues on virulence and modes of transmission. Vet Res *36*, 289-311.

Caprioli, J., Peng, L., and Remuzzi, G. (2005b). The hemolytic uremic syndromes. Curr Opin Crit Care *11*, 487-492.

Carey, C.M., Kostrzynska, M., Ojha, S., and Thompson, S. (2008). The effect of probiotics and organic acids on Shiga-toxin 2 gene expression in enterohemorrhagic *Escherichia coli* O157:H7. J Microbiol Methods *73*, 125-132.

Caron, E., Crepin, V.F., Simpson, N., Knutton, S., Garmendia, J., and Frankel, G. (2006). Subversion of actin dynamics by EPEC and EHEC. Curr Opin Microbiol *9*, 40-45.

Castanie-Cornet, M.P., Penfound, T.A., Smith, D., Elliott, J.F., and Foster, J.W. (1999). Control of acid resistance in *Escherichia coli*. Journal of bacteriology *181*, 3525-3535.

Chandler, W.L., Jelacic, S., Boster, D.R., Ciol, M.A., Williams, G.D., Watkins, S.L., Igarashi, T., and Tarr, P.I. (2002). Prothrombotic coagulation abnormalities preceding the hemolytic-uremic syndrome. The New England journal of medicine *346*, 23-32.

Chen, H.D., and Frankel, G. (2005). Enteropathogenic *Escherichia coli*: unravelling pathogenesis. FEMS Microbiol Rev *29*, 83-98.

Cheng, H.C., Skehan, B.M., Campellone, K.G., Leong, J.M., and Rosen, M.K. (2008). Structural mechanism of WASP activation by the enterohaemorrhagic *E. coli* effector EspF$_U$. Nature *454*, 1009-1013.

Chiu, J., March, P.E., Lee, R., and Tillett, D. (2004). Site-directed, Ligase-Independent Mutagenesis (SLIM): a single-tube methodology approaching 100% efficiency in 4 h. Nucleic acids research *32*, e174.

Cimolai, N., Morrison, B.J., and Carter, J.E. (1992). Risk factors for the central nervous system manifestations of gastroenteritis-associated hemolytic-uremic syndrome. Pediatrics *90*, 616-621.

Cleary, J., Lai, L.C., Shaw, R.K., Straatman-Iwanowska, A., Donnenberg, M.S., Frankel, G., and Knutton, S. (2004). Enteropathogenic *Escherichia coli* (EPEC) adhesion to intestinal epithelial cells: role of bundle-forming pili (BFP), EspA filaments and intimin. Microbiology *150*, 527-538.

Clements, A., Smollett, K., Lee, S.F., Hartland, E.L., Lowe, M., and Frankel, G. (2011). EspG of enteropathogenic and enterohemorrhagic *E. coli* binds the Golgi matrix protein GM130 and disrupts the Golgi structure and function. Cellular microbiology *13*, 1429-1439.

Coad, N.A., Marshall, T., Rowe, B., and Taylor, C.M. (1991). Changes in the postenteropathic form of the hemolytic uremic syndrome in children. Clin Nephrol *35*, 10-16.

Cody, S.H., Glynn, M.K., Farrar, J.A., Cairns, K.L., Griffin, P.M., Kobayashi, J., Fyfe, M., Hoffman, R., King, A.S., Lewis, J.H.*, et al.* (1999). An outbreak of *Escherichia coli* O157:H7 infection from unpasteurized commercial apple juice. Ann Intern Med *130*, 202-209.

Cohen, A., Hannigan, G.E., Williams, B.R., and Lingwood, C.A. (1987). Roles of globotriosyl- and galabiosylceramide in verotoxin binding and high affinity interferon receptor. The Journal of biological chemistry *262*, 17088-17091.

Crane, J.K., McNamara, B.P., and Donnenberg, M.S. (2001). Role of EspF in host cell death induced by enteropathogenic *Escherichia coli*. Cell Microbiol *3*, 197-211.

Crepin, V.F., Girard, F., Schuller, S., Phillips, A.D., Mousnier, A., and Frankel, G. (2010). Dissecting the role of the Tir:Nck and Tir:IRTKS/IRSp53 signalling pathways *in vivo*. Mol Microbiol *75*, 308-323.

Croxen, M.A., and Finlay, B.B. (2010). Molecular mechanisms of *Escherichia coli* pathogenicity. Nature reviews Microbiology *8*, 26-38.

Crump, J.A., Sulka, A.C., Langer, A.J., Schaben, C., Crielly, A.S., Gage, R., Baysinger, M., Moll, M., Withers, G., Toney, D.M.*, et al.* (2002). An outbreak of *Escherichia coli* O157:H7 infections among visitors to a dairy farm. The New England journal of medicine *347*, 555-560.

Dahan, S., Wiles, S., La Ragione, R.M., Best, A., Woodward, M.J., Stevens, M.P., Shaw, R.K., Chong, Y., Knutton, S., Phillips, A.*, et al.* (2005). EspJ is a prophage-carried type III effector protein of attaching and effacing pathogens that modulates infection dynamics. Infect Immun *73*, 679-686.

Daniell, S.J., Takahashi, N., Wilson, R., Friedberg, D., Rosenshine, I., Booy, F.P., Shaw, R.K., Knutton, S., Frankel, G., and Aizawa, S. (2001). The filamentous type III secretion translocon of enteropathogenic *Escherichia coli*. Cell Microbiol *3*, 865-871.

Datsenko, K.A., and Wanner, B.L. (2000). One-step inactivation of chromosomal genes in *Escherichia coli* K-12 using PCR products. Proc Natl Acad Sci U S A *97*, 6640-6645.

de Grado, M., Abe, A., Gauthier, A., Steele-Mortimer, O., DeVinney, R., and Finlay, B.B. (1999). Identification of the intimin-binding domain of Tir of enteropathogenic *Escherichia coli*. Cell Microbiol *1*, 7-17.

de Verdugo, U.R., Selinka, H.C., Huber, M., Kramer, B., Kellermann, J., Hofschneider, P.H., and Kandolf, R. (1995). Characterization of a 100-kilodalton binding protein for the six serotypes of coxsackie B viruses. J Virol *69*, 6751-6757.

de Vries, G.E., Raymond, C.K., and Ludwig, R.A. (1984). Extension of bacteriophage lambda host range: selection, cloning, and characterization of a constitutive lambda receptor gene. Proceedings of the National Academy of Sciences of the United States of America *81*, 6080-6084.

Dean-Nystrom, E.A., Bosworth, B.T., Cray, W., Jr., and Moon, H.W. (1997). Pathogenicity of *Escherichia coli* O157:H7 in the intestines of neonatal calves. Infection & Immunity *65*, 1842-1848.

Dean-Nystrom, E.A., Bosworth, B.T., and Moon, H.W. (1999). Pathogenesis of *Escherichia coli* O157:H7 in weaned calves. Advances in experimental medicine and biology *473*, 173-177.

Dean-Nystrom, E.A., Bosworth, B.T., Moon, H.W., and O'Brien, A.D. (1998). *Escherichia coli* O157:H7 Requires Intimin for Enteropathogenicity in Calves. Infect Immun *66*, 4560-4563.

Dean-Nystrom, E.A., Stoffregen, W.C., Bosworth, B.T., Moon, H.W., and Pohlenz, J.F. (2008). Early attachment sites for Shiga-toxigenic *Escherichia coli* O157:H7 in experimentally inoculated weaned calves. Applied and environmental microbiology *74*, 6378-6384.

Dean, P., and Kenny, B. (2004). Intestinal barrier dysfunction by enteropathogenic *Escherichia coli* is mediated by two effector molecules and a bacterial surface protein. Mol Microbiol *54*, 665-675.

Dean, P., and Kenny, B. (2011). Cell-surface nucleolin is sequestered into EPEC microcolonies and may play a role during infection. Microbiology *157*, 1761-1767.

Deng, W., Li, Y., Vallance, B.A., and Finlay, B.B. (2001). Locus of enterocyte effacement from *Citrobacter rodentium*: sequence analysis and evidence for horizontal transfer among attaching and effacing pathogens. Infect Immun *69*, 6323-6335.

Deng, W., Puente, J.L., Gruenheid, S., Li, Y., Vallance, B.A., Vazquez, A., Barba, J., Ibarra, J.A., O'Donnell, P., Metalnikov, P.*, et al.* (2004). Dissecting virulence: systematic and functional analyses of a pathogenicity island. Proc Natl Acad Sci U S A *101*, 3597-3602.

Deng, W., Vallance, B.A., Li, Y., Puente, J.L., and Finlay, B.B. (2003). *Citrobacter rodentium* translocated intimin receptor (Tir) is an essential virulence factor needed for

actin condensation, intestinal colonization and colonic hyperplasia in mice. Mol Microbiol *48*, 95-115.

DeVinney, R., Gauthier, A., Abe, A., and Finlay, B.B. (1999a). Enteropathogenic *Escherichia coli*: a pathogen that inserts its own receptor into host cells. Cell Mol Life Sci *55*, 961-976.

DeVinney, R., Stein, M., Reinscheid, D., Abe, A., Ruschkowski, S., and Finlay, B.B. (1999b). Enterohemorrhagic *Escherichia coli* O157:H7 produces Tir, which is translocated to the host cell membrane but is not tyrosine phosphorylated. Infect Immun *67*, 2389-2398.

Donnenberg, M.S., and Kaper, J.B. (1991). Construction of an *eae* deletion mutant of enteropathogenic *Escherichia coli* by using a positive-selection suicide vector. Infection and Immunity *59*, 4310-4317.

Donnenberg, M.S., Tacket, C.O., James, S.P., Losonsky, G., Nataro, J.P., Wasserman, S.S., Kaper, J.B., and Levine, M.M. (1993a). Role of the *eaeA* gene in experimental enteropathogenic *Escherichia coli* infection. J Clin Invest *92*, 1412-1417.

Donnenberg, M.S., Tzipori, S., McKee, M.L., O'Brien, A.D., Alroy, J., and Kaper, J.B. (1993b). The role of the *eae* gene of enterohemorrhagic *Escherichia coli* in intimate attachment *in vitro* and in a porcine model. Journal of Clinical Investigation *92*, 1418-1424.

Donohue-Rolfe, A., Kondova, I., Oswald, S., Hutto, D., and Tzipori, S. (2000). *Escherichia coli* O157:H7 strains that express Stx2 alone are more neurotropic for gnotobiotic piglets than are isotypes producing Stx1 alone or both toxins. Journal of Infectious Disease *in press*.

Doyle, M.E., and Pariza, M.W. (2001). Foodborne microbial pathogens and the food research institute. Adv Appl Microbiol *49*, 143-161.

Dziva, F., van Diemen, P.M., Stevens, M.P., Smith, A.J., and Wallis, T.S. (2004). Identification of *Escherichia coli* O157:H7 genes influencing colonization of the bovine gastrointestinal tract using signature-tagged mutagenesis. Microbiology *150*, 3631-3645.

Eaton, K.A., Friedman, D.I., Francis, G.J., Tyler, J.S., Young, V.B., Haeger, J., Abu-Ali, G., and Whittam, T.S. (2008). Pathogenesis of renal disease due to enterohemorrhagic *Escherichia coli* in germ-free mice. Infect Immun *76*, 3054-3063.

Ebel, F., Podzadel, T., Rohde, M., Kresse, A.U., Kramer, S., Deibel, C., Guzman, C.A., and Chakraborty, T. (1998). Initial binding of Shiga toxin-producing *Escherichia coli* to host cells and subsequent induction of actin rearrangements depend on filamentous EspA-containing surface appendages. Mol Microbiol *30*, 147-161.

Echtenkamp, F., Deng, W., Wickham, M.E., Vazquez, A., Puente, J.L., Thanabalasuriar, A., Gruenheid, S., Finlay, B.B., and Hardwidge, P.R. (2008). Characterization of the NleF effector protein from attaching and effacing bacterial pathogens. FEMS microbiology letters *281*, 98-107.

Eklund, M., Leino, K., and Siitonen, A. (2002). Clinical *Escherichia coli* strains carrying stx genes: stx variants and stx-positive virulence profiles. Journal of clinical microbiology *40*, 4585-4593.

Elliott, E., Li, Z., Bell, C., Stiel, D., Buret, A., Wallace, J., Brzuszczak, I., and O'Loughlin, E. (1994). Modulation of host response to *Escherichia coli* O157:H7 infection by anti-CD18 antibody in rabbits. Gastroenterology *106*, 1554-1561.

Ellis, T.N., and Kuehn, M.J. (2010). Virulence and immunomodulatory roles of bacterial outer membrane vesicles. Microbiol Mol Biol Rev *74*, 81-94.

Endo, Y., Tsurugi, K., Yutsudo, T., Takeda, Y., Ogasawara, T., and Igarashi, K. (1988). Site of action of a Vero toxin (VT2) from *Escherichia coli* O157:H7 and of Shiga toxin on eukaryotic ribosomes. RNA N-glycosidase activity of the toxins. Eur J Biochem *171*, 45-50.

Erdem, A.L., Avelino, F., Xicohtencatl-Cortes, J., and Giron, J.A. (2007). Host protein binding and adhesive properties of H6 and H7 flagella of attaching and effacing *Escherichia coli*. Journal of bacteriology *189*, 7426-7435.

Ergonul, Z., Hughes, A.K., and Kohan, D.E. (2003). Induction of apoptosis of human brain microvascular endothelial cells by shiga toxin 1. The Journal of infectious diseases *187*, 154-158.

Farmer, J.J., 3rd, Potter, M.E., Riley, L.W., Barrett, T.J., Blake, P.A., Bopp, C.A., Cohen, M.L., Kaufmann, A., Morris, G.K., Remis, R.S.*, et al.* (1983). Animal models to study *Escherichia coli* O157:H7 isolated from patients with haemorrhagic colitis. Lancet *1*, 702-703.

Fiederling, F., Boury, M., Petit, C., and Milon, A. (1997). Adhesive factor/rabbit 2, a new fimbrial adhesin and a virulence factor from *Escherichia coli* O103, a serogroup enteropathogenic for rabbits. Infection and immunity *65*, 847-851.

Finlay, B.B., and Falkow, S. (1988). Comparison of the invasion strategies used by *Salmonella cholerae-suis*, *Shigella flexneri* and *Yersinia enterocolitica* to enter cultured animal cells: endosome acidification is not required for bacterial invasion or intracellular replication. Biochimie *70*, 1089-1099.

Fitzhenry, R.J., Pickard, D.J., Hartland, E.L., Reece, S., Dougan, G., Phillips, A.D., and Frankel, G. (2002). Intimin type influences the site of human intestinal mucosal colonisation by enterohaemorrhagic *Escherichia coli* O157:H7. Gut *50*, 180-185.

Flynn, A.N., and Buret, A.G. (2008). Tight junctional disruption and apoptosis in an *in vitro* model of *Citrobacter rodentium* infection. Microb Pathog *45*, 98-104.

Foster, G.H., Armstrong, C.S., Sakiri, R., and Tesh, V.L. (2000). Shiga toxin-induced tumor necrosis factor alpha expression: requirement for toxin enzymatic activity and monocyte protein kinase C and protein tyrosine kinases. Infection and immunity *68*, 5183-5189.

Foster, J.W. (2004). *Escherichia coli* acid resistance: tales of an amateur acidophile. Nature reviews Microbiology *2*, 898-907.

Frank, C., Werber, D., Cramer, J.P., Askar, M., Faber, M., an der Heiden, M., Bernard, H., Fruth, A., Prager, R., Spode, A.*, et al.* (2011). Epidemic profile of Shiga-toxin-producing *Escherichia coli* O104:H4 outbreak in Germany. The New England journal of medicine *365*, 1771-1780.

Frankel, G., Candy, D.C., Everest, P., and Dougan, G. (1994). Characterization of the C-terminal domains of intimin-like proteins of enteropathogenic and enterohemorrhagic *Escherichia coli*, *Citrobacter freundii*, and *Hafnia alvei*. Infection & Immunity *62*, 1835-1842.

Frankel, G., Candy, D.C., Fabiani, E., Adu-Bobie, J., Gil, S., Novakova, M., Phillips, A.D., and Dougan, G. (1995). Molecular characterization of a carboxy-terminal eukaryotic-cell-binding domain of intimin from enteropathogenic *Escherichia coli*. Infection and immunity *63*, 4323-4328.

Frankel, G., Lider, O., Hershkoviz, R., Mould, A.P., Kachalsky, S.G., Candy, D., Cahalon, L., Humphries, M.J., and Dougan, G. (1996a). The cell-binding domain of intimin from enteropathogenic *Escherichia coli* binds to beta1 integrins. Journal of Biological Chemistry *271*, 20359-20364.

Frankel, G., Philips, A.D., Novakova, M., Batchelor, M., Hicks, S., and Dougan, G. (1998). Generation of *Escherichia coli* intimin derivatives with differing biological activities using site-directed mutagenesis of the intimin C- terminus domain Mol Microbiol *29*, 559-570.

Frankel, G., and Phillips, A.D. (2008). Attaching effacing *Escherichia coli* and paradigms of Tir-triggered actin polymerization: getting off the pedestal. Cellular microbiology *10*, 549-556.

Frankel, G., Phillips, A.D., Novakova, M., Field, H., Candy, D.C., Schauer, D.B., Douce, G., and Dougan, G. (1996b). Intimin from enteropathogenic *Escherichia coli* restores murine virulence to a *Citrobacter rodentium eaeA* mutant: induction of an immunoglobulin A response to intimin and EspB. Infect Immun *64*, 5315-5325.

Friedrich, A.W., Bielaszewska, M., Zhang, W.L., Pulz, M., Kuczius, T., Ammon, A., and Karch, H. (2002). *Escherichia coli* harboring Shiga toxin 2 gene variants: frequency and association with clinical symptoms. The Journal of infectious diseases *185*, 74-84.

Fujii, J., Kita, T., Yoshida, S., Takeda, T., Kobayashi, H., Tanaka, N., Ohsato, K., and Mizuguchi, Y. (1994). Direct evidence of neuron impairment by oral infection with verotoxin-producing *Escherichia coli* O157:H- in mitomycin-treated mice. Infection and immunity *62*, 3447-3453.

Gamage, S.D., Strasser, J.E., Chalk, C.L., and Weiss, A.A. (2003). Nonpathogenic *Escherichia coli* can contribute to the production of Shiga toxin. Infection and immunity *71*, 3107-3115.

Gansheroff, L.J., and O'Brien, A.D. (2000). *Escherichia coli* O157:H7 in beef cattle presented for slaughter in the U.S.: higher prevalence rates than previously estimated. Proceedings of the National Academy of Sciences of the United States of America *97*, 2959-2961.

Garcia-Angulo, V.A., Deng, W., Thomas, N.A., Finlay, B.B., and Puente, J.L. (2008). Regulation of expression and secretion of NleH, a new non-locus of enterocyte effacement-encoded effector in *Citrobacter rodentium*. Journal of bacteriology *190*, 2388-2399.

Garcia, A., Bosques, C.J., Wishnok, J.S., Feng, Y., Karalius, B.J., Butterton, J.R., Schauer, D.B., Rogers, A.B., and Fox, J.G. (2006). Renal injury is a consistent finding in Dutch Belted rabbits experimentally infected with enterohemorrhagic *Escherichia coli*. The Journal of infectious diseases *193*, 1125-1134.

Garcia, A., Marini, R.P., Feng, Y., Vitsky, A., Knox, K.A., Taylor, N.S., Schauer, D.B., and Fox, J.G. (2002). A naturally occurring rabbit model of enterohemorrhagic *Escherichia coli*-induced disease. The Journal of infectious diseases *186*, 1682-1686.

Garmendia, J., Frankel, G., and Crepin, V.F. (2005). Enteropathogenic and enterohemorrhagic *Escherichia coli* infections: translocation, translocation, translocation. Infect Immun *73*, 2573-2585.

Garmendia, J., Phillips, A.D., Carlier, M.F., Chong, Y., Schuller, S., Marches, O., Dahan, S., Oswald, E., Shaw, R.K., Knutton, S.*, et al.* (2004). TccP is an enterohaemorrhagic *Escherichia coli* O157:H7 type III effector protein that couples Tir to the actin-cytoskeleton. Cell Microbiol *6*, 1167-1183.

Gerber, A., Karch, H., Allerberger, F., Verweyen, H.M., and Zimmerhackl, L.B. (2002). Clinical course and the role of shiga toxin-producing *Escherichia coli* infection in the hemolytic-uremic syndrome in pediatric patients, 1997-2000, in Germany and Austria: a prospective study. The Journal of infectious diseases *186*, 493-500.

Ghaem-Maghami, M., Simmons, C.P., Daniell, S., Pizza, M., Lewis, D., Frankel, G., and Dougan, G. (2001). Intimin-specific immune responses prevent bacterial colonization by the attaching-effacing pathogen *Citrobacter rodentium*. Infection and immunity *69*, 5597-5605.

Gibson, D.L., Ma, C., Bergstrom, K.S., Huang, J.T., Man, C., and Vallance, B.A. (2008). MyD88 signalling plays a critical role in host defence by controlling pathogen burden and promoting epithelial cell homeostasis during *Citrobacter rodentium*-induced colitis. Cell Microbiol *10*, 618-631.

Ginisty, H., Sicard, H., Roger, B., and Bouvet, P. (1999). Structure and functions of nucleolin. Journal of cell science *112 (Pt 6)*, 761-772.

Girard, F., Batisson, I., Frankel, G.M., Harel, J., and Fairbrother, J.M. (2005). Interaction of enteropathogenic and Shiga toxin-producing *Escherichia coli* and porcine intestinal mucosa: role of intimin and Tir in adherence. Infect Immun *73*, 6005-6016.

Girard, F., Crepin, V.F., and Frankel, G. (2009a). Modelling of infection by enteropathogenic *Escherichia coli* strains in lineages 2 and 4 *ex vivo* and *in vivo* by using *Citrobacter rodentium* expressing TccP. Infect Immun *77*, 1304-1314.

Girard, F., Dziva, F., Stevens, M.P., and Frankel, G. (2009b). Interactions of typical and atypical enteropathogenic *Escherichia coli* strains with the calf intestinal mucosa *ex vivo*. Appl Environ Microbiol *75*, 5991-5995.

Girard, F., Frankel, G., Phillips, A.D., Cooley, W., Weyer, U., Dugdale, A.H., Woodward, M.J., and La Ragione, R.M. (2008). Interaction of enterohemorrhagic *Escherichia coli* O157:H7 with mouse intestinal mucosa. FEMS Microbiol Lett *283*, 196-202.

Giron, J.A., Donnenberg, M.S., Martin, W.C., Jarvis, K.G., and Kaper, J.B. (1993). Distribution of the bundle-forming pilus structural gene (*bfpA*) among enteropathogenic *Escherichia coli*. The Journal of infectious diseases *168*, 1037-1041.

Giron, J.A., Ho, A.S.Y., and Schoolnik, G.K. (1991). An inducible bundle-forming pilus of enteropathogenic *Escherichia coli*. Science *254*, 710-713.

Giron, J.A., Torres, A.G., Freer, E., and Kaper, J.B. (2002). The flagella of enteropathogenic *Escherichia coli* mediate adherence to epithelial cells. Molecular microbiology *44*, 361-379.

Gobius, K.S., Higgs, G.M., and Desmarchelier, P.M. (2003). Presence of activatable Shiga toxin genotype (stx2d) in Shiga toxigenic *Escherichia coli* from livestock sources. J Clin Microbiol *41*, 3777-3783.

Goldberg, M.B. (2001). Actin-based motility of intracellular microbial pathogens. Microbiol Mol Biol Rev *65*, 595-626, table of contents.

Goley, E.D., and Welch, M.D. (2006). The ARP2/3 complex: an actin nucleator comes of age. Nat Rev Mol Cell Biol *7*, 713-726.

Goosney, D.L., DeVinney, R., Pfuetzner, R.A., Frey, E.A., Strynadka, N.C., and Finlay, B.B. (2000). Enteropathogenic *E. coli* translocated intimin receptor, Tir, interacts directly with alpha-actinin. Curr Biol *10*, 735-738.

Gorden, J., and Small, P. (1993). Acid resistance in enteric bacteria. Infect Immun *61*, 364-367.

Griffin, P.M., Ostroff, S.M., Tauxe, R.V., Greene, K.D., Wells, J.G., Lewis, J.H., and Blake, P.A. (1988). Illnesses associated with *Escherichia coli* O157:H7 infections. A broad clinical spectrum. Ann Intern Med *109*, 705-712.

Gruenheid, S., DeVinney, R., Bladt, F., Goosney, D., Gelkop, S., Gish, G.D., Pawson, T., and Finlay, B.B. (2001). Enteropathogenic *E. coli* Tir binds Nck to initiate actin pedestal formation in host cells. Nat Cell Biol *3*, 856-859.

Gruenheid, S., Sekirov, I., Thomas, N.A., Deng, W., O'Donnell, P., Goode, D., Li, Y., Frey, E.A., Brown, N.F., Metalnikov, P.*, et al.* (2004). Identification and characterization of NleA, a non-LEE-encoded type III translocated virulence factor of enterohaemorrhagic *Escherichia coli* O157:H7. Molecular microbiology *51*, 1233-1249.

Grys, T.E., Siegel, M.B., Lathem, W.W., and Welch, R.A. (2005). The StcE protease contributes to intimate adherence of enterohemorrhagic *Escherichia coli* O157:H7 to host cells. Infection and immunity *73*, 1295-1303.

Gunzer, F., Hennig-Pauka, I., Waldmann, K.H., Sandhoff, R., Grone, H.J., Kreipe, H.H., Matussek, A., and Mengel, M. (2002). Gnotobiotic piglets develop thrombotic microangiopathy after oral infection with enterohemorrhagic *Escherichia coli*. Am J Clin Pathol *118*, 364-375.

Guttman, J.A., Li, Y., Wickham, M.E., Deng, W., Vogl, A.W., and Finlay, B.B. (2006a). Attaching and effacing pathogen-induced tight junction disruption *in vivo*. Cell Microbiol *8*, 634-645.

Guttman, J.A., Samji, F.N., Li, Y., Vogl, A.W., and Finlay, B.B. (2006b). Evidence that tight junctions are disrupted due to intimate bacterial contact and not inflammation during attaching and effacing pathogen infection *in vivo*. Infect Immun *74*, 6075-6084.

Hanajima-Ozawa, M., Matsuzawa, T., Fukui, A., Kamitani, S., Ohnishi, H., Abe, A., Horiguchi, Y., and Miyake, M. (2007). Enteropathogenic *Escherichia coli*, *Shigella flexneri*, and *Listeria monocytogenes* recruit a junctional protein, zonula occludens-1, to actin tails and pedestals. Infection and immunity *75*, 565-573.

Hardwidge, P.R., Deng, W., Vallance, B.A., Rodriguez-Escudero, I., Cid, V.J., Molina, M., and Finlay, B.B. (2005). Modulation of host cytoskeleton function by the enteropathogenic *Escherichia coli* and *Citrobacter rodentium* effector protein EspG. Infect Immun *73*, 2586-2594.

Hartland, E.L., Batchelor, M., Delahay, R.M., Hale, C., Matthews, S., Dougan, G., Knutton, S., Connerton, I., and Frankel, G. (1999). Binding of intimin from enteropathogenic *Escherichia coli* to Tir and to host cells. Molecular microbiology *32*, 151-158.

Hartland, E.L., Huter, V., Higgins, L.M., Goncalves, N.S., Dougan, G., Phillips, A.D., MacDonald, T.T., and Frankel, G. (2000). Expression of intimin gamma from enterohemorrhagic *Escherichia coli* in *Citrobacter rodentium*. Infect Immun *68*, 4637-4646.

Hayward, R.D., Leong, J.M., Koronakis, V., and Campellone, K.G. (2006). Exploiting pathogenic *Escherichia coli* to model transmembrane receptor signalling. Nat Rev Microbiol *4*, 358-370.

Hemrajani, C., Berger, C.N., Robinson, K.S., Marches, O., Mousnier, A., and Frankel, G. (2010). NleH effectors interact with Bax inhibitor-1 to block apoptosis during enteropathogenic *Escherichia coli* infection. Proceedings of the National Academy of Sciences of the United States of America *107*, 3129-3134.

Hemrajani, C., Marches, O., Wiles, S., Girard, F., Dennis, A., Dziva, F., Best, A., Phillips, A.D., Berger, C.N., Mousnier, A*., et al.* (2008). Role of NleH, a type III secreted effector from attaching and effacing pathogens, in colonization of the bovine, ovine, and murine gut. Infection and immunity *76*, 4804-4813.

Henikoff, S., and Henikoff, J.G. (1992). Amino acid substitution matrices from protein blocks. Proceedings of the National Academy of Sciences of the United States of America *89*, 10915-10919.

Hernandez, V.J., Edlind, T.D., Young, R.F., and Ihler, G.M. (1985). The DNA between *Rz* and *cosR* in bacteriophage lambda is nonessential. Gene *33*, 363-365.

Hicks, S., Frankel, G., Kaper, J.B., Dougan, G., and Phillips, A.D. (1998). Role of intimin and bundle-forming pili in enteropathogenic *Escherichia coli* adhesion to pediatric intestinal tissue *in vitro*. Infection and immunity *66*, 1570-1578.

Ho, T.D., Davis, B.M., Ritchie, J.M., and Waldor, M.K. (2008). Type 2 secretion promotes enterohemorrhagic *Escherichia coli* adherence and intestinal colonization. Infection and immunity *76*, 1858-1865.

Hurley, B.P., Thorpe, C.M., and Acheson, D.W. (2001). Shiga toxin translocation across intestinal epithelial cells is enhanced by neutrophil transmigration. Infect Immun *69*, 6148-6155.

Ide, T., Laarmann, S., Greune, L., Schillers, H., Oberleithner, H., and Schmidt, M.A. (2001). Characterization of translocation pores inserted into plasma membranes by type III-secreted Esp proteins of enteropathogenic *Escherichia coli*. Cell Microbiol *3*, 669-679.

Imai, Y., Fukui, T., Kurohane, K., Miyamoto, D., Suzuki, Y., Ishikawa, T., Ono, Y., and Miyake, M. (2003). Restricted expression of shiga toxin binding sites on mucosal epithelium of mouse distal colon. Infection and immunity *71*, 985-990.

Isberg, R.R., and Leong, J.M. (1990). Multiple β1 chain integrins are receptors for invasin, a protein that promoted bacterial penetration into mammalian cells. Cell *60*, 861-871.

Isberg, R.R., Voorhis, D.L., and Falkow, S. (1987). Identification of invasin: a protein that allows enteric bacteria to penetrate cultured mammalian cells. Cell *50*, 769-778.

Isogai, E., Isogai, H., Kimura, K., Hayashi, S., Kubota, T., Fujii, N., and Takeshi, K. (1998). Role of tumor necrosis factor alpha in gnotobiotic mice infected with an *Escherichia coli* O157:H7 strain. Infection and immunity *66*, 197-202.

Ito, H., Terai, A., Kurazono, H., Takeda, Y., and Nishibuchi, M. (1990). Cloning and nucleotide sequencing of Vero toxin 2 variant genes from *Escherichia coli* O91:H21 isolated from a patient with the hemolytic uremic syndrome. Microbial pathogenesis *8*, 47-60.

Jarvis, K.G., Giron, J.A., Jerse, A.E., McDaniel, T.K., Donnenberg, M.S., and Kaper, J.B. (1995). Enteropathogenic *Escherichia coli* contains a putative type III secretion system necessary for the export of proteins involved in attaching and effacing lesion formation. Proc Natl Acad Sci U S A *92*, 7996-8000.

Jenkins, C., Pearce, M.C., Smith, A.W., Knight, H.I., Shaw, D.J., Cheasty, T., Foster, G., Gunn, G.J., Dougan, G., Smith, H.R*., et al.* (2003). Detection of *Escherichia coli*

serogroups O26, O103, O111 and O145 from bovine faeces using immunomagnetic separation and PCR/DNA probe techniques. Lett Appl Microbiol *37*, 207-212.

Jerse, A.E., Yu, J., Tall, B.D., and Kaper, J.B. (1990). A genetic locus of enteropathogenic *Escherichia coli* necessary for the production of attaching and effacing lesions on tissue culture cells. Proc Natl Acad Sci U S A *87*, 7839-7843.

Jerse, A.E., Yu, J., Tall, B.D., and Kaper, J.B. (1990). A genetic locus of enteropathogenic *Escherichia coli* necessary for the production of attaching and effacing lesions on tissue culture cells. Proc Nat Acad Sci, USA *87*, 7839-7843.

Jobling, M.G., and Holmes, R.K. (1990). Construction of vectors with the p15a replicon, kanamycin resistance, inducible *lacZ* alpha and pUC18 or pUC19 multiple cloning sites. Nucleic acids research *18*, 5315-5316.

Johnson, K.E., Thorpe, C.M., and Sears, C.L. (2006). The emerging clinical importance of non-O157 Shiga toxin-producing Escherichia coli. Clin Infect Dis *43*, 1587-1595.

Jones, D.H., and Winistorfer, S.C. (1993). Genome walking with 2- to 4-kb steps using panhandle PCR. PCR Methods Appl *2*, 197-203.

Kanack, K.J., Crawford, J.A., Tatsuno, I., Karmali, M.A., and Kaper, J.B. (2005). SepZ/EspZ is secreted and translocated into HeLa cells by the enteropathogenic *Escherichia coli* type III secretion system. Infection and immunity *73*, 4327-4337.

Kang, G., Pulimood, A.B., Koshi, R., Hull, A., Acheson, D., Rajan, P., Keusch, G.T., Mathan, V.I., and Mathan, M.M. (2001). A monkey model for enterohemorrhagic *Escherichia coli* infection. The Journal of infectious diseases *184*, 206-210.

Kaper, J.B., Nataro, J.P., and Mobley, H.L. (2004). Pathogenic *Escherichia coli*. Nat Rev Microbiol *2*, 123-140.

Karch, H., Tarr, P.I., and Bielaszewska, M. (2005). Enterohaemorrhagic *Escherichia coli* in human medicine. Int J Med Microbiol *295*, 405-418.

Karmali, M.A., Gannon, V., and Sargeant, J.M. (2009). Verocytotoxin-producing *Escherichia coli* (VTEC). Vet Microbiol *140*, 360-370.

Karpman, D., Connell, H., Svensson, M., Scheutz, F., Alm, P., and Svanborg, C. (1997). The role of lipopolysaccharide and Shiga-like toxin in a mouse model of *Escherichia coli* O157:H7 infection. The Journal of infectious diseases *175*, 611-620.

Keepers, T.R., Gross, L.K., and Obrig, T.G. (2007). Monocyte chemoattractant protein 1, macrophage inflammatory protein 1 alpha, and RANTES recruit macrophages to the

kidney in a mouse model of hemolytic-uremic syndrome. Infection and immunity *75*, 1229-1236.

Keepers, T.R., Psotka, M.A., Gross, L.K., and Obrig, T.G. (2006). A murine model of HUS: Shiga toxin with lipopolysaccharide mimics the renal damage and physiologic response of human disease. J Am Soc Nephrol *17*, 3404-3414.

Kelly, M., Hart, E., Mundy, R., Marches, O., Wiles, S., Badea, L., Luck, S., Tauschek, M., Frankel, G., Robins-Browne, R.M.*, et al.* (2006). Essential role of the type III secretion system effector NleB in colonization of mice by *Citrobacter rodentium*. Infection and immunity *74*, 2328-2337.

Kenny, B. (1999). Phosphorylation of tyrosine 474 of the enteropathogenic *Escherichia coli* (EPEC) Tir receptor molecule is essential for actin nucleating activity and is preceded by additional host modifications. Mol Microbiol *31*, 1229-1241.

Kenny, B. (2001). The enterohaemorrhagic *Escherichia coli* (serotype O157:H7) Tir molecule is not functionally interchangeable for its enteropathogenic *E. coli* (serotype O127:H6) homologue. Cell Microbiol *3*, 499-510.

Kenny, B., DeVinney, R., Stein, M., Reinscheid, D.J., Frey, E.A., and Finlay, B.B. (1997). Enteropathogenic *E. coli* (EPEC) transfers its receptor for intimate adherence into mammalian cells. Cell *91*, 511-520.

Kenny, B., Ellis, S., Leard, A.D., Warawa, J., Mellor, H., and Jepson, M.A. (2002). Co-ordinate regulation of distinct host cell signalling pathways by multifunctional enteropathogenic *Escherichia coli* effector molecules. Mol Microbiol *44*, 1095-1107.

Kenny, B., and Finlay, B.B. (1995). Protein secretion by enteropathogenic *Escherichia coli* is essential for transducing signals to epithelial cells. Proc Natl Acad Sci U S A *92*, 7991-7995.

Kenny, B., and Jepson, M. (2000). Targeting of an enteropathogenic *Escherichia coli* (EPEC) effector protein to host mitochondria. Cell Microbiol *2*, 579-590.

Khan, M.A., Ma, C., Knodler, L.A., Valdez, Y., Rosenberger, C.M., Deng, W., Finlay, B.B., and Vallance, B.A. (2006). Toll-like receptor 4 contributes to colitis development but not to host defense during *Citrobacter rodentium* infection in mice. Infection and immunity *74*, 2522-2536.

Knutton, S., Phillips, A.D., Smith, H.R., Gross, R.J., Shaw, R., Watson, P., and Price, E. (1991). Screening for enteropathogenic *Escherichia coli* in infants with diarrhea by the fluorescent-actin staining test. Infection and immunity *59*, 365-371.

Knutton, S., Rosenshine, I., Pallen, M.J., Nisan, I., Neves, B.C., Bain, C., Wolff, C., Dougan, G., and Frankel, G. (1998). A novel EspA-associated surface organelle of enteropathogenic *Escherichia coli* involved in protein translocation into epithelial cells. Embo J *17*, 2166-2176.

Kolling, G.L., and Matthews, K.R. (1999). Export of virulence genes and Shiga toxin by membrane vesicles of *Escherichia coli* O157:H7. Applied and environmental microbiology *65*, 1843-1848.

Kulasekara, B.R., Jacobs, M., Zhou, Y., Wu, Z., Sims, E., Saenphimmachak, C., Rohmer, L., Ritchie, J.M., Radey, M., McKevitt, M.*, et al.* (2009). Analysis of the genome of the Escherichia coli O157:H7 2006 spinach-associated outbreak isolate indicates candidate genes that may enhance virulence. Infection and immunity *77*, 3713-3721.

Kurioka, T., Yunou, Y., and Kita, E. (1998). Enhancement of susceptibility to Shiga toxin-producing *Escherichia coli* O157:H7 by protein calorie malnutrition in mice. Infection and immunity *66*, 1726-1734.

La Ragione, R.M., Cooley, W.A., and Woodward, M.J. (2000). The role of fimbriae and flagella in the adherence of avian strains of *Escherichia coli* O78:K80 to tissue culture cells and tracheal and gut explants. Journal of medical microbiology *49*, 327-338.

Lane, M.C., and Mobley, H.L. (2007). Role of P-fimbrial-mediated adherence in pyelonephritis and persistence of uropathogenic *Escherichia coli* (UPEC) in the mammalian kidney. Kidney Int *72*, 19-25.

LaRosa, D.F., Stumhofer, J.S., Gelman, A.E., Rahman, A.H., Taylor, D.K., Hunter, C.A., and Turka, L.A. (2008). T cell expression of MyD88 is required for resistance to *Toxoplasma gondii*. Proceedings of the National Academy of Sciences of the United States of America *105*, 3855-3860.

Lee, C.A. (1997). Type III secretion systems: machines to deliver bacterial proteins into eukaryotic cells? Trends in microbiology *5*, 148-156.

Lin, J., Lee, I.S., Frey, J., Slonczewski, J.L., and Foster, J.W. (1995). Comparative analysis of extreme acid survival in *Salmonella typhimurium*, *Shigella flexneri*, and *Escherichia coli*. Journal of bacteriology *177*, 4097-4104.

Lin, J., Smith, M.P., Chapin, K.C., Baik, H.S., Bennett, G.N., and Foster, J.W. (1996). Mechanisms of acid resistance in enterohemorrhagic *Escherichia coli*. Applied and environmental microbiology *62*, 3094-3100.

Lindgren, S.W., Melton, A.R., and O'Brien, A.D. (1993). Virulence of enterohemorrhagic *Escherichia coli* O91:H21 clinical isolates in an orally infected mouse model. Infect Immun *61*, 3832-3842.

Lingwood, C.A., Law, H., Richardson, S., Petric, M., Brunton, J.L., De Grandis, S., and Karmali, M. (1987). Glycolipid binding of purified and recombinant *Escherichia coli* produced verotoxin *in vitro*. The Journal of biological chemistry *262*, 8834-8839.

Litalien, C., Proulx, F., Mariscalco, M.M., Robitaille, P., Turgeon, J.P., Orrbine, E., Rowe, P.C., McLaine, P.N., and Seidman, E. (1999). Circulating inflammatory cytokine levels in hemolytic uremic syndrome. Pediatric nephrology *13*, 840-845.

Littman, D.R., and Pamer, E.G. (2011). Role of the commensal microbiota in normal and pathogenic host immune responses. Cell host & microbe *10*, 311-323.

Liu, B., Yin, X., Feng, Y., Chambers, J.R., Guo, A., Gong, J., Zhu, J., and Gyles, C.L. (2010). Verotoxin 2 enhances adherence of enterohemorrhagic *Escherichia coli* O157:H7 to intestinal epithelial cells and expression of beta1-integrin by IPEC-J2 cells. Applied and environmental microbiology *76*, 4461-4468.

Liu, H., Magoun, L., Luperchio, S., Schauer, D.B., and Leong, J.M. (1999). The Tir-binding region of enterohaemorrhagic *Escherichia coli* intimin is sufficient to trigger actin condensation after bacterial-induced host cell signalling. Mol Microbiol *34*, 67-81.

Liu, H., Radhakrishnan, P., Magoun, L., Prabu, M., Campellone, K.G., Savage, P., He, F., Schiffer, C.A., and Leong, J.M. (2002). Point mutants of EHEC intimin that diminish Tir recognition and actin pedestal formation highlight a putative Tir binding pocket. Mol Microbiol *45*, 1557-1573.

Lloyd, S.J., Ritchie, J.M., Rojas-Lopez, M., Blumentritt, C.A., Popov, V.L., Greenwich, J.L., Waldor, M.K., and Torres, A.G. (2012). A double long polar fimbriae mutant of *Escherichia coli* O157:H7 expresses curli and exhibits reduced *in vivo* colonization. Infection and immunity.

Lommel, S., Benesch, S., Rohde, M., Wehland, J., and Rottner, K. (2004). Enterohaemorrhagic and enteropathogenic *Escherichia coli* use different mechanisms for actin pedestal formation that converge on N-WASP. Cell Microbiol *6*, 243-254.

Lommel, S., Benesch, S., Rottner, K., Franz, T., Wehland, J., and Kuhn, R. (2001). Actin pedestal formation by enteropathogenic *Escherichia coli* and intracellular motility of *Shigella flexneri* are abolished in N-WASP-defective cells. EMBO Rep *2*, 850-857.

Loureiro, I., Frankel, G., Adu-Bobie, J., Dougan, G., Trabulsi, L.R., and Carneiro-Sampaio, M.M. (1998). Human colostrum contains IgA antibodies reactive to enteropathogenic *Escherichia coli* virulence-associated proteins: intimin, BfpA, EspA, and EspB. J Pediatr Gastroenterol Nutr *27*, 166-171.

Luo, Y., Frey, E.A., Pfuetzner, R.A., Creagh, A.L., Knoechel, D.G., Haynes, C.A., Finlay, B.B., and Strynadka, N.C. (2000). Crystal structure of enteropathogenic *Escherichia coli* intimin-receptor complex. Nature *405*, 1073-1077.

Luperchio, S.A., Newman, J.V., Dangler, C.A., Schrenzel, M.D., Brenner, D.J., Steigerwalt, A.G., and Schauer, D.B. (2000). *Citrobacter rodentium*, the causative agent of transmissible murine colonic hyperplasia, exhibits clonality: synonymy of *C. rodentium* and mouse-pathogenic *Escherichia coli*. J Clin Microbiol *38*, 4343-4350.

Luperchio, S.A., and Schauer, D.B. (2001). Molecular pathogenesis of *Citrobacter rodentium* and transmissible murine colonic hyperplasia. Microbes Infect *3*, 333-340.

Ma, C., Wickham, M.E., Guttman, J.A., Deng, W., Walker, J., Madsen, K.L., Jacobson, K., Vogl, W.A., Finlay, B.B., and Vallance, B.A. (2006). *Citrobacter rodentium* infection causes both mitochondrial dysfunction and intestinal epithelial barrier disruption *in vivo*: role of mitochondrial associated protein (Map). Cell Microbiol *8*, 1669-1686.

MacConnachie, A.A., and Todd, W.T. (2004). Potential therapeutic agents for the prevention and treatment of haemolytic uraemic syndrome in shiga toxin producing *Escherichia coli* infection. Curr Opin Infect Dis *17*, 479-482.

Mallick, E.M., Brady, M.J., Luperchio, S.A., Vanguri, V., Magoun, L., Liu, H., Sheppard, B.J., Mukherjee, J., Donohue-Rolfe, A., Tzipori, S.*, et al.* (2012). Allele- and Tir-independent functions of intimin in diverse animal infection models. Front Microbiol *3*.

Maluykova, I., Gutsal, O., Laiko, M., Kane, A., Donowitz, M., and Kovbasnjuk, O. (2008). Latrunculin B facilitates Shiga toxin 1 transcellular transcytosis across T84 intestinal epithelial cells. Biochim Biophys Acta *1782*, 370-377.

Malyukova, I., Murray, K.F., Zhu, C., Boedeker, E., Kane, A., Patterson, K., Peterson, J.R., Donowitz, M., and Kovbasnjuk, O. (2009). Macropinocytosis in Shiga toxin 1 uptake by human intestinal epithelial cells and transcellular transcytosis. American journal of physiology Gastrointestinal and liver physiology *296*, G78-92.

Marches, O., Batchelor, M., Shaw, R.K., Patel, A., Cummings, N., Nagai, T., Sasakawa, C., Carlsson, S.R., Lundmark, R., Cougoule, C.*, et al.* (2006). EspF of enteropathogenic *Escherichia coli* binds sorting nexin 9. Journal of bacteriology *188*, 3110-3115.

Marches, O., Covarelli, V., Dahan, S., Cougoule, C., Bhatta, P., Frankel, G., and Caron, E. (2008). EspJ of enteropathogenic and enterohaemorrhagic *Escherichia coli* inhibits opsono-phagocytosis. Cellular microbiology *10*, 1104-1115.

Marches, O., Ledger, T.N., Boury, M., Ohara, M., Tu, X., Goffaux, F., Mainil, J., Rosenshine, I., Sugai, M., De Rycke, J.*, et al.* (2003). Enteropathogenic and

enterohaemorrhagic *Escherichia coli* deliver a novel effector called Cif, which blocks cell cycle G2/M transition. Mol Microbiol *50*, 1553-1567.

Marches, O., Nougayrede, J.P., Boullier, S., Mainil, J., Charlier, G., Raymond, I., Pohl, P., Boury, M., De Rycke, J., Milon, A.*, et al.* (2000). Role of Tir and intimin in the virulence of rabbit enteropathogenic *Escherichia coli* serotype O103:H2. Infect Immun *68*, 2171-2182.

Marches, O., Wiles, S., Dziva, F., La Ragione, R.M., Schuller, S., Best, A., Phillips, A.D., Hartland, E.L., Woodward, M.J., Stevens, M.P.*, et al.* (2005). Characterization of two non-locus of enterocyte effacement-encoded type III-translocated effectors, NleC and NleD, in attaching and effacing pathogens. Infection and immunity *73*, 8411-8417.

Martinez-Argudo, I., Sands, C., and Jepson, M.A. (2007). Translocation of enteropathogenic *Escherichia coli* across an in vitro M cell model is regulated by its type III secretion system. Cellular microbiology *9*, 1538-1546.

Martinez, M.B., Taddei, C.R., Ruiz-Tagle, A., Trabulsi, L.R., and Giron, J.A. (1999). Antibody response of children with enteropathogenic *Escherichia coli* infection to the bundle-forming pilus and locus of enterocyte effacement-encoded virulence determinants. The Journal of infectious diseases *179*, 269-274.

Matsuzawa, T., Kuwae, A., and Abe, A. (2005). Enteropathogenic *Escherichia coli* type III effectors EspG and EspG2 alter epithelial paracellular permeability. Infect Immun *73*, 6283-6289.

Matsuzawa, T., Kuwae, A., Yoshida, S., Sasakawa, C., and Abe, A. (2004). Enteropathogenic *Escherichia coli* activates the RhoA signaling pathway via the stimulation of GEF-H1. Embo J *23*, 3570-3582.

McBee, M.E., Zheng, P.Z., Rogers, A.B., Fox, J.G., and Schauer, D.B. (2008). Modulation of acute diarrheal illness by persistent bacterial infection. Infection and immunity *76*, 4851-4858.

McCormick, B.A. (2007). Bacterial-induced hepoxilin A3 secretion as a pro-inflammatory mediator. The FEBS journal *274*, 3513-3518.

McDaniel, T.K., Jarvis, K.G., Donnenberg, M.S., and Kaper, J.B. (1995). A genetic locus of enterocyte effacement conserved among diverse enterobacterial pathogens. Proc Natl Acad Sci U S A *92*, 1664-1668.

McDaniel, T.K., and Kaper, J.B. (1997). A cloned pathogenicity island from enteropathogenic *Escherichia coli* confers the attaching and effacing phenotype on *E. coli* K-12. Mol Microbiol *23*, 399-407.

McDonough, M.A., and Butterton, J.R. (1999). Spontaneous tandem amplification and deletion of the shiga toxin operon in *Shigella dysenteriae* 1. Molecular microbiology *34*, 1058-1069.

McKee, M.L., Melton-Celsa, A.R., Moxley, R.A., Francis, D.H., and O'Brien, A.D. (1995). Enterohemorrhagic *Escherichia coli* O157:H7 requires intimin to colonize the gnotobiotic pig intestine and to adhere to HEp-2 cells. Infect Immun *63*, 3739-3744.

McKee, M.L., and O'Brien, A.D. (1995). Investigation of enterohemorrhagic *Escherichia coli* O157:H7 adherence characteristics and invasion potential reveals a new attachment pattern shared by intestinal *E. coli*. Infect Immun *63*, 2070-2074.

McNamara, B.P., Koutsouris, A., O'Connell, C.B., Nougayrede, J.P., Donnenberg, M.S., and Hecht, G. (2001). Translocated EspF protein from enteropathogenic *Escherichia coli* disrupts host intestinal barrier function. J Clin Invest *107*, 621-629.

Mead, P.S., and Griffin, P.M. (1998). *Escherichia coli* O157:H7. Lancet *352*, 1207-1212.

Melton-Celsa, A., Mohawk, K., Teel, L., and O'Brien, A. (2011). Pathogenesis of Shiga-Toxin Producing *Escherichia coli*. Curr Top Microbiol Immunol.

Melton-Celsa, A.R., Darnell, S.C., and O'Brien, A.D. (1996). Activation of Shiga-like toxins by mouse and human intestinal mucus correlates with virulence of enterohemorrhagic *Escherichia coli* O91:H21 isolates in orally infected, streptomycin-treated mice. Infection and immunity *64*, 1569-1576.

Melton-Celsa, A.R., Kokai-Kun, J.F., and O'Brien, A.D. (2002). Activation of Shiga toxin type 2d (Stx2d) by elastase involves cleavage of the C-terminal two amino acids of the A2 peptide in the context of the appropriate B pentamer. Molecular microbiology *43*, 207-215.

Menard, R., Sansonetti, P.J., and Parsot, C. (1993). Nonpolar mutagenesis of the ipa genes defines IpaB, IpaC, and IpaD as effectors of *Shigella flexneri* entry into epithelial cells. Journal of bacteriology *175*, 5899-5906.

Meyers, K.E., and Kaplan, B.S. (2000). Many cell types are Shiga toxin targets. Kidney Int *57*, 2650-2651.

Mohawk, K.L., Melton-Celsa, A.R., Robinson, C.M., and O'Brien, A.D. (2010a). Neutralizing antibodies to Shiga toxin type 2 (Stx2) reduce colonization of mice by Stx2-expressing *Escherichia coli* O157:H7. Vaccine *28*, 4777-4785.

Mohawk, K.L., Melton-Celsa, A.R., Zangari, T., Carroll, E.E., and O'Brien, A.D. (2010b). Pathogenesis of *Escherichia coli* O157:H7 strain 86-24 following oral infection of BALB/c mice with an intact commensal flora. Microbial pathogenesis *48*, 131-142.

Mohawk, K.L., and O'Brien, A.D. (2011). Mouse models of *Escherichia coli* O157:H7 infection and shiga toxin injection. J Biomed Biotechnol *2011*, 258185.

Moon, H.W. (1997). Comparative histopathology of intestinal infections. Advances in experimental medicine and biology *412*, 1-19.

Moon, H.W., Whipp, S.C., Argenzio, R.A., Levine, M.M., and Giannella, R.A. (1983). Attaching and effacing activities of rabbit and human enteropathogenic *Escherichia coli* in pig and rabbit intestines. Infect Immun *41*, 1340-1351.

Mousnier, A., Whale, A.D., Schuller, S., Leong, J.M., Phillips, A.D., and Frankel, G. (2008). Cortactin recruitment by enterohemorrhagic *Escherichia coli* O157:H7 during infection *in vitro* and *ex vivo*. Infection and immunity *76*, 4669-4676.

Muhldorfer, I., Hacker, J., Keusch, G.T., Acheson, D.W., Tschape, H., Kane, A.V., Ritter, A., Olschlager, T., and Donohue-Rolfe, A. (1996). Regulation of the Shiga-like toxin II operon in *Escherichia coli*. Infection and immunity *64*, 495-502.

Mundy, R., MacDonald, T.T., Dougan, G., Frankel, G., and Wiles, S. (2005). *Citrobacter rodentium* of mice and man. Cell Microbiol *7*, 1697-1706.

Mundy, R., Petrovska, L., Smollett, K., Simpson, N., Wilson, R.K., Yu, J., Tu, X., Rosenshine, I., Clare, S., Dougan, G.*, et al.* (2004). Identification of a novel *Citrobacter rodentium* type III secreted protein, EspI, and roles of this and other secreted proteins in infection. Infection and immunity *72*, 2288-2302.

Mundy, R., Pickard, D., Wilson, R.K., Simmons, C.P., Dougan, G., and Frankel, G. (2003). Identification of a novel type IV pilus gene cluster required for gastrointestinal colonization of *Citrobacter rodentium*. Molecular microbiology *48*, 795-809.

Mundy, R., Schuller, S., Girard, F., Fairbrother, J.M., Phillips, A.D., and Frankel, G. (2007). Functional studies of intimin *in vivo* and *ex vivo*: implications for host specificity and tissue tropism. Microbiology *153*, 959-967.

Murata, A., Shimazu, T., Yamamoto, T., Taenaka, N., Nagayama, K., Honda, T., Sugimoto, H., Monden, M., Matsuura, N., and Okada, S. (1998). Profiles of circulating inflammatory- and anti-inflammatory cytokines in patients with hemolytic uremic syndrome due to *E. coli* O157 infection. Cytokine *10*, 544-548.

Murphy, K.C., and Campellone, K.G. (2003). Lambda Red-mediated recombinogenic engineering of enterohemorrhagic and enteropathogenic *E. coli*. BMC Mol Biol *4*, 11.

Myers, E.W., and Miller, W. (1988). Optimal alignments in linear space. Comput Appl Biosci *4*, 11-17.

Nagai, T., Abe, A., and Sasakawa, C. (2005). Targeting of enteropathogenic *Escherichia coli* EspF to host mitochondria is essential for bacterial pathogenesis: critical role of the 16th leucine residue in EspF. The Journal of biological chemistry *280*, 2998-3011.

Nagano, K., Taguchi, K., Hara, T., Yokoyama, S., Kawada, K., and Mori, H. (2003). Adhesion and colonization of enterohemorrhagic *Escherichia coli* O157:H7 in cecum of mice. Microbiol Immunol *47*, 125-132.

Nakao, H., and Takeda, T. (2000). *Escherichia coli* Shiga toxin. J Nat Toxins *9*, 299-313.

Nart, P., Naylor, S.W., Huntley, J.F., McKendrick, I.J., Gally, D.L., and Low, J.C. (2008). Responses of cattle to gastrointestinal colonization by *Escherichia coli* O157:H7. Infection and immunity *76*, 5366-5372.

Nataro, J.P., and Kaper, J.B. (1998). Diarrheagenic *Escherichia coli*. Clin Microbiol Rev *11*, 142-201.

Neild, G.H. (1994). Haemolytic-uraemic syndrome in practice. Lancet *343*, 398-401.

Newman, J.V., Zabel, B.A., Jha, S.S., and Schauer, D.B. (1999). *Citrobacter rodentium espB* is necessary for signal transduction and for infection of laboratory mice. Infect Immun *67*, 6019-6025.

Nicholls, L., Grant, T.H., and Robins-Browne, R.M. (2000). Identification of a novel genetic locus that is required for *in vitro* adhesion of a clinical isolate of enterohaemorrhagic *Escherichia coli* to epithelial cells. Mol Microbiol *35*, 275-288.

Nougayrede, J.P., Fernandes, P.J., and Donnenberg, M.S. (2003). Adhesion of enteropathogenic *Escherichia coli* to host cells. Cell Microbiol *5*, 359-372.

O'Brien, A.D., Tesh, V.L., Donohue-Rolfe, A., Jackson, M.P., Olsnes, S., Sandvig, K., Lindberg, A.A., and Keusch, G.T. (1992). Shiga toxin: biochemistry, genetics, mode of action, and role in pathogenesis. Curr Top Microbiol Immunol *180*, 65-94.

O'Loughlin, E.V., and Robins-Browne, R.M. (2001). Effect of Shiga toxin and Shiga-like toxins on eukaryotic cells. Microbes and infection / Institut Pasteur *3*, 493-507.

Obrig, T.G. (2010). *Escherichia coli* Shiga Toxin Mechanisms of Action in Renal Disease. Toxins (Basel) *2*, 2769-2794.

Ogino, T., Ohno, R., Sekiya, K., Kuwae, A., Matsuzawa, T., Nonaka, T., Fukuda, H., Imajoh-Ohmi, S., and Abe, A. (2006). Assembly of the type III secretion apparatus of enteropathogenic *Escherichia coli*. J Bacteriol *188*, 2801-2811.

Ostroff, S.M., Tarr, P.I., Neill, M.A., Lewis, J.H., Hargrett-Bean, N., and Kobayashi, J.M. (1989). Toxin genotypes and plasmid profiles as determinants of systemic sequelae in *Escherichia coli* O157:H7 infections. The Journal of infectious diseases *160*, 994-998.

Oswald, E., Schmidt, H., Morabito, S., Karch, H., Marches, O., and Caprioli, A. (2000). Typing of intimin genes in human and animal enterohemorrhagic and enteropathogenic *Escherichia coli*: characterization of a new intimin variant. Infect Immun *68*, 64-71.

Padrick, S.B., Cheng, H.C., Ismail, A.M., Panchal, S.C., Doolittle, L.K., Kim, S., Skehan, B.M., Umetani, J., Brautigam, C.A., Leong, J.M*., et al.* (2008). Hierarchical regulation of WASP/WAVE proteins. Mol Cell *32*, 426-438.

Pai, C.H., Kelly, J.K., and Meyers, G.L. (1986). Experimental Infection of Infant Rabbits with Verotoxin-Producing *Escherichia coli*. Infectiona nd Immuntiy *51*, 16-23.

Panda, A., Tatarov, I., Melton-Celsa, A.R., Kolappaswamy, K., Kriel, E.H., Petkov, D., Coksaygan, T., Livio, S., McLeod, C.G., Nataro, J.P*., et al.* (2010). *Escherichia coli* O157:H7 infection in Dutch belted and New Zealand white rabbits. Comp Med *60*, 31-37.

Paton, J.C., and Paton, A.W. (1998). Pathogenesis and diagnosis of Shiga toxin-producing *Escherichia coli* infections. Clin Microbiol Rev *11*, 450-479.

Pearce, M.C., Jenkins, C., Vali, L., Smith, A.W., Knight, H.I., Cheasty, T., Smith, H.R., Gunn, G.J., Woolhouse, M.E., Amyes, S.G*., et al.* (2004). Temporal shedding patterns and virulence factors of *Escherichia coli* serogroups O26, O103, O111, O145, and O157 in a cohort of beef calves and their dams. Applied and environmental microbiology *70*, 1708-1716.

Pennington, H. (2010). *Escherichia coli* O157. Lancet *376*, 1428-1435.

Perna, N.T., Plunkett, G., 3rd, Burland, V., Mau, B., Glasner, J.D., Rose, D.J., Mayhew, G.F., Evans, P.S., Gregor, J., Kirkpatrick, H.A*., et al.* (2001). Genome sequence of enterohaemorrhagic *Escherichia coli* O157:H7. Nature *409*, 529-533.

Persson, S., Olsen, K.E., Ethelberg, S., and Scheutz, F. (2007). Subtyping method for *Escherichia coli* shiga toxin (verocytotoxin) 2 variants and correlations to clinical manifestations. Journal of clinical microbiology *45*, 2020-2024.

Phillips, A.D., and Frankel, G. (2000). Intimin-mediated tissue specificity in enteropathogenic *Escherichia coli* interaction with human intestinal organ cultures. J Infect Dis *181*, 1496-1500.

Phillips, N., Hayward, R.D., and Koronakis, V. (2004). Phosphorylation of the enteropathogenic *E. coli* receptor by the Src-family kinase c-Fyn triggers actin pedestal formation. Nat Cell Biol *6*, 618-625.

Philpott, D.J., Ackerley, C.A., Kiliaan, A.J., Karmali, M.A., Perdue, M.H., and Sherman, P.M. (1997). Translocation of verotoxin-1 across T84 monolayers: mechanism of bacterial toxin penetration of epithelium. Am J Physiol *273*, G1349-1358.

Pierard, D., Muyldermans, G., Moriau, L., Stevens, D., and Lauwers, S. (1998). Identification of new verocytotoxin type 2 variant B-subunit genes in human and animal *Escherichia coli* isolates. Journal of clinical microbiology *36*, 3317-3322.

Poirier, K., Faucher, S.P., Beland, M., Brousseau, R., Gannon, V., Martin, C., Harel, J., and Daigle, F. (2008). *Escherichia coli* O157:H7 survives within human macrophages: global gene expression profile and involvement of the Shiga toxins. Infection and immunity *76*, 4814-4822.

Potter, M.E., Kaufmann, A.F., Thomason, B.M., Blake, P.A., and Farmer, J.J., 3rd (1985). Diarrhea due to *Escherichia coli* O157:H7 in the infant rabbit. The Journal of infectious diseases *152*, 1341-1343.

Proulx, F., Seidman, E.G., and Karpman, D. (2001). Pathogenesis of Shiga toxin-associated hemolytic uremic syndrome. Pediatr Res *50*, 163-171.

Proulx, F., Toledano, B., Phan, V., Clermont, M.J., Mariscalco, M.M., and Seidman, E.G. (2002). Circulating granulocyte colony-stimulating factor, C-X-C, and C-C chemokines in children with *Escherichia coli* O157:H7 associated hemolytic uremic syndrome. Pediatr Res *52*, 928-934.

Psotka, M.A., Obata, F., Kolling, G.L., Gross, L.K., Saleem, M.A., Satchell, S.C., Mathieson, P.W., and Obrig, T.G. (2009). Shiga toxin 2 targets the murine renal collecting duct epithelium. Infect Immun *77*, 959-969.

Quitard, S., Dean, P., Maresca, M., and Kenny, B. (2006). The enteropathogenic *Escherichia coli* EspF effector molecule inhibits PI-3 kinase-mediated uptake independently of mitochondrial targeting. Cellular microbiology *8*, 972-981.

Rasko, D.A., Webster, D.R., Sahl, J.W., Bashir, A., Boisen, N., Scheutz, F., Paxinos, E.E., Sebra, R., Chin, C.S., Iliopoulos, D*., et al.* (2011). Origins of the *E. coli* strain causing an outbreak of hemolytic-uremic syndrome in Germany. The New England journal of medicine *365*, 709-717.

Ray, P.E., and Liu, X.H. (2001). Pathogenesis of Shiga toxin-induced hemolytic uremic syndrome. Pediatric nephrology *16*, 823-839.

Raymond, B., Crepin, V.F., Collins, J.W., and Frankel, G. (2011). The WxxxE effector EspT triggers expression of immune mediators in an Erk/JNK and NF-kappaB-dependent manner. Cellular microbiology *13*, 1881-1893.

Richard, H.T., and Foster, J.W. (2003). Acid resistance in *Escherichia coli*. Adv Appl Microbiol *52*, 167-186.

Richardson, S.E., Karmali, M.A., Becker, L.E., and Smith, C.R. (1988). The histopathology of the hemolytic uremic syndrome associated with verocytotoxin-producing *Escherichia coli* infections. Hum Pathol *19*, 1102-1108.

Richardson, S.E., Rotman, T.A., Jay, V., Smith, C.R., Becker, L.E., Petric, M., Olivieri, N.F., and Karmali, M.A. (1992). Experimental verocytotoxemia in rabbits. Infection and immunity *60*, 4154-4167.

Riley, L.W., Remis, R.S., Helgerson, S.D., McGee, H.B., Wells, J.G., Davis, B.R., Hebert, R.J., Olcott, E.S., Johnson, L.M., Hargrett, N.T.*, et al.* (1983). Hemorrhagic colitis associated with a rare *Escherichia coli* serotype. N Engl J Med *308*, 681-685.

Riopel, M., Krishnamurthy, M., Li, J., Liu, S., Leask, A., and Wang, R. (2011). Conditional beta1-integrin-deficient mice display impaired pancreatic beta cell function. J Pathol *224*, 45-55.

Ritchie, J.M., Brady, M.J., Riley, K.N., Ho, T.D., Campellone, K.G., Herman, I.M., Donohue-Rolfe, A., Tzipori, S., Waldor, M.K., and Leong, J.M. (2008). EspF$_U$, a type III-translocated effector of actin assembly, fosters epithelial association and late-stage intestinal colonization by *E. coli* O157:H7. Cell Microbiol *10*, 836-847.

Ritchie, J.M., Thorpe, C.M., Rogers, A.B., and Waldor, M.K. (2003). Critical roles for stx2, *eae*, and *tir* in enterohemorrhagic *Escherichia coli*-induced diarrhea and intestinal inflammation in infant rabbits. Infect Immun *71*, 7129-7139.

Ritchie, J.M., and Waldor, M.K. (2005). The locus of enterocyte effacement-encoded effector proteins all promote enterohemorrhagic *Escherichia coli* pathogenicity in infant rabbits. Infection and immunity *73*, 1466-1474.

Rivera, G.M., Briceno, C.A., Takeshima, F., Snapper, S.B., and Mayer, B.J. (2004). Inducible clustering of membrane-targeted SH3 domains of the adaptor protein Nck triggers localized actin polymerization. Current biology : CB *14*, 11-22.

Robinson, C.M., Sinclair, J.F., Smith, M.J., and O'Brien, A.D. (2006). Shiga toxin of enterohemorrhagic *Escherichia coli* type O157:H7 promotes intestinal colonization. Proceedings of the National Academy of Sciences of the United States of America *103*, 9667-9672.

Roche, J.K., Keepers, T.R., Gross, L.K., Seaner, R.M., and Obrig, T.G. (2007). CXCL1/KC and CXCL2/MIP-2 are critical effectors and potential targets for therapy of *Escherichia coli* O157:H7-associated renal inflammation. Am J Pathol *170*, 526-537.

Rodriguez-Escudero, I., Hardwidge, P.R., Nombela, C., Cid, V.J., Finlay, B.B., and Molina, M. (2005). Enteropathogenic *Escherichia coli* type III effectors alter cytoskeletal function and signalling in *Saccharomyces cerevisiae*. Microbiology *151*, 2933-2945.

Rohatgi, R., Nollau, P., Ho, H.Y., Kirschner, M.W., and Mayer, B.J. (2001). Nck and phosphatidylinositol 4,5-bisphosphate synergistically activate actin polymerization through the N-WASP-Arp2/3 pathway. The Journal of biological chemistry *276*, 26448-26452.

Romer, W., Berland, L., Chambon, V., Gaus, K., Windschiegl, B., Tenza, D., Aly, M.R., Fraisier, V., Florent, J.C., Perrais, D.*, et al.* (2007). Shiga toxin induces tubular membrane invaginations for its uptake into cells. Nature *450*, 670-675.

Rose, R.E. (1988). The nucleotide sequence of pACYC184. Nucleic Acids Res *16*, 355.

Rosenshine, I., Ruschkowski, S., Stein, M., Reinscheid, D.J., Mills, S.D., and Finlay, B.B. (1996). A pathogenic bacterium triggers epithelial signals to form a functional bacterial receptor that mediates actin pseudopod formation. EMBO J *15*, 2613-2624.

Ross, N.T., and Miller, B.L. (2007). Characterization of the binding surface of the translocated intimin receptor, an essential protein for EPEC and EHEC cell adhesion. Protein Sci *16*, 2677-2683.

Rovin, B.H., and Phan, L.T. (1998). Chemotactic factors and renal inflammation. Am J Kidney Dis *31*, 1065-1084.

Ruggenenti, P., Noris, M., and Remuzzi, G. (2001). Thrombotic microangiopathy, hemolytic uremic syndrome, and thrombotic thrombocytopenic purpura. Kidney Int *60*, 831-846.

Rutjes, N.W., Binnington, B.A., Smith, C.R., Maloney, M.D., and Lingwood, C.A. (2002). Differential tissue targeting and pathogenesis of verotoxins 1 and 2 in the mouse animal model. Kidney Int *62*, 832-845.

Sallee, N.A., Rivera, G.M., Dueber, J.E., Vasilescu, D., Mullins, R.D., Mayer, B.J., and Lim, W.A. (2008). The pathogen protein EspF(U) hijacks actin polymerization using mimicry and multivalency. Nature *454*, 1005-1008.

Sandvig, K. (2001). Shiga toxins. Toxicon *39*, 1629-1635.

Sandvig, K., and van Deurs, B. (1996). Endocytosis, intracellular transport, and cytotoxic action of Shiga toxin and ricin. Physiol Rev *76*, 949-966.

Sanger, J.M., Chang, R., Ashton, F., Kaper, J.B., and Sanger, J.W. (1996). Novel form of actin-based motility transports bacteria on the surfaces of infected cells. Cell Motil Cytoskeleton *34*, 279-287.

Sauter, K.A., Melton-Celsa, A.R., Larkin, K., Troxell, M.L., O'Brien, A.D., and Magun, B.E. (2008). Mouse model of hemolytic-uremic syndrome caused by endotoxin-free Shiga toxin 2 (Stx2) and protection from lethal outcome by anti-Stx2 antibody. Infection and immunity *76*, 4469-4478.

Schauer, D.B., and Falkow, S. (1993a). Attaching and effacing locus of a *Citrobacter freundii* biotype that causes transmissible murine colonic hyperplasia. Infect Immun *61*, 2486-2492.

Schauer, D.B., and Falkow, S. (1993b). The *eae* gene of *Citrobacter freundii* biotype 4280 is necessary for colonization in transmissible murine colonic hyperplasia. Infect Immun *61*, 4654-4661.

Scheiring, J., Andreoli, S.P., and Zimmerhackl, L.B. (2008). Treatment and outcome of Shiga-toxin-associated hemolytic uremic syndrome (HUS). Pediatric nephrology *23*, 1749-1760.

Scheiring, J., Rosales, A., and Zimmerhackl, L.B. (2010). Clinical practice. Today's understanding of the haemolytic uraemic syndrome. Eur J Pediatr *169*, 7-13.

Schmidt, H. (2001). Shiga-toxin-converting bacteriophages. Res Microbiol *152*, 687-695.

Schuller, S. (2011). Shiga toxin interaction with human intestinal epithelium. Toxins *3*, 626-639.

Schuller, S., Chong, Y., Lewin, J., Kenny, B., Frankel, G., and Phillips, A.D. (2007). Tir phosphorylation and Nck/N-WASP recruitment by enteropathogenic and enterohaemorrhagic *Escherichia coli* during *ex vivo* colonization of human intestinal mucosa is different to cell culture models. Cell Microbiol *9*, 1352-1364.

Schuller, S., Frankel, G., and Phillips, A.D. (2004). Interaction of Shiga toxin from *Escherichia coli* with human intestinal epithelial cell lines and explants: Stx2 induces epithelial damage in organ culture. Cellular microbiology *6*, 289-301.

Sebbag, H., Lemelle, J.L., Moller, C., and Schmitt, M. (1999). Colonic stenosis after hemolytic-uremic syndrome. Eur J Pediatr Surg *9*, 119-120.

Sekiya, K., Ohishi, M., Ogino, T., Tamano, K., Sasakawa, C., and Abe, A. (2001). Supermolecular structure of the enteropathogenic *Escherichia coli* type III secretion system and its direct interaction with the EspA-sheath-like structure. Proc Natl Acad Sci U S A *98*, 11638-11643.

Shames, S.R., Croxen, M.A., Deng, W., and Finlay, B.B. (2011). The type III system-secreted effector EspZ localizes to host mitochondria and interacts with the translocase of inner mitochondrial membrane 17b. Infection and immunity *79*, 4784-4790.

Shames, S.R., Deng, W., Guttman, J.A., de Hoog, C.L., Li, Y., Hardwidge, P.R., Sham, H.P., Vallance, B.A., Foster, L.J., and Finlay, B.B. (2010). The pathogenic *E. coli* type III effector EspZ interacts with host CD98 and facilitates host cell prosurvival signalling. Cellular microbiology *12*, 1322-1339.

Shaner, N.C., Sanger, J.W., and Sanger, J.M. (2005). Actin and alpha-actinin dynamics in the adhesion and motility of EPEC and EHEC on host cells. Cell Motil Cytoskeleton *60*, 104-120.

Shaw, R.K., Cleary, J., Murphy, M.S., Frankel, G., and Knutton, S. (2005a). Interaction of enteropathogenic *Escherichia coli* with human intestinal mucosa: role of effector proteins in brush border remodeling and formation of attaching and effacing lesions. Infection and immunity *73*, 1243-1251.

Shaw, R.K., Smollett, K., Cleary, J., Garmendia, J., Straatman-Iwanowska, A., Frankel, G., and Knutton, S. (2005b). Enteropathogenic *Escherichia coli* type III effectors EspG and EspG2 disrupt the microtubule network of intestinal epithelial cells. Infect Immun *73*, 4385-4390.

Sheoran, A.S., Chapman-Bonofiglio, S., Harvey, B.R., Mukherjee, J., Georgiou, G., Donohue-Rolfe, A., and Tzipori, S. (2005). Human antibody against shiga toxin 2 administered to piglets after the onset of diarrhea due to *Escherichia coli* O157:H7 prevents fatal systemic complications. Infection and immunity *73*, 4607-4613.

Sherman, P.M., and Boedeker, E.C. (1987). Regional differences in attachment of enteroadherent *Escherichia coli* strain RDEC-1 to rabbit intestine: luminal colonization but lack of mucosal adherence in jejunal self-filling blind loops. J Pediatr Gastroenterol Nutr *6*, 439-444.

Shifflett, D.E., Clayburgh, D.R., Koutsouris, A., Turner, J.R., and Hecht, G.A. (2005). Enteropathogenic *E. coli* disrupts tight junction barrier function and structure *in vivo*. Lab Invest *85*, 1308-1324.

Shimizu, K., Asahara, T., Nomoto, K., Tanaka, R., Hamabata, T., Ozawa, A., and Takeda, Y. (2003). Development of a lethal Shiga toxin-producing *Escherichia coli*

infection mouse model using multiple mitomycin C treatment. Microbial pathogenesis *35*, 1-9.

Shimizu, T., Ohta, Y., Tsutsuki, H., and Noda, M. (2011). Construction of a novel bioluminescent reporter system for investigating Shiga toxin expression of enterohemorrhagic *Escherichia coli*. Gene *478*, 1-10.

Siebert, P.D., Chenchik, A., Kellogg, D.E., Lukyanov, K.A., and Lukyanov, S.A. (1995). An improved PCR method for walking in uncloned genomic DNA. Nucleic acids research *23*, 1087-1088.

Siegler, R.L. (1994). Spectrum of extrarenal involvement in postdiarrheal hemolytic-uremic syndrome. J Pediatr *125*, 511-518.

Siegler, R.L. (2003). Postdiarrheal Shiga toxin-mediated hemolytic uremic syndrome. Jama *290*, 1379-1381.

Siegler, R.L., Obrig, T.G., Pysher, T.J., Tesh, V.L., Denkers, N.D., and Taylor, F.B. (2003). Response to Shiga toxin 1 and 2 in a baboon model of hemolytic uremic syndrome. Pediatr Nephrol *18*, 92-96.

Simmons, C.P., Clare, S., Ghaem-Maghami, M., Uren, T.K., Rankin, J., Huett, A., Goldin, R., Lewis, D.J., MacDonald, T.T., Strugnell, R.A.*, et al.* (2003). Central role for B lymphocytes and CD4+ T cells in immunity to infection by the attaching and effacing pathogen *Citrobacter rodentium*. Infection and immunity *71*, 5077-5086.

Simon, M., Cleary, T.G., Hernandez, J.D., and Abboud, H.E. (1998). Shiga toxin 1 elicits diverse biologic responses in mesangial cells. Kidney Int *54*, 1117-1127.

Simovitch, M., Sason, H., Cohen, S., Zahavi, E.E., Melamed-Book, N., Weiss, A., Aroeti, B., and Rosenshine, I. (2010). EspM inhibits pedestal formation by enterohaemorrhagic *Escherichia coli* and enteropathogenic *E. coli* and disrupts the architecture of a polarized epithelial monolayer. Cellular microbiology *12*, 489-505.

Simpson, N., Shaw, R., Crepin, V.F., Mundy, R., FitzGerald, A.J., Cummings, N., Straatman-Iwanowska, A., Connerton, I., Knutton, S., and Frankel, G. (2006). The enteropathogenic *Escherichia coli* type III secretion system effector Map binds EBP50/NHERF1: implication for cell signalling and diarrhoea. Mol Microbiol *60*, 349-363.

Sinclair, J.F., Dean-Nystrom, E.A., and O'Brien, A.D. (2006). The established intimin receptor Tir and the putative eucaryotic intimin receptors nucleolin and beta1 integrin localize at or near the site of enterohemorrhagic *Escherichia coli* O157:H7 adherence to enterocytes *in vivo*. Infect Immun *74*, 1255-1265.

Sinclair, J.F., and O'Brien, A.D. (2002). Cell surface-localized nucleolin is a eukaryotic receptor for the adhesin intimin-gamma of enterohemorrhagic *Escherichia coli* O157:H7. J Biol Chem *277*, 2876-2885.

Sinclair, J.F., and O'Brien, A.D. (2004). Intimin types alpha, beta, and gamma bind to nucleolin with equivalent affinity but lower avidity than to the translocated intimin receptor. J Biol Chem *279*, 33751-33758.

Small, P., Blankenhorn, D., Welty, D., Zinser, E., and Slonczewski, J.L. (1994). Acid and base resistance in *Escherichia coli* and *Shigella flexneri*: role of *rpoS* and growth pH. Journal of bacteriology *176*, 1729-1737.

Smollett, K., Shaw, R.K., Garmendia, J., Knutton, S., and Frankel, G. (2006). Function and distribution of EspG2, a type III secretion system effector of enteropathogenic *Escherichia coli*. Microbes Infect *8*, 2220-2227.

Snapper, S.B., Takeshima, F., Anton, I., Liu, C.H., Thomas, S.M., Nguyen, D., Dudley, D., Fraser, H., Purich, D., Lopez-Ilasaca, M.*, et al*. (2001). N-WASP deficiency reveals distinct pathways for cell surface projections and microbial actin-based motility. Nat Cell Biol *3*, 897-904.

Soberon, X., Covarrubias, L., and Bolivar, F. (1980). Construction and characterization of new cloning vehicles. IV. Deletion derivatives of pBR322 and pBR325. Gene *9*, 287-305.

Spears, K.J., Roe, A.J., and Gally, D.L. (2006). A comparison of enteropathogenic and enterohaemorrhagic *Escherichia coli* pathogenesis. FEMS Microbiol Lett *255*, 187-202.

Staley, T.E., Jones, E.W., and Corley, L.D. (1969). Attachment and penetration of *Escherichia coli* into intestinal epithelium of the ileum in newborn pigs. Amer J Path *56*, 371-392.

Stradal, T.E., and Scita, G. (2006). Protein complexes regulating Arp2/3-mediated actin assembly. Curr Opin Cell Biol *18*, 4-10.

Sueyoshi, M., and Nakazawa, M. (1994). Experimental infection of young chicks with attaching and effacing *Escherichia coli*. Infection and immunity *62*, 4066-4071.

Swimm, A., Bommarius, B., Li, Y., Cheng, D., Reeves, P., Sherman, M., Veach, D., Bornmann, W., and Kalman, D. (2004a). Enteropathogenic *E. coli* Use Redundant Tyrosine Kinases to Form Actin Pedestals. Mol Biol Cell.

Swimm, A., Bommarius, B., Li, Y., Cheng, D., Reeves, P., Sherman, M., Veach, D., Bornmann, W., and Kalman, D. (2004b). Enteropathogenic *Escherichia coli* use redundant tyrosine kinases to form actin pedestals. Mol Biol Cell *15*, 3520-3529.

Tabor, S., and Richardson, C.C. (1985). A bacteriophage T7 RNA polymerase/promoter system for controlled exclusive expression of specific genes. Proceedings of the National Academy of Sciences of the United States of America *82*, 1074-1078.

Tacket, C.O., Sztein, M.B., Losonsky, G., Abe, A., Finlay, B.B., McNamara, B.P., Fantry, G.T., James, S.P., Nataro, J.P., Levine, M.M.*, et al.* (2000). Role of EspB in experimental human enteropathogenic *Escherichia coli* infection. Infect Immun *68*, 3689-3695.

Taguchi, H., Takahashi, M., Yamaguchi, H., Osaki, T., Komatsu, A., Fujioka, Y., and Kamiya, S. (2002). Experimental infection of germ-free mice with hyper-toxigenic enterohaemorrhagic *Escherichia coli* O157:H7, strain 6. Journal of medical microbiology *51*, 336-343.

Takeda, K., and Akira, S. (2004). TLR signaling pathways. Semin Immunol *16*, 3-9.

Takeuchi, A., Inman, L.R., O'Hanley, P.D., Cantey, J.R., and Lushbaugh, W.B. (1978). Scanning and transmission electron microscopic study of *Escherichia coli* O15 (RDEC-1) enteric infection in rabbits. Infection and immunity *19*, 686-694.

Tarr, P.I., Gordon, C.A., and Chandler, W.L. (2005). Shiga-toxin-producing *Escherichia coli* and haemolytic uraemic syndrome. Lancet *365*, 1073-1086.

Taylor, F.B., Jr., Tesh, V.L., DeBault, L., Li, A., Chang, A.C., Kosanke, S.D., Pysher, T.J., and Siegler, R.L. (1999). Characterization of the baboon responses to Shiga-like toxin: descriptive study of a new primate model of toxic responses to Stx-1. Am J Pathol *154*, 1285-1299.

te Loo, D.M., Monnens, L.A., van Der Velden, T.J., Vermeer, M.A., Preyers, F., Demacker, P.N., van Den Heuvel, L.P., and van Hinsbergh, V.W. (2000). Binding and transfer of verocytotoxin by polymorphonuclear leukocytes in hemolytic uremic syndrome. Blood *95*, 3396-3402.

Te Loo, D.M., van Hinsbergh, V.W., van den Heuvel, L.P., and Monnens, L.A. (2001). Detection of verocytotoxin bound to circulating polymorphonuclear leukocytes of patients with hemolytic uremic syndrome. Journal of the American Society of Nephrology : JASN *12*, 800-806.

Teel, L.D., Melton-Celsa, A.R., Schmitt, C.K., and O'Brien, A.D. (2002). One of two copies of the gene for the activatable shiga toxin type 2d in *Escherichia coli* O91:H21 strain B2F1 is associated with an inducible bacteriophage. Infection and immunity *70*, 4282-4291.

Tesh, V.L., Burris, J.A., Owens, J.W., Gordon, V.M., Wadolkowski, E.A., O'Brien, A.D., and Samuel, J.E. (1993). Comparison of the relative toxicities of Shiga-like toxins type I and type II for mice. Infection and immunity *61*, 3392-3402.

Tesh, V.L., Ramegowda, B., and Samuel, J.E. (1994). Purified Shiga-like toxins induce expression of proinflammatory cytokines from murine peritoneal macrophages. Infection and immunity *62*, 5085-5094.

Thorpe, C.M., Hurley, B.P., Lincicome, L.L., Jacewicz, M.S., Keusch, G.T., and Acheson, D.W. (1999). Shiga toxins stimulate secretion of interleukin-8 from intestinal epithelial cells. Infection and immunity *67*, 5985-5993.

Thorpe, C.M., Smith, W.E., Hurley, B.P., and Acheson, D.W. (2001). Shiga toxins induce, superinduce, and stabilize a variety of C-X-C chemokine mRNAs in intestinal epithelial cells, resulting in increased chemokine expression. Infection and immunity *69*, 6140-6147.

Tilden, J., Jr., Young, W., McNamara, A.M., Custer, C., Boesel, B., Lambert-Fair, M.A., Majkowski, J., Vugia, D., Werner, S.B., Hollingsworth, J.*, et al.* (1996). A new route of transmission for *Escherichia coli*: infection from dry fermented salami. Am J Public Health *86*, 1142-1145.

Torres, A.G., Giron, J.A., Perna, N.T., Burland, V., Blattner, F.R., Avelino-Flores, F., and Kaper, J.B. (2002). Identification and characterization of lpfABCC'DE, a fimbrial operon of enterohemorrhagic *Escherichia coli* O157:H7. Infect Immun *70*, 5416-5427.

Torres, A.G., Kanack, K.J., Tutt, C.B., Popov, V., and Kaper, J.B. (2004). Characterization of the second long polar (LP) fimbriae of *Escherichia coli* O157:H7 and distribution of LP fimbriae in other pathogenic *E. coli* strains. FEMS Microbiol Lett *238*, 333-344.

Torres, A.G., and Kaper, J.B. (2003). Multiple elements controlling adherence of enterohemorrhagic *Escherichia coli* O157:H7 to HeLa cells. Infect Immun *71*, 4985-4995.

Torres, A.G., Zhou, X., and Kaper, J.B. (2005). Adherence of diarrheagenic *Escherichia coli* strains to epithelial cells. Infection and immunity *73*, 18-29.

Touze, T., Hayward, R.D., Eswaran, J., Leong, J.M., and Koronakis, V. (2004). Self-association of EPEC intimin mediated by the beta-barrel-containing anchor domain: a role in clustering of the Tir receptor. Mol Microbiol *51*, 73-87.

Tran Van Nhieu, G., and Isberg, R.R. (1993). Bacterial internalization mediated by β_1 chain integrins is determined by ligand affinity and receptor density. EMBO J *12*, 1887-1895.

Tu, X., Nisan, I., Yona, C., Hanski, E., and Rosenshine, I. (2003). EspH, a new cytoskeleton-modulating effector of enterohaemorrhagic and enteropathogenic *Escherichia coli*. Molecular microbiology *47*, 595-606.

Tzipori, S., Gunzer, F., Donnenberg, M.S., de Montigny, L., Kaper, J.B., and Donohue-Rolfe, A. (1995). The role of the *eaeA* gene in diarrhea and neurological complications in a gnotobiotic piglet model of enterohemorrhagic *Escherichia coli* infection. Infection and immunity *63*, 3621-3627.

Tzipori, S., Robins-Browne, R.M., Gonis, G., Hayes, J., Withers, M., and McCartney, E. (1985). Enteropathogenic *Escherichia coli* enteritis: evaluation of the gnotobiotic piglet as a model of human infection. Gut *26*, 570-578.

Tzipori, S., Wachsmuth, I.K., Chapman, C., Birden, R., Brittingham, J., Jackson, C., and Hogg, J. (1986). The pathogenesis of hemorrhagic colitis caused by *Escherichia coli* O157:H7 in gnotobiotic piglets. J Infect Dis *154*, 712-716.

Vallance, B.A., Deng, W., Jacobson, K., and Finlay, B.B. (2003). Host susceptibility to the attaching and effacing bacterial pathogen *Citrobacter rodentium*. Infection and immunity *71*, 3443-3453.

Vallance, B.A., Deng, W., Knodler, L.A., and Finlay, B.B. (2002). Mice lacking T and B lymphocytes develop transient colitis and crypt hyperplasia yet suffer impaired bacterial clearance during *Citrobacter rodentium* infection. Infection and immunity *70*, 2070-2081.

van de Kar, N.C., Monnens, L.A., Karmali, M.A., and van Hinsbergh, V.W. (1992). Tumor necrosis factor and interleukin-1 induce expression of the verocytotoxin receptor globotriaosylceramide on human endothelial cells: implications for the pathogenesis of the hemolytic uremic syndrome. Blood *80*, 2755-2764.

van Setten, P.A., Monnens, L.A., Verstraten, R.G., van den Heuvel, L.P., and van Hinsbergh, V.W. (1996). Effects of verocytotoxin-1 on nonadherent human monocytes: binding characteristics, protein synthesis, and induction of cytokine release. Blood *88*, 174-183.

van Setten, P.A., van Hinsbergh, V.W., van den Heuvel, L.P., Preyers, F., Dijkman, H.B., Assmann, K.J., van der Velden, T.J., and Monnens, L.A. (1998). Monocyte chemoattractant protein-1 and interleukin-8 levels in urine and serum of patents with hemolytic uremic syndrome. Pediatr Res *43*, 759-767.

van Setten, P.A., van Hinsbergh, V.W., van der Velden, T.J., van de Kar, N.C., Vermeer, M., Mahan, J.D., Assmann, K.J., van den Heuvel, L.P., and Monnens, L.A. (1997). Effects of TNF alpha on verocytotoxin cytotoxicity in purified human glomerular microvascular endothelial cells. Kidney Int *51*, 1245-1256.

Vidal, J.E., and Navarro-Garcia, F. (2006). Efficient translocation of EspC into epithelial cells depends on enteropathogenic *Escherichia coli* and host cell contact. Infection and immunity *74*, 2293-2303.

Vidal, J.E., and Navarro-Garcia, F. (2008). EspC translocation into epithelial cells by enteropathogenic *Escherichia coli* requires a concerted participation of type V and III secretion systems. Cellular microbiology *10*, 1975-1986.

Vierzig, A., Roth, B., Querfeld, U., and Michalk, D. (1998). A 12-year-old boy with fatal hemolytic-uremic-syndrome, excessive neutrophilia and elevated endogenous granulocyte-colony-stimulating-factor serum concentrations. Clin Nephrol *50*, 56-59.

Vingadassalom, D., Campellone, K.G., Brady, M.J., Skehan, B., Battle, S.E., Robbins, D., Kapoor, A., Hecht, G., Snapper, S.B., and Leong, J.M. (2010). Enterohemorrhagic E. coli requires N-WASP for efficient type III translocation but not for EspFU-mediated actin pedestal formation. PLoS Pathog *6*.

Vingadassalom, D., Kazlauskas, A., Skehan, B., Cheng, H.C., Magoun, L., Robbins, D., Rosen, M.K., Saksela, K., and Leong, J.M. (2009). Insulin receptor tyrosine kinase substrate links the *E. coli* O157:H7 actin assembly effectors Tir and EspF$_U$ during pedestal formation. Proc Natl Acad Sci U S A *106*, 6754-6759.

Viswanathan, V.K., Koutsouris, A., Lukic, S., Pilkinton, M., Simonovic, I., Simonovic, M., and Hecht, G. (2004a). Comparative analysis of EspF from enteropathogenic and enterohemorrhagic *Escherichia coli* in alteration of epithelial barrier function. Infect Immun *72*, 3218-3227.

Viswanathan, V.K., Lukic, S., Koutsouris, A., Miao, R., Muza, M.M., and Hecht, G. (2004b). Cytokeratin 18 interacts with the enteropathogenic *Escherichia coli* secreted protein F (EspF) and is redistributed after infection. Cell Microbiol *6*, 987-997.

Vlisidou, I., Dziva, F., La Ragione, R.M., Best, A., Garmendia, J., Hawes, P., Monaghan, P., Cawthraw, S.A., Frankel, G., Woodward, M.J.*, et al.* (2006a). Role of intimin-tir interactions and the tir-cytoskeleton coupling protein in the colonization of calves and lambs by *Escherichia coli* O157:H7. Infect Immun *74*, 758-764.

Vlisidou, I., Lyte, M., van Diemen, P.M., Hawes, P., Monaghan, P., Wallis, T.S., and Stevens, M.P. (2004). The neuroendocrine stress hormone norepinephrine augments *Escherichia coli* O157:H7-induced enteritis and adherence in a bovine ligated ileal loop model of infection. Infection and immunity *72*, 5446-5451.

Vlisidou, I., Marches, O., Dziva, F., Mundy, R., Frankel, G., and Stevens, M.P. (2006b). Identification and characterization of EspK, a type III secreted effector protein of enterohaemorrhagic *Escherichia coli* O157:H7. FEMS Microbiol Lett *263*, 32-40.

Voorhis, D.L., Dillon, S., Formal, S.B., and Isberg, R.R. (1991). An O antigen can interfere with the function of the *Yersinia pseudotuberculosis* invasin protein. Molecular microbiology *5*, 317-325.

Wadolkowski, E.A., Burris, J.A., and O'Brien, A.D. (1990a). Mouse model for colonization and disease caused by enterohemorrhagic *Escherichia coli* O157:H7. Infect Immun *58*, 2438-2445.

Wadolkowski, E.A., Sung, L.M., Burris, J.A., Samuel, J.E., and O'Brien, A.D. (1990b). Acute renal tubular necrosis and death of mice orally infected with *Escherichia coli* strains that produce Shiga-like toxin type II. Infect Immun *58*, 3959-3965.

Wagner, P.L., Acheson, D.W., and Waldor, M.K. (2001a). Human neutrophils and their products induce Shiga toxin production by enterohemorrhagic *Escherichia coli*. Infection and immunity *69*, 1934-1937.

Wagner, P.L., Neely, M.N., Zhang, X., Acheson, D.W., Waldor, M.K., and Friedman, D.I. (2001b). Role for a phage promoter in Shiga toxin 2 expression from a pathogenic *Escherichia coli* strain. Journal of bacteriology *183*, 2081-2085.

Waldor, M.K., and Friedman, D.I. (2005). Phage regulatory circuits and virulence gene expression. Current opinion in microbiology *8*, 459-465.

Wales, A.D., Clifton-Hadley, F.A., Cookson, A.L., Dibb-Fuller, M.P., Laragione, R.M., Pearson, G.R., and Woodward, M.J. (2002). Production of attaching-effacing lesions in ligated large intestine loops of 6-month-old sheep by Escherichia coli O157:1H7. Journal of medical microbiology *51*, 755-763.

Wales, A.D., Pearson, G.R., Skuse, A.M., Roe, J.M., Hayes, C.M., Cookson, A.L., and Woodward, M.J. (2001). Attaching and effacing lesions caused by *Escherichia coli* O157:H7 in experimentally inoculated neonatal lambs. Journal of medical microbiology *50*, 752-758.

Wales, A.D., Woodward, M.J., and Pearson, G.R. (2005). Attaching-effacing bacteria in animals. J Comp Pathol *132*, 1-26.

Walters, M.D., Matthei, I.U., Kay, R., Dillon, M.J., and Barratt, T.M. (1989). The polymorphonuclear leucocyte count in childhood haemolytic uraemic syndrome. Pediatric nephrology *3*, 130-134.

Wehmeier, U., Sprenger, G.A., and Lengeler, J.W. (1989). The use of lambda plac-Mu hybrid phages in *Klebsiella pneumoniae* and the isolation of stable Hfr strains. Mol Gen Genet *215*, 529-536.

Weiss, S.M., Ladwein, M., Schmidt, D., Ehinger, J., Lommel, S., Stading, K., Beutling, U., Disanza, A., Frank, R., Jansch, L*., et al.* (2009). IRSp53 links the enterohemorrhagic *E. coli* effectors Tir and EspF$_U$ for actin pedestal formation. Cell Host Microbe *5*, 244-258.

Wiles, S., Clare, S., Harker, J., Huett, A., Young, D., Dougan, G., and Frankel, G. (2004). Organ specificity, colonization and clearance dynamics *in vivo* following oral challenges with the murine pathogen *Citrobacter rodentium*. Cell Microbiol *6*, 963-972.

Wilson, R.K., Shaw, R.K., Daniell, S., Knutton, S., and Frankel, G. (2001). Role of EscF, a putative needle complex protein, in the type III protein translocation system of enteropathogenic *Escherichia coli*. Cell Microbiol *3*, 753-762.

Wong, C.S., Jelacic, S., Habeeb, R.L., Watkins, S.L., and Tarr, P.I. (2000). The risk of the hemolytic-uremic syndrome after antibiotic treatment of Escherichia coli O157:H7 infections. The New England journal of medicine *342*, 1930-1936.

Woods, J.B., Schmitt, C.K., Darnell, S.C., Meysick, K.C., and O'Brien, A.D. (2002). Ferrets as a model system for renal disease secondary to intestinal infection with *Escherichia coli* O157:H7 and other Shiga toxin-producing *E. coli*. The Journal of infectious diseases *185*, 550-554.

Xicohtencatl-Cortes, J., Monteiro-Neto, V., Ledesma, M.A., Jordan, D.M., Francetic, O., Kaper, J.B., Puente, J.L., and Giron, J.A. (2007). Intestinal adherence associated with type IV pili of enterohemorrhagic *Escherichia coli* O157:H7. The Journal of clinical investigation *117*, 3519-3529.

Yanisch-Perron, C., Vieira, J., and Messing, J. (1985). Improved M13 phage cloning vectors and host strains: nucleotide sequences of the M13mp18 and pUC19 vectors. Gene *33*, 103-119.

Yi, Y., Ma, Y., Gao, F., Mao, X., Peng, H., Feng, Y., Fan, Z., Wang, G., Guo, G., Yan, J*., et al.* (2010). Crystal structure of EHEC intimin: insights into the complementarity between EPEC and EHEC. PLoS One *5*, e15285.

Yokoyama, K., Horii, T., Yamashino, T., Hashikawa, S., Barua, S., Hasegawa, T., Watanabe, H., and Ohta, M. (2000). Production of shiga toxin by *Escherichia coli* measured with reference to the membrane vesicle-associated toxins. FEMS microbiology letters *192*, 139-144.

Yoon, J.W., and Hovde, C.J. (2008). All blood, no stool: enterohemorrhagic *Escherichia coli* O157:H7 infection. J Vet Sci *9*, 219-231.

Zhang, Q., Donohue-Rolfe, A., Krautz-Peterson, G., Sevo, M., Parry, N., Abeijon, C., and Tzipori, S. (2009). Gnotobiotic piglet infection model for evaluating the safe use of

antibiotics against *Escherichia coli* O157:H7 infection. The Journal of infectious diseases *199*, 486-493.

Zoja, C., Corna, D., Farina, C., Sacchi, G., Lingwood, C., Doyle, M.P., Padhye, V.V., Abbate, M., and Remuzzi, G. (1992). Verotoxin glycolipid receptors determine the localization of microangiopathic process in rabbits given verotoxin-1. J Lab Clin Med *120*, 229-238.